




Universitat Autònoma de Barcelona

ADVERTIMENT. L'accés als continguts d'aquesta tesi queda condicionat a l'acceptació de les condicions d'ús establertes per la següent llicència Creative Commons:  http://cat.creativecommons.org/?page_id=184

ADVERTENCIA. El acceso a los contenidos de esta tesis queda condicionado a la aceptación de las condiciones de uso establecidas por la siguiente licencia Creative Commons:  <http://es.creativecommons.org/blog/licencias/>

WARNING. The access to the contents of this doctoral thesis it is limited to the acceptance of the use conditions set by the following Creative Commons license:  <https://creativecommons.org/licenses/?lang=en>



**Universitat Autònoma
de Barcelona**

PhD in Medicine

Departament of Medicine

Tumor immune microenvironment in B-cell lymphoid malignancies

Doctoral thesis presented by

Isabel Jiménez Bernal

to qualify for the degree of

Doctor

Supervisors

Dr Francesc Bosch Albareda

Dra Marta Crespo Maull

Tutor

Dr Francesc Bosch Albareda

Barcelona, 2020

List of abbreviations

A

ABC-DLBCL	Activated B-cell diffuse large B-cell lymphoma
AID	Activation-induced cytidine deaminase
APC	Antigen presenting cell
APRIL	Proliferation-inducing ligand
ARG	Arginase
ASCT	Autologous stem cell transplant
aSHM	Aberrant somatic hypermutation
ATM	Ataxia telangiectasia mutated

B

β 2m	Beta-2-microglobulin
BAFF	B-cell activating factor
BBB	Blood-brain barrier
BCL-6	B-cell lymphoma 6
BCL-10	B-cell lymphoma 10
BCR	B-cell receptor
BIRC3	Baculoviral IAP repeat-containing 3
BLI	Bioluminescence imaging
BLIMP-1	B lymphocyte-induced maturation protein-1
BM	Bone marrow
BMSC	Bone marrow stromal cell
BTK	Bruton tyrosine kinase

C

CAR	Chimeric antigen receptor
CARD11	Caspase recruitment domain family member 11

TIME in B-cell lymphoid malignancies

CBA	Chromosome-banding analysis
CCF	Cancer cell fraction
CDKN2A	Cyclin-dependent kinase inhibitor 2A
CDKN2B	Cyclin-dependent kinase inhibitor 2B
CDR3	Complementary determining region 3
CI	Combination index
CIT	Chemo-immunotherapy
CK	Complex karyotype
CLL	Chronic lymphocytic leukemia
CLP	Common lymphoid progenitor
CMP	Common myeloid progenitor
CNS	Central nervous system
CNV	Copy-number variant
COO	Cell of origin
CR	Complete response
CSF	Cerebro-spinal fluid
CSR	Class-switch recombination
CT	Computed tomography
CTLA-4	Cytotoxic T-lymphocyte-associated protein 4

D

DC	Dendritic cell
DLBCL	Diffuse large B-cell lymphoma
DZ	Dark zone

E

EBV	Epstein-Barr virus
EC	Endothelial cell
EM	Effector memory
ERIC	European Research Initiative in Chronic Lymphocytic Leukemia

ESCCA	European Society for Clinical Cell Analysis
ET-1	Endothelin-1
ETAT	Endothelin subtype A receptor

F

FBS	Fetal bovine serum
FBXW7	F-Box and WD40 domain protein-7
FCR	Fludarabine cyclophosphamide rituximab
FDA	Food and drug administration
FDC	Follicular dendritic cell
FISH	Fluorescence in situ hybridation
FMO	Fluorescence minus one

G

GC	Germinal center
GCB-DLBCL	Germinal center B diffuse large B-cell lymphoma
GEP	Gene expression profile
GMP	Granulocyte/macrophage progenitor

H

Hb	Hemoglobin
HD	Healthy donor
HD-MTX	High-dose of methotrexate
HIV	Human immunodeficiency virus
HLA	Human leukocyte antigen
HR	Hazard ratio
HSC	Hematopoietic stem cell
HSCT	Hematopoietic stem cell transplantation

TIME in B-cell lymphoid malignancies

I

ID50	Inhibitory dose 50
IDO	Indoleamine 2,3-dioxygenase
IELSG	International Extranodal Lymphoma Study Group
IFN γ	Interferon gamma
Ig	Immunoglobulin
IgH	Immunoglobulin heavy chain
IGHV	Immunoglobulin heavy chain variable region
IgL	Immunoglobulin light chain
IHC	Immunohistochemistry
IL	Interleukin
IL-7	Interleukin-7
IL-7R	Interleukin-7 receptor
Indel	Insertion and deletion
IPI	International prognostic index
IR	Inhibitory receptor
IRAK1	Interleukin-1 receptor-associated kinase 1
IRF4	Interferon regulatory factor 4
ITK	Interleukin-2-inducible T-cell kinase
iwCLL	International workshop on Chronic Lymphocytic Leukemia

K

KLRG1	Killer cell lectin-like receptor subfamily G member 1
-------	---

L

LCMV	Lymphocytic choriomeningitis virus
LDH	Lactate dehydrogenase
LDT	Lymphocyte doubling time
LN	Lymph node
LPS	Lipopolysaccharide

LT-HSC	Long-term hematopoietic stem cell
LZ	Light zone
M	
mAb	Monoclonal antibody
MALT1	Mucosa-associated lymphoid tissue lymphoma translocation 1
MBL	Monoclonal B-cell lymphocytosis
M-CLL	Mutated chronic lymphocytic leukemia
MDSC	Myeloid-derived suppressor cell
MEP	Megakaryocyte/erythrocyte progenitor
MHC	Major histocompatibility complex
M-IGHV	Mutated immunoglobulin heavy chain variable region
MPP	Multipotent progenitor
MRI	Magnetic resonance imaging
MSKCC	Memorial Sloan Kettering Cancer Center
MTX	Methotrexate
MVEC	Microvascular endothelial cell
MYD88	Myeloid differentiation primary response gene 88
N	
NF- κ B	Non-canonical nuclear factor-kappa B
NGS	Next-generation sequencing
NHEJ	Non-homologous end-joining
NHL	Non-Hodgkin lymphoma
NK	Natural killer
NLC	Nurse-like cell
NOS	Nitric-oxide synthase
NOTCH1	Notch homolog 1
NPC	Nuclear pore complex

TIME in B-cell lymphoid malignancies

O

OS Overall survival

P

PAX5 Paired box 5

PB Peripheral blood

PBMC Peripheral blood mononuclear cell

PCNSL Primary central nervous system lymphoma

PD-1 Programmed death 1

PD-L1 Programmed death ligand 1

PD-L2 Programmed death ligand 2

PDX Patient-derived xenograft

PFS Progression-free survival

Ph/s Photons per second

PI Propidium iodide

PI3K Phosphoinositide 3-kinase

PKC β II Protein kinase C beta II

POT1 Protection of telomeres 1

PR Partial response

Q

qRT-PCR Quantitative reverse transcription polymerase chain reaction

R

R/R Relapsed/refractory

RNI Reactive nitrogen intermediate

ROI Reactive oxygen intermediate

RPS15 Ribosomal protein S15

RS Richter's syndrome

S

SF3B1	Splicing factor 3B subunit 1
SHM	Somatic hypermutation
SINE	Selective inhibitor of nuclear exportin
SIRP α	Signal regulatory protein alpha
SLC	Surrogate light chain
SLL	Small lymphocytic lymphoma
SNV	Single nucleotide variant
STAT	Signal transducer and activator of transcription 6
ST-HSC	Short-term hematopoietic stem cell

T

TAM	Tumor-associated macrophage
TCF1	Transcription factor T-cell factor 1
TCR	T-cell receptor
TGF β	Transforming growth factor beta
TIL	Tumor-infiltrating lymphocyte
TIME	Tumor immune microenvironment
TK	Thymidine kinase
TLR	Toll-like receptor
TME	Tumor microenvironment
TNFAIP3	TNF alpha induced protein 3
TOX	Thymocyte selection-associated HMG box
TP53	Tumor protein 53
TTFT	Time to first treatment
TTT	Time to treatment

U

UM-CLL	Unmutated chronic lymphocytic leukemia
UM-IGHV	Unmutated immunoglobulin heavy chain variable region

TIME in B-cell lymphoid malignancies

V

VAF	Variant allele frequency
VEGF	Vascular endothelial growth factor
VLA-4	Very-late antigen 4

W

WBRT	Whole-brain radiotherapy
WES	Whole-exome sequencing
WHO	World Health Organization

X

XBPI	X-box binding protein 1
XPO1	Exportin 1

Z

ZAP-70	Zeta-chain-associated protein 70
--------	----------------------------------

Table of contents

Summary	19
Resumen.....	21
1. Introduction.....	25
1.1. Origin and development of B lymphocytes	27
1.1.1. Hematopoiesis.....	27
1.1.2. Development and differentiation of B lymphocytes.....	28
1.1.2.1. From HSCs towards immature B lymphocytes in the BM	28
1.1.2.2. Towards mature B lymphocytes in secondary lymphoid organs.....	30
1.2. B-cell lymphoid malignancies	33
1.3. Tumor immune microenvironment	34
1.3.1. Overview	34
1.3.2. Cancer immunoediting	34
1.3.3. Evasion from tumor immunosurveillance	35
1.3.3.1. Mechanisms of the innate response: TAMs	35
1.3.3.2. Mechanisms of the adaptive response: T-cell exhaustion	37
1.4. Chronic lymphocytic leukemia	40
1.4.1. Definition and epidemiology.....	40
1.4.2. Diagnosis	41
1.4.3. Prognosis	42
1.4.3.1. Clinical prognostic factors	42
1.4.3.2. Biological prognostic factors.....	43
1.4.4. Pathogenesis.....	45
1.4.5. Genetic alterations	47
1.4.5.1. Chromosomal aberrations	47
1.4.5.2. Somatic mutations.....	48
1.4.5.3. Clonal evolution	50
1.4.6. Treatment.....	52
1.4.7. TIME in CLL	54
1.4.7.1. Cellular components	54
1.4.7.2. Soluble components	59
1.4.7.3. BCR signaling pathway	60
1.4.7.4. TIME during CLL progression	62
1.5. Primary central nervous system lymphoma	64

1.5.1. Definition and epidemiology.....	64
1.5.2. Diagnosis	64
1.5.3. Prognosis	65
1.5.4. Pathogenesis.....	66
1.5.5. Genetic alterations.....	67
1.5.6. Treatment.....	69
1.5.7. TIME in PCNSL.....	70
1.5.7.1. Cellular components	70
1.5.7.2. Soluble components.....	73
1.5.7.3. BCR and NF- κ B signaling pathways.....	74
2. Hypothesis.....	79
3. Objectives	85
3.1. Main objective.....	87
3.2. Specific objectives	87
Part I – The genetic and immune landscapes in clinical progression of CLL	87
Part II – New therapeutic strategies in PCNSL and immunomodulatory effects	87
4. Materials & Methods.....	89
5. Results	105
Part I - The genetic and immune landscapes of clinical progression in CLL.....	107
5.1. CLL cells show limited and non-recurrent genetic changes at clinical progression....	109
5.2. At CLL progression, CD8 ⁺ T cells are enriched in PD-1 ⁺ effector memory subsets and show increased co-expression of inhibitory receptors.....	121
5.3. Terminally exhausted CD8 ⁺ T cells accumulate at CLL progression.....	124
5.4. T cells acquire a distinct transcriptional profile at CLL progression.....	126
5.5. PD-1 expression in CD8 ⁺ T cells is induced by malignant cells via soluble factors including IL-10	130
Part II - New therapeutic strategies in PCNSL and immunomodulatory effects	135
5.6. DLBCL cell lines have equivalent sensitivity to selinexor regardless of their COO	137
5.7. Selinexor blocks tumor growth and prolongs survival in a orthotopic mouse model of PCNSL	138
5.8. The combination of selinexor and ibrutinib synergizes <i>in vitro</i> in DLBCL cell lines and increases the survival of mice with CNS lymphoma.....	142
5.9. CNS lymphoma is infiltrated by M2-like macrophages expressing PD-1 and SIRP α .	146
5.10. Treatment with selinexor and ibrutinib favors TAM polarization toward a pro-inflammatory M1-like phenotype and diminishes PD-1 and SIRP α expression in M2-like TAMs.....	151
6. Discussion.....	159
7. Conclusions.....	169

8. Prospective research opportunities	173
9. Bibliography	179
10. Annexes	211
10.1. Scientific articles and communications	213

Summary

The tumor immune microenvironment (TIME) plays a critical role in the early formation of tumors and their progression. Targeting the TIME has offered new therapeutic approaches and improved current ones in several cancers, including B-cell malignancies. Nonetheless, further investigation is needed in order to more deeply understand immune evasion mechanisms that lead to tumor progression and to design therapies that modulate the immune system more precisely. Here, our main objectives are to provide new insights into immune mechanisms that favor tumor progression and a pre-clinical rationale for the design of new therapeutic strategies with immunomodulatory potential. To accomplish these goals our study will focus on chronic lymphocytic leukemia (CLL) and primary central nervous system lymphoma (PCNSL).

Mechanisms driving the progression of CLL from its early stages are not fully understood. This hampers detecting progression in advance and developing therapies that could intervene in the early stages. Although the limited acquisition of molecular changes suggests that CLL progression is not mainly driven by clonal evolution, a deeper analysis of the immune microenvironment that demonstrates immune variations over time that contribute to progression has not been performed. Hence, we longitudinally studied the immune and genetic landscapes of untreated progressing and non-progressing patients. Our results show that progressed CLL patients experience an increase in effector memory and terminally exhausted T-bet^{mid}/Eomes^{hi}PD^{hi} CD8⁺ T cells over time, not observed in non-progressing patients. In addition, T cells at progression acquire a distinct transcriptional profile. This is accompanied by enhanced immunosuppressive properties in leukemic cells at progression. We prove that progressed CLL cells are intrinsically more capable of inducing CD8⁺ T-cell exhaustion in T cells affected by CLL and healthy T cells by a mechanism dependent on soluble factors including IL-10. In addition, the reduced genetic changes we found by whole-exome sequencing in our cohort indicate these immune variations are fundamental for progression in CLL.

TIME in B-cell lymphoid malignancies

Patients diagnosed with PCNSL often face dismal outcomes due to the limited availability of therapeutic options. PCNSL cells frequently have deregulated B-cell receptor (BCR) signaling, but its inhibition using ibrutinib only offers a brief effective response in PCNSL patients. Nonetheless, the BCR pathway can also be blocked by inhibiting the nuclear exportin XPO1 using selinexor. Selinexor is able to cross the blood–brain barrier and has shown positive clinical activity in a patient with refractory diffuse large B-cell lymphoma in the CNS. Accordingly, we evaluated the effects of selinexor alone and also combined it with ibrutinib in pre-clinical mouse models of PCNSL. Our analysis shows that selinexor blocks tumor growth and prolongs survival in a bioluminescent mouse model and its combination with ibrutinib further increases survival. We demonstrate that CNS lymphomas in mice are infiltrated by tumor-promoting M2-like macrophages expressing PD-1 and SIRP α . Moreover, the treatment with selinexor and ibrutinib favors an anti-tumoral immune response by shifting macrophage polarization toward an inflammatory phenotype and diminishing the expression of PD-1 and SIRP α in M2 tumor-associated macrophages.

On one hand, our CLL data highlight that malignant cells displaying increased immunosuppressive features over the course of the disease engage in a positive feed-back system with T cells that further increase T-cell exhaustion. This boosts the evasion of T-cell surveillance and facilitates the transition from diagnosis to progression in CLL. On the other hand, our analysis in PCNSL proposes a pathogenic role of the innate immune microenvironment in PCNSL and provides pre-clinical evidence for the development of selinexor and ibrutinib as a new therapeutic option with cytotoxic and immunomodulatory potential.

Resumen

El microambiente inmune tumoral juega un papel fundamental en las etapas tempranas de la formación de los tumores y en la progresión de éstos. Terapias dirigidas a este microambiente ofrecen nuevas opciones terapéuticas y también sirven para mejorar las terapias actuales frente a muchos cánceres, incluyendo los que afectan a las células B. Sin embargo, son necesarias más investigaciones para entender en mayor profundidad los mecanismos de evasión del sistema inmune que favorecen la progresión de los tumores y diseñar inmunoterapias más precisas. Aquí, nuestros principales objetivos son aportar nuevas evidencias sobre mecanismos inmunes asociados a la progresión tumoral y las bases pre-clínicas para el desarrollo de nuevas estrategias terapéuticas con potencial inmuno-modulador. Para ello, nos centramos en la leucemia linfática crónica (LLC) y en el linfoma cerebral primario (LCP).

Los mecanismos de progresión en LLC desde estadios tempranos no son conocidos en su totalidad. Esto dificulta detectar de forma precoz aquellos pacientes que progresarán y desarrollar terapias que puedan ser beneficiosas en estadios iniciales. Aunque la adquisición de alteraciones moleculares es escasa sugiriendo que la LLC no progresa exclusivamente por mecanismos de evolución clonal, todavía no se ha llevado a cabo un análisis exhaustivo del microambiente inmune que demuestre que la progresión sí pueda deberse a cambios inmunes. Por ello, hemos realizado un estudio longitudinal abarcando tanto los escenarios genéticos como inmunológicos en pacientes de LLC sin tratar que han progresado clínicamente y en pacientes asintomáticos durante un largo periodo de tiempo. Nuestros resultados muestran que los pacientes que progresan experimentan un incremento de células T CD8⁺ efectoras de memoria y terminalmente exhaustas T-bet^{mid}/Eomes^{hi}PD^{hi} a la progresión. Este incremento no se observa en los pacientes de LLC que no han progresado. Además, las células T a la progresión adquieren un perfil transcripcional diferente. Esto va acompañado de un aumento en las propiedades inmunosupresoras de las células leucémicas a la progresión. Demostramos que las células de LLC en el momento de la progresión tienen mayor capacidad de inducir exhaustión tanto en células T

TIME in B-cell lymphoid malignancies

CD8⁺ de LLC como aquellas procedentes de individuos sanos, y que lo hacen mediante un mecanismo dependiente de factores solubles que incluye IL-10. Finalmente, los escasos cambios genéticos que encontramos tras secuenciar el exoma de nuestros pacientes nos permiten concluir que las variaciones inmunes que hemos identificado son fundamentales para la progresión de la LLC.

El desenlace de los pacientes diagnosticados con LCP es normalmente desfavorable debido a la escasez de opciones terapéuticas efectivas. Las células malignas de LCP presentan con frecuencia una desregulación de la vía del receptor de la célula B (del inglés, BCR), pero su inhibición mediante ibrutinib muestra respuestas muy breves en pacientes. Sin embargo, la vía del BCR también puede bloquearse mediante la inhibición de la exportina nuclear XPO1 con selinexor. Selinexor atraviesa la barrera hemato-encefálica y ha mostrado actividad en un paciente diagnosticado con linfoma difuso de células grandes B con recaída en el sistema nervioso central. Por consiguiente, decidimos evaluar los efectos de selinexor en monoterapia y combinado con ibrutinib en modelos pre-clínicos murinos de LCP. Nuestro análisis muestra que selinexor bloquea el crecimiento tumoral y prolonga la supervivencia en un modelo de ratón bioluminiscente y la combinación con ibrutinib prolonga aún más la supervivencia. Demostramos que los linfomas cerebrales en ratón están infiltrados con macrófagos pro-tumorales M2 que expresan PD-1 y SIRP α . Además, el tratamiento con selinexor e ibrutinib favorece la respuesta inmune anti-tumoral induciendo un cambio en la polarización de los macrófagos hacia un perfil más pro-inflamatorio y reduciendo la expresión de PD-1 y SIRP α en los macrófagos M2 asociados al tumor.

Por un lado, nuestros datos en LLC destacan que las células malignas, con mayores propiedades inmunosupresoras durante el curso de la enfermedad, participan en un sistema de retroalimentación con las células T que induce un aumento en su exhaustión. Esto fomenta la evasión de vigilancia de las células T y favorece el paso desde el diagnóstico a la progresión. Por otro lado, nuestro análisis en LCP propone la implicación del microambiente inmune innato en la patogénesis de este linfoma y proporciona evidencias pre-clínicas para el desarrollo de

selinexor e ibrutinib como nueva opción terapéutica con potencial citotóxico e inmunomodulador.

1. Introduction

1.1. Origin and development of B lymphocytes

1.1.1. Hematopoiesis

All blood cellular components originate from the same progenitor cell, the *hematopoietic stem cell* (HSC), which comprises a pool of long-lived and self-renewing cells that reside in special microenvironments in the bone marrow (BM) called *HSC niches*. HSCs are able to differentiate into multi-lineage progenitors and lineage-committed precursors through a traditionally-considered stepwise process: the *hematopoiesis* (1,2).

The survival of HSCs and maintenance of the niches are tightly regulated by the interactions between HSCs and other cell-types and also by soluble factors. In the adult BM, HSCs can localize adjacent to osteoblasts which produce thrombopoietin to keep HSCs in a quiescent state. Furthermore, *stromal* and *endothelial cells* (ECs) secrete CXCL12. CXCL12 binds to CXCR4 expressed in HSCs favoring the migration of HSCs to vascular cells. This contributes to the formation and maintenance of the niches (3).

The classical hematopoietic hierarchy considers hematopoiesis as a tree-branched process and HSCs as a homogeneous population that can be classified into long-term HSCs (LT-HSCs) and short-term HSCs (ST-HSCs). ST-HSCs differentiate into *multipotent progenitors* (MPPs) which can turn into *common myeloid progenitors* (CMPs) or *common lymphoid progenitors* (CLPs). These progenitors will evolve into erythrocytes and myeloid cells or lymphoid cells, respectively (detailed in **Figure 1A**). Advances in the field of single-cell transcriptomics have revealed that considering hematopoiesis a continuous process would be more accurate. HSCs have come to encompass a heterogeneous pool of cells with differentiation properties (**Figure 1B**). Recently, a new model suggests that hematopoiesis is a continuum of differentiation in which undifferentiated stem and progenitor cells will progressively transform to lineage-restricted cells through the suppression of cell division-related genes and activation of lineage-specific genes (**Figure 1C**) (2).

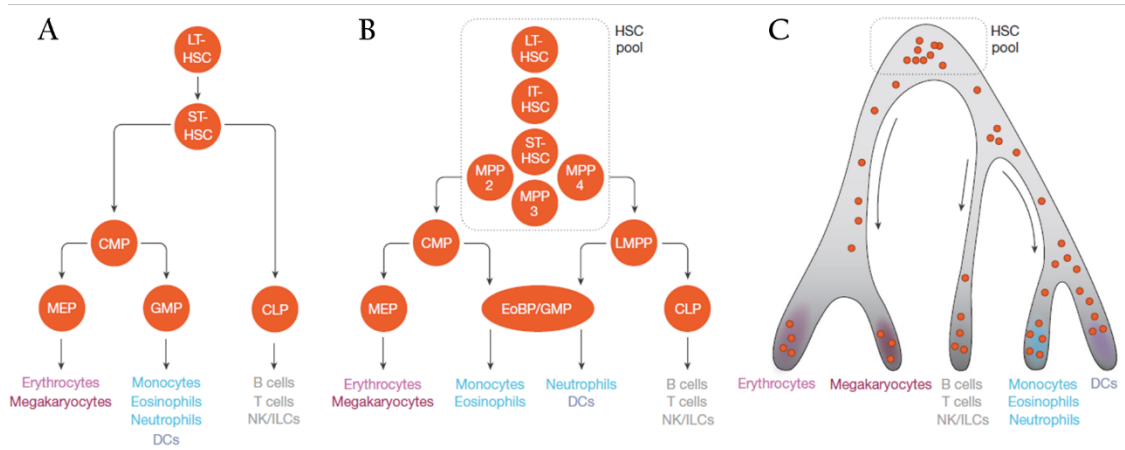


Figure 1. The evolution of hematopoietic models. (A) A classical hematopoietic hierarchy model was first considered. (B) Then, HSCs were classified into different pools of cells with differentiation properties. (C) Hematopoiesis as a continuum of differentiation. From Laurenti E. & Göttgens B. Nat. Rev. 2018.

1.1.2. Development and differentiation of B lymphocytes

B-cell lymphopoiesis generates mature B cells from multipotent stem cells. It takes place early in the BM and later in secondary lymphoid organs. Survival and differentiation of B-cell progenitors are regulated by CXCL12 and interleukin-7 (IL-7) secreted by stromal cells in the BM. Multipotent stem cells are highly CXCL12-dependent and are attached to CXCL12-producing cells whereas more differentiated B cells move away CXCL12-producing cells and become closer to IL-7 producing cells (3,4). The main characteristic of B-cell lymphopoiesis is the rearrangement of the immunoglobulin (Ig) gene loci for the formation of the *B-cell receptor (BCR)*. Different checkpoints control the BCR formation in order to guaranty the central tolerance to autoantigens in the BM and assure the responsiveness of the BCR to foreign antigens (5).

1.1.2.1. From HSCs towards immature B lymphocytes in the BM

B-cell development starts in the BM from multipotent stem cells that possess the Ig gene loci in a germline configuration. The rearrangement of the Ig heavy chain (IgH) locus is initiated by

recombinases *RAG1* and *RAG2* which cut the DNA at the recombination signal sequences in CLPs or *pro-B* cells. Then *non-homologous end-joining proteins (NHEJ)* repair and join the cleaved double strands of DNA and diversity (D) and joining (J) regions of the IgH gene are assembled in CLPs or early stages of *pro-B* cells. Then the variable (V) regions are rearranged to the DJ rearrangements in late stages of *pro-B* cells. This process is known as *V(D)J rearrangement (Figure 2A)* (6,7).

Productive *V(D)J* rearrangements express the Ig heavy ($Ig\mu$) chain on the surface of large *pre-B* cells. Large *pre-B* cells express a *pre-BCR* on their surface composed of two $Ig\mu$ chains and a germline-encoded surrogate light chain (SLC). The SLC is encoded by two separate genes, *VpreB* and $\lambda 5$, transcribed in *pro-* and *pre-B* cells respectively. Once the *pre-BCR* is formed, it combines with the signaling subunits $Ig\alpha$ and $Ig\beta$ (Figure 3). Although the *pre-BCR* is transiently expressed, it is needed for two fundamental checkpoints. In the first one, the SLC tests the $Ig\mu$ chain fitness to pair with an Ig light (IgL) chain. And in the second one, a recognition of nuclear antigens by the non-Ig components of SLC drives the positive or negative selection of *pre-B* cells.

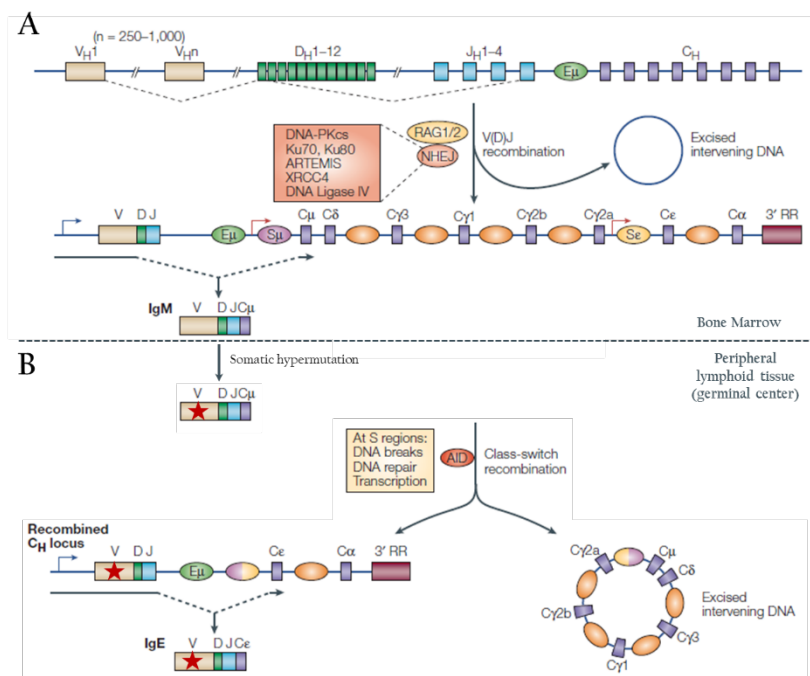


Figure 2. Rearrangement mechanisms at the Ig gene loci. (A) *V(D)J* rearrangement and (B) somatic hypermutation and class-switch recombination mechanisms. From Chaudhuri J. & Alt F. W., *Nat Rev Immunol.* 2004 (modified).

TIME in B-cell lymphoid malignancies

Importantly, the aggregation of pre-BCRs and subsequent signaling is mainly initiated by the non-Ig component of $\lambda 5$ subunit. This subunit is positively charged and polyreactive. This facilitates the interaction of the pre-BCR with multiple molecules (nucleic acids, insulin or heparin sulphates) creating pre-BCR complexes to initiate the signaling. Signals from the pre-BCR induce clonal proliferation and pre-BCR downregulation. As a result, the recombination of the IgL genes to generate a complete molecule of BCR is initiated in small pre-B cells. The BCR molecule is formed by two Ig μ chains (IgH) and two Ig κ or Ig λ chains (IgL) associated to Ig α and Ig β and it is expressed on the surface of *immature B cells* (Figure 3) (5,8).

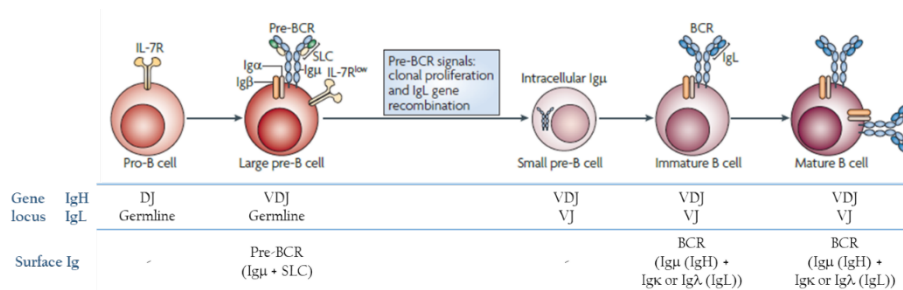


Figure 3. B-cell differentiation stages. From Herzog S. *et al.*, Nat. Rev. Immunol. 2009.

Immature B cells are subjected to a third checkpoint which consists of the presentation of autoantigens, such as insulin or DNA, and positive selection of those B cells carrying low-affinity autoreactive BCRs. Positively selected B cells are approximately 25% of total immature B cells and are the ones that exit the BM. In contrast, immature B cells with high-affinity autoreactive BCRs are negatively selected and eliminated by apoptosis. Therefore, negative selection assures central B tolerance by eliminating the vast majority of the BCR repertoire initially formed in the BM (8).

1.1.2.2. Towards mature B lymphocytes in secondary lymphoid organs

Immature B cells that have undergone successful V(D)J rearrangements and possess a functional non-self-reactive BCR are able to migrate from the BM to secondary lymphoid organs as *mature*

naïve B cells. In lymphoid tissues, these naïve B cells become activated by the interaction of CD40 with its ligand, CD40L, expressed on the surface of CD4⁺ T cells as well as by the interaction with antigen-presenting *follicular dendritic cells (FDCs)*. Then they aggregate into primary follicles which eventually originate the *germinal centers (GC)*. GCs are histological structures composed by a *dark zone (DZ)* of highly proliferating B cells and a *light zone (LZ)* in which the positive selection of B cells with increased affinity for foreign antigens takes place. After passing through the GC reaction, B cells reach their final differentiation stage in which *memory B cells* and *plasma cells* are formed. Plasma cells will be able to produce high affinity antibodies of different isotype classes (8,9).

The GC reaction. During the GC reaction, two processes of Ig gene remodeling occur: *somatic hypermutation (SHM)* in the DZ and *class-switch recombination (CSR)* later in the LZ (**Figure 2B**). By SHM, mainly single nucleotide changes, but also deletions and duplications, are introduced in the antigen-binding variable region of the IgH (IGHV). CSR consists of the replacement of the constant region (C_H) of the IgH (C_μ for IgM) with a set of downstream constant-region genes C_γ, C_α or C_ε by the enzyme *activation-induced cytidine deaminase (AID)*. As a result, the antigen-binding variable region remains unaltered but a diversity of isotype classes (IgG, IgA or IgE, respectively) with different functions arise. Only IgD is originated by an alternative splicing of the germline transcripts that encode IgM, not by CSR (6,7). Interestingly, although CSR has always been considered to take place in the LZ, a recent study suggests that it takes place during the initial interaction between T and B cells before the GC formation and it diminishes as B cells differentiate and SHM starts (10). GC formation and its subsequent maintenance are strictly regulated by the activation and repression of a broad collection of *transcription factors*. The center of this transcriptional network is the transcriptional repressor *B-cell lymphoma 6 (BCL-6)*. BCL-6 increases the threshold of response to DNA damage regulating genes such as *tumor protein 53 (TP53)* and *ataxia telangiectasia mutated (ATM)* and, therefore, allowing SHM and CSR to occur. BCL-6 also interferes with several signaling pathways in order to avoid a premature B-cell exit

TIME in B-cell lymphoid malignancies

from the GC. When BCL-6 is expressed, *interferon regulatory factor 4* (IRF4) is repressed. Consequently, the plasma cell master regulator *B lymphocyte-induced maturation protein-1* (BLIMP-1) is blocked which impedes plasma cell differentiation. BCL-6 is activated in naïve B cells that interact with CD4⁺ T cells for the GC formation and in B cells in the DZ. However, it is switched off in the LZ when BLIMP-1 is upregulated (Figure 4) (9,11-13).

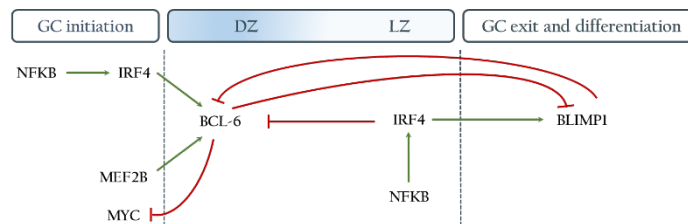


Figure 4. Main transcriptional regulation in the GC. Based on Basso K. & Dalla-Favera R. Nat Rev Immunol. 2015.

Notably, the GC reaction should not be considered a unidirectional process as there is a cyclic re-entry of B cells from the LZ to the DZ, so more rounds of SHM can take place until the eventual exit of B cells from the GC. Specifically, the subset of B cells that re-express MYC in the LZ is positively selected for re-entry in the DZ (14). Differentiation into memory B cells and plasma cells depends on the transcriptional factor *paired box 5* (PAX5). PAX5 blocks the expression of *X-box binding protein 1* (XBPI), which is key for the acquisition of the antibody-secreting phenotype of plasma cells. Thus, PAX5 is continuously expressed in mature B cells, except those restricted to turn into plasma cells (Figure 5). XBPI, together with BLIMP1 (encoded by PRDM1), NFKB and IRF4, conform the transcriptional program for plasma cell differentiation (Figure 5) (9,15,16).

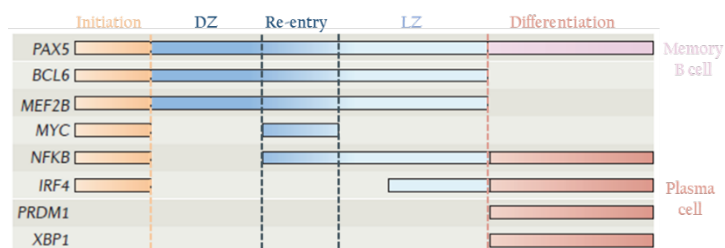


Figure 5. Gene expression during the GC reaction. From Basso K. and Dalla-Favera R. Nat. Rev. Immunol. 2015 (modified).

1.2. B-cell lymphoid malignancies

The deregulation of the same genetic mechanisms that generate functional BCRs and transcriptional programmes involved in the GC entail the malignant transformation of B cells. Malignant B cells usually retain some characteristics of their cell of origin. Although most B-cell lymphomas arise from GC or post-GC B cells, the exact origin of some B-cell malignancies is still unknown (Figure 6) (9,17).

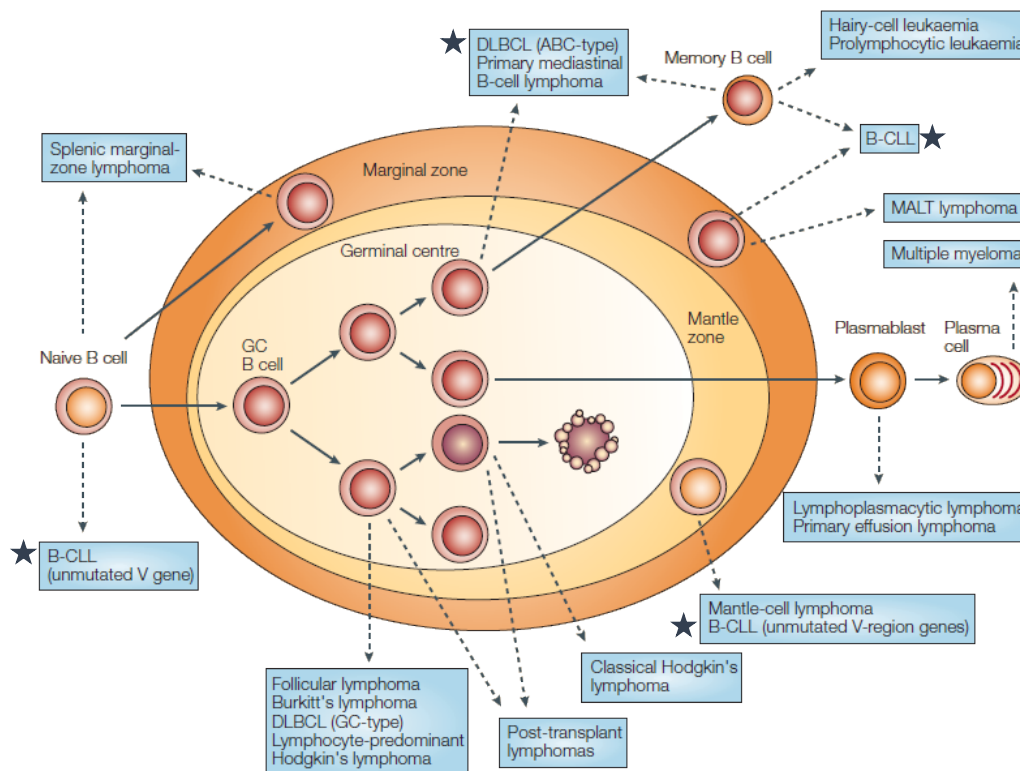


Figure 6. Origin of B-cell lymphoid malignancies. Those malignancies marked with an asterisk will be covered in this thesis: B-CLL and PCNSL (mainly classified as ABC-DLBCL). From Küppers R. Nat. Rev. Cancer 2005.

This doctoral thesis will be focused on two mature B-cell lymphoid malignancies, chronic lymphocytic leukemia (section 1.4) and primary central nervous system lymphoma (section 1.5).

1.3. Tumor immune microenvironment

1.3.1. Overview

The *tumor microenvironment (TME)* is defined as the environment around a tumor in which non-malignant cells from the immune system, vasculature and lymphatic system interact with tumor cells. Soluble factors including chemokines, cytokines and growth factors secreted by tumor cells and non-malignant cells also take part in these interactions. The *tumor immune microenvironment (TIME)* is specifically formed by immune cells, as well as related soluble factors with immune impact that interact with tumor cells. The TIME has received special attention due to the development of immunotherapies. Some immunotherapeutic approaches have shown excellent responses in some types of cancer, but not every type, highlighting different implications of the TIME among malignancies. Further investigations are needed to better understand the role of the TIME in cancer. This will aid in designing more effective immunotherapies and identifying predictors of response to these therapies (18).

1.3.2. Cancer immunoediting

The immune system is composed of the *innate* and *adaptive* immune cells. Innate cells (monocytes, macrophages, granulocytes and NK cells) are the body's first defense barrier and they rapidly trigger an inflammatory response against pathogens. However, the innate response is unspecific and limited. Adaptive immune cells (T and B cells), however, recognize the pathogen with specificity. This leads to an effective response that will also induce memory (19).

The immune system is also the principal defense barrier against tumors (20). The mechanisms by which immune cells are able to distinguish transformed cells at early stages and eliminate them are called *immunosurveillance mechanisms*. However, immune cells can also facilitate tumor progression. This dual role is named *cancer immunoediting* and it comprises three phases: elimination, equilibrium and escape (Figure 7). During the elimination phase, innate and adaptive immune cells cooperate to detect and eliminate transformed cells before the tumor is

clinically detectable. Nonetheless, some transformed cells enter in an equilibrium stage in which they stay dormant and clinically indiscernible. Dormant malignant cells could eventually develop mechanisms to escape from immunosurveillance either by changes in the expression of surface molecules and secretion of specific soluble factors or by inducing changes in patients' immune cells. These changes are devoted to create an immunosuppressed environment that favors the end of dormancy and, therefore, the progression of the tumor (20,21).

(20,21).

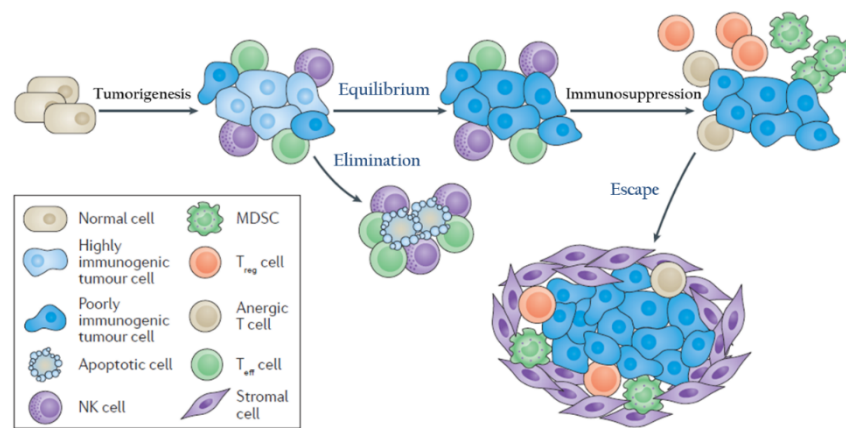


Figure 7. Phases of cancer immunoediting. Adapted from Yarchoan M. *et al.* Nat. Rev. Cancer 2017.

1.3.3. Evasion from tumor immunosurveillance

1.3.3.1. Mechanisms of the innate response: TAMs

Monocytes and macrophages are myeloid cells with high plasticity and differentiation potential towards more specialized cellular subtypes. Their polarization depends on the signals they receive. Macrophages are found at high frequencies in the TIME where they exhibit anti-inflammatory properties that favor tumor progression as well as tumor metastasis (22).

Macrophage polarization. Macrophages are mainly classified into two subtypes: the *classically activated macrophages (M1)* and *alternatively activated macrophages (M2)* (22). M1 macrophages are effective antigen presenting cells (APCs) and exhibit inflammatory properties for the elimination

TIME in B-cell lymphoid malignancies

of pathogens and tumor cells. The M1 phenotype is induced by lipopolysaccharide (LPS) from bacteria and interferon γ (IFN γ) secreted by T helper 1 (Th1) cells. M1 macrophages display a cytokine and chemokine profile, including IL-12, IL-23, tumor necrosis factor alpha (TNF α), CXCL9 and CXCL10, that attracts Th1 cells and NK cells. Also, M1 macrophages express high levels of MHC-II and the co-stimulatory molecule CD86 (22,23) (Figure 8A). On the other hand, M2 macrophages phagocytose and eliminate parasites, reduce inflammation and promote tissue remodeling. They are also able to favor tumor progression. Polarization towards M2 macrophages is induced by IL-4 and IL-13 secreted by Th2 cells. Other cytokines associated to Th2 responses, IL-33 and IL-21, have also M2 polarization properties. The M2 phenotype is characterized by high expression of mannose, galactose and the scavenger receptor CD163 as well as high IL-10, IL-1 decoy receptor and IL-1RA and low IL-12 surface expression. The M2 chemokine profile is based on the secretion of CCL17, CCL22 and CCL24 which further promotes Th2 responses (22–24) (Figure 8B) (25,26).

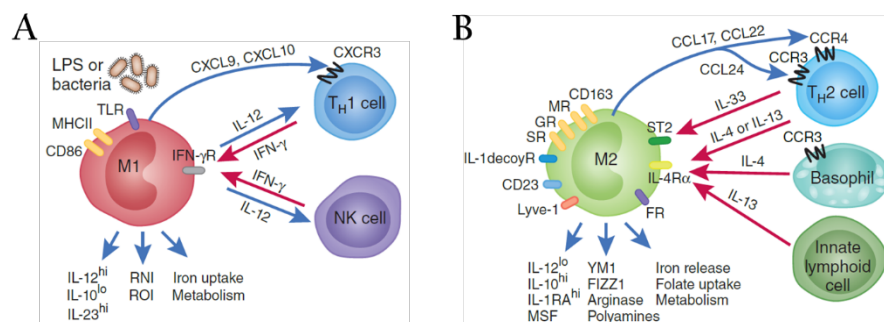


Figure 8. Macrophage polarization towards (A) M1 and (B) M2 phenotypes. From Biswas S. K. & Mantovani A. Nat. Rev. Immunol. 2010.

Tumor-associated macrophages. Macrophages are activated by the inflammatory environment that dominates early stages of tumor development. Once a tumor is formed, there is a switch towards an immunosuppressive environment. Anti-inflammatory cytokines transform Th1 responses into Th2 which, in turn, induce an M2-like polarization in macrophages. These M2-like macrophages are named *tumor-associated macrophages (TAMs)*. TAMs and Th2 cells engage in a positive-loop and attract immunosuppressive cells like *regulatory T cells (Tregs)* and *myeloid-derived suppressor cells*

(MDSCs) to the tumor site. Transforming growth factor β (TGF β) and IL-10 secreted by both tumor cells and immunosuppressive cells also favor the M2-like phenotype (high levels of CD206, CD163 and CCL18 and low HLA-DR) (22,27–29). Expression of angiogenic factors (30), classical and non-classical MHC-I molecules (31,32) and *programmed death 1* (PD-1) and *cytotoxic T-lymphocyte-associated protein 4* (CTLA-4) ligands (PD-L1, PD-L2, B7-1 and B7-2) are common pro-tumoral mechanisms in TAMs (29,33–36). Recently, PD-1 expression has also been observed in TAMs playing a similar role as the *signal regulatory protein α* (SIRP α). SIRP α inhibits phagocytosis in TAMs upon binding to CD47 in tumor cells. This enables the escape of tumor cells from macrophage-mediated phagocytosis (29,33). TAMs also secrete cytokines (IL-10, TGF β) and enzymes (nitric-oxide synthase and arginase I) with pro-tumoral effects by the inhibition of T-cell responses (30).

1.3.3.2. Mechanisms of the adaptive response: T-cell exhaustion

During the escape phase of cancer immunoediting different mechanisms impair the adaptive immune response against tumor cells such as *T-cell exhaustion*. T-cell exhaustion was first observed in chronic infections and later in tumors. It is characterized by a progressive T-cell dysfunction caused by a continuous antigen stimulation. Exhausted T cells show reduced effector functions, high expression of inhibitory receptors (IR) and a distinct transcriptional profile (37).

When CD8⁺ naïve T cells encounter its antigen during an infection, they receive co-stimulatory signals to differentiate into functional *effector CD8⁺ T cells*. Effector T cells express CD127, the *killer cell lectin-like receptor subfamily G member 1* (KLRG1) and transcription factors like *T-bet*. They also produce inflammatory cytokines (IFN γ , TNF α and IL-2) and display cytolytic potential that enable the clearance of the antigen. A subset of effector T cells remains afterwards as *memory T cells* in which the expression of CD127 is maintained and KLRG1 is lost. Memory T cells can survive without the presence of their antigen and they exhibit long-term self-renewal capacity

TIME in B-cell lymphoid malignancies

via IL-7 and IL-15 (Figure 9). Moreover, if memory T cells re-encounter its antigen they will proliferate and reactivate their effector functions rapidly (38–40). However, an antigen is not always completely cleared and it can persist for a long period of time. As a consequence, T cells lose their effector functions progressively and become dysfunctional or ‘exhausted’. T cells first lose their ability to produce IL-2 as well as their proliferative and cytolytic potential; then, they lose TNF α production and lastly, IFN γ production and the degranulation ability. At this point, T cells have acquired a severe exhausted degree and finally, they die (Figure 9) (37).

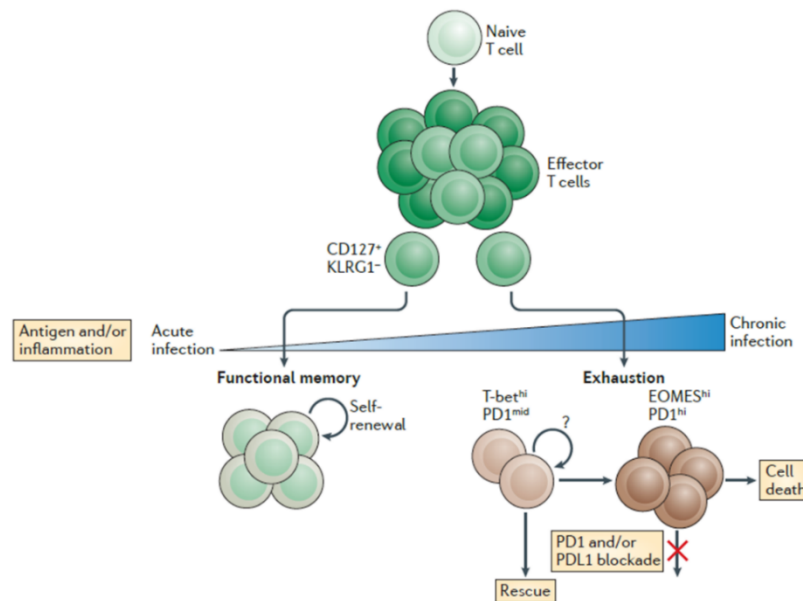


Figure 9. T-cell memory formation and T-cell exhaustion. From Wherry E.J. & Kurachi M. Nat. Rev. Immunol. 2015.

Transcriptional factors in exhausted T cells. The transcription factors T-bet and Eomes were first described as responsible for sustaining T-cell exhaustion. Paley *et al.* identified two distinct CD8⁺ T-cell exhausted subpopulations based on the differential expression of T-bet and Eomes with PD-1: the *progenitor exhausted* subpopulation (T-bet^{hi}Eomes^{dim/-}PD-1^{mid}) that conserved proliferative potential, and the *terminally exhausted* subpopulation (T-bet^{dim/-}Eomes^{hi}PD-1^{hi}) characterized by high co-expression of PD-1 and other IR and a severe dysfunction (40–42). Other transcription factors in exhausted T cells have been further identified (Table 1). Importantly, in 2019 Yao *et al.* and Khan *et al.* identified *thymocyte selection-associated HMG box (TOX)*

as the key transcription factor for the formation of exhausted T cells. As opposed to other factors that are also necessary for effector and memory T-cell differentiation, TOX is exclusive of exhausted T cells (43,44).

Transcription factor	Function
Blimp-1	<ul style="list-style-type: none"> • Encoded by PRDM1. • Control of terminal effector CD8⁺ T-cell differentiation. • Expressed in lower levels in memory CD8⁺ T cells, in high levels in effector CD8⁺ T cells and in the highest levels in exhausted CD8⁺ T cells. • Co-expressed with IR (PD-1, LAG-3, CD160 and CD244). • Blimp-1 inhibition blocks IR expression and restores CD127 expression.
T-bet	<ul style="list-style-type: none"> • Control of terminal differentiation of CD8⁺ T cells similar to Blimp-1. • Inhibition of IR in exhausted T cells.
Eomes	<ul style="list-style-type: none"> • Control of central memory T-cell formation. • Highly expressed in terminally exhausted T cells.
NFAT2	<ul style="list-style-type: none"> • Encoded by NFATc1. • Highly expressed in exhausted CD8⁺ T cells, but its translocation to the nucleus is impaired in chronic infections. • Low NFATc1 function related to low cytokine production with normal cytotoxicity. • Up-regulation of PD-1 <i>in vitro</i>.
BATF	<ul style="list-style-type: none"> • Dimer formation with c-Jun and blockade AP-1 transcription in T cells.
TCF1	<ul style="list-style-type: none"> • Encoded by TCF7. • Induction of Th2 formation and inhibition of Th1 cells by promoting the expression of GATA3 and IL-4 while limiting IFNγ in CD4⁺ T cells. • Highly expressed in certain subsets of CD8⁺ T cells during chronic infections leading to a stem-cell like phenotype with proliferative capacity. • Defines the proliferative PD1⁺CD8⁺ T-cell population after PD-1 blockade therapies.
TOX	<ul style="list-style-type: none"> • Key transcription factor for exhausted T-cell formation.

Table 1. Transcription factors involved in T-cell exhaustion. Based on Wherry E. J. & Kurachi M. Nat. Rev. Immunol. 2015; Maier E. *et al.*, J. Biol. Chem. 2011; Im S. J. *et al.*, Nat. 2016; Yao C. *et al.*, Nat. Immunol. 2019; and Khan O. *et al.*, Nat 2019.

Regulatory pathways in T-cell exhaustion. Besides persistent antigen exposure, additional negative regulatory pathways maintain T-cell exhaustion. Constant and/or high expression of IR is the main feature of exhausted T cells. IR are induced upon T-cell activation and transiently expressed in activated T cells, but their expression is maintained in exhausted T cells. PD-1 and its ligand PD-L1 are considered the main axis of T-cell inhibition during exhaustion. In addition, other relevant IR have been identified both in animal models of chronic infections and cancer and in humans including *CD244 (2B4)*, *CD160*, *LAG-3*, *TIM-3* and *CTLA-4 (37,41)*. The exposure to soluble factors and immunosuppressive cells also acts as a negative regulatory pathway in T-cell exhaustion. IL-10 and TGF β contribute to the maintenance of a dysfunctional state in T cells in chronic processes and cancer (38). Tregs are frequently abundant in chronic infections as well as in the TIME and have T-cell suppression functions (45,46). APCs, TAMs, MDSCs, NKs and some

TIME in B-cell lymphoid malignancies

subsets of regulatory CD8⁺ T cells are additional immunoregulatory cells that also contribute to T-cell dysfunction by direct contact or by the production of cytokines (37).

Exhausted T cells and response to immunotherapies. Exhausted CD8⁺ T cells are not a homogeneous pool of cells but they comprise different subsets with partial or severe exhaustion degrees mainly dependent on PD-1 expression. Immunotherapies using PD-1/PD-L1 inhibitors show effects in reversing exhaustion in CD8⁺ T cells with intermediate expression of PD-1. However, severely exhausted CD8⁺ T cells expressing higher levels of PD-1 are resistant to this type of therapy (Figure 9) (47). Studies in different types of cancers describe that subpopulations of exhausted CD8⁺ T cells can respond to immunotherapies differently so they can have predictive potential. For instance, the frequency of TCF7⁺CD8⁺ T cells in melanoma tumors is positively correlated with the clinical response to checkpoint inhibitors and survival rates (48). Progenitor tumor infiltrating lymphocytes (TILs) in melanoma also respond better to IR blockade. High ratios of progenitor TCF1⁺ cells out of PD-1⁺CD8⁺ cells are associated with increased progression-free survival (PFS) and overall survival (OS) after nivolumab (anti-PD-1) and ipilimumab (anti-CTLA-4) therapies (49,50).

1.4. Chronic lymphocytic leukemia

1.4.1. Definition and epidemiology

Chronic lymphocytic leukemia (CLL) is the most common form of adult leukemia in the US and Europe (51). In 2019, the estimated number of new cases was 20,720 which corresponded to 1.2% of all new cancer cases in the US and an estimated number of 3,930 deaths (52). Regarding its incidence, approximately 4.9 new CLL cases per 100,000 individuals are diagnosed in the US and 4.92 per 100,000 individuals in Europe. The diagnosis of CLL occurs at a median age of 70 years, being more frequent in men than in women (1.3:1 in the US and 1.5:1 in Europe) (52,53).

CLL is characterized by the clonal expansion of CD5⁺ B lymphocytes in peripheral blood (PB), BM, lymph nodes (LN) and spleen (54). CLL is a heterogeneous disease with an uncertain origin. Despite the introduction of new approaches for the management of patients in the clinical practice and approval of new therapies, CLL remains incurable (55,56).

1.4.2. Diagnosis

The diagnosis of CLL is mainly based on the assessment of the blood count and immunophenotype of the expanded B-cell population (56).

CLL requires for its diagnosis the presence of $\geq 5,000$ B clonal lymphocytes/ μL in PB maintained for at least 3 months (51,56). The number of B lymphocytes in PB allows for the differentiation of CLL from other presentations also characterized by high absolute counts of B lymphocytes without exceeding 5,000 clonal B lymphocytes/ μL in PB: *small lymphocytic lymphoma (SLL)* and *monoclonal B-cell lymphocytosis (MBL)*. SLL is the non-leukemic presentation of CLL. In SLL, malignant B cells preferentially accumulate in the LN causing lymphadenopathies (57). On the other hand, MBL is characterized by $< 5,000$ clonal B lymphocytes/ μL in PB in absence of physical manifestations (58). MBL is found in approximately 12% of healthy individuals older than 40 and it evolves to CLL/SLL at a rate of 1-2% per year due to unknown mechanisms (59,60). Since 2016, MBL is considered an independent mature B-cell lymphoid malignancy by the WHO (51).

Immunophenotyping of CLL cells determines the clonality of B lymphocytes in PB. CLL cells co-express the T-cell antigen CD5 and classical B-cell antigens (CD19, CD20 and CD23), and clones are restricted to the expression of κ or λ IgL chains. Moreover, CLL cells display lower levels of surface Ig, CD200 and CD79b than normal B cells (**Table 2**) (61–63).

Required markers	CD19, CD5, CD20, CD23, κ and λ
Recommended markers	CD43, CD79b, CD81, CD200, CD10 or RORI

Table 2. Markers for CLL diagnosis by flow cytometry. In 2018, members from the European Research Initiative in CLL (ERIC) and the European Society for Clinical Cell Analysis (ESCCA) published a consensus for required and recommended markers in order to develop a reproducible diagnostic approach among laboratories.

1.4.3. Prognosis

The median survival of patients diagnosed with CLL is approximately 10 years but its clinical course is highly variable. The vast majority of patients with CLL are diagnosed at early asymptomatic stages. Approximately half of them experience an indolent form of the disease that does not interfere with their normal life span while, within months to years, the other half will eventually progress and exhibit an aggressive leukemia needing treatment. Patients that progress have a median survival from the start of therapy to approximately 6 years (64,65). The identification at early stages of those patients that are likely to progress or *high-risk* patients is crucial for their proper follow-up and eventual treatment. In this regard, it is important to assess clinical and biological prognostic factors at diagnosis.

1.4.3.1. Clinical prognostic factors

Clinical staging systems. Two clinical staging systems are widely used in CLL: the *Rai staging system* and the *Binet staging system* (56). Both systems are based on patient's physical examinations and standard blood tests (Table 3 and Table 4).

Risk	Stage*	Description
Low	0	Lymphocytosis in PB and BM
Intermediate	I	Lymphocytosis + lymphadenopathy
	II	Lymphocytosis + hepatomegaly or splenomegaly +/- lymphadenopathy
High	III	Lymphocytosis + anemia (Hb<11 g/dL)
	IV	Lymphocytosis + thrombocytopenia (<100·10 ⁹ platelets/L)

Table 3. The modified Rai staging system. *Former Rai classification.

Risk	Stage	Description
Low	A	<3 areas affected**
Intermediate	B	>3 areas affected**
High	C	Anemia (Hb<11 g/dL) +/- thrombocytopenia (<100·10 ⁹ platelets/L)

Table 4. The Binet staging system. **Areas affected (head and neck, axillae, groins, spleen and liver) defined as the presence of enlarged nodes (>1cm in diameter) or organomegaly.

Lymphocyte doubling time (LDT). LDT is the number of months that are necessary to duplicate the absolute count of lymphocytes. If LDT is less than 12 months, the patient tends to experience an aggressive disease with shorter survival (66).

1.4.3.2. Biological prognostic factors

Serum markers. Beta-2-microglobulin (β 2m), lactate dehydrogenase (LDH), thymidine kinase (TK) and soluble CD23 have prognostic impact in CLL as their serum levels are associated with poor PFS and OS (67–70). In addition, these serum markers correlate with other relevant prognostic factors in CLL (detailed below). For instance, high levels of β 2m, LDH and soluble CD23 are associated with high expression of CD38 and *zeta-chain-associated protein 70 (ZAP-70)* in leukemic cells (71–74).

IGHV mutational status. CLL can be classified into two categories according to the presence and levels of SHM within IGHV genes. CLL patients can have *mutated IGHV genes (M-IGHV and M-CLL)* when germline identity is below 98% or *unmutated IGHV genes (U-IGHV and U-CLL)* if they show a germline identity equal to 98% or higher (75). U-CLL and M-CLL are different in terms of their clinical course and their biological characteristics. U-CLL cases have worse clinical outcome and exhibit a more aggressive disease than M-CLL cases (76,77). Moreover, there are cases with a germline identity between 97% and 98% which are considered '*borderline*'. In some series borderline cases have shown a different prognosis compared to cases with <98% identity (78). Interestingly, several studies have found that the diversity of BCRs among CLL patients is not as high as the one expected for a natural V(D)J rearrangement and CLL cells display '*stereotyped BCRs*'. This was clearly proven in a study conducted by Tobin *et al.* in 2003 that demonstrated that almost half of patients using the IGHV3-21 gene showed practically identical *heavy complementary determining regions 3 (VH CDR3)* and a restricted usage of IgL genes (79). This restriction is also observed among unrelated CLL patients with other IGHV gene usage, both in U-CLL and M-CLL cases (80–83). In 2012, an exhaustive study from Agathangelidis *et al.*

TIME in B-cell lymphoid malignancies

including almost 7,500 patients identified stereotyped BCRs in approximately 30% of patients. Also, the authors classified stereotyped BCRs into different subsets according to their specific usage of IgH genes and sequence motifs in the VH CDR3 region. Specifically, they identified 19 major subsets (20-213 sequences) in approximately 12% of patients (84). Afterwards, four out of these 19 subsets (subsets #1, #2, #4 and #8) were associated with distinct clinical outcomes. For instance, IGHV3-21 included in the subset #2 identifies CLL patients with poor OS regardless of IGHV mutational status (79,85,86). Despite this, the analysis of BCR stereotypy is not currently recommended for daily clinical practice by the iwCLL (56).

IGHV mutational status surrogates. ZAP-70 is a 70 kDa protein that belongs to the Syk family of tyrosine kinases. Its expression measured by flow cytometry has been consistently considered a reliable IGHV mutational status surrogate: patients with at least 20% of ZAP-70-positive malignant cells show absence of somatic mutations in their IGHV genes (87,88). CD38, a 45 kDa transmembrane glycoprotein important for B-cell development (89), was also proposed as a surrogate of IGHV mutational status (76). CLL patients with more than 30% of CD38-positive leukemic cells showed shorter OS (74,90). However, its implementation is still controversial since CD38 is heterogeneously expressed among CLL patients and its expression can also vary throughout the course of the disease (91,92).

CD49d (or VLA- α 4). CD49d constitutes the 150 kDa α 4 subunit of the *very-late antigen (VLA)-4*, member of the integrin family of cell adhesion proteins. CD49d is an independent predictor of progressive disease and OS in CLL patients (93–95) and the strongest flow cytometry-based predictor of OS (96). Bulian *et al.* analyzed a pool of almost 3,000 CLL patients and, after considering those patients with at least 30% of leukemic cells expressing CD49d as positive, CD49d was able to identify patients with shorter OS and treatment-free survival reliably and independently of ZAP-70 and CD38, and with greater prognostic value (96).

Chromosomal aberrations and somatic mutations. Copy-number variants (CNVs) with demonstrated prognostic impact include deletions in the long arm of chromosome 13 (*del(13q)*) and chromosome 11 (*del(11q)*), deletion in the short arm of chromosome 17 (*del(17p)*) and trisomy in chromosome 12

(*tri(12)*) (see **section 1.4.5.1**) (97). The mutational burden in CLL is very low in comparison to that observed in other lymphoid neoplasms and solid tumors (98). However, deep sequencing analysis have been able to identify genetic alterations with adverse prognostic impact and adverse predictive value to chemo-immunotherapy (CIT) such as somatic mutations in *TP53*. The analysis of *TP53* alterations must be performed at least before therapy (see **section 1.4.5.2**) (56).

1.4.4. Pathogenesis

The biology of CLL and its *cell of origin* (COO) is still a subject up for discussion. The COO of any malignancy refers to the non-malignant cell where the malignant transformation starts and, therefore, it constitutes a relevant source of information about the changes that are needed for the conversion to malignant cell. A large amount of publications have reported the B-CLL normal counterpart in mature B cells. Whether they are pre-GC, post-GC or GC-independent may depend on different factors. In addition, some studies have proposed HSCs as the COO of CLL.

Early studies pointed out normal CD5⁺ B cells as the origin of the malignant B-CLL population (99–101). These CD5⁺ B cells, also called B1 cells, are abundant at early life but their frequency decreases with age, representing the 10–25% of the B-cell population in PB in adults. Normal CD5⁺ B cells constitute a distinct B-cell lineage characterized by the production of polyreactive IgM antibodies and, as opposed to CD5⁻ B cells, by the absence of SHM in their IGHV genes which highlights their T-cell independent development (101–103). Nonetheless, CD5⁺ B cells are increased in autoimmune processes in which they do harbor mutations in the IGHV genes (104,105), as CLL cells also do, indicating that only disease-related CD5⁺ B cells might have a post-GC origin. Therefore, the GC reaction would allegedly come with higher risk of autoimmune diseases and malignant B-cell transformation.

However, subsequent studies showed that 35–40% of CLL patients also displayed UM-IGHV genes (75). In fact, as was explained in **section 1.4.3.2**, CLL patients can be divided into two different subgroups regarding the mutational status of the IGHV genes, UM-IGHV or M-IGHV (76,77). This suggests a different COO for each subset: while M-IGHV CLLs would have

TIME in B-cell lymphoid malignancies

experienced the GC reaction and would emerge from post-GC mature B cells, UM-IGHV CLLs would evolve from pre-GC naïve B cells (106). Surprisingly, gene expression analysis of M-IGHV and UM-IGHV malignant cells later showed that both subtypes shared a similar gene expression signature related to CD27⁺ antigen-experienced B cells and different from the one observed in normal CD5⁺ B cells, thereby proposing CD27⁺ memory B cells as the common COO of CLL (107,108). In these studies, normal CD5⁺ B cells used as controls were isolated from cord blood. As published later, the proportion of transitional CD27⁻ naïve B cells over mature B cells out of total CD5⁺ cells in cord blood is extremely high (109,110) which might have altered the gene expression analysis. Consequently, new gene expression studies were performed using different subpopulations of healthy B cells as controls, including naïve, mature CD5⁺ and memory B cells. After this, it was demonstrated that the B-CLL normal counterpart was different in the two subgroups: CD27⁻CD5⁺ post-GC B cells in M-IGHV and CD27⁻CD5⁺ naïve B cells in UM-IGHV (Figure 10) (111).

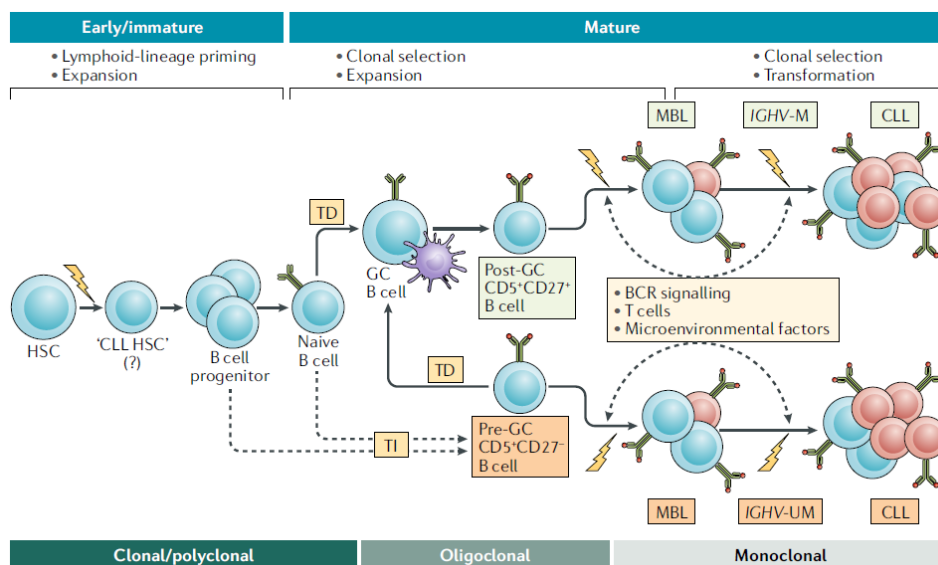


Figure 10. The COO of CLL. From Bosch F. & Dalla Favera R. Nat. Rev. Clin. Oncol. 2019.

Other studies support the theory that CLL cells arise from HSCs. Kikushige *et al.* described that the differentiation of CD34⁺CD38⁻ HSC population in the BM from CLL patients (CLL-HSCs) compared to healthy donors was skewed towards CD34⁺CD19⁺ pro-B cells with polyclonal IGHV rearrangements. In addition, mature B cells formed after xenogeneic transplantation of CLL-

HSCs showed oligoclonal and monoclonal IGHV rearrangements, indicating that a clonal selection had taken place (112). This may also suggest that genetic alterations that trigger clonal selection and the eventual malignant transformation are already present in the HSC compartment of CLL patients (Figure 10). However, considering HSCs as the COO of CLL is still controversial. Particularly, due to the complexity in obtaining pure HSCs fractions free of CLL cells (113).

Regardless of the COO, the natural history of CLL is well established. Oligoclonal B progenitors evolve to a pre-malignant state or MBL which can turn into CLL. Virtually all CLL cases are preceded by a MBL stage (section 1.4.2). The transition from MBL to CLL is apparently caused by the expansion of clones harboring driver lesions at the MBL stage since the genetic alterations that have been found in MBL are very similar to those present in CLL (114). The BCR signaling and other microenvironmental factors might also contribute to the MBL expansion and eventual CLL emergence. However, the exact mechanisms are not fully understood. Also, CLL can transform into lymphoma named *Richter's syndrome (RS)*. RS occurs in 0,5% of diagnosed CLL cases per year and gives rise to two different manifestations: DLBCL, in the vast majority of cases, or a Hodgkin lymphoma variant (51,115). As opposed to MBL, genetic studies have revealed that the malignant B-cell population responsible for RS comes from the original CLL clone that acquires additional lesions in most cases (see section 1.4.5.3) (116,117).

1.4.5. Genetic alterations

1.4.5.1. Chromosomal aberrations

Chromosomal aberrations or CNVs are the most common genetic alterations in patients diagnosed with CLL as 80% of them show at least one. In 2000, a remarkable study by Döhner *et al.* analyzed the prognostic impact of chromosomal aberrations detected by *fluorescence in situ hybridization (FISH)* using a cohort of more than 300 patients (97). Del(13q) was identified as the most prevalent CNV found in approximately 55% of patients. In addition, tri(12) was detected in 18% of patients; del(11q), in 16%; and del(17p), in 7%. Lower percentages of patients harbored

TIME in B-cell lymphoid malignancies

other alterations affecting chromosomes 3 (tri(3q)), 6 (del(6q)) and 8 (tri(8q)) and translocations on chromosome 14 (t(14q32). Importantly, del(17p) was linked to the shortest survival (median of 32 months) and treatment-free interval (median of 9 months) followed by del(11q) (median survival of 79 months and treatment-free interval of 13 months). On the other hand, patients with del(13q) as the sole abnormality showed the highest survival and treatment-free interval (median of 133 and 92 months, respectively) even beyond normal karyotype (median of 111 and 49 months, respectively) (Figure II). The same hierarchy in CNVs was identified in subsequent studies (118–121). Other studies also associated tri(12) and the absence of del(13q) with increased predisposition for RS (122,123). Additionally, *chromosome-banding analysis (CBA)* allows for the identification of patients with *complex karyotype (CK; 3 or more chromosomal aberrations)*. CK is associated with poor clinical outcomes and a limited response to chemotherapy in CLL (124,125). Nonetheless, recent studies suggest that CK should not be necessarily considered as an unfavorable feature in CLL because it actually comprises a heterogeneous group of patients with variable clinical outcomes (126,127).

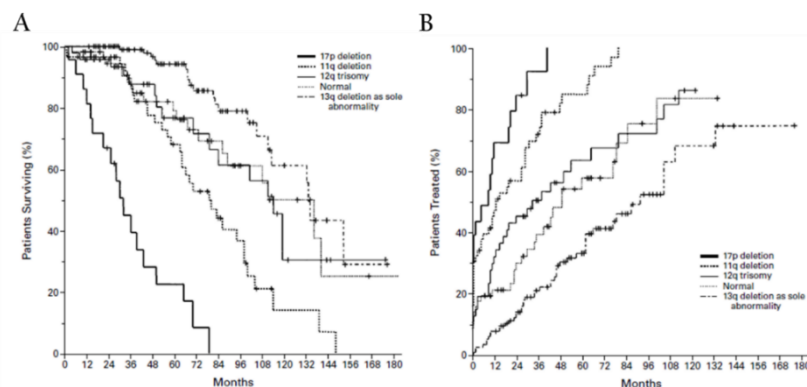


Figure II. Survival from (A) diagnosis and (B) treatment-free interval in CLL patients with del(17p), del(11q), tri(12), del(13q) or normal karyotype. From Döhner H. *et al*, NEJM 2000.

1.4.5.2. Somatic mutations

The mutational landscape of CLL has been broadly characterized during the last decade by next-generation sequencing (NGS) techniques. Approximately 0.9 mutations per megabase (including point mutations, CNVs and rare chromosomal translocations) and approximately 20

non-silent alterations per patient have been detected by whole-exome sequencing (WES) (128–131). Also, recurrent mutations with prognostic and predictive impact have been identified in CLL affecting *NOTCH1*, *TP53*, *ATM*, *BIRC3*, *SF3B1* and *MYD88* genes. Non-recurrent mutated genes in CLL include *FBXW7*, *XPO1*, *RPS15* and *POT1*. Alterations in these genes are present at very low frequencies which difficult the study of their role as prognostic or predictive markers (132–136).

NOTCH1. Mutations in *Notch homolog 1 (NOTCH1)* are the most common mutations detected at diagnosis in CLL (8–22%), mostly enriched at advanced stages (137–139). *NOTCH1* mutations in CLL include del7544_45 in 89,5% of cases and also non-coding mutations in the 3'UTR region. These alterations avoid the degradation of the intracellular *NOTCH1* (ICNI) domain by the proteasome and, therefore, genes involved in proliferation and survival are constitutively activated (140). Patients with mutated *NOTCH1* show unfavorable prognosis and frequently display tri(12), UM-IGHV genes and increased risk of RS (55,116,139).

TP53. Mutations in *TP53* are detected in 5% of early-staged CLL and their frequency arise up to 10% in advanced stages (132,137,141–143). Missense mutations in *TP53* are commonly accompanied by del(17p) in the second allele, which typically affects the entire short arm of the chromosome 17 and comprise the locus of *TP53* (142,144,145). *TP53* mutations deregulate p53 protein and consequently, impair apoptosis and cell proliferation (146). Alterations in this gene are associated with UM-IGHV, RS and shorter time to first treatment (TTFT) and OS (137,141,142,147,148). Importantly, malignant cells harboring *TP53* alterations show fitness advantage after CIT due to their resistance to DNA damage agents. This leads to an increase of *TP53* mutated clones and presence of *TP53* alterations in up to 40% of CIT-resistant patients (55,128,149,150).

ATM. Mutations in *ATM* are present in up to 14% of CLL at diagnosis (138,151,152). *ATM* acts as an upstream regulator of *TP53* and it is located in the 11q22-23 region. Almost 40% of CLL patients with del(11q) also harbor *ATM* mutations in the remaining allele (153). Alterations in

TIME in B-cell lymphoid malignancies

ATM are associated with young patients, bulky disease at diagnosis, UM-IGHV and shorter TTFT and OS (138,152,154).

BIRC3. Mutations in *baculoviral IAP repeat-containing 3 (BIRC3)* are found in 2-4% of CLL at diagnosis, being more common in advanced stages (137,138,155–157). *BIRC3* negatively regulates the *non-canonical nuclear factor- κ B (NF- κ B)* pathway which will be constitutively activated if *BIRC3* is mutated (158). This induces resistance of mutated malignant cells to chemotherapies. Moreover, patients with mutated *BIRC3* frequently show del(11q), tri(12) and U-IGHV(137,138).

SF3B1. Mutations in *splicing factor 3B subunit 1 (SF3B1)* have been detected in 5-15% of CLL and up to 21% of patients with advanced clinical stage at diagnosis (129,137,138,155,159,160). Alterations in *SF3B1* have impact in a wide range of cellular processes, from DNA damage response and telomere maintenance to Notch signaling (161). *SF3B1* mutations are associated with adverse prognostic factors, including high levels of β 2m and UM-IGHV, and are independent prognostic indicators regardless of ZAP-70 or CD38 expression (130,137).

MYD88. Mutations in *myeloid differentiation primary response gene 88 (MYD88)* are detected in 2-4% of diagnosed CLL patients (132,137,162). *MYD88* encodes for a protein involved in IL-1 and *Toll-like receptor (TLR)* pathways and pleiotropic activity in B cells (132). The vast majority of patients with alterations in *MYD88* genes are young and show good prognosis and predictive factors compared to patients with wild-type *MYD88*: M-IGHV, Binet A stage, isolated del(13q) and low levels of ZAP-70 and CD38 (132,137,162) as well as higher OS (162).

1.4.5.3. Clonal evolution

Deciphering the temporal order of genetic events can bring to light the natural history of tumors and also the interactions within the TME that contribute to tumor development. In CLL, several questions behind its natural history remain unanswered. Clonal evolution mechanisms have been explored in order to unveil what triggers the emergence of CLL from the earliest stage of MBL

and why approximately half of patients will experience clinical progression and, in some cases, lymphoma transformation.

MBL. MBL is characterized by low tumor load and a similar amount of mutated driver genes to CLL but lower when compared to ultra-stable CLLs (155,156,163). Longitudinal genetic analysis of MBLs progressing to CLL are scarce. These studies have pointed out that clonal evolution mechanisms from MBL to CLL are unlikely. In this regard, Barrio *et al.* found that CLL patients harbored alterations in the MBL stage long before the emergence of CLL (median of 41 months prior to CLL) (114). Moreover, genetic alterations considered CLL early events, such as del(13q) and tri(12q), are predominant in MBL while somatic mutations in *NOTCH1*, *TP53* and *XPO1* have lower incidence in MBL compared to CLL (114,128,156).

CLL. Longitudinal studies in CLL patients from diagnosis to the time of progression before treatment have demonstrated that the acquisition of new alterations at progression is a rare phenomenon. This indicates that, although genetic fluctuations could explain some progressing cases, clinical progression in CLL is not exclusively driven by clonal evolution. In fact, clonal evolution has also been identified in non-progressing patients at long-term follow-up (131,164–173). On the contrary, sequential genetic analysis in CLL patients at progression before and after chemotherapy have confirmed the importance of clonal selection after a therapeutic intervention. These analysis have identified that only alterations in *TP53* have clear clonal advantage after chemotherapy (128). When clonal changes over time occur, genetic alterations involved are very heterogeneous but those affecting *TP53* and chromosome 13 are the most frequent (165,167,168,171). Epigenetic changes in CLL have also been explored by longitudinal studies. Patients showing genetic evolution before or after treatment as well as patients with static disease can present higher CpG methylation over time (169,170,174). Therefore, methylation changes are neither associated with progression nor therapy.

RS. Patients with *TP53* and *NOTCH1* alterations as well as those expressing IGHV4-39 genes (subset #8) have shown higher risk of transformation to lymphoma (175). Approximately 40-50% of diagnosed CLL patients with *NOTCH1* activating mutations will potentially develop RS

TIME in B-cell lymphoid malignancies

(116,139,176,177). RS also displays higher frequencies of tri(12) compared to CLL (122) and lacks del(13q) (123). Compared to *de novo* DLBCL, RS exhibits a different genomic landscape. Lesions in *MYC*, *TP53*, *cyclin-dependent kinase inhibitor 2A (CDKN2A)* and *2B (CDKN2B)* genes are found in approximately 90% of RS and are also observed in *de novo* DLBCLs (*MYC* in 10-14% of GCB-DLBCL; *TP53* in 20% of all DLBCL and *CDKN2A/2B* in 30% of ABC-DLBCL). However, other alterations characteristic of DLBCL, such as *TNF alpha induced protein 3 (TNFAIP3)* and *BLIMP1*, are scarce in RS (116,117,178). In 2013, Fabbri *et al.* conducted a longitudinal genetic study in 9 CLL cases who experienced RS. In this study only a small proportion of genetic alterations at Richter stage were identified subclonally at early CLL stages, suggesting a clonal selection mechanism during the lymphoma transformation (116). Additional longitudinal analysis have demonstrated that RS experiences an increase in chromosomal aberrations (179) and, although it can appear in both M-IGHV and UM-IGHV CLLs, it is more likely in UM-IGHV cases. In M-IGHV cases, lymphomas could arise as secondary neoplasms (180).

1.4.6. Treatment

Early therapeutic interventions in CLL patients do not offer any benefit over interventions at CLL progression. What is more, they could induce processes of clonal selection, early toxicities or secondary malignancies. CLL patients will only be treated when they show signs of clinical progression or active disease (such as marrow failure, symptomatic splenomegaly and/or lymphadenopathy) according to the International Workshop on CLL (iwCLL) criteria (56). The assessment of IGHV mutational status, cytogenetic abnormalities by FISH and *TP53* alterations are mandatory before therapy in order to decide which regimen would be more suitable (56).

First-line treatment. The presence of alterations in *TP53* defines which first-line therapy is the most suitable in CLL patients. If a patient shows alterations in this gene, the consensus is to use the *Bruton tyrosine kinase (BTK)* inhibitor ibrutinib as first therapeutic choice. Patients with *TP53* mutations receiving ibrutinib show a PFS >30 months (181) while those receiving FCR exhibit a PFS of 18 months on average (142). If patients with *TP53* alterations are not eligible for ibrutinib

therapy due to comorbidities or interactions with other drugs, the *B-cell lymphoma 2 (BCL-2)* inhibitor venetoclax will be chosen as the best alternative (55,131,138,182). In treatment-naïve patients without *TP53* alterations, therapies are chosen according to IGHV mutational status, chromosomal alterations and patient's physical fitness and age (see **Figure 12** for details). Patients with low-risk prognostic factors (M-IGHV, del(13q) or tri(12)) can tolerate CIT (124,183–185). However, recent data from independent clinical trials have revealed that ibrutinib may have similar effects as CIT in terms of PFS in these patients (186–188). This indicates that unfit CLL patients with wild-type *TP53* could also benefit from ibrutinib which, in addition, is safer than CIT. Ibrutinib is also preferred in patients with UM-IGHV genes or del(11q) without *TP53* alterations as it leads to superior PFS than CIT (183) (**Figure 12**). IGHV mutational status has actually no effect in the response to ibrutinib therapy (186–189).

Second-line treatment in R/R CLL patients. In refractory patients, a new therapy can be administered if toxicities to first therapy, if existed, are resolved. In relapsed cases with an increase in lymphocytosis, it will be necessary that symptoms appear again to provide a second-line therapy (56). Second-line treatment for R/R patients is chosen based on three different scenarios. In the first one, a patient received CIT as first-line treatment and then progressed. Targeted therapies using ibrutinib or rituximab combined with venetoclax or with the *phosphoinositide 3-kinase δ* (*PI3K δ*) inhibitor idelalisib would be more appropriate as second-line regimes (189–191). Idelalisib is restricted as second-line therapy in patients who had already received it as front-line therapy due to toxicities and it is only administered in R/R patients after ibrutinib or venetoclax (55,192). In the second scenario, a patient does not tolerate ibrutinib and is rescued with rituximab plus venetoclax or rituximab plus idelalisib (55). And in the last scenario, a patient progressed after ibrutinib (approximately 15%). Venetoclax is used as salvage therapy in most cases since 65% of patients show a median TTP of approximately 2 years (193). Other options include idelalisib plus rituximab, clinical trials and, eventually, the consideration for cellular therapies (allo-HSCT and CAR-T cell therapy) (**Figure 12**).

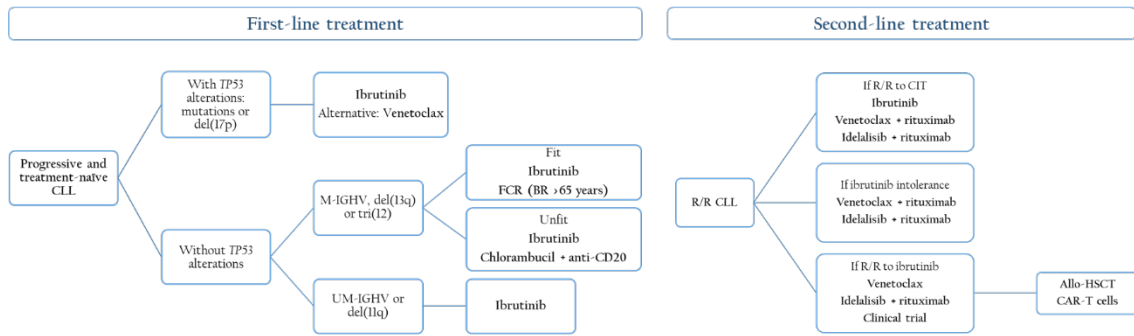


Figure 12. Algorithms for the treatment of CLL patients. FCR (fludarabine plus cyclophosphamide plus rituximab); BR (bendamustine plus rituximab); Allo-HSCT (hematopoietic stem cell transplantation); CAR-T (chimeric antigen receptor (CAR)-T cell). Based on Bosch F. & Dalla Favera R. Nat. Rev. Clin. Oncol. 2019.

1.4.7. TIME in CLL

CLL cells profoundly rely on the microenvironment for their proliferation and survival. Leukemic cells establish a bidirectional cross-talk with cellular and soluble components from the TME that provides signals for the migration of quiescent CLL cells in PB to BM and LNs as well as for the clonal expansion of CLL cells. Moreover, interactions between CLL cells and the TIME promote an immunosuppressive environment that facilitates the evasion from immunosurveillance.

1.4.7.1. Cellular components

Several cellular types have been identified in the CLL microenvironment: from non-immune cells, such as BMSCs and ECs, to immune cells, such as T cells, monocytes, NK cells and follicular dendritic cells (194). Their contribution to the development of the disease will be reviewed in this section.

Bone marrow stromal cells. BMSCs secrete CXCL12 for the homing of CLL cells to the BM (195). Upon CXCL12 binds to its receptor CXCR4, the expression of CXCR4 on the surface of CLL cells decreases. The CXCR4^{dim}CD5^{hi} subpopulation is, therefore, identified as the *proliferative compartment* of the whole CLL population, those CLL cells that just left secondary lymphoid organs (194). BMSCs induce high expression of aggressive disease-related markers in leukemic cells, such as CD38 and ZAP-70. BMSCs also induce CD20 downregulation in leukemic cells

leading to resistance to anti-CD20 therapies (196). Interestingly, it has been described that BMSCs influence on the glucose metabolism of CLL cells. CLL cells in contact with stromal cells experience an increase in glucose uptake and expression of glucose transporters and glycolytic enzymes via NOTCH-mediated c-Myc activation and this enhances drug resistance (197). On the other hand, CLL cells activate BMSCs by stimulating the expression of *protein kinase C beta II* (*PKC β II*) and the NF- κ B signaling pathway (198).

Endothelial cells. CLL cells can adhere to *microvascular endothelial cells* (MVECs) and the interactions between the *endothelin subtype A receptor* (ETAT) in MVECs and *endothelin-1* (ET-1) in CLL cells promotes proliferation and survival. Also, MVECs express β 1 and β 2 integrins, *B-cell activating factor* (BAFF) and *proliferation-inducing ligand* (APRIL) that interact with their respective receptors in leukemic cells to trigger proliferative and survival signals (199,200).

CD4⁺ T cells. Compared to healthy donors (HDs), CLL patients show higher frequencies of antigen-experienced effector and memory CD4⁺ T cells with high expression of IR, including PD-1, CD160 and TIGIT and the activation molecule HLA-DR. CD4⁺ T cells from CLL also display signs of being more activated than healthy CD4⁺ T cells as they exhibit higher expression of the proliferation marker Ki-67 (201–203). Naïve CD4⁺ T cells can differentiate into different subsets of specialized T cells depending on the stimuli they receive. Table 5 details the CD4⁺ T-cell subsets that have been investigated in CLL: *T helper (Th) cells*, including Th1, Th2 and Th17 cells, *T follicular helper (Tfh) cells* and *Tregs* (204).

Subtype	Th1	Th2	Th17	Tfh	Tregs
Stimuli	IFN γ IL-12	IL-4 IL33	TGF β IL-6, IL-23	IL-6 IL-21	TGF β
Transcription factor	T-bet	GATA3	ROR γ t	Bcl-6	FOXP3
Marker	CXCR3	CCR4	CCR6	CXCR5	CD25
Cytokines	IL-2 IFN γ TNF α	IL-4, IL-5, IL-9, IL-10, IL-13	IL-17, IL-22, IL-6	IL-4, IL-21	IL-10, TGF β

Table 5. CD4⁺ T-cell subtypes identified in CLL patients. Naïve CD4⁺ T cells differentiate into different subsets depending on stimuli. Each subtype is formed upon the activation of a distinct transcription factor and expresses different surface molecules and cytokines.

TIME in B-cell lymphoid malignancies

Absolute numbers of Th1 and Th2 subtypes in PB are higher in CLL patients compared to HDs. The production of IFN γ by Th1 cells has been associated with high levels of CD38 in CLL cells and increase proliferation ability. In this regard, the Th1 subset seems to be predominant in progressed CLL patients (205,206). Nonetheless, whether Th1 or Th2 cells are predominant in CLL is controversial. Görgün *et al.* showed that T cells from CLL have a distinct gene expression profile (GEP) compared to T cells from HDs. They found that CD4⁺ T cells exhibited downregulated genes that were related to Ras-Jnk and p38-MAPK pathways. These pathways are important for IFN γ production and Th1 differentiation. Therefore, their results suggests that CD4⁺ T cells in CLL are skewed towards a Th2 subtype (207). In addition, CLL patients show high numbers of IL-4-producing CD4⁺ T cells, and conditioned media from primary CLL cells can induce IL-4 secretion in healthy lymphocytes. This supports the idea that Th2 differentiation is preferred in CLL (208,209). However, mononuclear cells from CLL samples show increased production of IFN γ after PMA and ionomycin stimulation *in vitro* in comparison to mononuclear cells from healthy samples which is related to Th1 differentiation (203). Also, an increased accumulation of Th1-like cells compared to Th2 is found in TCL1 mice, an animal model that recapitulates the immune dysfunction observed in CLL patients (210).

Regarding Th17 cells, their numbers in CLL are higher in comparison to HDs but lower when compared to the numbers of Th1 and Th2 cells. The main cytokine produced by Th17 cells, IL-17, is also increased in plasma from CLL patients (211).

Absolute numbers of Tfh cells in PB are high in CLL. A role in CLL progression has been proposed for this subset since Tfh cells produce IL-21 which is able to induce CLL proliferation *in vitro* (212).

Tregs, a CD4⁺ T-cell subpopulation that stands out for its immunosuppressive ability, are found at higher frequencies in CLL patients compared to HDs. Tregs in CLL produce IL-10 and TGF β and express CTLA-4. Moreover, high absolute numbers of Tregs have been associated with advanced stages, unfavorable prognostic factors and shorter TTFT (213–215).

CD8⁺ T cells. The *CD8⁺* population is a central player in the adaptive immune response against tumors. Both *CD8⁺* and *CD4⁺* T cells differentiate from naïve T cells into central memory (CM) and effector memory (EM) T cells, and lastly they re-express CD45RA (EMRA). Each differentiation stage has a different phenotype based on CCR7 and CD45RA expression (Table 6) (216).

Naïve	Central Memory (CM)	Effector Memory (EM)	EM CD45RA ⁺ (EMRA)
CCR7 ⁺ CD45RA ⁺	CCR7 ⁺ CD45RA ⁻	CCR7 ⁻ CD45RA ⁻	CCR7 ⁻ CD45RA ⁺

Table 6. T-cell differentiation subsets based on CCR7 and CD45RA expression.

CLL patients at diagnosis display an accumulation of antigen-experienced effector *CD8⁺* T cells (EM and EMRA *CD8⁺* T cells) and an inversion in the CD4:CD8 ratio. Inverted CD4:CD8 ratios have been associated to shorter TTFT and PFS (203,205,217). Moreover, a distinct memory signature has been identified in *CD8⁺* T cells from CLL patients that will need therapy within 6 months after the phenotypic analysis (218). Multiple expression of IR is a key feature of *CD8⁺* T cells from diagnosed CLL patients. PD-1, CD244 and CD160 expression is higher in *CD8⁺* T cells from CLL (T-CLL) in comparison with healthy *CD8⁺* T cells. Interestingly, although *CD8⁺* T-CLL cells show increased expression of IR, they still produce inflammatory cytokines (IFN γ , TNF α and IL-2) and even in higher amounts than healthy *CD8⁺* T cells (203,219). This gives them a ‘pseudo-exhausted’ status. Another T-cell exhaustion-related feature in *CD8⁺* T-CLL cells is a defective glucose metabolism (220). In addition, defects in cytoskeleton formation, vesicle trafficking and cytotoxicity are observed in *CD8⁺* T-CLL cells. These defects were first described at the genetic level by using the GEP analysis performed by Görgün *et al.* They found deregulated genes involved in these cellular processes and identified that lower levels of granzyme B in *CD8⁺* T cells also contributed to an impaired cytolysis (207). Then, Ramsay *et al.* demonstrated that the polarization of *F-actin* and recruitment of several cytoskeletal proteins at the contact-site between T and CLL cells is impaired. This led to a defective *immunologic synapse* formation (Figure 13) (221). An effective immunologic synapse is needed for triggering effector functions in T cells.

TIME in B-cell lymphoid malignancies

As this process is impaired in CLL, leukemic cells can evade the immune T-cell response. The same authors demonstrated later that interactions between IR in T cells and their ligands in leukemic cells targeted T-cell Rho-GTPase activation and, consequently, actine polarizarion. The immunomodulatory drug lenalidomide was able to reduce the expression of IR in T cells and restore the immunologic synapse (219).

Notably, the dysfunctional status of T cells in CLL patients probably determines the low functionality of CAR-T cells derived from CLL patients (222).

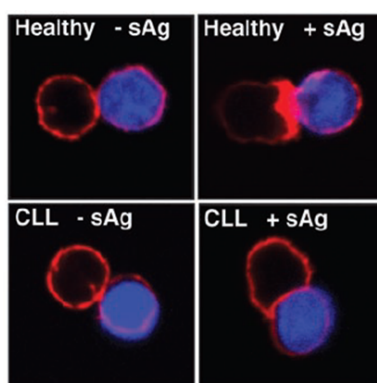


Figure 13. Defective immunologic synapse in CLL. T cells from CLL patients or healthy T cells from age-matched donors are conjugated with autologous CLL cells (blue) pulsed with or without staphylococcal antigens (sAg). F-actin polarization at the synapse site is impaired (red). From Ramsay A. G. *et al.* J. Clin. Invest. 2008.

Monocytes. In CLL, the CD14⁺ monocytic population from PB preferentially displays a classical phenotype (CD14⁺⁺CD16⁻). This is also observed in age-matched HDs. Nonetheless, TIE-2⁺ non-classical or activated monocytes (CD14⁺CD16⁺⁺) are higher in CLL patients compared to HDs, especially in those patients with high-risk FISH. Activated monocytes have inflammatory properties in HDs, but in CLL monocytes seem to be immunosuppressive: they show an altered gene expression profile that suggests defective inflammatory and phagocytic properties (223). Moreover, monocytes from CLL patients secrete CCL2 and soluble CD14 that favor survival of CLL cells by the activation of the NF- κ B pathway (224). When CD14⁺ cells are cultured with CLL cells, they develop a M2-like TAM phenotype and are named *nurse-like cells* (NLCs). NLCs are found *in vivo* in lymphoid tissues from CLL patients. They secrete BAFF and APRIL and also

express the BCR-antigens vimentin and calreticulin and the ligand of CD38, CD31. This allows NLCs to activate the BCR signaling and NF- κ B pathway in leukemic cells. In addition, they also favor CLL migration to the LNs by secreting CXCL12 and CXCL13 (198).

A population of immunosuppressive CD14⁺ cells named MDSCs is found at higher frequencies in PB from CLL patients compared to HDs. These cells, defined as CD14⁺HLA-DR1^o, suppress effector T-cell properties and attract other immunosuppressive cells. MDSCs in CLL inhibit T-cell activation and induce a regulatory T-cell phenotype *in vitro* mainly by the secretion of *indoleamine 2,3-dioxygenase (IDO)*, an enzyme that degrades tryptophan. When tryptophan levels are low, T cells enter in cell cycle arrest and anergy. Higher percentages of circulating MDSCs have been correlated with advanced disease stages and higher levels of CD38 and ZAP-70 (225,226).

Natural killer cells. Absolute numbers of NK cells in CLL patients are increased when compared to HDs. However, NK-cell numbers are highly variable among diagnosed patients. At progression, NK cells seem stable (227,228). The low expression of NKp30 and NKG2D in NK cells from CLL patients might cause a defective NK-mediated cytotoxicity. It has been described that BAFF secretion contributes to CLL drug-resistance and it also interferes in NK-mediated lysis after rituximab therapy (227,229).

Follicular dendritic cells. FDCs are cells with mesenchymal origin found in the primary follicles and GC. In CLL, they play a role in the correct localization of CLL cells within the lymphoid follicles via CXCR5-CXCL13 and lymphotoxin $\alpha\beta$ (LT $\alpha\beta$) signaling pathway (230).

1.4.7.2. Soluble components

Cytokines, chemokines and angiogenic factors are secreted by immune and non-immune cells from the microenvironment of CLL. Chemokines (CXCL12, CXCL13, CCL17, CCL22) and angiogenic factors (VEGF, neutrophilin-1, β FGF, PDGF) mediate in CLL homing towards secondary lymphoid organs and in the maintenance of BM architecture and homeostasis,

TIME in B-cell lymphoid malignancies

respectively. Cytokines (IL-10, TGF β , IFN γ , TNF α , IL-2, IL-21, IL-6, IL-8, IL-17) are important to establish and maintain the immunosuppressive microenvironment.

CLL cells also release soluble factors. CCL3 and CCL4 are secreted by CLL cells in response to BCR stimulation as well as in co-cultures with NLCs. Higher serum levels of CCL3 and CCL4 are also found in patients and are associated with unfavorable clinical outcomes. CLL cells also secrete CCL17 and CCL22 upon CD40 activation and this can attract T cells (198). In addition, CLL cells exhibit features of *regulatory B cells* and are able to secrete IL-10. This regulatory B-cell properties are also enhanced via CD40 (231,232).

1.4.7.3. BCR signaling pathway

Interactions between CLL cells and cells from the microenvironment, especially those with T cells and NLCs, trigger the activation of signaling pathways for leukemia proliferation and survival. This includes BCR and Notch signaling as well as inflammatory pathways through TLR and IL-1R activation.

The BCR is the central player in the pathogenesis of CLL (**section 1.4.4**). All BCR downstream signaling components are intact in terms of somatic mutations in both U-CLL and M-CLL cells. However, interactions between the BCR and the antigen in U-CLL cells compared to M-CLL cells might be different in terms of the intensity and quantity of the signal. U-CLL cells likely experience higher BCR signaling than M-CLL cells which leads to poorer outcomes and an aggressive disease in U-CLL patients (76,77). In this sense, U-CLL cells usually express higher levels of surface IgM compared to M-CLL cells and also have lower affinity for antigens (233).

During selection and clonal expansion of malignant B cells an antigenic selection process may take place as it is suggested by the BCR stereotypy observed among patients (see **section 1.4.3.2**) (81,82). Moreover, CLL cells display a constitutive activation of the BCR. This activation may occur through an antigen-dependent mechanism and several autoantigens have been identified (calreticulin, vimentin, LPS and DNA). However, it has been described that CDR3 regions are also able to induce an antigen-independent cell-autonomous BCR signaling (234). Therefore,

whether the BCR activation in CLL cells is antigen-dependent or not is not clear. In any case, the activation of the BCR leads to the formation of clusters involving the BCR molecule and CD19, CD20 and CXCR4 on the surface of CLL cells as well as LYN in the cytoplasm. Then, the signal activates the ITAM domains in the cytoplasmic tail of the *BCR complex-associated molecules CD79A* and *CD79B* and, consequently, downstream kinase proteins are activated, including SYK, BTK, PI3K and *phospholipase C gamma 2 (PLC γ 2)*. The signaling is further amplified downstream leading to calcium mobilization and activation of PKC and, then, ERK as well as NF- κ B. This favors proliferation and survival in CLL cells and induce secretion of CCL3 and CCL4. In addition, signals from chemokine receptors and integrins for the migration of leukemic cells to secondary lymphoid organs also involve SYK, BTK and PI3K proteins as well as ZAP-70 when expressed in CLL cells (Figure 14) (235).

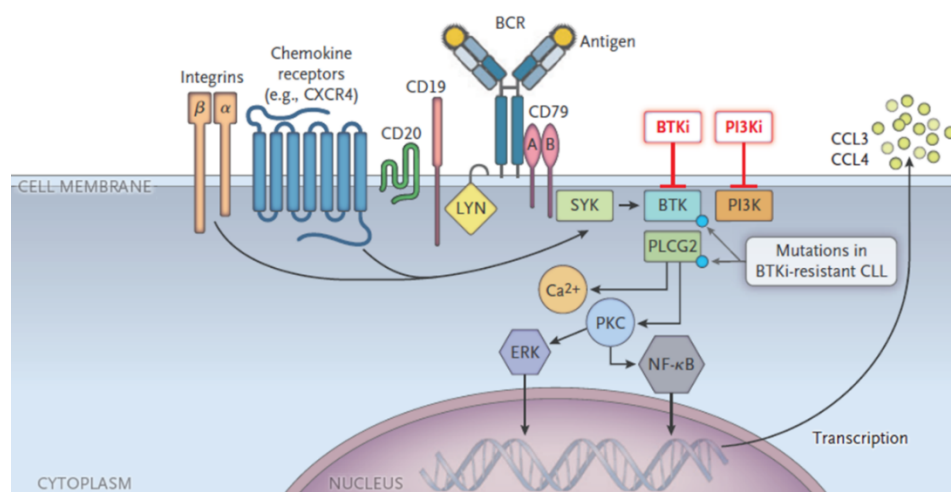


Figure 14. BCR signaling pathway. From Burger J. A. NEJM 2020.

Targeting the BCR signaling pathway has transformed the treatment of CLL and targeted BCR therapies have been approved since 2010. The most effective are BTK (ibrutinib and acalabrutinib) and PI3K inhibitors (idelalisib and duvelisib) (235). Interestingly, acquired BTK mutations are observed in relapsed patients after ibrutinib and acalabrutinib therapies. Activating mutations in *PLC γ 2* are also associated with resistance to ibrutinib (236,237).

1.4.7.4. TIME during CLL progression

Despite the great advances that have been made in understanding the biology of CLL over the last decade, the underlying mechanisms that drive clinical progression from early stages are still not fully understood. Within months to years, approximately half of them will progress to advanced clinical stages needing treatment, while the other half will remain stable. A myriad of prognostic factors have been used to identify those patients who are likely to progress from early stages (see section 1.4.3). In addition, longitudinal studies performed at the time of diagnosis and progression before treatment show that only a small proportion of patients experience genetic changes over time and that *de novo* acquisition of molecular alterations is a rare phenomenon (section 1.4.5.3). Changes in the gene expression profile of leukemic cells are also infrequent at progression (166). These findings point out that CLL progression from early stages is not mainly driven by genetic evolution and highlight the role of the leukemic microenvironment in the evolution of the disease. The growth of CLL cells is facilitated by the evasion from immunosurveillance (Figure 15), although the exact mechanisms leading to CLL progression are unknown.

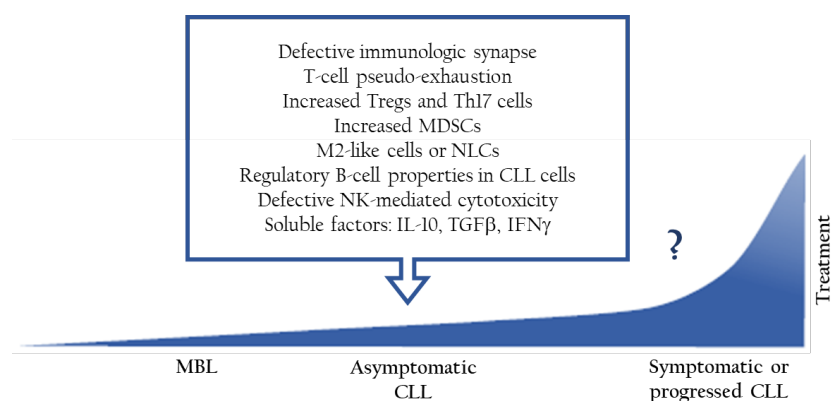


Figure 15. Clinical course and immune evasion mechanism in CLL. Based on Purroy N. & Wu. C. J. Cold Spring Harb. Perspect. Med. 2017.

Focusing on T cells, their role in CLL progression is not completely clear. Some studies indicate that T cells could have a pro-tumoral role but others performed in mouse models suggest that T cells could control the leukemia.

In vitro cultures of primary CLL cells and *in vivo* experiments in mouse models suggest that the main function of CD4⁺ T cells is pro-tumoral. CLL cells cultured with CD4⁺ T-cell-derived cytokines, such as IFN γ , IL-4 and IL-21 (238–240), or co-cultured with autologous CD4⁺ T cells after depletion of PD-1 or TIGIT, or both, show decreased survival *in vitro*. The capacity of TIGIT⁺CD4⁺ T cells to produce IFN γ and IL-10 may explain such effect (202). In addition, lower numbers of CD4⁺ T cells are associated with increased PFS (241). On the other hand, studies using the TCL1 mouse model have identified anti-tumoral properties in CD4⁺ T cells. CD4⁺ T cells are able to control CLL progression since TCL1 adoptive transfer into mice lacking CD4⁺ T cells leads to increased CLL formation. However, no changes are found when adoptive transfer is performed in wild-type mice after CD4⁺ T-cell depletion using specific antibodies (242,243). Whether CD8⁺ T cells facilitate or delay the disease is not clear. Although the *pseudo-exhausted* status in CD8⁺ T cells from CLL patients indicates that they might have a pro-tumoral role, studies of TCL1 adoptive transfer have reported a delay in the development of CLL when CD8⁺ T cells were present (243). Also, TCR analysis in this model indicate an enrichment in clonally expanded CD8⁺ T cells that is also observed in T cells from CLL patients (243,244). This suggests that the accumulation of CD8⁺ T cells in CLL might be caused by an antigenic selection. In summary, the expanded CD8⁺ T cells could recognize CLL cells but they fail in controlling the leukemia as a consequence of pseudo-exhaustion. As opposed to this, at least in TCL1 mice CD8⁺ T cells are still able to control the disease.

Therapies aimed at reversing the immunosuppressed state and activating T cells have shown interesting results in mouse models (245,246), but a better understanding is needed to translate these approaches to humans. In addition, the lack of immune parameters that can be monitored over time beyond the gradual increase in whole blood count hampers catching progression in advance and testing early therapeutic interventions on the immune system to prevent or delay progression.

1.5. Primary central nervous system lymphoma

1.5.1. Definition and epidemiology

Primary central nervous system lymphoma (PCNSL) is an aggressive and rare form of extranodal non-Hodgkin lymphoma (NHL). PCNSL accounts for up to 1% of all lymphomas, 4% of intracranial neoplasms and 4-6% of extranodal lymphomas (247). In 2019, the estimated number of new cases was 1,500 in the US with an incidence of approximately 0,5 new cases per 100,000 individuals (248). In immunocompetent patients, PCNSL is diagnosed at a median age of 55 years, being more frequent in males than in females (2:1). However, approximately 6-20% of diagnosed patients are infected with HIV, in whom the median age of diagnosis is lower (35 years) and 95% are males. PCNSL is also frequently found with other immunodeficiencies with low CD4⁺ T-cell counts (<50 cells/mL) cells and *Epstein-Barr virus (EBV)* infection (249).

PCNSL is confined to the *central nervous system (CNS)* including brain, eyes, leptomeninges and spinal cord. Approximately 90% of PCNSL are classified as *diffuse large B-cell lymphoma (DLBCL)* according to their histology (250) but their prognosis is much worse than extracerebral DLBCL (251). Survival rates of patients diagnosed with PCNSL are usually inferior to other types of lymphomas. Therefore, managing patients is challenging, and the exploration of new therapeutic approaches is of great necessity. In addition, CNS infiltration can occur concomitantly or recurrently in systemic lymphomas and are called *secondary CNS lymphomas (SCNSLs)*. Up to 5% of patients with DLBCL and 30% of Burkitt's lymphomas exhibit CNS infiltration (252).

1.5.2. Diagnosis

The diagnosis of PCNSL is mainly based on imaging techniques for determining the localization and extension of the malignancy as well as histopathology techniques for confirming the lymphoma diagnosis and discarding other brain diseases (249).

For an optimal image of the brain parenchyma, gadolinium-enhanced *magnetic resonance imaging* (MRI) scan is recommended (Figure 16). In those patients in whom MRI is contraindicated, a contrast-enhanced *computed tomography* (CT) can be performed (253).

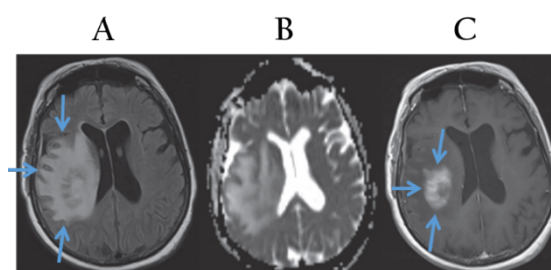


Figure 16. MRI scan from a patient with PCNSL. (A) Lesion is located in the right temporal lobe indicated by arrows. (B) The lesion displays reduced diffusion coefficient compared to surrounding areas. (C) Tumor with intense contrast enhancement in a gadolinium MRI image. From Korfel A. & Schlegel U. Nat. Rev. Neurol. 2013.

Once the lesion has been located, a stereotactic needle biopsy is needed to confirm the diagnosis of PCNSL by histopathology. This procedure is essential because there are other pathologies affecting the CNS (multiple sclerosis, sarcoidosis and some gliomas) that display a similar magnetic resonance image as the one from PCNSL. When possible, *cerebro-spinal fluid* (CSF) should be obtained by lumbar puncture before or at least one week after biopsy in all patients. This enables to perform cytology, protein analysis and, especially, flow cytometry which is more sensitive (254). In addition, the analysis of circulating DNA in the CSF can help monitor CNS lymphoma patients more precisely than the same analysis using plasma and flow cytometry (255).

1.5.3. Prognosis

A physical and neurological examination should be performed in newly diagnosed cases. Two clinical scoring systems are accepted for the evaluation of PCNSL patients: the *International Extranodal Lymphoma Study Group* (IELSG) score (Table 7A) and the *Memorial Sloan Kettering Cancer Center* (MSKCC) score (Table 7B) (256,257). Both allow for the classification of patients in three

TIME in B-cell lymphoid malignancies

different groups of risk: low, intermediate and high risk, with a median OS of 8,5, 3,2 and 1,1 years, respectively (257).

A			B			
Risk	Score	Parameter	Favorable (+0)	Unfavorable (+1)	Risk	Description
Low	0-1	Age	<60 years	>60 years	Low	<50 years
Intermediate	2-3	PS	0-1	>1	Intermediate	≥50 years KPS ≥70
		LDH	Normal	Elevated		
High	4-5	Deep brain involvement*	No	Yes	High	≥50 years KPS <70

Table 7. Clinical scoring systems in PCNSL. (A) The IELSG and (B) the MSKCC scoring system. *Periventricular regions, basal ganglia, brainstem and/or cerebellum.

Some biological prognostic factors have been identified in PCNSL. LDH has independent prognostic value in PCNSL and serum levels must be determined in all patients at diagnosis. High LDH concentrations are associated with poor survival (256). Also, high levels of IL-10 and CXCL13 in CSF are related to poor PFS and OS rates (258,259).

1.5.4. Pathogenesis

The vast majority of PCNSLs are histologically classified as DLBCLs (>90%) while the remaining can be classified as Burkitt's lymphomas, low-grade lymphomas or both peripheral and anaplastic T-cell lymphomas (250,260).

The expression of *BCL-6*, the main regulator of the GC reaction, in approximately 60-80% of PCNSLs indicates that the COO in PCNSL is likely situated in a *post-GC B-cell* (261). *BCL-6* is overexpressed in PCNSL patients and has been associated with good prognosis in some studies: *BCL6*-positive patients showed better PFS than *BCL-6*-negative patients (median PFS of 20.5 vs 10.1 months) (262) as well as higher OS (median OS of 101 vs 14.7 months) (263). On the contrary, in shorter retrospective studies, *BCL-6* expression was related to reduced PFS (264). Hypermutation frequencies in Ig genes from B cells in PCNSLs are higher than in Ig genes from other DLBCL types and show a preferential usage of the V4-34 gene segment which suggests an autoantigen stimulation (265,266). The expression of memory B cell-related genes rather than

GC B cell-genes is also higher in PCNSL (261). These findings point out that malignant B cells in PCNSL are ready to leave the GC. However, *BCL-6* in PCNSL is simultaneously expressed with the plasma cell differentiation factor *IRF4* and, in addition, malignant cells show surface expression of IgM with absence of plasma cell markers, such as CD38 and CD138. This indicates that further B-cell differentiation is altered and PCNSL B cells are arrested in terminal B-cell differentiation. Thus, malignant cells from PCNSLs correspond to *late GC-exit B cells* (267).

What is not clear is whether the disease arises from a B-cell resident in the CNS or outside the brain. B cells can be recruited to the brain as part of an immune response and they could experiment a malignant transformation and eventually form lymphoma in the brain. On the contrary, B cells could also experiment the malignant transformation outside the brain and then migrate towards the CNS. There, the immune control is limited which may favor the growth of the disease. Nonetheless, no chemokine or adhesion molecule that selectively favors B-cell migration to the brain has been identified to date (see **section 1.5.6.2**). Therefore, this second possibility would be less plausible (267).

1.5.5. Genetic alterations

Genetic alterations have a profound impact on PCNSL development, especially translocations affecting IgH genes or the *BCL-6* gene loci (268). As discussed below, hypermutation rates in proto-oncogenes as well as somatic mutations in genes related to proliferation, survival and regulatory pathways are also high in PCNSL.

GC arrest. A study conducted by Pasqualucci *et al.* in 2001 proved that SHM mechanisms are aberrant in DLBCL. More than half of systemic DLBCL tumors analyzed (28 in total) presented SHM affecting the proto-oncogenes *PIMI*, *c-MYC*, *RhoH/TTF* and *PAX5*, while this was not detected in non-GC B cells or in other types of GC-derived lymphomas (269). However, *aberrant SHM (aSHM)* in these proto-oncogenes is found in almost all PCNSLs with a mutational frequency 2 to 5-fold times higher than in systemic DLBCLs (265), likely contributing to tumorigenesis. Moreover, translocations in *BCL-6*, alone or combined with *del(6)(q22)*, are present in 17% to

TIME in B-cell lymphoid malignancies

47% of PCNSL patients and are related to poor OS (268,270,271). *PRDMI*, a gene transactivated by *IRF4* and encoding *BLIMP1*, shows mutations due to aSHM and deletions in the 6q21 region in 19-21% and 53% of PCNSLs, respectively (272,273), leading to *BLIMP1* protein loss and plasma cell differentiation blockade. The constitutive activation of *BCL-6* and loss of *BLIMP1* lead to the arrest of malignant B cells in PCNSL in a GC stage.

Constitutive activation of the NF- κ B pathway. Alterations in genes involved in the BCR and TLR signaling pathways constitutively activate the NF- κ B pathway in PCNSL. Mutations in *CD79B* and *SHIP* are the most frequent (20%) and can lead to increased expression of surface BCR and chronic BCR stimulation (274). In addition, the most recurrent chromosomal alteration in PCNSL is gain of 18q21 (37%) and involves *MALT1*. *MALT1*, together with *CARD11* and *BCL-10*, form the *CBM signalosome complex* which receives signals from the BCR and ultimately activates the NF- κ B pathway. Activating mutations in *CARD11* have been also detected in PCNSL patients (16%) (268,271,273). The TLR signaling pathway is altered in PCNSL mainly due to *MYD88* mutations which are found in 36 to 50% of patients (274-276).

Immune evasion. Chromosomal aberrations, copy gains or translocations involving the 9q24.1 region which includes PD-1 ligands (*PD-L1* and *PD-L2*) loci are common in PCNSLs (67% CNs of *PD-L1* and 52% CNs of *PD-L2*) (277,278). Loss or downregulation of *major histocompatibility complex (MHC)-II* molecules is a key mechanism of immune evasion in lymphomas. In PCNSL, the expression MHC-II on the surface of malignant cells is lost at higher rates. This can be explained by the presence of genetic alterations directly affecting MHC-II genes. The 6p21.32 region, which involves genes encoding for MHC-II molecules, is affected by partial or total losses or partial disomies in 73% of PCNSLs (267,279,280).

Proliferation and cell adhesion. These cellular properties are affected in PCNSL due to losses in 9p21 (71%; involving *CDKN2A* loci), gains in 12q (71%) (249,281) and deletions in 6q (66%; leading to *PTPRK* inhibition, a tyrosine phosphatase involved in cell adhesion) (281).

1.5.6. Treatment

In PCNSL systemic chemotherapy is the standard of care. It can be followed by brain radiotherapy or intrathecal chemotherapy while surgical interventions are generally limited to stereotactic biopsy.

First-line treatment. MTX is the most effective chemotherapeutic option for the treatment of PCNSL. It acts as a folate analog and avoids *de novo* synthesis of purines by the inhibition of the enzyme dihydrofolate reductase. First-line therapy of newly diagnosed patients consists of high doses of methotrexate (HD-MTX), being 3g/m² the most frequent dosing and effective in crossing the *blood-brain barrier (BBB)* (249). HD-MTX is usually administered with rituximab and other chemotherapeutic compounds able to cross the BBB. Rituximab administered with MTX, procarbazine and vincristine (R-MPV) with whole-brain radiotherapy (WBRT) or cytarabine as consolidation therapy has shown higher response rates and disease control as well as lower toxicity (60% of patients with CR; median PFS and OS of 7,7 and 6,6 years, respectively) (282). Naïve-treatment PCNSL patients receiving MTX-cytarabine plus rituximab and thiotepa (MATRix regimen) have shown CR in 49% of cases vs. 23% of patients receiving only MTX-cytarabine and 30% of patients treated with MTX-cytarabine plus rituximab (283). WBRT as first-line treatment in PCNSL does not offer benefits over chemotherapy and it leads to poor survival and increase relapse rates alongside neurotoxicity (284,285). In general, surgery has also low efficacy due to the infiltrating and diffuse growing pattern of PCNSL which difficults a complete tumor resection. Other options in the treatment of PCNSL include *autologous stem cell transplant (ASCT)*. ASCT has shown good results, even in large cohorts, with 5-year OS in 79% of patients (286). However, it has no clear benefits as consolidation therapy in patients with CR after chemotherapy (287).

Second-line treatment in R/R PCNSL patients. Approximately half of patients who responded to first-line treatment will relapse in a median time of 10-18 months. In addition, one-third of PCNSLs are primary refractory. In these cases the prognosis is very poor (median survival of 2 months)

TIME in B-cell lymphoid malignancies

unless a second-line treatment is provided (288,289). Effective second-line choices consist of additional HD-MTX therapy, which leads to CR in 73-75% of patients and a median OS of 41-62 months (290,291), or intense chemotherapy followed by ASCT with 2-year OS in 69% (286). Targeted therapies using ibrutinib and immunotherapies based on pomalidomide have also been considered to treat R/R PCNSL patients. Ibrutinib has shown good brain penetrance and effectiveness but brief responses (see section 1.5.6.3) (292,293) while pomalidomide has shown moderate results (CR in 24% of patients treated with pomalidomide-dexamethasone) (294). Moreover, due to the importance of PD-1/PD-L1 evasion mechanisms in PCNSL, nivolumab was also tested in a small group of 4 R/R PCNSL patients who showed activity (295).

1.5.7. TIME in PCNSL

PCNSL is confined to the CNS which is considered an *immunoprivileged site* thanks to the tight regulation that the BBB exerts. The BBB is responsible for the homeostasis of the CNS. It allows for an efficient and bidirectional transport between the CNS and circulation, the efflux of toxic cellular byproducts and the influx of molecules from circulation to the brain. When a neuroinflammatory process occurs, some immune cells are able to cross the BBB. Importantly, tumors affecting the CNS can impair the integrity of the BBB to make it more permeable to molecules and cells that would not be able to cross it under normal conditions (296).

1.5.7.1. Cellular components

Analysis of tumor-infiltrating immune cells, mainly by immunohistochemistry (IHC), show that tumor cells from PCNSL are accompanied by T cells and macrophages. Although studies focused on the TIME in PCNSL are still limited they have revealed that immune infiltrations can have prognostic value and specific localizations as well as an immune heterogeneity among patients.

CD4⁺ T cells. CD4⁺ T cells are scarce in PCNSL. Both Tregs, defined as CD4⁺FoxP3⁺, and Tfh cells, CD4⁺PD-1⁺, are also very rare. When present, CD4⁺ T cells are localized in the perivascular area while Tregs and Tfh cells localize in the central tumor areas (297). T cells expressing CXCL13

have been identified in PCNSL as well as CXCL13⁺ tumor cells similar to late GC B cells which attract Tfh cells. In addition, malignant cells and 10% of TILs in PCNSLs express *IRF4* which is involved in Th2 and Th17 differentiation and is upregulated in late GC B cells (298).

CD8⁺ T cells. Infiltrates of CD8⁺ T cells in PCNSL usually accumulate in the perivascular areas (297,298) and show granzyme B and Ki-67 positive stainings. This indicates that these CD8⁺ T cells have cytotoxic capacity and proliferative *in situ* (Figure 17). Nonetheless, these abilities are restricted to certain CD8⁺ T cells as not all of them expressed these markers in the study that Venetz *et al.* conducted (56% CD8⁺GrzB⁺ and 15% CD8⁺Ki-67⁺) (298). Localization of TILs in the perivascular areas is fostered by CXCL9 secreted by pericytes and perivascular macrophages. CXCL12, a chemokine that favors migration of CD8⁺ T cells and malignant cells, has been found to be co-expressed with CXCL9 in the tumor vasculature of PCNSL (298).

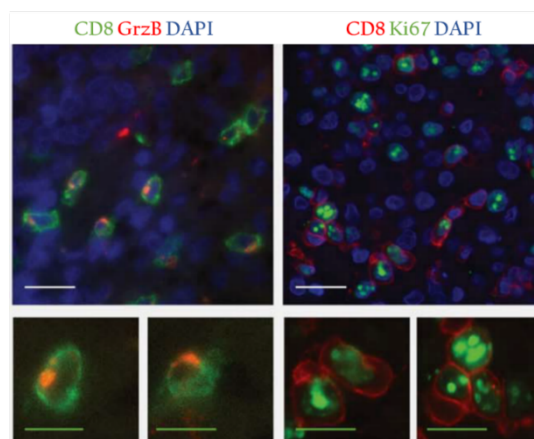


Figure 17. CD8⁺ TILs from PCNSL expressing granzyme B (GrzB) and Ki-67. Scale bars: 20 μ m and 10 μ m in upper and lower panels, respectively. From Venetz D. *et al.*, Int. J. Cancer 2010.

Compared to DLBCLs, PCNSLs at diagnosis show less infiltrates of effector CD45RO⁺ T cells and lower levels of cytotoxic T cells with less granzyme expression (Figure 18) (299). Therefore, PCNSL have lower immunogenicity in comparison to DLBCL and this could lead to poorer OS rates. Moreover, lymphoma cells from PCNSL show less HLA-DR expression than malignant cells from DLBCL (Figure 18) (299). Loss or downregulation of MHC-II genes, such as HLA-DR, is associated with less infiltrates of CD8⁺ TILs and poor survival in DLBCL (300). However, a

TIME in B-cell lymphoid malignancies

study that compared different types of lymphomas found higher levels of cytotoxic T cells in aggressive lymphomas developed in immunocompromised locations (this included PCNSL and peripheral testicular lymphoma) in comparison to nodal, skin and stomach lymphomas (301). This indicates that the role of cytotoxic lymphocytes in PCNSL is not clear. Interestingly, a recent study suggests that the relationship between CD8⁺ T cells and patients' survival could depend on corticosteroid therapies prior to biopsy. In this study, Marcelis *et al.* observed that higher levels of CD8⁺ T cells at any location were associated with superior OS rates. However, if patients who received corticosteroids were excluded from the analysis only low CD8⁺ T-cell counts within the tumor could predict poor OS (297).

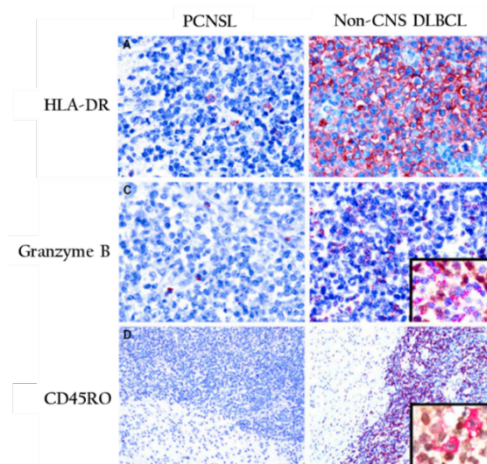


Figure 18. (A) HLA-DR, (C) granzyme B and (D) CD45RO in immune infiltrations in PCNSL and non-CNS DLBCL. From Chang C. *et al.* Histopathology 2015.

Macrophages. Based on CD68 and CD163 expression, both M1 (CD68⁺CD163^{lo}) and M2 (CD68⁺CD163^{hi}) TAMs are present in PCNSL. CD163⁺ cells seem to accumulate within the tumor area preferentially (297). Moreover, higher levels of CD68⁺ TAMs were associated with poor PFS in patients that received MTX and radiotherapy, and a similar association was observed with CD163⁺ TAMs. However, no associations with OS were found. The presence of cells with double staining for CD68 or CD163 and IL-10 points out that TAMs in PCNSL produce this cytokine. In addition, levels of IL-10 in CSF correlate with CD68⁺ and CD163⁺ TAMs (302).

Expression of immune check-points. Tumor cells, TILs and TAMs express PD-1 and/or its ligand PD-L1 in the vast majority of PCNSLs (90%). By IHC techniques, Berghoff *et al.* analyzed 20 biopsies from PCNSL patients and found that 60% of them displayed PD-1-positive TILs both intratumor and peritumor. The expression of PD-L1 in TAMs was less frequent (20% of patients) as well as PD-1 and PD-L1 in tumor cells (20% and 10%, respectively; **Figure 19**). It should be noted that specific markers for B cells, macrophages or T cells were not included. Therefore, cells expressing PD-1 and PD-L1 were highly dependent on the pathologist examination (303).

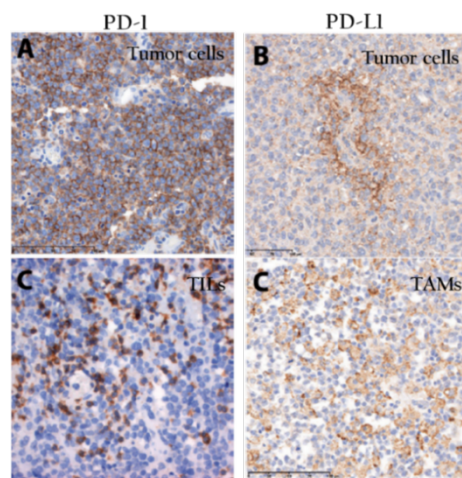


Figure 19. PD-1 and PD-L1 expression by IHC in PCNSL. (A, left) PD-1 expression in PCNSL tumor cells and (C, left) TILs. (B, right) PD-L1 expression in perivascular PCNSL tumor cells and (C, right) TAMs. Magnification of 400x for all images. Based on Berghoff A. S. *et al.* Clin. Neuropathol. 2013.

A recent study conducted by Ou *et al.* found that PD-1 is also more abundant than PD-L1. However, they detected higher proportions than Berghoff *et al.* Up to 86% of patients showed PD-1 expression while high and intermediate PD-L1 expression were found in 37% and 29% of PCNSLs, respectively. In addition, 33% of patients did not display PD-L1, and there was no relationship between PD-1 and PD-L1 levels (304).

1.5.7.2. Soluble components

Chemokines and cytokines are important for the localization of malignant and immune cells within the brain and some of them have also prognostic impact. Their role in immune evasion mechanisms in PCNSL needs to be further studied.

TIME in B-cell lymphoid malignancies

Chemokines. Tumor cells express CXCR4 and CXCR5 as well as their ligands CXCL12 and CXCL13 and they also express CCR7. CXCL12 and CXCL13 are secreted by ECs while astrocytes and microglial cells secrete CXCL12 and express CCR5 and CCR6. Interactions between these chemokines and their receptors in tumor cells and brain resident cells could be essential for the recruitment of B cells to the CNS and their dissemination (271). CXCL9 and CXCL12 contribute to CD8⁺ TILs localization in the brain (see section 1.5.6.1). Moreover, levels of CXCL13 in CSF have shown prognostic value, stronger if combined with IL-10 (259,298).

Cytokines. Tumor cells and M2 TAMs in PCNSL might produce IL-10 according to IHC analysis (258,302). The presence of increased levels of this cytokine in CSF has demonstrated prognostic impact since patients with low IL-10 show better PFS and OS rates (258,259). After chemotherapy, IL-10 in CSF decreases, and it rises again at relapse in most patients (258). *In vitro* studies using PCNSL-derived cell lines have demonstrated that tumor cells secrete soluble factors that induce high levels of PD-L1 and IDO mRNAs in differentiated human macrophages as well as IL-6, IL-1 β , VEGF, TNF α and PD-L2, but not IL-10, TGF β or HLA-G (305).

Other soluble factors. Analysis of serum samples from PCNSL patients confirm the presence of higher levels of soluble PD-L1 in comparison to HDs. Increase PD-L1 serum levels have been associated with shorter PFS and OS rates. Moreover, patients with the highest levels of soluble PD-L1 display higher frequencies of relapse after HD-MTX (78%). On the other hand, in patients with low levels of soluble PD-L1 the frequency of relapse decreases to 50% (306).

1.5.7.3. BCR and NF- κ B signaling pathways

PCNSL cells rely heavily on NF- κ B signaling for survival and proliferation. The transcriptional activation of NF- κ B is regulated by the MYD88/IRAK complex and the BCR signaling pathway as well as by PIM kinases, PI3K/mTOR and JAK/STAT pathways (Figure 20). The activation of these pathways provides survival, proliferation and invasion signals to malignant cells (307). As explained in section 1.5.4, NF- κ B signaling pathway is constitutively activated in PCNSL cells due to genetic alterations affecting MYD88 and genes related to BCR signaling.

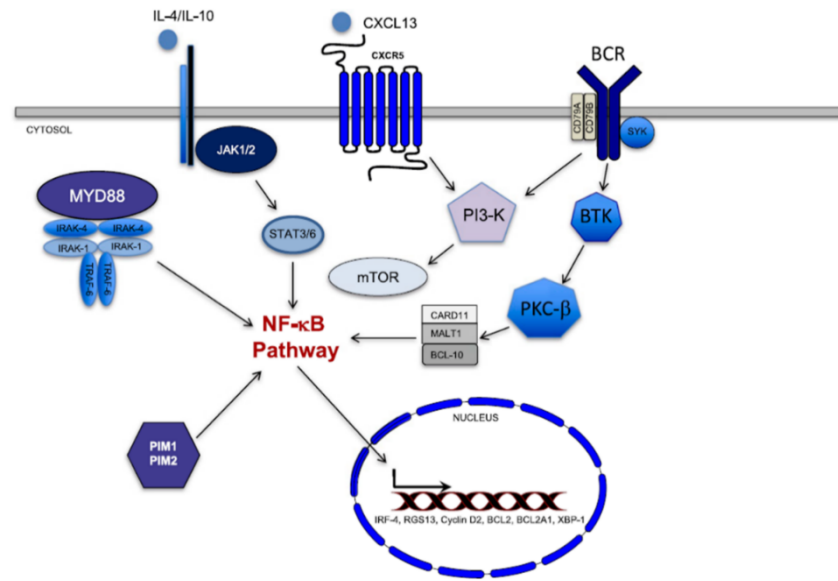


Figure 20. NF- κ B signaling pathway in PCNSL. From Rubenstein J. L. American Society of Hematology Educ. Program 2017.

Targeted therapies in R/R PCNSL patients are being explored as an alternative to conventional treatments.

BTK inhibitors. The efficacy and safety of ibrutinib monotherapy in CNS lymphomas were evaluated by Grommes *et al.* in a phase I clinical trial that included R/R PCNSL and SCNSL patients. Ibrutinib exhibited brain penetrance and clinical responses were observed in 10 out of the 13 PCNSL patients (77%) included in this study. However, the response was brief (median PFS of 4,6 months). Incomplete responses were found in patients with *CD79B* mutations, and one patient with mutated *CARD11* showed complete resistance to ibrutinib (292). Ibrutinib was also tested in combination with chemotherapy: tumor reductions were observed in 94% of the 18 PCNSL patients, including patients with *CD79B* and *MYD88* mutations, and 86% of 14 evaluable patients showed complete remissions in a phase 1b clinical trial (293).

PI3K/mTOR inhibitors. Temsirolimus is an mTOR inhibitor that was evaluated as monotherapy in R/R PCNSL patients. In a phase II clinical trial overall responses were achieved in 54% of patients but only 13% showed complete responses. Median PFS was brief (2,1 months) (308).

TIME in B-cell lymphoid malignancies

Selective inhibitors of nuclear exportins (SINEs). Transport across the nuclear membrane depends on the size of the molecules. While small molecules can be passively transported through the *nuclear pore complex (NPC)*, bigger molecules (>40 kDa) require the association of the NPC with different transport receptors, including exportin proteins like XPO1. Then, the NPC and transport receptors can bind to cargo proteins via Ran-GTPases regulation. Exportins recognize cargo proteins by the nuclear export sequence (NES) (Figure 21). XPO1 is a 120 kDa protein responsible for the transport of tumor suppressors and growth regulators (p53, p21, FOXO, IκB and eIF4E, among others) between the cytoplasm and nucleus (309,310). SINEs bind to the cargo binding pocket of XPO1 and inhibit its activity leading to anti-tumoral effects. Several SINEs targeting XPO1 have been developed. Nonetheless, only KPT-330 or selinexor has reached clinical trials. In a phase I clinical trial including different subtypes of R/R NHLs, 31% of patients who received selinexor achieved a certain response, partial in most cases (in 18 out of 22 patients) (311). Presently, selinexor is approved for the treatment of R/R multiple myeloma and DLBCL (312,313). A compassionate therapy with selinexor was administered in our institution to one R/R DLBCL patient who developed isolate CNS lymphoma after several lines of treatment. After 5 months of treatment, this patient exhibited a complete resolution of the brain lesions (314). Pre-clinical studies are needed to formally evaluate selinexor for the treatment of PCNSL.

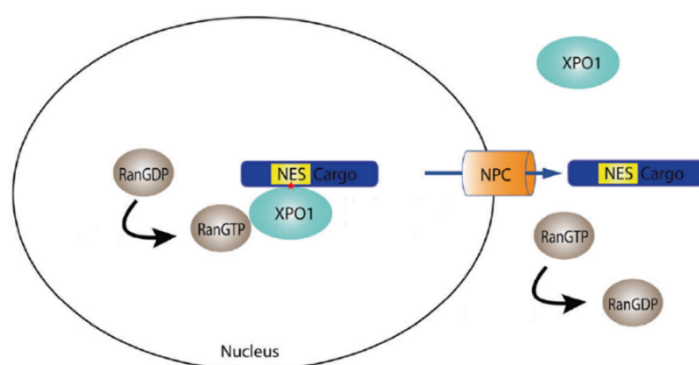


Figure 21. Nuclear export of cargo proteins by XPO-1. From Nachmias B. & Schimmer A. D. Leukemia 2020 (modified).

2. Hypothesis



The TIME plays a critical role not only in the early formation of tumors but later in their progression. Cellular and soluble components from the TIME interact with tumor cells facilitating their evasion from immunosurveillance. Moreover, targeting the TIME with immunotherapies offers therapeutic alternatives and improves current ones in several cancers, including B-cell malignancies. Great contributions have been made in this field during the last few years. However, further investigations are needed to deeper understand immune evasion mechanisms that lead to tumor progression. CLL, a slow growing leukemia with limited genetic alterations, provides a good model to explore this. Moreover, the design of novel therapies that modulate the immune system more precisely in aggressive diseases with limited therapeutic options, such as PCNSL, are also needed.

In CLL, the vast majority of patients are diagnosed at early asymptomatic stages. Within months to years, approximately half of them will progress to advanced clinical stages needing treatment, while the other half will remain stable. The underlying mechanisms that drive clinical progression from its early stages are still not fully understood. This also limits catching progression in advance or improving the current therapeutic options. Longitudinal studies performed at the time of diagnosis and progression before treatment show limited acquisition of molecular changes over time and suggest that CLL progression is not mainly driven by clonal evolution. Moreover, the growth of CLL cells is facilitated by the escape of immunosurveillance. We hypothesized that disease-induced immunological changes could aid this escape, driving CLL from early asymptomatic stages to clinical progression.

TIME in B-cell lymphoid malignancies

In PCNSL, patients often face dismal outcomes due to the limited availability of therapeutic options. PCNSL cells frequently have deregulated BCR signaling, but the effectiveness of BTK inhibition using ibrutinib has been brief. Interestingly, the BCR signaling pathway can also be inhibited by blocking nuclear export using selinexor. Selinexor covalently binds to XPO1 and is able to cross the BBB. Recently, it has shown clinical activity in a patient with refractory DLBCL in the CNS. We hypothesized that selinexor alone or in combination with ibrutinib could provide a novel therapeutic strategy for patients diagnosed with PCNSL.

3. Objectives

3.1. Main objective

To provide new insights into immune mechanisms that favor tumor progression and a pre-clinical rationale for the design of new therapeutic strategies with immunomodulatory potential focusing on CLL and PCNSL.

3.2. Specific objectives

Part I – The genetic and immune landscapes in clinical progression of CLL

1. To perform a longitudinal analysis of the genetic and immune landscapes in progressing and non-progressing CLL patients using paired samples at diagnosis and clinical progression before treatment or long-term asymptomatic follow-up, respectively.
2. To investigate *in vitro* the contribution of immune alterations to CLL progression.

Part II – New therapeutic strategies in PCNSL and immunomodulatory effects

3. To determine *in vivo* the impact of XPO1 inhibition using selinexor monotherapy and its combination with BTK inhibition using ibrutinib in xenograft orthotopic PCNSL mouse models.
4. To analyze *in vivo* the immunomodulatory effects of selinexor and ibrutinib in tumor cells and TAMs from xenograft orthotopic PCNSL mouse models.

4. Materials & Methods

Primary samples from CLL patients

Thirty eight patients diagnosed with CLL were enrolled in the study. Peripheral blood mononuclear cells (PBMCs) were isolated from whole blood by Ficoll-Paque Plus (GE Healthcare, Chicago, IL, USA) density gradient and cryopreserved in RPMI-1640 medium (Biowest, Nuaille, France) with 10% dimethyl sulfoxide (DMSO, Sigma-Aldrich, St. Louis, MO, USA) and 10% heat-inactivated fetal bovine serum (FBS, Gibco™, ThermoFisher Scientific, Waltham, MA, USA). Simultaneously, granulocytes were isolated by sedimentation with 2% dextran (Sigma-Aldrich). Plasma was obtained from EDTA blood and stored at -80°C.

Samples were collected at two time points: diagnosis and progression before treatment or long-term asymptomatic follow-up. Definition of progression and requirement for treatment were established following the iwCLL criteria (56). For most of the experiments, only a subgroup of the patients is represented due to availability of samples. For co-culture assays, PBMCs from age-matched HDs were used (n=17; 64 years old).

Isolation of B and T lymphocytes

B-CLL and T-CLL cells were immunomagnetically isolated using the EasySep™ Human B cell Enrichment Kit without CD43 Depletion and the EasySep™ Human T cell Isolation Kit (StemCell, Vancouver, Canada). The purity of isolated cells was >90% CD19⁺CD5⁺ and >85% CD3⁺ as assessed by flow cytometry.

DNA and RNA preparation for WES and RNA-Seq

DNA was extracted from isolated B-CLL cells and T cells or granulocytes from CLL patients (germline controls) using the AllPrep DNA/RNA (Qiagen, Hilden, Germany). RNA was also extracted from isolated T-CLL cells.

WES and data processing

Sample preparation and sequencing. 200ng of tumor or germline (T cells or granulocytes) DNA were used for SureSelect Human All Exon V5 (Agilent Technologies, Santa Clara, CA, USA) whole exome capture-based library preparation. Genomic DNA was sheared on a Covaris E210 and purified/size selected with AMPure XP beads (Beckman Coulter, Brea, CA, USA). The sheared DNA was end-repaired, 3' adenylated and ligated to NGS sequencing adapters. The adapter-modified DNA was amplified pre-capture through 10 PCR cycles. The PCR product was quality controlled on the Agilent 2100 Bioanalyzer 7500 chip (Agilent Technologies) to confirm size range (200 to 350bp) and quantity and hybridized for 24h at 65°C. The hybridization mix was washed and the eluate was post-capture PCR amplified (12 cycles) in order to add the index tags. The final library size and concentration were determined on Agilent 2100 Bioanalyzer 7500 chip. Libraries were sequenced on HiSeq2500 (Illumina, San Diego, CA, USA) with a read length of 100bp paired-end using TruSeq SBS Kit v4 (Illumina). Each sample was sequenced multiple times to achieve 110x mean depth of coverage.

Data analysis. Raw data was processed using the Real Time Analysis software (RTA 1.18.66.3, Illumina) to generate FASTQ sequence files, which were processed using the bioinformatics software HD Genome One (DREAMgenics, Oviedo, Spain), certified with IVD/CE-marking (315). The analysis workflow was as follows: raw FASTQ files were evaluated using quality control checks from FastQC (<https://www.bioinformatics.babraham.ac.uk/projects/fastqc/>) and Trimmomatic (316) was employed to remove low quality bases, adapters and other technical sequences. Then, alignment to the human reference genome (GRCh37/hg19) was done using BWA-mem (317), generating sorted BAM files with SAMtools (318). Optical and PCR duplicates were removed using Sambamba (319).

Variant calling and annotation. SNVs and indels were identified using a variation of Sidrón algorithm, as previously described (320), with the following parameters: total read depth ≥ 6 , mutated allele count ≥ 3 , variant frequency ≥ 0.01 , base quality ≥ 10 , and mapping quality ≥ 20 .

Indels realignment was performed to correct underestimated allele frequencies. Variants were annotated using several databases containing functional (Ensembl, CCDS, RefSeq, Pfam), population (dbSNP, 1000 Genomes, ESP6500, ExAC, gnomAD) and cancer-related (COSMIC – Release 87, ICGC – Release 27) information; as well as 14 scores from algorithms for prediction of the impact caused by variants on the protein structure and function (SIFT, SIFT 4G (321), PROVEAN (322), Mutation Assessor (323), Mutation Taster (324), LRT (325), MetaLR, MetaSVM (326), FATHMM, FATHMM-MKL, FATHMM-XF (327), primateAI (328) and Deogen2 (329)), and one score for evolutionary conservation of the affected nucleotide (GERP++) (330).

Variant filtering. Variants with high frequency in the population (>0.01) were discarded. A minimum coverage of 20 reads and a minimum variant allele frequency (VAF) of 0.1 in at least one time point were also established. Somatic status of each variant was defined using the Fisher Exact Test to compare tumor and germline control samples ($p\text{-value}<0.01$ and effect Size >2.5). Only variants with a consistent damaging impact on protein were considered.

Copy number variants. The exome2cnv algorithm used for CNVs detection incorporated a combination of read depth and allelic imbalance computations for copy number assessment (331). For tumor samples, the algorithm employed a pool of all control samples as background.

Cancer cell fraction. The CCF and the 95% CI were computed using the R package Palimpsest (332). The purity of samples was determined by flow cytometry and the ploidy was based on the copy number and the allele frequency. A significant change in CCF over time was determined if the 95% confidence interval of the CCF in the diagnosis and progression sample did not overlap (128).

Targeted sequencing of CLL genetic drivers

Sequencing of 9 CLL driver genes (*TP53*, *BIRC3*, *ATM*, *NOTCH1*, *SF3B1*, *XPO1*, *MYD88*, *FBXW7* and *POT1*) was performed using amplicon-based library preparation (CLL MASTR Plus assay; Multiplicom, Agilent) starting from 200ng of tumor DNA. Libraries were sequenced on

TIME in B-cell lymphoid malignancies

HiSeq2500 (Illumina) with a read length of 250bp paired-end, achieving 2 000x mean depth of coverage. Limit of detection was set at a minimum coverage of 100 reads and a minimum of 0.05 VAF in at least one time point. Data analysis was performed using DNAnexus (DNAnexus, Mountain View, CA, USA).

RNA-Seq and data processing

Sample preparation and sequencing. 10ng of full-length T-cell-RNA were used to prepare sequencing libraries using the SMARTer Stranded Total RNA-Seq Kit v2 - Pico Input Mammalian (Takara, Kusatsu, Japan). Total T-cell-RNA was reverse transcribed and Illumina compatible adapters and indexes were added to the cDNA followed by a purification using Agencourt Ampure XP beads (Beckman Coulter). Next, ribosomal (18S and 28S) and mitochondrial (m12S and m16) cDNA transcripts were depleted and final libraries were amplified during 16 PCR cycles. After two consecutive purification steps, the product size distribution and quantity were assessed using Bioanalyzer High Sensitivity DNA Kit (Agilent Technologies). Libraries were sequenced on HiSeq2500 (Illumina) using TruSeq SBS Kit v4 (Illumina). On average, 50 M paired-end reads were obtained per sample and 90% mapped to the reference genome.

Data analysis. Reads were mapped against the human reference genome (GENCODE release 28) using STAR version 2.5.3a (333) with the parameter `outFilterMultimapNmax=1`. Genes were quantified with RSEM version 1.3.0 (334) using the GENCODE release 28 human annotation. Differential expression analysis was performed adjusting for patient with DESeq2 version 1.18.1 (335). Genes with adjusted P value (padj) <0.05 were considered significant and filtered out if $\text{padj}>0.05$ and $|\text{shrunken fold change}|<1.5$. Heatmap showing the top-50 differentially expressed genes was performed with the regularized log transformation of the counts using the heatmap R package with the option `scale="row"`.

In vivo modeling of PCNSL

All animal experiments were approved by the local Ethical Committee for the Use of Experimental Animals.

Orthotopic xenograft cell line model. Eight-week-old athymic female mice (NMRI-*Foxn1^{nu/nu}* mice; Janvier Labs) were used to develop an orthotopic xenograft model of PCNSL using OCI-Ly10 cells stably transfected with luciferase (Fluc2 gene). For this, $15 \cdot 10^6$ cells at $1 \cdot 10^6$ cells/mL were electroporated ($960 \mu\text{F}/250\text{V}$) in the presence of 5pM of pGL4_Luc2_CMV_neo plasmid and 48 hours after electroporation 400 $\mu\text{g}/\text{ml}$ neomycin was added to culture media. After two weeks of selection, the bioluminescence of cells was analyzed by bioluminescence imaging (BLI) using IVIS[®] Spectrum system and Living Image software (PerkinElmer). $1 \cdot 10^5$ cells in 5 μl PBS were injected intracerebrally (coordinates: 1mm anterior, 1.8mm lateral right to the bregma and 2.5mm deep from the dura) with a Hamilton syringe with 26-gauge needle at a rate of 1 $\mu\text{l}/\text{min}$ using a stereotactic platform (Stoelting Just For Mice[™]). Tumor growth was monitored by BLI using an IVIS[®] Spectrum system (PerkinElmer) twice a week starting at day 4 post-intracerebral injection. Mice were anesthetized with isofluorane (1-2%) before intraperitoneal injection of luciferin at a dose of 150mg/kg. Tumor size was analyzed and quantified using Living Image software (PerkinElmer) and the total photons per second (ph/s) were recorded.

Patient-derived xenograft model. PDX model was established by intracerebral implantation of $2 \cdot 10^5$ human lymphoma cells isolated from brain biopsy by mechanical tissue dissociation in eight-week-old NOD-SCID gamma (NSG) female mice (NOD.Cg-Prkdc^{scid} Il2^{tm1Wjl}/SzJ; Charles River Laboratories). Malignant human CD19⁺ cells were sequentially expanded and passaged 3 times *in vivo* until the generation of a stable PDX model. Once a stable PDX in NSG mice was generated, the number of human tumor cells was sufficient for their implantation in athymic mice for the study of the innate immune response after drug treatments. Thus, $2 \cdot 10^5$ low-passage CD19⁺ patient-derived tumor cells were stereotactically inoculated into the brain parenchyma of eight-week-old athymic female mice as specified above. Human tumor sample

TIME in B-cell lymphoid malignancies

was obtained from a patient diagnosed with PCNSL at Hospital Universitari Joan XIII, Tarragona (Spain) after approval from the local Clinical Research Ethics Committee according to the principles of the Declaration of Helsinki and obtaining written informed consent from the patient. PDX tumors were confirmed to be negative for EBV via *in situ* hybridization (ISH) for EBV-encoded RNA (EBER). ISH was performed on a Ventana BenchMark Ultra autostainer (Ventana Corporation, Tucson, AZ, USA) using EBER probes and the Ventana ISH iVIEW Blue Detection Kit according to manufacturer's instructions.

For survival experiments, mice were euthanized when end point criteria were met, including neurological symptoms (seizures, circling or hind limb paralysis) or a significant weight loss (>20%).

Treatment regimens. Mice treated with selinexor were dosed with 5 mg/kg of drug or vehicle via oral gavage three times or twice a week when combined with ibrutinib as detailed in the results section. Ibrutinib was administered daily at 25 mg/kg in drinking water.

Flow cytometry analysis of human and mice samples

Monoclonal antibodies. In Table 8 monoclonal antibodies (mAbs) used for the staining of human and mouse samples are detailed.

Primary cells from CLL patients. Cryopreserved PBMCs were thawed and stained with mAbs for 15min at room temperature. Then, cells were resuspended in staining buffer (PBS with 1% bovine serum albumin and 0.1% sodium azide (Sigma-Aldrich)) and acquired in the flow cytometer. For the staining of transcription factors and intracellular cytokines, cells were permeabilized for 30min at 4°C using the Foxp3/Transcription Factor Staining Buffer Set (eBioscience, San Diego, CA, USA) and incubated with mAbs for 30min at room temperature.

For the assessment of intracellular IL-10 produced by CLL cells, PBMCs were co-cultured for 48 hours with UE6E7T-2 cells, CD40L (Peprotech, Rocky Hill, NJ, USA) and TLR9L (CpG ODN2006, Invivogen, San Diego, CA, USA) as previously described (194). Cells were stimulated

with Leukocyte Activation Cocktail (BD Biosciences, Franklin Lakes, NJ, USA) for 5 hours prior to staining.

Dissociation of mouse brain tissue. Mice brains were collected in cold RPMI-1640 medium immediately after euthanasia and the two hemispheres were separated with a razor blade. One hemisphere was used for immunochemical determinations and the other one was processed for flow cytometry analysis as previously described (336). Briefly, brain was dissected and minced through a 100 μ m cell strainer. Tissue pellets were digested with 25 μ g/ml Liberase (Roche), filtered through a 70 μ m cell strainer and further treated with 10 μ g/ml DNase I (Roche). Myelin and cell debris were removed by Percoll (Sigma-Aldrich) density gradient. Cell pellets were further washed and resuspended in 100 μ l FACS staining buffer (PBS with 1% bovine serum albumin and 0.1% sodium azide (Sigma-Aldrich)). When needed, remaining erythrocytes were lysed using the ACK lysing buffer (Gibco). Cells were blocked with 1 μ g rat serum IgG per 10⁶ cells (Sigma-Aldrich) for 15min at 4°C before the incubation with mAbs for 20min at 4°C. Dead cells were discarded using the LIVE/DEAD™ Fixable Violet Dead Stain Cell kit (Invitrogen). TAMs were identified as CD45⁺ Gr1^{low/-} CD11b⁺ F4/80⁺ ; M1 mouse TAMs as CD206⁻ and M2 mouse TAMs as CD206⁺ (29).

Acquisition and analysis. Cells were acquired by a Navios™ cytometer (Beckman Coulter, Brea, CA, USA). Data were analyzed using the FlowJo v10 software (TreeStar, Ashland, OR, USA) and the Cytobank platform (Santa Clara, CA, USA). Compensation was performed with single-stained tubes with VersaComp Antibody Capture beads (Beckman Coulter). The gating strategy used included only singlets and forward and side scatter live cells. All gates were based on fluorescence minus one (FMO) or isotype controls.

TIME in B-cell lymphoid malignancies

Species	mAb	Clone	Company
Human	CD3-APC-A750	UCHL1	Beckman Coulter
Human	CD4-PC5.5	13B8.2	Beckman Coulter
Human	CD4-Krome Orange	13B8.2	Beckman Coulter
Human	CD5-PC7	BL1a	Beckman Coulter
Human	CD8-Pacific Blue	B9.11	Beckman Coulter
Human	CD19-APC-A750	J3-119	Beckman Coulter
Human	CD45-Krome Orange	J33	Beckman Coulter
Human	CD45RA-Alexa Fluor 700	2H4LDH11LDB9	Beckman Coulter
Human	CD197(CCR7)-PE	G043H7	Beckman Coulter
Human	CD197(CC7)-PC7	G043H7	Beckman Coulter
Human	CD279(PD-1)-PC5.5	PD1.3	Beckman Coulter
Human	HLA-DR-PC5.5	Immu357	Beckman Coulter
Human	CD5-APC	L17F12	BD Biosciences
Human	CD14-FITC	M5E2	BD Biosciences
Human	CD86-Alexa Fluor 700	2331 (FUN-1)	BD Biosciences
Human	CD184(CXCR4)-APC	12G5	BD Biosciences
Human	CXCR5-BV421	RF8B2	BD Biosciences
Human	CD47-FITC	B6H12	eBioscience
Human	CD244-FITC	eBioDM244	eBioscience
Human	CD274(B7-H1)-PE (PD-L1)	MIH1	eBioscience
Human	IL-10-PE	JES3-9D7	eBioscience
Human/mouse	T-bet-PE	eBio4B10	eBioscience
Human	Eomes-eFluor 660	WD1928	eBioscience
Human	rat IgG1 κ isotype control-PE	eBRG1	eBioscience
Human	mouse IgG1 κ isotype control-eFluor 660	P3.6.2.8.1	eBioscience
Human	CD172a(SIRP α)-PerCP eFluor710	15-414	eBioscience
Human	CD206-APC	19.2	eBioscience
Human	CD48-FITC	BJ40	Biologend
Human	CD279(PD-1)-Alexa Fluor 700	EH12.2H7	Biologend
Human	CD16-PE/Cy7	B73.1	Biologend
Human	CD163-Brilliant Violet 605	GHI/61	Biologend
Human	CD279-A700	EH12.2H7	Biologend
Human	CD20-APC	2H7	Biologend
Human/mouse	CD11b-PerCP Cy5.5	M1/70	Biologend
Mouse	CD19-FITC	1D3/CD19	Biologend
Mouse	CD45-Brilliant Violet 510	30-F11	Biologend
Mouse	CD206-PE/Cy7	BM8	Biologend
Mouse	Gr1-FITC	RB6-8C5	Biologend
Mouse	CD279(PD-1)-PE	29F.1A12	Biologend
Mouse	F4/80-APC/Cy7	BM8	Biologend
Mouse	CD172a(SIRP α)-APC	P84	eBioscience

Table 8. mAbs for flow cytometry staining of human and mice samples.

Co-cultures of B and T lymphocytes from CLL

After negative selection, B-CLL cells or B cells from HDs were co-cultured with T cells from CLL or HDs at 1:2 and 1:10 T to B-cell ratios. Co-cultures were maintained in AIM VTM Medium

(Gibco™, ThermoFisher Scientific) supplemented with 2% human plasma and 50µM β-mercaptoethanol (Gibco™, ThermoFisher Scientific). Co-cultures were stimulated with 1µg/mL anti-CD3 (Clone OKT3; Miltenyi Biotec, Bergisch Gladbach, Germany) and 1µg/mL anti-CD28 (Clone 15E8, Miltenyi Biotec). When indicated, 10µg/ml LEAF™ purified anti-human IL-10 (BioLegend, San Diego, CA, USA) was added. After 7 days, cells were analyzed by flow cytometry. Assays were also performed using HTS Transwell-96 well plates (pore size 0.4µm; Corning, NY, USA).

Determination of soluble IL-10

Concentrations of IL-10 in plasma from CLL patients were measured using the Simple Plex™ Assay for the detection of human IL-10 (R&D Systems) on Ella™ Automated ELISA Platform following the manufacturer's instructions.

For the determination of IL-10 in the media of primary M2 macrophages cultures we used the ELISA MAX Deluxe Set Human IL-10 (Biolegend) following manufacturer's instructions. Previously, medium was removed at day 7 and replaced with RPMI free of M-CSF and IL-10. Supernatants were collected after 24h with 1µg/ml LPS (Sigma) and stored at -80°C before the analysis.

Quantitative real-time PCR

XPO1 relative expression was determined by quantitative reverse transcription PCR (qRT-PCR) using the $\Delta\Delta\text{CT}$ method and RIVA cells as calibrator.

Cell proliferation assay and assessment of apoptosis

Cell proliferation was measured using the CellTiter96™ Cell Proliferation Assay (MTS, Promega). Apoptosis was assessed analyzing the binding of Annexin-V-FITC and the incorporation of propidium iodide (PI) by flow cytometry (Bender Medsystems). Annexin-V⁺PI⁺ cells were considered viable cells.

IHC analysis of brain tumors

Antigen retrieval, IHC detection and counterstaining were performed at an Autostainer Link 48 (DAKO) using antibodies against human CD20 (PA5-16701, Thermo Fisher Scientific), human Ki-67 (Clone 30-9, Ventana Medical Systems Inc), mouse F4/80 (Clone SP115, Abcam) and mouse Iba-1 (Clone EPR16588, Abcam). Slides were scanned using NanoZoomer 2.0 HT Digital slide scanner C9600 and visualized using NDP.view 2 (Hamamatsu Photonics K.K).

Western blot

Jurkat and Ramos cells treated with the phosphatase-inhibitor pervanadate (3 mM H₂O₂/1 mM Na₃VO₄) for 5min at 37°C were used as positive controls for phospho-proteins. Whole cell protein extracts were prepared using lysis buffer (20 mM Tris pH 7.4, 1 mM EDTA, 140 mM NaCl, 1% NP-40, 2 mM Na₃VO₄ and protease inhibitor cocktail (Sigma-Aldrich)) for 1h at 4°C. Equal amounts of denatured protein were resolved by 10% SDS-PAGE and transferred to Immobilon-P membranes (Millipore). Blocked membranes were incubated overnight at 4°C with the following primary antibodies: phospho-BTK^{Tyr551}/ITK^{Tyr511}, BTK (BD Biosciences), phospho-SYK^{Tyr352}/phospho-ZAP70^{Tyr319}, phospho-AKT^{Ser473}, AKT, phospho-ERK1/2^{Thr202/Tyr204}, ERK1/2 and β-actin (Cell Signaling Technology) and SYK (Upstate Cell Signaling). Images were quantified using ImageJ software. Values of phosphoproteins are expressed as relative to total protein and loading control.

Culture of human macrophages

Primary monocytes were isolated from cryopreserved PBMCs from HDs by adherence in culture plates. For macrophage differentiation, monocytes were cultured for 5 days in RPMI-1640 (Biowest) supplemented with 10% FBS (Gibco) and 50ng/ml M-CSF (StemCell). At day 5, human macrophages were pre-incubated with drugs for 30min and then 10ng/ml IL-10 (Peprotech) was added for 48h to promote M2 differentiation. At day 7, cells were analyzed by flow cytometry and >90% CD14⁺CD16⁺ cells expressed CD206.

Phagocytosis assay

The phagocytic capacity of primary macrophages was evaluated using Phagocytosis Assay Kit Red E. coli (Abcam) following manufacturer's instructions.

Cell lines

Cell lines were obtained from Riken Cell Bank (Ibakari, Japan) and authenticated using short tandem repeat method. The UE6E7T-2 human BMSC cell line was cultured at 37°C in 5% CO₂ atmosphere in DMEM (Biowest) supplemented with 10% FBS, 2mM L-glutamine and 50µg/mL penicillin/streptomycin (Biowest). ABC-DLBCL cell lines RIVA, SUDHL2 and TMD8 and GCB-DLCBCL cell lines OCI-Ly4, SUDHL4, SUDHL5 and Karpas422 were grown in IMDM with 10% fetal calf serum, 100 µg/ml penicillin and streptomycin. OCI-Ly8 (GCB-DLBCL) were grown in equally supplemented RPMI-1640 media. OCI-Ly10 (ABC-DLBCL) cells were grown in IMDM with 20% human plasma, 100 µg/ml penicillin and streptomycin and 50 µM β-mercaptoethanol.

Reagents

Selinexor was kindly provided by Karyopharm. Ibrutinib was kindly provided by Pharmacyclics. Vehicle for oral selinexor was 0.6% plasdone PVP K-29/32 and 0.6% poloxamer pluronic F-68. Vehicle for oral ibrutinib was 1% HP-β-CD (Sigma).

Statistical analysis

Comparisons were performed using the Wilcoxon matched-pairs rank test and the Mann-Whitney U test or one or two-way ANOVA in unpaired samples. Differences were considered statistically significant if $P < 0.05$. Survival curves were generated using the Kaplan and Meier method, and statistically compared by the log-rank test. The synergistic nature of drug interactions was analyzed using isobologram analysis (337) and the combination index (CI) was calculated according to the Chou–Talalay method (338). All the statistical analyses were carried out and graphed using the GraphPad Prism version 6.0 software.

Data sharing statement

WES and RNA-Seq data are deposited at EGA and GEO under accession numbers EGAS00001004116 and GSE141787, respectively.

5. Results

Part I - The genetic and immune landscapes of
clinical progression in CLL

5.1. CLL cells show limited and non-recurrent genetic changes at clinical progression

In a series of 25 patients (median age: 63 years, range 40–82 years) that experienced clinical progression (median TTP: 29 months, range 5-96 months), we collected serial paired samples at diagnosis and at the time of progression before treatment. As a control group, 13 patients that did not progress (median age: 66 years, range 47–81 years; median time to second sampling: 39 months, range 30-77 months) were included in the study, and serial samples at diagnosis and asymptomatic follow-up (hereinafter called ‘non-progression’) were taken. For this group, the median follow-up was 77 months (range 41-101 months) and only one patient (CLL46) progressed 19 months after the second sampling. Clinical characteristics are detailed in Table 9 and Table 10.

	Progressed		Non-progressed	
	Median	Range	Median	Range
Gender	M (68%)		M (69%)	
BINET/RAI stage at diagnosis	A0 (72%)		A0 (92%)	
IGHV Status	UM (56%)		UM (8%)	
Age at diagnosis	63	40-82	66	47-81
TTP (months)	29	5-96	-	-
Follow-up without progression (months)	-	-	77	41-101
Time to second sampling (months)	29	5-96	39	30-77
Lymphocytes·10⁹/L at diagnosis	12,20	3,3-65,8	10,40	3,8-31,2
Lymphocytes·10⁹/L at second sampling	73,05	2,3-287,1	22,40	5,2-85,3

Table 9. Summary of clinical characteristics of progressing and non-progressing CLL patients.

For the purpose of analyzing potential genetic changes related to clinical progression, we performed longitudinal WES in paired samples from 12 patients at diagnosis and progression. With a mean read depth of 110X, the limit of detection was set at a minimum coverage of 20 reads and a minimum of 0.1 VAF. In accordance with previous WES studies in CLL, tumor mutational burden at both time points was low and consisted of a mean \pm SEM of 12.2 \pm 3.3 (range 6-17) somatic single nucleotide variants (SNVs) and insertions and deletions (indels) per patient (Table 11). We then screened for clonal shifts from diagnosis to progression by calculating significant changes in the CCF of alterations detected in each patient. A significant change was

TIME in B-cell lymphoid malignancies

determined if the 95% CI of the CCF in the diagnosis and progression sample did not overlap (128). We found that 50% of patients showed significant changes at progression affecting the CCF of at least one alteration. Specifically, a linear pattern characterized four patients (CLL05, CLL51, CLL03 and CLL19) while two showed a branched evolution pattern (CLL17 and CLL31) (131). The remaining 50% of progressing patients exhibited clonal stability (**Figure 22A** and **22B**). At diagnosis, mutations in CLL driver genes (128,339) were found in 9 out of 12 (75%) patients (mean \pm SEM of 1.4 ± 1.2 drivers per patient) (**Figure 22A**). However, at progression, only one patient (CLL51) harbored alterations in driver genes with clonal advantage: two variants in *NFKBIE* and *ATM* genes rised at progression (**Figure 22B**, in bold red). Also in this patient, two additional variants in the same genes displayed fixed CCF between time points (**Figure 22B**, in bold black). Furthermore, one patient (CLL31) amidst those without alterations in driver genes acquired a new mutation affecting the gene *TENMI* (CCF=0.31) (**Figure 22B**), not previously associated with CLL.

We also analyzed the mutational status of 9 CLL driver genes (*TP53*, *BIRC3*, *ATM*, *NOTCH1*, *SF3BL1*, *XPO1*, *MYD88*, *FBXW7* and *POT1*) using higher depth sequencing (mean read depth of 2000X, the limit of detection was set at a minimum coverage of 100 reads and a minimum of 0.05 VAF) but no additional changes over time affecting these drivers were observed (**Table 12**).

Next, we evaluated changes in CNVs by WES. At diagnosis, CNVs were detected in 10 out of 12 (83%) patients with a mean \pm SEM of 4.0 ± 4.1 (range 1-12) CNVs per patient (**Table 13**). Seven out of 12 (58%) patients had recurrent CNVs associated with CLL (del(13q), tri(12), del(11q) and del(17p)), but all remained stable over time. Nonetheless, the same patient that showed increased CCF in driver genes (CLL51) also acquired CNVs at progression. We observed acquisition of del(8p) and del(15p) with a CCF of 72% and 44%, respectively, at progression in this patient (**Figure 23**).

Regarding patients without clinical progression, we analyzed the panel of CLL driver genes in paired B-CLL cells at diagnosis and non-progression from 9 patients. We identified mutations at diagnosis in 4 out of 9 (44%) patients. One of them (CLL23) displayed increased VAF in one

ATM variant, and another one (CLL47) showed reduced VAF in one mutation affecting *FBXW7* at second sampling (Table 12).

The genetic analysis in our series indicates that genetic fluctuations in malignant cells are not always detected during the progression of CLL from early stages, as previously reported by others (131,165,168–170,172). Accordingly, these data support the role of the leukemic microenvironment in the evolution of the disease and prompt us to study changes in the immune system that may drive CLL clinical progression.

TIME in B-cell lymphoid malignancies

Patient ID	Gender	Age at diagnosis	BINET/RAI stage at diagnosis	IGHV Status	IGHV (% identity)	FISH ^a	Mutated drivers at diagnosis ^b	Progression	TTP (months)	Follow-up without progression (months)	Time to second sampling (months)	Lymphocytes-10 ⁹ /L at diagnosis	Lymphocytes-10 ⁹ /L at second sampling	C criteria for active disease
CLL02	M	82	A0	N/A	N/A	del(13q); del(11q)	TP53	Yes	5	-	5	21	120,5	(1) (2) (4)
CLL03	F	78	A1	N/A	N/A	Neg	No	Yes	21	-	21	7,6475	719	(1) (4)
CLL04	F	63	A0	UM	IGHV3-1 [*] 01(100)	tri(12)	No	Yes	26	-	26	3,3	2,3	(3)
CLL05	M	45	A0	M	IGHV3-7 [*] 01(96,5)	del(13q)	SF3B1, ATM ^c	Yes	37	-	37	12,3	814	(1)
CLL06	M	60	A0	UM	IGHV3-66 [*] 02 (99)	del(13q)	No	Yes	13	-	13	34	53,7	(1) (4)
CLL07	F	63	A0	UM	IGHV1-69 [*] 01(100)	Neg	No	Yes	19	-	19	4,9	23,3	(1) (3) (4)
CLL09	F	68	A0	M	IGHV3-48 [*] 03 (87,1)	N/A	N/A	Yes	54	-	54	6,2	26,4	(3)
CLL10	M	47	A1	UM	IGHV3-13 [*] 01(100)	tri(12)	N/A	Yes	63	-	63	4,8	N/A	(1) (4)
CLL11	M	60	A1	N/A	N/A	N/A	N/A	Yes	29	-	29	N/A	26,1	(3)
CLL17	M	68	A0	M	IGHV3-30 [*] 02 (94,8)	del(13q)	MYD88	Yes	46	-	46	22	106,3	(1) (2) (4)
CLL18	M	63	B1	M	IGHV1-2 [*] 04 (93,8)	del(13q)	No	Yes	51	-	51	10	272,5	(1)
CLL19	F	67	A0	UM	IGHV1-8 [*] 01(100)	del(17p); tri(12)	No	Yes	24	-	24	44	70,8	(1)
CLL20	M	79	A0	UM	IGHV1-2 [*] 02 (100)	tri(12)	No	Yes	13	-	13	16	20,5	(1) (4)
CLL24	M	69	A0	UM	IGHV3-64D [*] 06 (100)	tri(12)	No	Yes	63	-	63	5,2	224,4	(2) (3)
CLL29	M	70	A0	N/A	N/A	Neg	No	Yes	16	-	16	19	11,9	(4)
CLL30	F	40	A0	UM	IGHV4-39 [*] 01(100)	tri(12)	No	Yes	47	-	47	14,3	52	(1) (3) (4)
CLL31	F	44	A0	M	IGHV1-69 [*] 06 (97,6)	del(13q)	No	Yes	43	-	43	36	179,8	(1)
CLL32	F	56	A0	UM	IGHV4-39 [*] 01(100)	del(13q)	NOTCH1	Yes	12	-	12	65,8	287,1	(1) (4)
CLL50	M	59	A0	UM	IGHV1-69 [*] 01(100)	N/A	ATM	Yes	72	-	72	13	74,2	(1) (4)
CLL51	M	49	A1	UM	IGHV1-69 [*] 01(100)	del(13q); del(11q)	ATM ^d	Yes	96	-	96	12	125,2	(1) (4)
CLL53	M	62	A0	UM	IGHV1-69 [*] 15 (99,7)	N/A	N/A	Yes	33	-	33	12,1	60,6	(1) (4)
CLL54	M	72	A1	N/A	N/A	N/A	N/A	Yes	29	-	29	22,8	60,2	(1) (4)
CLL55	M	71	A0	UM	IGHV1-69 [*] 06 (100)	Neg	N/A	Yes	74	-	74	7,7	234	(1) (2) (4)
CLL56	M	62	N/A	N/A	N/A	del(13q); del(11q)	N/A	Yes	19	-	19	6,6	75,6	(1) (4)
CLL57	M	64	A0	UM	IGHV1-69 [*] 01(99,7)	del(13q); del(11q)	N/A	Yes	21	-	21	11,7	123,3	(1) (2) (4)
CLL21	M	63	A0	M	IGHV3-7 [*] 01(94,1)	N/A	FBXW7	No	-	97	35	312	12	-
CLL22	M	57	A0	M	IGHV1-2 [*] 02 (93,4)	N/A	No	No	-	95	36	31	60,6	-
CLL23	F	81	A0	M	IGHV4-34 [*] 01(96,1)	N/A	ATM	No	-	41	36	11,2	67,5	-
CLL26	M	79	A0	M	IGHV3-33 [*] 01(94,4)	Neg	No	No	-	83	30	11,2	23,5	-
CLL42	M	60	A0	UM	IGHV3-30-3 [*] 01(100)	del(17p); tri(12)	NOTCH1	No	-	86	58	7,5	16,4	-
CLL43	F	66	A0	N/A	N/A	tri(12)	N/A	No	-	101	77	7,1	5,2	-
CLL44	M	53	A0	M	IGHV1-2 [*] 02 (91)	Neg	No	No	-	88	61	4,2	16,8	-
CLL45	M	68	A0	N/A	N/A	del(13q)	No	No	-	77	53	10,2	24,2	-
CLL46	M	65	A0	M	IGHV4-34 [*] 01(91,6)	del(13q); del(17p); tri(12)	FBXW7, ATM	No	-	58	39	17,7	85,3	-
CLL47	M	79	A0	M	IGHV3-9 [*] 01(94,8)	del(13q)	FBXW7	No	-	58	30	10,8	11,4	-
CLL48	F	67	A0	M	IGHV5-10-1 [*] 03 (93,4)	N/A	No	No	-	47	35	5,3	7,7	-
CLL58	F	81	A0	M	IGHV5-51 [*] 01(91,7)	del(13q)	N/A	No	-	72	59	10,4	22,4	-
CLL59	M	47	A1	M	IGHV3-15 [*] 01(96,9)	del(13q)	N/A	No	-	64	45	3,8	32	-

(1) B C stages (2) Lymphocyte doubling time <12 months (3) Constitutional symptoms (4) Progressive or symptomatic lymphadenopathy and/or visceromegaly

^aRecurrent CNVs in CLL: del(13q), del(11q), del(17p) and tri(12)

^bTP53, BIRC3, ATM, NOTCH1, SF3B1, XPO1, MYD88, FBXW7 and POT1 by NGS

^cOne of the two mutations detected in SF3B1 and the mutation in ATM were only detected by NGS

^dTwo mutations detected in ATM

N/A not available

Table 10. Detailed clinical characteristics from progressing and non-progressing CLL patients included in the study.

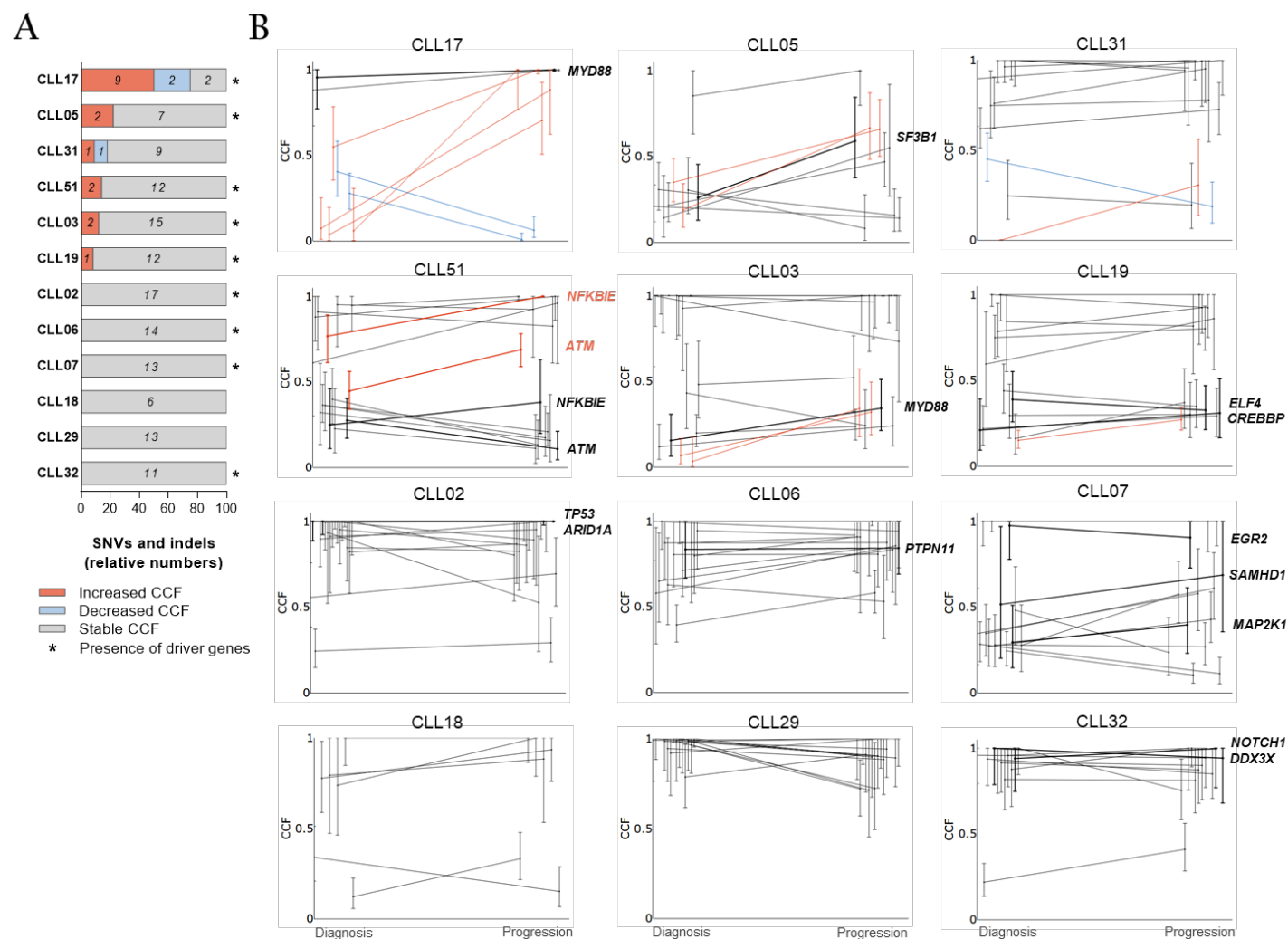


Figure 22. Longitudinal analysis of the CCF of SNVs and indels from paired B-CLL cells at diagnosis and progression before treatment. (A) Relative numbers of SNVs and indels with significantly increased (red) or decreased (blue) CCF and stable (grey) CCF between diagnosis and progression. Patients harboring CLL driver genes are marked with an asterisk. Absolute numbers of SNVs and indels detected per patient are detailed in italics inside bars. (B) Comparison of the CCF with 95% CI for each alteration detected per patient (n=12) between diagnosis and progression. Significantly increased (red lines) or decreased (blue lines) CCF and stable CCF (grey lines) are shown. CLL driver genes are plotted with bold lines and labeled with gene name: significantly increased (bold red) and stable CCF (bold black) driver genes are shown.

TIME in B-cell lymphoid malignancies

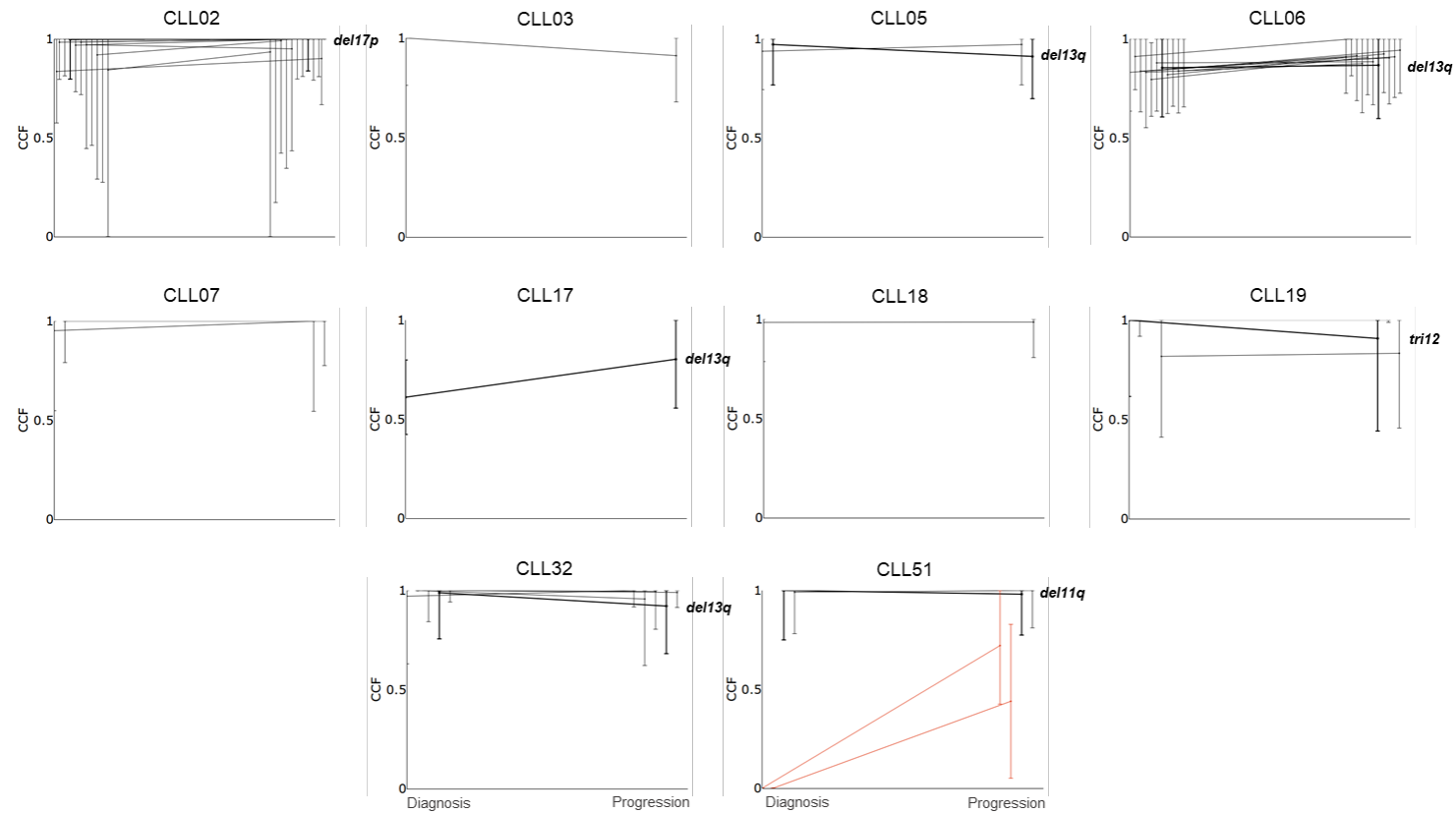


Figure 23. Longitudinal analysis of the CCF of CNVs from paired B-CLL cells at diagnosis and progression before treatment. Comparison of the CCF with 95% CI for each CNV detected per patient (n=10) between diagnosis and progression. Significantly increased (red lines) and stable CCF (grey lines) are shown. Recurrent CNVs in CLL (del(13q), del(11q), del(17p) and tri(12)) are plotted with bold lines and labeled with CNV name: stable CCF (bold black) is shown.

Patient	Chr	Coordinate	Gene	Protein Effect	Region	c.Hgvs	D Variant Frequency	P Variant Frequency	D Coverage	P Coverage	D Copy Number	D Purity	P Purity	D CCF.adj	D CCF.min	D CCF.max	D Clonality	P Copy Number	P CCF.adj	P CCF.min	P CCF.max	P Clonality
CLL02	16	2376203	ABC A3	N O_SYN	EXON	c.127C>T	0.27	0.33	99,00	103,00	2	0.98	0.95	0.56	0.38	0.76	subclonal	2	0.69	0.51	0.90	subclonal
CLL02	17	7578217	TP53	N O_SYN	EXON	c.632C>T	0.94	1.00	50,00	41,00	1	0.98	0.95	1.00	0.89	1.05	clonal	1	1.00	1.01	1.11	clonal
CLL02	11	10327898	ADM	N O_SYN	EXON	c.268A>T	0.12	0.14	151,00	137,00	2	0.98	0.95	0.24	0.15	0.37	subclonal	2	0.29	0.28	0.44	subclonal
CLL02	22	24836897	ADORA2A	N O_SYN	EXON	c.679A>G	0.44	0.48	157,00	143,00	2	0.98	0.95	0.90	0.74	1.06	clonal	2	1.00	0.82	1.18	clonal
CLL02	1	27059264	ARID1A	STOP_GAINED	EXON	c.1901C>G	1.00	1.00	24,00	32,00	1	0.98	0.95	1.00	0.92	1.08	clonal	1	1.00	0.98	1.10	clonal
CLL02	8	27516873	SCARA3	N O_SYN	EXON	c.1186C>T	0.49	0.51	162,00	160,00	2	0.98	0.95	1.00	0.83	1.16	clonal	2	1.00	0.90	1.23	clonal
CLL02	17	28326990	EFC A85	SPLICING_GAINED	EXON_DONOR	c.1043_1044+1del	0.46	0.25	24,00	32,00	2	0.98	0.95	0.94	0.52	1.37	clonal	2	0.53	0.24	0.91	subclonal
CLL02	13	36909901	SPG 20	N O_SYN	EXON	c.67G>A	0.45	0.45	38,00	42,00	2	0.98	0.95	0.91	0.58	1.26	clonal	2	0.95	0.63	1.29	clonal
CLL02	17	40359630	STAT5B	N O_SYN	EXON	c.2023A>G	0.53	0.42	81,00	85,00	2	0.98	0.95	1.00	0.85	1.31	clonal	2	0.89	0.67	1.13	clonal
CLL02	11	46563815	AM BRA1	STOP_GAINED	EXON	c.1482G>A	0.97	0.97	62,00	64,00	1	0.98	0.95	1.00	0.96	1.07	clonal	1	1.00	1.02	1.14	clonal
CLL02	11	61630454	FADS2	N O_SYN	EXON	c.893G>C	0.51	0.48	168,00	153,00	2	0.98	0.95	1.00	0.87	1.19	clonal	2	1.00	0.83	1.18	clonal
CLL02	12	8111015	MYF5	N O_SYN	EXON	c.173C>T	0.47	0.41	105,00	88,00	2	0.98	0.95	0.95	0.75	1.16	clonal	2	0.86	0.64	1.09	clonal
CLL02	15	83793513	TM 6SF1_HDG_FRP3	STOP_GAINED	EXON_DOWNSTREAM	c.693C>A	0.51	0.50	178,00	175,00	2	0.98	0.95	1.00	0.89	1.20	clonal	2	1.00	0.89	1.21	clonal
CLL02	9	96031031	WNK2	SPLICING	INTRON_DONOR	c.4033+3A>T	1.00	1.00	72,00	71,00	2	0.98	0.95	1.00	0.97	1.02	clonal	2	1.00	1.00	1.05	clonal
CLL02	2	109513427	EDAR	N O_SYN	EXON	c.1283G>T	0.42	0.39	106,00	79,00	2	0.98	0.95	0.85	0.65	1.05	clonal	2	0.83	0.60	1.07	clonal
CLL02	7	122763200	SLC 13A1	N O_SYN	EXON	c.1330G>A	0.40	0.41	67,00	80,00	2	0.98	0.95	0.82	0.58	1.08	clonal	2	0.87	0.64	1.11	clonal
CLL02	10	124036354	BTBD16	N O_SYN	EXON	c.67C>A	0.52	0.38	63,00	55,00	2	0.98	0.95	1.00	0.80	1.33	clonal	2	0.80	0.53	1.10	clonal
CLL03	1	6662185	KLHL21	INFRAME	EXON	c.691_693delinsTCT	0.41	0.33	32,00	30,00	2	0.81	0.91	1.00	0.59	1.47	clonal	2	0.73	0.38	1.16	clonal
CLL03	1	6662490	KLHL21	STOP_GAINED	EXON	c.388C>T	0.42	0.46	121,00	97,00	2	0.81	0.91	1.00	0.82	1.27	clonal	2	1.00	0.80	1.25	clonal
CLL03	16	10273946	GRIN2A	N O_SYN	EXON	c.323C>T	0.55	0.56	143,00	106,00	2	0.81	0.91	1.00	1.15	1.57	clonal	2	1.00	1.00	1.44	clonal
CLL03	1	14108437	PRDM 2	N O_SYN	EXON	c.4147G>T	0.05	0.11	126,00	101,00	2	0.81	0.91	0.12	0.04	0.25	subclonal	2	0.24	0.12	0.41	subclonal
CLL03	8	15480637	TU SC 3	N O_SYN	EXON	c.187C>T	0.49	0.62	61,00	55,00	2	0.81	0.91	1.00	0.89	1.54	clonal	2	1.00	1.05	1.64	clonal
CLL03	7	24325004	NPY	N O_SYN	EXON	c.145T>G	0.42	0.49	85,00	90,00	2	0.81	0.91	1.00	0.78	1.32	clonal	2	1.00	0.84	1.31	clonal
CLL03	X	38147160	TM 4SF21RPGR	INFRAME	INTRON_EXON	c.172-378212_172-378207del;c.1701_1706del	0.79	0.83	94,00	77,00	1	0.81	0.91	1.00	1.12	1.40	clonal	1	1.00	1.00	1.24	clonal
CLL03	3	38182025	MYD88	N O_SYN	EXON	c.649G>T	0.06	0.16	112,00	122,00	2	0.81	0.91	0.15	0.06	0.31	subclonal	2	0.34	0.21	0.51	subclonal
CLL03	6	65336130	EYS	N O_SYN	EXON	c.3452C>A	0.48	0.58	31,00	26,00	2	0.81	0.91	1.00	0.74	1.65	clonal	2	1.00	0.81	1.68	clonal
CLL03	12	76763508	OSPL8	N O_SYN	EXON	c.2149G>T	0.40	0.44	109,00	105,00	2	0.81	0.91	1.00	0.77	1.24	clonal	2	0.96	0.75	1.18	clonal
CLL03	9	90263723	DAPK1	N O_SYN	EXON	c.157G>C	0.03	0.15	149,00	110,00	2	0.81	0.91	0.07	0.02	0.17	subclonal	2	0.32	0.19	0.50	subclonal
CLL03	9	96863893	PTPDC 1	N O_SYN	EXON	c.2053G>A	0.38	0.50	40,00	28,00	2	0.81	0.91	0.93	0.56	1.34	clonal	2	1.00	0.67	1.52	clonal
CLL03	5	11374180	KCN N2	N O_SYN	EXON	c.628A>T	0.17	0.11	63,00	73,00	2	0.81	0.91	0.43	0.22	0.72	subclonal	2	0.24	0.11	0.45	subclonal
CLL03	5	13692331	TRPC 7	N O_SYN	EXON	c.745T>G	0.52	0.48	96,00	80,00	2	0.81	0.91	1.00	1.03	1.54	clonal	2	1.00	0.80	1.30	clonal
CLL03	5	150923520	FAT2	N O_SYN	EXON	c.7168G>A	0.01	0.15	77,00	71,00	2	0.81	0.91	0.03	0.00	0.17	subclonal	2	0.34	0.18	0.57	subclonal
CLL03	5	170346569	RANBP17	N O_SYN	EXON	c.1226C>T	0.08	0.11	225,00	243,00	2	0.81	0.91	0.20	0.12	0.30	subclonal	2	0.24	0.16	0.34	subclonal
CLL03	2	233407987	CHRN G	N O_SYN	EXON	c.808G>A	0.20	0.24	82,00	76,00	2	0.81	0.91	0.48	0.29	0.73	subclonal	2	0.52	0.32	0.77	subclonal
CLL05	11	1993302	MUC 2	INFRAME	EXON	c.5130_5135del	0.10	0.07	149,00	129,00	2	0.96	0.99	0.21	0.12	0.33	subclonal	2	0.14	0.07	0.26	subclonal
CLL05	18	22806851	ZNF521	N O_SYN	EXON	c.1031C>T	0.15	0.08	122,00	90,00	2	0.96	0.99	0.31	0.19	0.46	subclonal	2	0.16	0.06	0.31	subclonal
CLL05	21	22838960	NCA M 2	N O_SYN	EXON	c.1688C>T	0.07	0.27	44,00	33,00	2	0.96	0.99	0.14	0.03	0.39	subclonal	2	0.55	0.27	0.92	subclonal
CLL05	6	26247069	HISTH4G	N O_SYN	EXON	c.137G>A	0.10	0.23	136,00	125,00	2	0.96	0.99	0.21	0.12	0.23	subclonal	2	0.47	0.33	0.64	subclonal
CLL05	7	107830115	NRC A M	N O_SYN	EXON	c.2009G>A	0.17	0.33	161,00	135,00	2	0.96	0.99	0.35	0.24	0.49	subclonal	2	0.66	0.50	0.83	subclonal
CLL05	9	133799687	FIBCD1	N O_SYN	EXON	c.649C>T	0.09	0.33	100,00	100,00	2	0.96	0.99	0.19	0.09	0.34	subclonal	2	0.67	0.48	0.87	subclonal
CLL05	2	170058137	LRP2	CANONICAL_SPLICING	INTRON_DONOR	c.8452+1G>A	0.15	0.04	89,00	50,00	2	0.96	0.99	0.30	0.17	0.49	subclonal	2	0.08	0.01	0.28	subclonal
CLL05	3	176769516	TBLKR1	CANONICAL_SPLICING	INTRON_ACCEPTOR	c.205-2A>T	0.41	0.50	83,00	94,00	2	0.96	0.99	0.85	0.63	1.09	clonal	2	1.00	0.80	1.22	clonal
CLL05	2	198266834	SF3B1	N O_SYN	EXON	c.2098A>G	0.13	0.29	80,00	65,00	2	0.96	0.99	0.26	0.13	0.45	subclonal	2	0.59	0.38	0.84	subclonal
CLL06	11	4566796	OR52M 1	N O_SYN	EXON	c.376G>A	0.50	0.47	66,00	90,00	2	0.97	0.99	1.00	0.77	1.29	clonal	2	0.94	0.73	1.16	clonal
CLL06	9	4834165	RCL1	N O_SYN	EXON	c.484G>C	0.28	0.42	32,00	33,00	2	0.97	0.99	0.58	0.28	0.96	clonal	2	0.86	0.51	1.23	clonal
CLL06	8	16012572	MSR1	CANONICAL_SPLICING	INTRON_DONOR	c.898+1G>T	0.32	0.41	57,00	63,00	2	0.97	0.99	0.65	0.41	0.93	subclonal	2	0.83	0.59	1.10	clonal
CLL06	17	39619109	KRT32	N O_SYN	EXON	c.1190G>A	0.60	0.56	30,00	27,00	2	0.97	0.99	1.00	0.84	1.59	clonal	2	1.00	0.71	1.51	clonal
CLL06	19	42824492	TM EM 145	N O_SYN	EXON	c.1097G>A	0.42	0.43	92,00	83,00	2	0.97	0.99	0.87	0.66	1.10	clonal	2	0.88	0.66	1.11	clonal
CLL06	11	49207313	FOLH1	N O_SYN	EXON	c.734G>A	0.31	0.26	59,00	57,00	2	0.97	0.99	0.63	0.40	0.90	subclonal	2	0.53	0.31	0.80	subclonal
CLL06	11	55703485	OR511	N O_SYN	EXON	c.392C>A	0.39	0.40	110,00	105,00	2	0.97	0.99	0.81	0.62	1.01	clonal	2	0.81	0.62	1.01	clonal
CLL06	11	56468281	OR9G 1	N O_SYN	EXON	c.418T>C	0.19	0.29	230,00	222,00	2	0.97	0.99	0.39	0.29	0.51	subclonal	2	0.58	0.46	0.71	subclonal
CLL06	11	78380515	TEN M 4	N O_SYN	EXON	c.6875G>A	0.83	0.98	52,00	41,00	1	0.97	0.99	1.00	0.87	1.15	clonal	1	1.00	0.98	1.12	clonal
CLL06	10	107015473	SORCS 3	N O_SYN	EXON	c.325T>A	0.35	0.42	159,00	151,00	2	0.97	0.99	0.71	0.56	0.88	subclonal	2	0.84	0.68	1.01	clonal
CLL06	12	112888211	PTPN11	N O_SYN	EXON	c.227A>G	0.41	0.42	143,00	170,00	2	0.97	0.99	0.84	0.67	1.01	clonal	2	0.84	0.69	1.00	clonal
CLL06	4	115891737	FNDST4	N O_SYN	EXON	c.1070C>A	0.42	0.45	33,00	20,00	2	0.97	0.99	0.87	0.53	1.25	clonal	2	0.91	0.47	1.38	clonal
CLL06	1	120307073	HMGCS 2	N O_SYN	EXON	c.281G>A	0.39	0.45	80,00	91,00	2	0.97	0.99	0.80	0.58	1.04	clonal	2	0.91	0.70	1.13	clonal
CLL06	2	232393197	NMUR1	N O_SYN	EXON	c.535C>T	0.46	0.46	85,00	90,00	2	0.97	0.99	0.95	0.72	1.18	clonal	2	0.92	0.71	1.14	clonal

TIME in B-cell lymphoid malignancies

Cont.

Patient	Chr	Coordinate	Gene	Protein Effect	Region	c.Hgvs	D Variant Frequency	P Variant Frequency	D Coverage	P Coverage	D Copy Number	D Purity	P Purity	D CCF.adj	D CCF.min	D CCF.max	D Clonality	P Copy Number	P CCF.adj	P CCF.min	P CCF.max	P Clonality
CLL07	10	3149488	PFKP	NO_SYN	EXON	c.857A>T	0.16	0.28	56,00	64,00	2	0.93	0.97	0.35	0.16	0.61	subclonal	2	0.58	0.36	0.84	subclonal
CLL07	19	4817089	TICAM1	NO_SYN	EXON	c.1301C>T	0.13	0.05	167,00	166,00	2	0.93	0.97	0.28	0.18	0.41	subclonal	2	0.11	0.05	0.21	subclonal
CLL07	17	8526291	M YH10	NO_SYN	EXON	c.274G>A	0.47	0.49	214,00	208,00	2	0.93	0.97	1.00	0.86	1.15	clonal	2	1.00	0.86	1.15	clonal
CLL07	20	9561039	PAK7	NO_SYN	EXON	c.743A>G	0.16	0.30	118,00	98,00	2	0.93	0.97	0.35	0.21	0.52	subclonal	2	0.61	0.43	0.82	subclonal
CLL07	1	10421883	KIF1B	SPLICING NO_SYN	EXON_DONOR	c.4166C>T	0.13	0.21	119,00	135,00	2	0.93	0.97	0.27	0.16	0.43	subclonal	2	0.43	0.29	0.59	subclonal
CLL07	8	11606569	GATA4	NO_SYN	EXON	c.758A>T	0.54	0.50	102,00	102,00	2	0.93	0.97	1.00	0.94	1.37	clonal	2	1.00	0.82	1.24	clonal
CLL07	15	28389334	HERC2	NO_SYN	EXON	c.1188A>G	0.13	0.13	100,00	138,00	2	0.93	0.97	0.28	0.15	0.46	subclonal	2	0.27	0.16	0.41	subclonal
CLL07	20	35545425	SAMHD1	STOP_P_GAINED	EXON	c.880A>T	0.24	0.33	25,00	30,00	2	0.93	0.97	0.52	0.20	0.97	clonal	2	0.69	0.36	1.09	clonal
CLL07	15	50929741	TRPM7	NO_SYN	EXON	c.710T>A	0.11	0.05	202,00	260,00	2	0.93	0.97	0.24	0.16	0.36	subclonal	2	0.10	0.06	0.17	subclonal
CLL07	10	64573332	EGR2	NO_SYN	EXON	c.1066G>A	0.45	0.44	119,00	132,00	2	0.93	0.97	0.98	0.78	1.18	clonal	2	0.91	0.73	1.09	clonal
CLL07	15	66727455	MAP2K1	NO_SYN	EXON	c.171G>T	0.14	0.19	73,00	78,00	2	0.93	0.97	0.29	0.15	0.51	subclonal	2	0.40	0.23	0.61	subclonal
CLL07	1	156640082	NES	NO_SYN	EXON	c.3898C>A	0.22	0.11	67,00	70,00	2	0.93	0.97	0.48	0.28	0.74	subclonal	2	0.24	0.10	0.44	subclonal
CLL07	4	169312773	DDX60L	NO_SYN	EXON	c.3833T>C	0.13	0.28	62,00	111,00	2	0.93	0.97	0.28	0.12	0.51	subclonal	2	0.58	0.41	0.77	subclonal
CLL17	11	21135189	NELL1	NO_SYN	EXON	c.1355T>C	0.40	0.53	106,00	147,00	2	0.90	0.91	0.88	0.67	1.10	clonal	2	1.00	0.99	1.36	clonal
CLL17	3	38182641	MYD88	NO_SYN	EXON	c.794T>C	0.43	0.53	142,00	141,00	2	0.90	0.91	0.95	0.77	1.15	clonal	2	1.00	0.99	1.37	clonal
CLL17	22	42277655	SREBF2	STOP_P_GAINED	EXON	c.1318C>A	0.03	0.40	61,00	68,00	2	0.90	0.91	0.07	0.01	0.25	subclonal	2	0.88	0.62	1.16	clonal
CLL17	6	78172002	HTR1B	NO_SYN	EXON	c.1187T>A	0.02	0.32	61,00	101,00	2	0.90	0.91	0.04	0.00	0.20	subclonal	2	0.70	0.51	0.93	subclonal
CLL17	12	106461476	NUAK1	NO_SYN	EXON	c.1090C>T	0.25	0.54	85,00	114,00	2	0.90	0.91	0.55	0.36	0.78	subclonal	2	1.00	0.98	1.40	clonal
CLL17	7	117250712	C FTR	NO_SYN	EXON	c.3128T>C	0.18	0.03	121,00	178,00	2	0.90	0.91	0.40	0.26	0.58	subclonal	2	0.06	0.02	0.14	subclonal
CLL17	2	211476925	CP51	NO_SYN	EXON	c.2476C>T	0.13	0.00	208,00	272,00	2	0.90	0.91	0.28	0.19	0.40	subclonal	2	0.01	0.00	0.05	subclonal
CLL17	1	216256878	USH2A	NO_SYN	EXON	c.5218A>T	0.03	0.49	38,00	49,00	2	0.90	0.91	0.06	0.00	0.31	subclonal	2	1.00	0.76	1.41	clonal
CLL18	17	7557556	ATP1B2	NO_SYN	EXON	c.533T>C	0.17	0.07	108,00	107,00	2	0.98	0.99	0.34	0.21	0.51	subclonal	2	0.15	0.07	0.29	subclonal
CLL18	9	33135245	B4GALT1	NO_SYN	EXON	c.590A>G	0.38	0.46	105,00	134,00	2	0.98	0.99	0.78	0.59	0.98	clonal	2	0.93	0.76	1.11	clonal
CLL18	13	72440901	DACH1	NO_SYN	EXON	c.76T>T	0.39	0.44	36,00	32,00	2	0.98	0.99	0.79	0.47	1.15	clonal	2	0.88	0.53	1.26	clonal
CLL18	18	74968157	GALR1	NO_SYN	EXON	c.710A>C	0.36	0.54	47,00	46,00	2	0.98	0.99	0.74	0.46	1.05	clonal	2	1.00	0.79	1.40	clonal
CLL18	8	98991117	MATN2	NO_SYN	EXON	c.962T>C	0.50	0.51	144,00	155,00	2	0.98	0.99	1.00	0.85	1.19	clonal	2	1.00	0.87	1.19	clonal
CLL18	9	118974017	PAPPA	NO_SYN	EXON	c.1724G>A	0.06	0.16	151,00	140,00	2	0.98	0.99	0.12	0.06	0.22	subclonal	2	0.33	0.22	0.48	subclonal
CLL19	16	3778029	CREBBP	FRAMESHIFT	EXON	c.7018dupA	0.10	0.15	78,00	81,00	2	0.98	0.96	0.21	0.09	0.39	subclonal	2	0.31	0.16	0.51	subclonal
CLL19	16	21213251	ZP2	CANONICAL_SPLICING	INTRON_DONOR	c.1379+2T>C	0.11	0.14	131,00	114,00	2	0.98	0.96	0.22	0.12	0.35	subclonal	2	0.29	0.17	0.45	subclonal
CLL19	3	39448221	RPSA	NO_SYN	EXON JUTR5	c.-68C>G	0.29	0.41	48,00	46,00	2	0.98	0.96	0.60	0.35	0.90	subclonal	2	0.86	0.56	1.18	clonal
CLL19	3	51893896	DOCK3	NO_SYN	EXON	c.4475G>C	0.55	0.44	116,00	142,00	2	0.98	0.96	1.00	0.93	1.31	clonal	2	0.92	0.75	1.10	clonal
CLL19	6	56438593	DST	STOP_P_GAINED	EXON	c.13027C>T	0.37	0.38	245,00	252,00	2	0.98	0.96	0.75	0.63	0.88	subclonal	2	0.80	0.68	0.93	subclonal
CLL19	12	66275610	RPI1	NO_SYN	EXON INTRON	c.155T>A c.249+43261A>T	0.25	0.31	306,00	323,00	3	0.98	0.96	0.79	0.64	0.95	subclonal	3	0.92	0.78	1.08	clonal
CLL19	16	66761704	DYNCL12	NO_SYN	EXON	c.1148C>G	0.55	0.49	58,00	47,00	2	0.98	0.96	1.00	0.85	1.39	clonal	2	1.00	0.71	1.33	clonal
CLL19	4	73175230	ADAMTS3	NO_SYN	EXON	c.2063G>A	0.22	0.17	144,00	132,00	2	0.98	0.96	0.44	0.31	0.59	subclonal	2	0.35	0.22	0.50	subclonal
CLL19	2	103340366	MFS9	NO_SYN	EXON	c.430A>T	0.41	0.39	46,00	51,00	2	0.98	0.96	0.84	0.55	1.16	clonal	2	0.82	0.54	1.12	clonal
CLL19	1	116941320	ATPIA1	NO_SYN	EXON	c.2202G>C	0.14	0.14	90,00	90,00	2	0.98	0.96	0.29	0.16	0.48	subclonal	2	0.30	0.17	0.49	subclonal
CLL19	X	129208091	ELF4	FRAMESHIFT	EXON	c.271_272dupAC	0.19	0.16	126,00	147,00	2	0.98	0.96	0.39	0.26	0.55	subclonal	2	0.33	0.21	0.47	subclonal
CLL19	5	168098455	SLIT3	NO_SYN	EXON	c.3875G>A	0.08	0.18	102,00	90,00	2	0.98	0.96	0.16	0.07	0.30	subclonal	2	0.37	0.22	0.57	subclonal
CLL19	5	178410189	GFM6	NO_SYN	EXON	c.2158C>T	0.07	0.13	436,00	471,00	2	0.98	0.96	0.15	0.10	0.21	subclonal	2	0.27	0.21	0.34	subclonal
CLL29	20	3641933	GFR4	STOP_P_GAINED	EXON	c.50C>A	0.48	0.54	84,00	70,00	2	0.96	0.99	0.99	0.76	1.23	clonal	2	1.00	0.85	1.34	clonal
CLL29	11	5776386	OR52N4 TRIM5	NO_SYN	EXON UPSTREAM	c.416C>T	0.50	0.44	180,00	156,00	2	0.96	0.99	1.00	0.88	1.20	clonal	2	0.89	0.73	1.06	clonal
CLL29	8	35631913	UNC5D	NO_SYN	EXON	c.2575C>A	0.47	0.47	167,00	165,00	2	0.96	0.99	0.99	0.82	1.15	clonal	2	0.94	0.79	1.10	clonal
CLL29	2	37543459	PRKD3	NO_SYN	EXON	c.209G>A	0.45	0.44	130,00	105,00	2	0.96	0.99	0.95	0.76	1.13	clonal	2	0.89	0.69	1.09	clonal
CLL29	3	38087055	DLEC1	NO_SYN	EXON	c.433C>T	0.44	0.56	77,00	54,00	2	0.96	0.99	0.92	0.68	1.17	clonal	2	1.00	0.84	1.40	clonal
CLL29	10	5053197	C10orf71	NO_SYN	EXON	c.807T>A	0.56	0.45	140,00	125,00	2	0.96	0.99	1.00	0.98	1.34	clonal	2	0.91	0.73	1.09	clonal
CLL29	6	50805755	TFAP2B	NO_SYN	EXON	c.889G>A	0.47	0.36	91,00	67,00	2	0.96	0.99	0.98	0.76	1.21	clonal	2	0.72	0.49	0.98	clonal
CLL29	4	72400019	SLC4A4	NO_SYN	EXON	c.2356A>T	0.51	0.44	90,00	81,00	2	0.96	0.99	1.00	0.84	1.29	clonal	2	0.90	0.67	1.13	clonal
CLL29	8	74922307	LY96	STOP_P_GAINED	EXON	c.274G>T	0.51	0.35	75,00	51,00	2	0.96	0.99	1.00	0.81	1.30	clonal	2	0.71	0.45	1.01	clonal
CLL29	15	75092771	CSK	NO_SYN	EXON	c.481G>A	0.38	0.45	135,00	93,00	2	0.96	0.99	0.79	0.62	0.97	clonal	2	0.91	0.70	1.13	clonal
CLL29	4	87080500	M APK10	NO_SYN	EXON	c.73C>T	0.47	0.51	167,00	139,00	2	0.96	0.99	0.99	0.82	1.15	clonal	2	1.00	0.86	1.20	clonal
CLL29	4	149357927	NR3C2	NO_SYN	EXON	c.86C>T	0.46	0.36	177,00	157,00	2	0.96	0.99	0.97	0.81	1.12	clonal	2	0.72	0.57	0.88	subclonal
CLL29	2	163291729	KCNH7	NO_SYN	EXON	c.1933A>G	0.52	0.45	243,00	220,00	2	0.96	0.99	1.00	0.95	1.22	clonal	2	0.91	0.77	1.05	clonal

Cont.

Patient	Chr	Coordinate	Gene	Protein Effect	Region	c.Hgvs	D Variant Frequency	P Variant Frequency	D Coverage	P Coverage	D Copy Number	D Purity	P Purity	D CCF.adj	D CCF.min	D CCF.max	D Clonality	P Copy Number	P CCF.adj	P CCF.min	P CCF.max	P Clonality
CLL31	12	3692375	PRM T8	CANONICAL_SPLICING	INTRON_DONOR	c.979+1G>A	0.43	0.53	6100	49,00	2	0.95	0.95	0.90	0.63	1.18	clonal	2	100	0.81	1.42	clonal
CLL31	1	1236713	VPS13D	NO_SYN	EXON	c.3068A>G	0.29	0.35	299,00	197,00	2	0.95	0.95	0.62	0.51	0.74	subclonal	2	0.73	0.59	0.88	subclonal
CLL31	X	19021048	GPR64	NO_SYN	EXON	c.2137G>C	0.21	0.09	173,00	124,00	2	0.95	0.95	0.45	0.33	0.59	subclonal	2	0.19	0.09	0.32	subclonal
CLL31	22	22314776	TOP3B	NO_SYN	EXON	c.1571G>A	0.36	0.37	12100	73,00	2	0.95	0.95	0.75	0.57	0.94	subclonal	2	0.78	0.55	1.03	clonal
CLL31	16	30455955	SEPHS2	NO_SYN	EXON	c.1094G>A	0.36	0.45	205,00	126,00	2	0.95	0.95	0.76	0.62	0.91	subclonal	2	0.95	0.77	1.14	clonal
CLL31	15	44202081	FRM D5	SPLICING SYN	EXON_DONOR	c.426A>G	0.52	0.47	94,00	72,00	2	0.95	0.95	1.00	0.88	1.32	clonal	2	0.99	0.74	1.25	clonal
CLL31	X	123663783	TENM1	NO_SYN	EXON	c.2702T>G	0.00	0.15	87,00	55,00	2	0.95	0.95	0.00	0.00	0.09	subclonal	2	0.31	0.14	0.56	subclonal
CLL31	4	125590576	ANKRD50	FRAMESHIFT	EXON	c.3855dupA	0.46	0.48	568,00	337,00	2	0.95	0.95	0.96	0.88	1.05	clonal	2	1.00	0.89	1.12	clonal
CLL31	6	146993542	ADGB	FRAMESHIFT	EXON	c.1029delA	0.12	0.09	77,00	54,00	2	0.95	0.95	0.25	0.12	0.44	subclonal	2	0.19	0.06	0.43	subclonal
CLL31	6	151687999	ZBTB2	NO_SYN	EXON	c.202A>C	0.56	0.45	6100	44,00	2	0.95	0.95	1.00	0.89	1.44	clonal	2	0.96	0.64	1.29	clonal
CLL31	4	107454940	RP1F 215A19.2 MTNRIA	NO_SYN	INTRON EXON	c.129+21396T>C c.956T>C	0.49	0.45	138,00	87,00	2	0.95	0.95	1.00	0.86	1.22	clonal	2	0.94	0.72	1.18	clonal
CLL32	12	4919776	KCNA6 GALNT8	NO_SYN	EXON DOWNSTREAM	c.569T>C	0.46	0.47	157,00	137,00	2	0.97	0.99	0.96	0.79	1.13	clonal	2	0.94	0.77	1.12	clonal
CLL32	8	22064854	BM P1	NO_SYN	EXON	c.2400T>G	0.11	0.20	189,00	143,00	2	0.97	0.99	0.22	0.14	0.33	subclonal	2	0.41	0.28	0.56	subclonal
CLL32	15	28116353	OCA2	NO_SYN	EXON	c.2191G>A	0.45	0.42	176,00	190,00	2	0.97	0.99	0.94	0.78	1.10	clonal	2	0.85	0.71	1.00	clonal
CLL32	X	41205604	RN75L EP DDX3X	NO_SYN	PROMOTER EXON	c.1438A>G	0.48	0.47	97,00	60,00	2	0.97	0.99	1.00	0.79	1.21	clonal	2	0.94	0.68	1.21	clonal
CLL32	6	42018317	TAF8 CCND3	NO_SYN	EXON UPSTREAM	c.38C>T	0.45	0.45	123,00	101,00	2	0.97	0.99	0.92	0.74	1.11	clonal	2	0.90	0.70	1.11	clonal
CLL32	12	50344867	AQP2	NO_SYN	EXON	c.254G>T	0.44	0.43	142,00	104,00	2	0.97	0.99	0.91	0.74	1.09	clonal	2	0.87	0.68	1.08	clonal
CLL32	5	53839102	SNXB	FRAMESHIFT	EXON	c.1717_1718del	0.40	0.40	126,00	107,00	2	0.97	0.99	0.82	0.64	1.01	clonal	2	0.81	0.62	1.01	clonal
CLL32	16	78142365	WWOX	NO_SYN	EXON	c.153A>C	0.46	0.55	127,00	89,00	2	0.97	0.99	0.96	0.77	1.14	clonal	2	1.00	0.89	1.33	clonal
CLL32	16	88696940	ZC3H1B	STOP_GAINED	EXON	c.2614G>T	0.43	0.50	87,00	66,00	2	0.97	0.99	0.88	0.66	1.11	clonal	2	1.00	0.76	1.26	clonal
CLL32	9	139390648	NOTCH1	FRAMESHIFT	EXON	c.754_17542del	0.46	0.49	114,00	81,00	2	0.97	0.99	0.94	0.75	1.14	clonal	2	1.00	0.77	1.23	clonal
CLL32	5	176710863	NSD1	NO_SYN	EXON	c.6085A>G	0.49	0.37	168,00	126,00	2	0.97	0.99	1.00	0.85	1.17	clonal	2	0.75	0.58	0.94	subclonal
CLL51	5	5186203	ADAMTS16	NO_SYN	EXON	c.802C>T	0.29	0.47	31,00	34,00	2	0.95	0.98	0.61	0.30	1.01	clonal	2	0.96	0.61	1.32	clonal
CLL51	19	7998369	TIMM44	CANONICAL_SPLICING	INTRON_DONOR	c.769+1G>T	0.42	0.49	213,00	203,00	2	0.95	0.98	0.88	0.74	1.03	clonal	2	1.00	0.86	1.15	clonal
CLL51	5	16685902	MYO10	NO_SYN	EXON	c.3935C>T	0.43	0.40	88,00	84,00	2	0.95	0.98	0.91	0.69	1.14	clonal	2	0.83	0.61	1.06	clonal
CLL51	10	29776096	SVIL	NO_SYN	EXON	c.4481C>T	0.15	0.08	46,00	39,00	2	0.95	0.98	0.32	0.13	0.61	subclonal	2	0.16	0.03	0.43	subclonal
CLL51	15	32403989	CHRNA7	CANONICAL_SPLICING	INTRON_ACCEPTOR	c.241+2A>G	0.17	0.13	214,00	139,00	2	0.95	0.98	0.36	0.26	0.48	subclonal	2	0.21	0.13	0.32	subclonal
CLL51	15	43023473	CDAN1	NO_SYN	EXON	c.1796A>G	0.17	0.08	93,00	71,00	2	0.95	0.98	0.36	0.21	0.56	subclonal	2	0.17	0.06	0.36	subclonal
CLL51	6	44232738	NFKBIE	FRAMESHIFT	EXON	c.759_762del	0.73	0.65	48,00	43,00	2	0.95	0.98	0.77	0.61	0.89	subclonal	2	1.00	1.00	1.61	clonal
CLL51	6	44232759	NFKBIE	FRAMESHIFT	EXON	c.725_741del	0.12	0.19	68,00	59,00	2	0.95	0.98	0.25	0.11	0.46	subclonal	2	0.38	0.20	0.63	subclonal
CLL51	11	46900692	LRP4	NO_SYN	EXON	c.2989C>T	0.19	0.06	111,00	93,00	2	0.95	0.98	0.40	0.25	0.58	subclonal	2	0.13	0.05	0.28	subclonal
CLL51	X	53105981	GPR173	FRAMESHIFT	EXON	c.179_186del	0.11	0.05	56,00	55,00	2	0.95	0.98	0.23	0.08	0.46	subclonal	2	0.11	0.02	0.31	subclonal
CLL51	15	83335612	AP3B2	NO_SYN	EXON	c.1739G>A	0.45	0.45	73,00	53,00	2	0.95	0.98	0.95	0.71	1.21	clonal	2	0.92	0.64	1.22	clonal
CLL51	11	108186735	ATM C1orf65	SPLICING	INTRON_ACCEPTOR DOWNSTREAM	c.6096_16096del	0.24	0.10	75,00	70,00	1	0.95	0.98	0.27	0.17	0.40	subclonal	1	0.11	0.04	0.21	subclonal
CLL51	11	108186796	ATM C1orf65	FRAMESHIFT	EXON DOWNSTREAM	c.6156_6163del	0.39	0.64	105,00	119,00	1	0.95	0.98	0.45	0.34	0.56	subclonal	1	0.69	0.59	0.78	subclonal
CLL51	1	155204986	GBA	SPLICING NO_SYN	EXON_DONOR	c.1505G>A	0.45	0.56	200,00	153,00	2	0.95	0.98	0.95	0.80	1.10	clonal	2	1.00	0.98	1.31	clonal

Table II. SNVs and Indels analysis by WES in progressing CLL patients. Data analysis was performed as detailed in Materials & Methods. CLL driver genes are highlighted in bold red; D (diagnosis); P (progression); Chr (chromosome); Hgvs (Human genome variation society nomenclature); CCFadj (adjusted cancer cell fraction); CCF.min (minimum confidence interval CCF); CCF.max (maximum confidence interval CCF); NO_SYN (non-synonymous); del (deletion); ins (insertion).

TIME in B-cell lymphoid malignancies

Patient	Time Point	Gene	Variant	VAF %
CLL02	Diagnosis	TP53	Ex 6: c.632C>T; p.Thr211Ile (T211I); M issense	96,7%
	Progression	TP53	Ex 6: c.632C>T; p.Thr211Ile (T211I); M issense	80,0%
CLL03	Diagnosis	MYD88	Ex 3: c.649G>T; p.Val217Phe (V217F); M issense	5,3%
	Progression	MYD88	Ex 3: c.649G>T; p.Val217Phe (V217F); M issense	10,9%
CLL05	Diagnosis	SF3B1	Ex 16: c.2225G>A; p.Gly742Asp (G742D); M issense	8,0%
		SF3B1	Ex 15: c.2098A>G; p.Lys700Glu (K700E); M issense	10,9%
		ATM	Ex 42: c.6188G>T; p.Gly2063Val (G2063V); M issense	1,8%
	Progression	SF3B1	Ex 16: c.2225G>A; p.Gly742Asp (G742D); M issense	5,8%
		SF3B1	Ex 15: c.2098A>G; p.Lys700Glu (K700E); M issense	35,5%
		ATM	Ex 42: c.6188G>T; p.Gly2063Val (G2063V); M issense	6,9%
CLL06	Diagnosis	NO MUTATIONS		
	Progression	NO MUTATIONS		
CLL07	Diagnosis	NO MUTATIONS		
	Progression	NO MUTATIONS		
CLL17	Diagnosis	MYD88	Ex 5: c.818T>C; p.Leu273Pro; M issense	36,0%
	Progression	MYD88	Ex 5: c.818T>C; p.Leu273Pro; M issense	49,30%
CLL18	Diagnosis	NO MUTATIONS		
	Progression	NO MUTATIONS		
CLL19	Diagnosis	NO MUTATIONS		
	Progression	NO MUTATIONS		
CLL29	Diagnosis	NO MUTATIONS		
	Progression	NO MUTATIONS		
CLL31	Diagnosis	NO MUTATIONS		
	Progression	NO MUTATIONS		
CLL32	Diagnosis	NOTCH1	Ex 34: c.7541_7542del; p.Pro2514Argfs*4; Frameshift	40,1%
	Progression	NOTCH1	Ex 34: c.7541_7542del; p.Pro2514Argfs*4; Frameshift	44,6%
CLL51	Diagnosis	ATM	Ex: 42: c.6096-2_6096-1del; Splicing	29,3%
		ATM	Ex 42: c.6156_6163del; p.Glu2052Aspfs*33; Frameshift	34,0%
	Progression	ATM	Ex: 42: c.6096-2_6096-1del; Splicing	14,7%
		ATM	Ex 42: c.6156_6163del; p.Glu2052Aspfs*33; Frameshift	61,4%
CLL22	Diagnosis	NO MUTATIONS		
	Non-progression	NO MUTATIONS		
CLL23	Diagnosis	ATM	Ex 7: c.5616del; p.Cys1873Valfs*44; Frameshift	63,5%
	Non-progression	ATM	Ex 7: c.5616del; p.Cys1873Valfs*44; Frameshift	97,1%
CLL26	Diagnosis	NO MUTATIONS		
	Non-progression	NO MUTATIONS		
CLL42	Diagnosis	NOTCH1	Ex 34: c.7541_7542del; p.Pro2514Argfs*4; Frameshift	1,4%
	Non-progression	NOTCH1	Ex 34: c.7541_7542del; p.Pro2514Argfs*4; Frameshift	5,4%
CLL44	Diagnosis	NO MUTATIONS		
	Non-progression	NO MUTATIONS		
CLL45	Diagnosis	NO MUTATIONS		
	Non-progression	NO MUTATIONS		
CLL46	Diagnosis	FBXW7	Ex10: c.1513C>T; p.Arg505Cys (R505C); M issense	8,1%
		ATM	Ex 56: c.8264_8268del; p.Tyr2755Cysfs*12; Frameshift	45,9%
	Non-progression	FBXW7	Ex10: c.1513C>T; p.Arg505Cys (R505C); M issense	5,4%
		ATM	Ex 56: c.8264_8268del; p.Tyr2755Cysfs*12; Frameshift	52,5%
CLL47	Diagnosis	FBXW7	Ex11: c.1429G>A; p.Gly477Ser (G477S); M issense	19,9%
	Non-progression	FBXW7	Ex11: c.1429G>A; p.Gly477Ser (G477S); M issense	6,90%
CLL48	Diagnosis	NO MUTATIONS		
	Non-progression	NO MUTATIONS		

Table 12. Analysis of CLL driver genes by next-generation sequencing in progressing and non-progressing patients. TP53, BIRC3, ATM, NOTCH1, SF3B1, XPO1, MYD88, FBXW7 and POT1 were analyzed. Data analysis was performed as detailed in Materials & Methods. Ex (exon); VAF (variant allele frequency).

Patient	Chr	Start	End	Copy Number	Type	Purity	CCF adj	CCF.min	CCF.max
CLL02D	1	24301437	24417123	1,02	Deletion	0,98	1,00	0,81	1,00
CLL02D	1	31194144	32936135	1,05	Deletion	0,98	0,97	0,73	1,00
CLL02D	1	25883483	29481119	1,04	Deletion	0,98	0,98	0,72	1,00
CLL02D	9	65602470	141071559	2,00	LOH	0,98	1,00	1,00	1,00
CLL02D	11	34378111	46921237	1,04	Deletion	0,98	0,98	0,80	1,00
CLL02D	12	27165389	34178661	1,18	Deletion	0,98	0,84	0,57	1,00
CLL02D	12	38711864	77252681	2,95	Amplification	0,98	0,97	0,45	1,00
CLL02D	12	247254	5153148	3,96	Amplification	0,98	1,00	0,46	1,00
CLL02D	12	19512203	27128324	2,90	Amplification	0,98	0,92	0,29	1,00
CLL02D	12	18234060	19467617	4,24	Amplification	0,98	1,00	0,28	1,00
CLL02D	12	5603307	17141843	1,17	Deletion	0,98	0,84	0,00	1,00
CLL02D	17	7463945	9281713	1,02	Deletion	0,98	1,00	0,80	1,00
CLL02P	1	31194144	32936135	1,04	Deletion	0,95	1,00	0,81	1,00
CLL02P	1	25883483	29481119	0,99	Deletion	0,95	1,00	0,80	1,00
CLL02P	1	24301437	24417123	0,97	Deletion	0,95	1,00	0,79	1,00
CLL02P	9	65602470	141071559	2,00	LOH	0,95	1,00	1,00	1,00
CLL02P	11	34378111	46921237	1,04	Deletion	0,95	1,00	0,81	1,00
CLL02P	12	27165389	34178661	1,14	Deletion	0,95	0,90	0,67	1,00
CLL02P	12	38711864	77252681	2,90	Amplification	0,95	0,95	0,43	1,00
CLL02P	12	19512203	27128324	2,94	Amplification	0,95	0,99	0,42	1,00
CLL02P	12	247254	5153148	4,43	Amplification	0,95	1,00	0,35	1,00
CLL02P	12	18234060	19467617	4,41	Amplification	0,95	1,00	0,17	1,00
CLL02P	12	5603307	17141843	1,11	Deletion	0,95	0,93	0,00	1,00
CLL02P	17	7463945	9281713	1,00	Deletion	0,95	1,00	0,84	1,00
CLL03D	X	2724695	154736429	1,15	Deletion	0,81	1,00	0,76	1,00
CLL03P	X	2724695	154736429	1,17	Deletion	0,91	0,91	0,68	1,00
CLL05D	13	46942048	50589483	1,07	Deletion	0,96	0,97	0,77	1,00
CLL05D	22	23089657	23246981	1,10	Deletion	0,96	0,94	0,74	1,00
CLL05P	13	46942048	50589483	1,10	Deletion	0,99	0,91	0,70	1,00
CLL05P	22	23089657	23246981	1,04	Deletion	0,99	0,97	0,77	1,00
CLL06D	2	9347093	9676651	1,19	Deletion	0,97	0,83	0,63	1,00
CLL06D	2	24468890	26568884	1,19	Deletion	0,97	0,84	0,63	1,00
CLL06D	2	127451321	128283591	1,18	Deletion	0,97	0,85	0,66	1,00
CLL06D	2	68691248	69783882	1,17	Deletion	0,97	0,85	0,66	1,00
CLL06D	2	32188011	32613711	1,19	Deletion	0,97	0,83	0,55	1,00
CLL06D	2	37310288	39082051	1,15	Deletion	0,97	0,88	0,64	1,00
CLL06D	11	34111604	35282282	1,23	Deletion	0,97	0,79	0,61	0,98
CLL06D	11	59131854	63481261	1,21	Deletion	0,97	0,82	0,62	1,00
CLL06D	11	75562751	85961181	1,19	Deletion	0,97	0,84	0,63	1,00
CLL06D	13	47266539	51600665	1,17	Deletion	0,97	0,85	0,61	1,00
CLL06D	22	23089657	23222797	1,12	Deletion	0,97	0,91	0,74	1,00
CLL06P	2	9347093	9676651	1,10	Deletion	0,99	0,91	0,73	1,00
CLL06P	2	37310288	39082051	1,12	Deletion	0,99	0,88	0,67	1,00
CLL06P	2	32188011	32613711	1,13	Deletion	0,99	0,88	0,63	1,00
CLL06P	2	68691248	69783882	1,10	Deletion	0,99	0,90	0,67	1,00
CLL06P	2	24468890	26568884	1,09	Deletion	0,99	0,92	0,69	1,00
CLL06P	2	127451321	128283591	1,07	Deletion	0,99	0,94	0,73	1,00
CLL06P	11	34111604	35282282	1,10	Deletion	0,99	0,91	0,72	1,00
CLL06P	11	75562751	85961181	1,10	Deletion	0,99	0,91	0,70	1,00
CLL06P	11	59131854	63481261	1,08	Deletion	0,99	0,92	0,73	1,00
CLL06P	13	47266539	51600665	1,14	Deletion	0,99	0,87	0,60	1,00
CLL06P	22	23089657	23222797	1,00	Deletion	0,99	1,00	0,81	1,00
CLL07D	6	69348437	170889055	1,02	Deletion	0,93	1,00	0,79	1,00
CLL07D	6	396993	54804386	2,89	Amplification	0,93	0,95	0,55	1,00
CLL07P	6	69348437	170889055	1,01	Deletion	0,97	1,00	0,78	1,00
CLL07P	6	396993	54804386	2,99	Amplification	0,97	1,00	0,54	1,00
CLL17D	13	49852352	51854488	1,45	Deletion	0,9	0,61	0,42	0,80
CLL17P	13	48570990	53307093	1,28	Deletion	0,9	0,80	0,56	1,00

TIME in B-cell lymphoid malignancies

Cont.

Patient	Chr	Start	End	Copy Number	Type	Purity	CCF adj	CCF.min	CCF.max
CLL18D	22	22730360	23246981	1,04	Deletion	0,98	0,98	0,79	1,00
CLL18P	22	22730360	23246981	1,02	Deletion	0,99	0,99	0,81	1,00
CLL19D	2	89246801	89513068	0,03	Deletion	0,98	1,00	0,92	1,00
CLL19D	9	100372495	101990088	2,80	Amplification	0,98	0,82	0,41	1,00
CLL19D	12	247254	133803479	3,04	Amplification	0,98	1,00	0,62	1,00
CLL19P	2	89246801	89513068	0,01	Deletion	0,96	1,00	0,99	1,00
CLL19P	9	100372495	101990088	2,80	Amplification	0,96	0,83	0,46	1,00
CLL19P	12	247254	133803479	2,87	Amplification	0,96	0,91	0,44	1,00
CLL32D	2	89246801	89533835	0,02	Deletion	0,97	1,00	0,94	1,00
CLL32D	8	38676941	38965128	0,99	Deletion	0,97	1,00	0,84	1,00
CLL32D	13	46942048	61985259	1,04	Deletion	0,97	0,99	0,76	1,00
CLL32D	22	23090045	23114651	0,01	Deletion	0,97	1,00	1,00	1,00
CLL32D	22	22781810	23089657	1,06	Deletion	0,97	0,97	0,63	1,00
CLL32P	2	89246801	89533835	0,04	Deletion	0,99	0,99	0,91	1,00
CLL32P	8	38676941	38965128	1,01	Deletion	0,99	1,00	0,80	1,00
CLL32P	13	46942048	61985259	1,09	Deletion	0,99	0,92	0,68	1,00
CLL32P	22	22781810	22892069	0,96	Deletion	0,99	1,00	0,92	1,00
CLL32P	22	23029112	23090045	0,10	Deletion	0,99	0,96	0,62	1,00
CLL5D	11	118451811	118939819	1,06	Deletion	0,95	0,99	0,78	1,00
CLL5D	11	105775786	115085174	1,04	Deletion	0,95	1,00	0,75	1,00
CLL5P	8	401162	29924163	1,29	Deletion	0,98	0,72	0,43	1,00
CLL5P	11	105775786	115085174	1,04	Deletion	0,98	0,98	0,77	1,00
CLL5P	11	118451811	118939819	1,02	Deletion	0,98	1,00	0,81	1,00
CLL5P	15	20169886	42976180	1,57	Deletion	0,98	0,44	0,05	0,83

Table 13. CNVs analysis by WES in progressing CLL patients. Data analysis was performed as detailed in Materials & Methods. Recurrent CNVs in CLL (del(13q), del(11q), del(17p) and tri(12)) are highlighted in bold red. Chr (chromosome); CCF (cancer cell fraction); CCF.min (minimum confidence interval CCF); CCF.max (maximum confidence interval CCF); LOH (loss of heterozygosity).

5.2. At CLL progression, CD8⁺ T cells are enriched in PD-1⁺ effector memory subsets and show increased co-expression of inhibitory receptors

The immune system is fundamental for controlling tumor growth by the recognition and elimination of malignant cells through innate and adaptive responses. Tumor cells often develop mechanisms to escape from autologous immune responses which contributes to tumor progression. In CLL, the growth of leukemic cells is facilitated by the evasion of immune surveillance, although the exact mechanisms are unknown. Prior studies in patients diagnosed with CLL have shown an accumulation of defective circulating CD8⁺ T cells displaying a terminally differentiated phenotype at all clinical stages (203,205,219,221,340,341). This highlights the importance of CD8⁺ T cells in CLL. However, how these CD8⁺ T cells potentially evolve from diagnosis to clinical progression using longitudinal samples has not yet been studied. To investigate this, we analyzed the T-cell immunophenotype in paired PBMC samples from 19 patients at the time of diagnosis and progression before treatment and in 10 patients at diagnosis and non-progression.

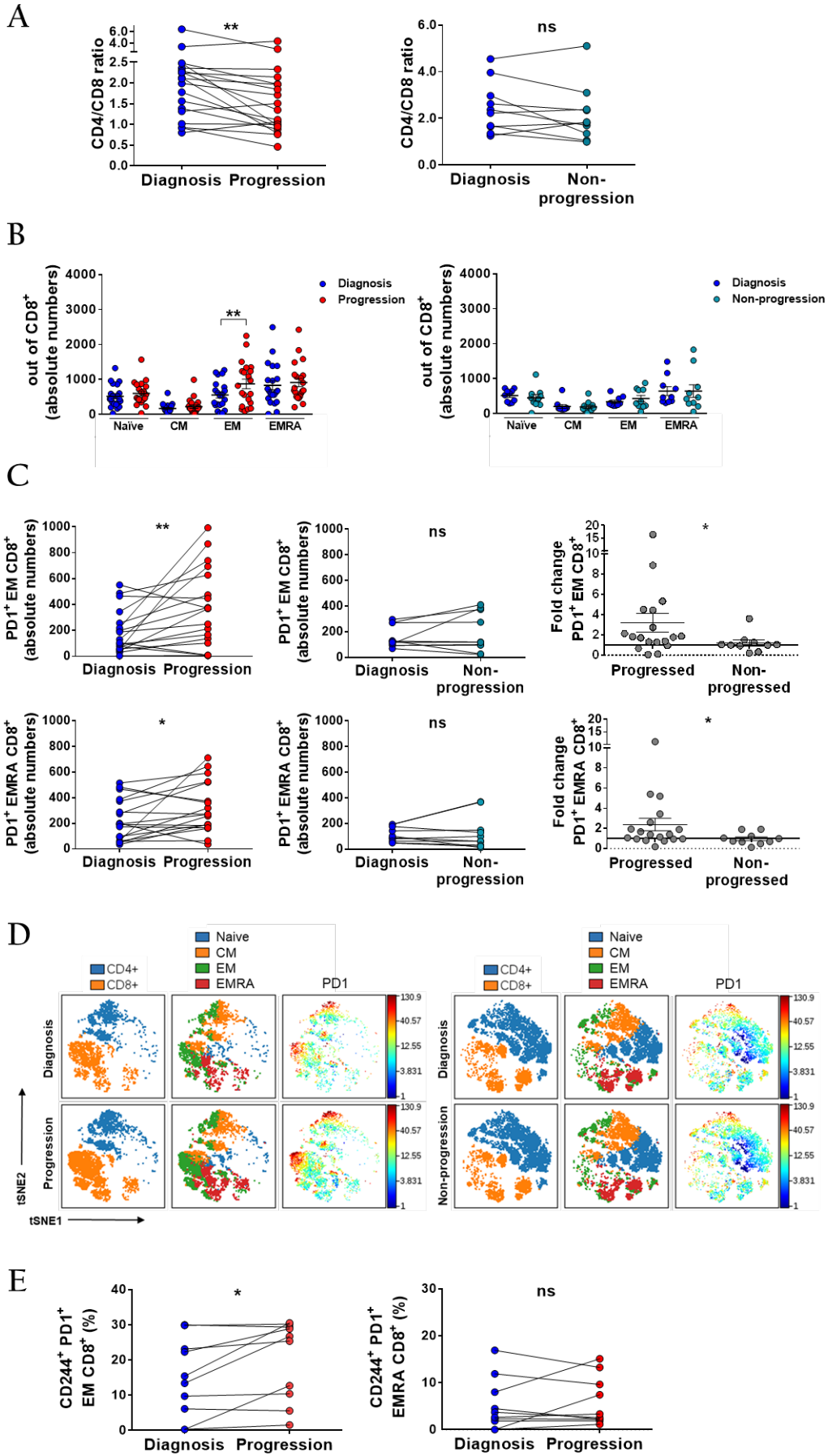
Firstly, the CD4/CD8 ratio at the second sampling was significantly decreased only in progressors, in whom effector memory CD8⁺ T cells (T_{EM}: CCR7⁺CD45RA⁻) were the sole expanded T-cell subset at progression, whereas no significant changes were found in non-progressors (Figure 24A and 24B). PD-1, expressed in chronically stimulated CD8⁺ T cells and known to have a relevant role in T-cell exhaustion (342,343), has been described as prevalent in CD8⁺ T_{EM} and T_{EM}CD45RA⁺ cells (T_{EMRA}: CCR7⁺CD45RA⁺) in CLL compared to healthy controls (203,205). Progressing patients showed an enrichment in PD-1⁺ T_{EM} and PD-1⁺ T_{EM}CD45RA⁺ (T_{EMRA}) CD8⁺ subsets, which in contrast was not observed at non-progression (Figure 24C and 24D). In addition, the increased T_{EM} CD8⁺ subset in progressing patients gained features of severe exhaustion at the time of progression as denoted by higher co-expression of PD-1 and

TIME in B-cell lymphoid malignancies

CD244, not observed in the T_{EMRA} CD8⁺ subset (Figure 24E). We also analyzed by flow cytometry the expression of the ligands of PD-1 and CD244 (PD-L1 and CD48, respectively) in CLL cells from progressors and non-progressors. At progression, the increase in the co-expression of PD-L1 and CD48 in CLL cells was mild (data not shown). Moreover, other key molecules in CLL including chemokine receptors involved in B-cell migration (CCR7, CXCR4, CXCR5) and activation molecules (HLA-DR, CD86) were analyzed and no changes in their expression were found over time (data not shown).

In summary, while CLL cells barely changed genetically and phenotypically at progression, (in terms of the migration and activation B-cell markers analyzed), CD8⁺ T cells did. The longitudinal increase of antigen-experienced effector memory CD8⁺ subsets with increased co-expression of inhibitory receptors we observed in progressors and not in non-progressors may significantly contribute to the progression of the disease.

Figure 24 (right). Longitudinal analysis of CD8⁺ T-cell exhaustion in progressing and non-progressing CLL patients. (A) CD4/CD8 ratio in progressing (n=19) and non-progressing patients (n=10) at diagnosis and progression or non-progression. **(B)** Absolute numbers of CD8⁺ T-cell differentiation subsets (naïve: CCR7⁺CD45RA⁺; central memory, CM: CCR7⁺CD45RA⁻; effector memory, EM: CCR7⁻CD45RA⁻ and EM CD45RA⁺, EMRA: CCR7⁻CD45RA⁺) in progressing (n=19) and non-progressing patients (n=10) at diagnosis and progression or non-progression. **(C)** Absolute numbers of PD-1⁺EM and PD-1⁺EMRA CD8⁺ cells in progressors (n=18) and non-progressors (n=10) at diagnosis and progression or diagnosis and non-progression, respectively; fold change between time points in progressors (n=18) and non-progressors (n=10). **(D)** Representative viSNE plots of T-cell differentiation subsets and PD-1 expression in CD4⁺ and CD8⁺ T cells at the two time points from one representative patient from each group. **(E)** Percentages of EM and EMRA CD8⁺ cells co-expressing CD244 and PD-1 in progressors (n=10). Mean±SEM or paired values; Wilcoxon matched paired test or Mann-Whitney test; *P<0.05; **P<0.01.



5.3. Terminally exhausted CD8⁺ T cells accumulate at CLL progression

Several studies pointed out that the T-box transcription factors T-bet and Eomes that regulate the differentiation process of CD8⁺ T cells after antigen encounters and cooperate in the maintenance of long-term immunity, also have roles in CD8⁺ T-cell exhaustion. Thus, differential expression of T-bet and Eomes with moderate or high PD-1 levels defines two distinctly exhausted CD8⁺ pools: the progenitor (T-bet^{hi}Eomes^{dim/}PD-1^{mid}) and the terminal progeny (T-bet^{dim/}Eomes^{hi}PD-1^{hi}) (40) (Figure 25).

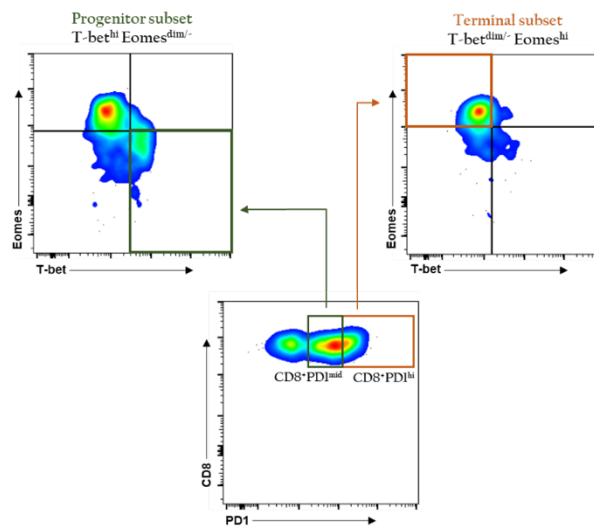


Figure 25. Progenitor and terminally exhausted CD8⁺ T cells. Gating strategy followed for the identification of progenitor (T-bet^{hi}Eomes^{dim/}PD-1^{mid}) and terminally (T-bet^{dim/}Eomes^{hi}PD-1^{hi}) exhausted CD8⁺ subsets by flow cytometry.

Since we observed that CD8⁺ T cells from CLL patients gained features of more severe exhaustion at progression, we hypothesized that the terminal progeny would also be increased at progression. Indeed, we found that the CD8⁺ progenitor subset remained mainly stable over time in both progressors and non-progressors, while the terminally exhausted CD8⁺ subpopulation was significantly increased only in progressing patients (Figure 26A-C). These findings confirm that CD8⁺ T cells at progression exhibit a terminally severe exhaustion condition likely losing their ability to control malignant growth.

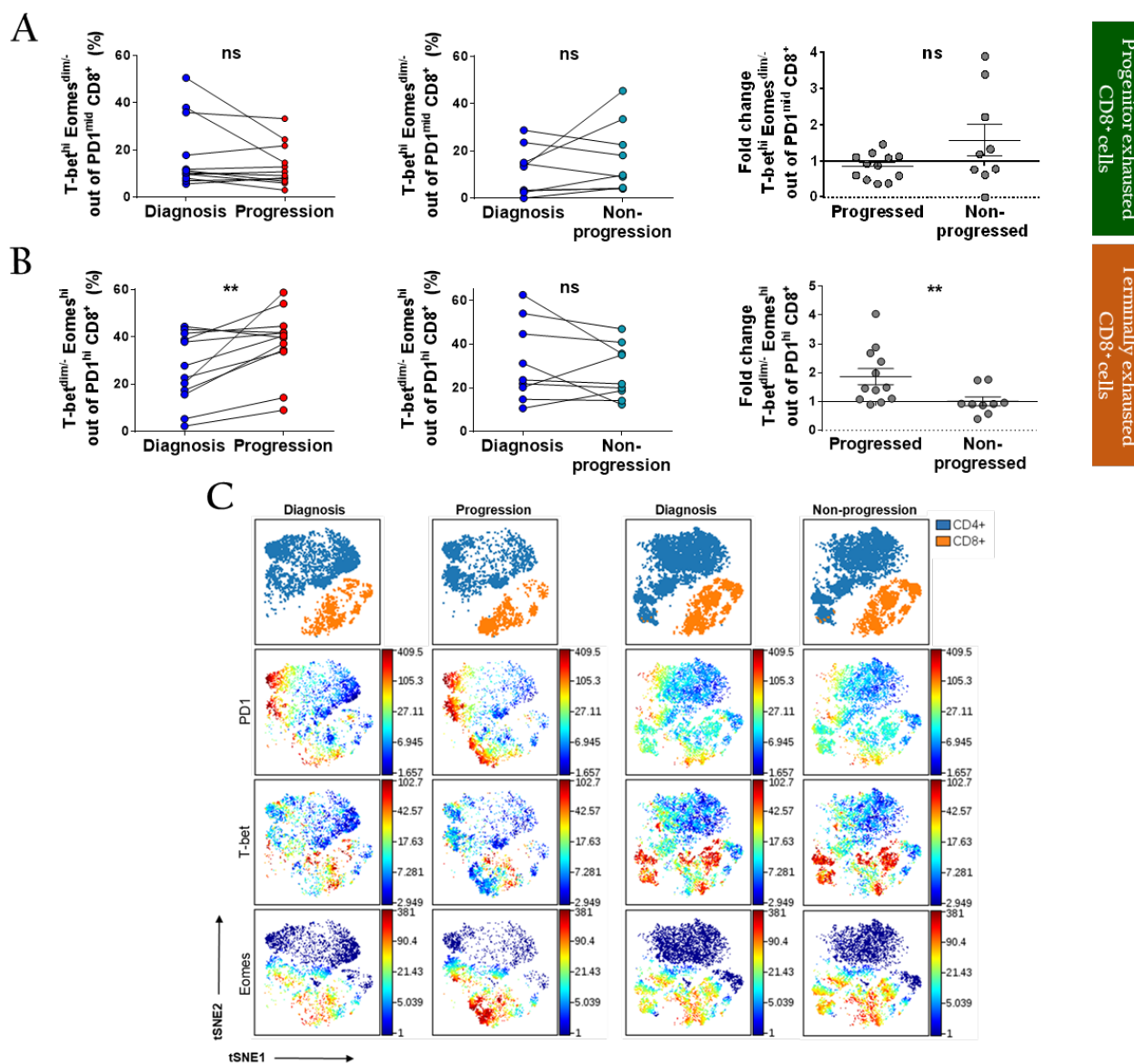


Figure 26. Progenitor (T-bet^{hi}Eomes^{dim/-}/PD-1^{mid}) and terminally (T-bet^{dim/-}/Eomes^{hi}PD-1^{hi}) exhausted CD8⁺ T cells in progressing and non-progressing CLL patients. (A) Percentages of T-bet^{hi}Eomes^{dim/-} out of PD-1^{mid}CD8⁺ cells and (B) T-bet^{dim/-}/Eomes^{hi} out of PD-1^{hi}CD8⁺ cells in progressing (left, n=12) and non-progressing patients (middle, n=9) at diagnosis and progression or non-progression. Fold change between time points of both subsets comparing progressing and non-progressing patients (right). (C) Representative viSNE plots of PD-1, T-bet and Eomes expression in CD4⁺ and CD8⁺ T cells at the two time points from one representative patient from each group. Graphs show mean ± SEM or paired values. P value was calculated by Wilcoxon matched paired test or Mann-Whitney test. **P<0.01

5.4. T cells acquire a distinct transcriptional profile at CLL progression

In CLL, T cells have a different gene expression profile compared to healthy T cells affecting genes involved in differentiation and cytoskeleton formation (207). In order to broadly characterize the alterations that occur over time in T-CLL cells related to clinical progression, we performed RNA-Seq of isolated T cells from paired samples at the two time points (n=13 progressors and 6 non-progressors; mean purity of 92%). After selecting uniquely mapped reads, the hierarchical clustering analysis of paired samples from progressing patients defined two main clusters: one corresponding exclusively to T cells at progression and another one to T cells at diagnosis plus two samples at progression, highlighting that the transcriptional profile of T cells at progression was clearly distinct from that of T cells at diagnosis (**Figure 27**). A total of 80 genes (including protein coding and lncRNA transcripts) were significantly up or downregulated in T cells from diagnosis to progression, while in contrast only 3 genes were differentially expressed in T cells from non-progressed patients at the time of follow-up (all genes $p_{adj} < 0.05$ are detailed in **Table 14**). Moreover, those 3 differentially expressed genes found in non-progressing patients were also found at progression. Briefly, the transcriptional profile of T cells at progression suggests lower mobility and differentiation capacity as well as an impairment in mitochondrial oxidative phosphorylation (**Table 15**), essential processes for the maintenance of T-cell effector functions (344). Additionally, genes related to fatty acids and amino acids catabolism and glucose transporters were upregulated, while lower levels of genes related to the synthesis of cellular components and RNA processing mechanisms were identified at progression, suggesting a potentially dysregulated T-cell metabolism. T cells at progression also showed an upregulation of genes associated with immune response and known to be expressed during exhaustion (345–347). Collectively, these results point towards an impaired cytoskeleton formation, mitochondrial metabolism and immune dysregulation, consistent with the exhausted and dysfunctional status of T cells that is aggravated at CLL progression.

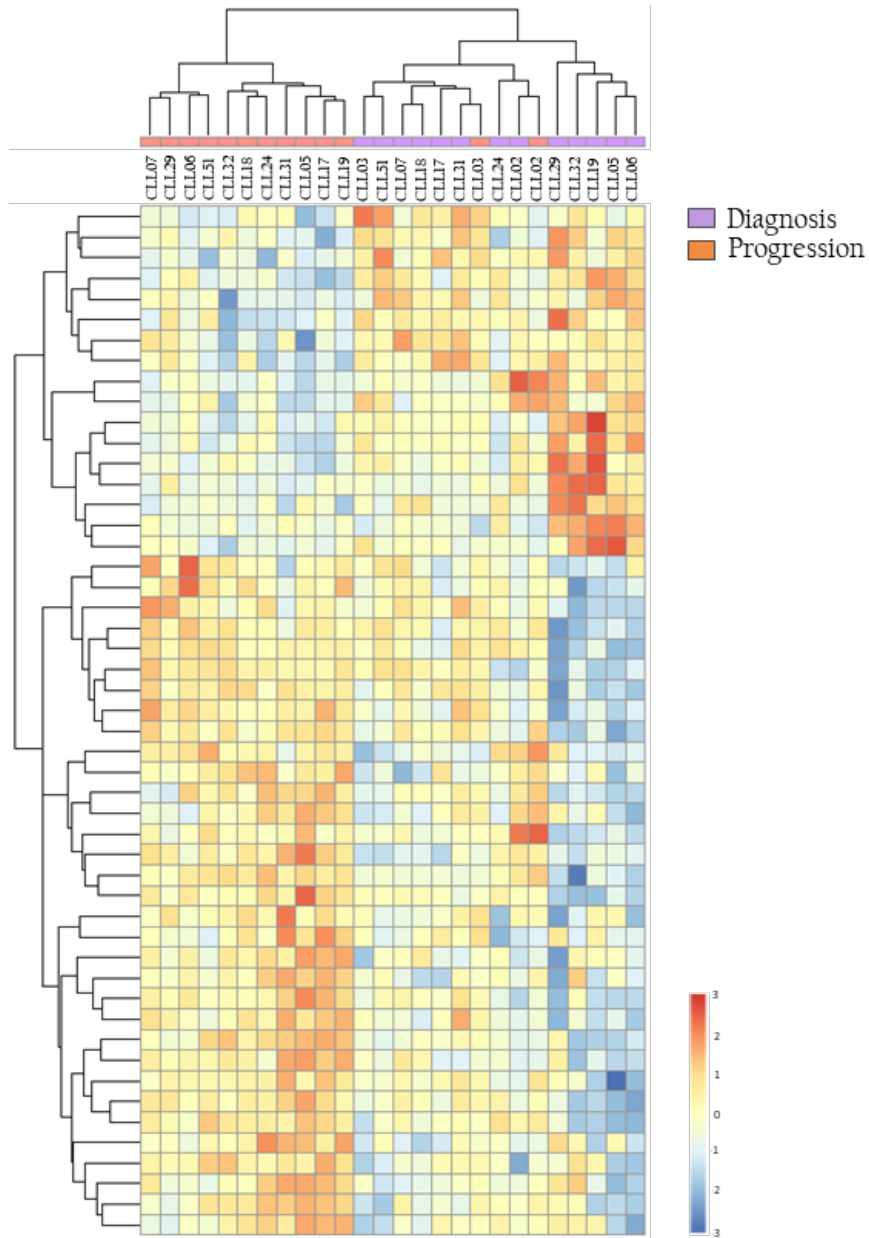


Figure 27. RNA-Seq of T cells from progressing CLL patients. Heatmap showing the top-50 differentially expressed genes from paired sorted T cells at diagnosis and progression (n=13).

TIME in B-cell lymphoid malignancies

Diagnosis vs Progression	baseMean	log2FoldChange	shrunkenlfc	lfcSE	stat	pvalue	padj
ENSG00000184956.15, MUC 6, protein_coding	86,73066	-1.682417518	-1.2709809	0,334092	-5,03579	4,76E-07	0,000444
ENSG00000095066.11, HOOK2, protein_coding	1527,367	1,24951998	0,97686632	0,249453	5,009048	5,47E-07	0,000444
ENSG00000142039.3, C, C, C, C, 97, protein_coding	118,2865	-1,103992671	-0,954436	0,221672	-4,98029	6,35E-07	0,000444
ENSG00000059804.15, SLC 2A3, protein_coding	27,08992	1,89062246	0,9816954	0,249303	4,769539	1,85E-06	0,000876
ENSG00000117481.10, NSUN 4, protein_coding	33,0124	1,26409343	0,90142993	0,240873	4,676368	2,92E-06	0,001079
ENSG00000178460.17, MCMDC 2, protein_coding	23,35057	1,357258253	1,01386956	0,29094	4,665088	3,08E-06	0,001079
ENSG00000161013.16, MGAT 4B, protein_coding	44,10828	-0,951564185	-0,8382207	0,206966	-4,59768	4,27E-06	0,001329
ENSG00000106246.17, PT CD1, protein_coding	141,1329	0,96241424	0,7954825	0,222138	4,332506	1,47E-05	0,004126
ENSG00000183508.4, FAM46C, protein_coding	34,76904	1,214141816	0,88565381	0,286273	4,241198	2,22E-05	0,004445
ENSG0000011077.17, TNS2, protein_coding	27,68712	-0,94279822	-0,8074451	0,220718	-4,2715	1,94E-05	0,004445
ENSG00000259807.1, RP11-426C22.4, lincRNA	175,3101	-0,941793244	-0,8257919	0,220722	-4,26687	1,98E-05	0,004445
ENSG00000164099.3, PRSS12, protein_coding	45,85069	1,098301058	0,85435139	0,260063	4,223204	2,41E-05	0,004494
ENSG00000180098.9, T RNAU 14P, protein_coding	34,21435	1,165535362	0,91194697	0,278905	4,178964	2,93E-05	0,004822
ENSG0000013369.8, ARRC3, protein_coding	26,40323	1,227380321	0,88276605	0,30518	4,021821	5,77E-05	0,008507
ENSG00000099974.18, PT RH2, protein_coding	6154998	-0,959389028	-0,872199	0,240078	-3,99615	6,44E-05	0,008581
ENSG00000163082.9, SGPP2, protein_coding	28,67321	-1,018961307	-0,794621	0,259185	-3,9314	8,45E-05	0,010745
ENSG00000021571.5, T MEM 167B, protein_coding	24,66937	1,019795824	0,81275082	0,26083	3,909816	9,24E-05	0,010747
ENSG00000125740.13, FOSB, protein_coding	397,5613	0,874626276	0,734854	0,224234	3,900507	9,60E-05	0,010747
ENSG00000079333.19, CDC 14A, protein_coding	20,84034	1,064745154	0,81416143	0,277492	3,837026	0,000125	0,012168
ENSG00000129696.12, C8orf41, protein_coding	294,9043	-0,915325449	-0,8440771	0,23826	-3,84171	0,000122	0,012168
ENSG00000099219.18, ERMP1, protein_coding	42,07987	-0,955167927	-0,7620164	0,249575	-3,82717	0,000133	0,012168
ENSG00000033170.16, FUT 8, protein_coding	18,82688	1,156667447	0,84305874	0,302783	3,820125	0,000133	0,012168
ENSG00000103014.3, CABP7, protein_coding	24,50633	1,248220655	0,78769475	0,326966	3,817588	0,000135	0,012168
ENSG00000105982.16, RN F32, protein_coding	68,23536	-0,661863151	-0,6045838	0,173794	-3,80831	0,00014	0,012329
ENSG00000197912.15, SPG7, protein_coding	35,13742	-0,860761241	-0,7519604	0,227023	-3,79152	0,00015	0,012326
ENSG00000174243.19, DDX 23, protein_coding	28,82073	-0,973962045	-0,8432773	0,258239	-3,77155	0,000162	0,012768
ENSG00000006607.13, FARP2, protein_coding	17,2973	-1,100001656	-0,8419213	0,298831	-3,68101	0,000232	0,016673
ENSG00000177606.6, JUN, protein_coding	268,4259	1,084799967	0,78367051	0,298491	3,63428	0,000279	0,01858
ENSG0000015498.11, ACAD8, protein_coding	100,4411	0,83368015	0,7045381	0,228922	3,641767	0,000271	0,01858
ENSG00000158062.20, UBXN 11, protein_coding	336,9921	1,196496578	0,73521042	0,331518	3,609142	0,000307	0,019543
ENSG00000103249.17, CLCN 7, protein_coding	28,54769	-1,082770478	-0,9330998	0,301999	-3,58534	0,000337	0,020857
ENSG00000131400.7, NAPA5, protein_coding	35,74809	0,912464907	0,7501332	0,254834	3,580621	0,000343	0,020857
ENSG00000188177.13, ZC3H6, protein_coding	36,05083	0,860558165	0,69256134	0,241101	3,569288	0,000358	0,020914
ENSG00000099974.17, DDT 1, protein_coding	44,19627	1,280187889	0,7032431	0,358719	3,568775	0,000359	0,020914
ENSG00000109118.13, PHF 12, protein_coding	30,94286	1,000173527	0,7294076	0,281005	3,559277	0,000372	0,021243
ENSG00000084092.6, NOA1, protein_coding	25,72007	0,903834462	0,71776304	0,255312	3,54019	0,0004	0,02195
ENSG00000171307.13, ZDHHC 16, protein_coding	20,4644	-0,802608916	-0,6802265	0,227226	-3,53221	0,000412	0,022182
ENSG0000017620.14, SLC 35A3, protein_coding	133,8784	1,070462537	0,7021827	0,304088	3,520236	0,000431	0,02277
ENSG00000111087.9, GLI1, protein_coding	49,62292	0,817254137	0,6569927	0,233495	3,500097	0,000465	0,024107
ENSG00000087074.7, PPP1R15A, protein_coding	192,6129	0,765563027	0,64242164	0,220215	3,47644	0,000508	0,024962
ENSG00000053438.8, NNAT, protein_coding	22,99512	-0,760501665	-0,6676001	0,218766	-3,47632	0,000508	0,024962
ENSG00000167964.12, RAB26, protein_coding	21,77421	1,04711048	0,7501369	0,302089	3,466237	0,000528	0,025233
ENSG00000186352.8, ANKRD37, protein_coding	26,4412	0,848696944	0,67873579	0,246804	3,438746	0,000584	0,026141
ENSG00000110367.11, DDX 6, protein_coding	48,09615	0,862406716	0,67983452	0,250925	3,436912	0,000588	0,026141
ENSG00000278743.1, RP11-707G18.1, lincRNA	3182543	0,923405144	0,73611808	0,267655	3,449989	0,000561	0,026141
ENSG00000215790.1, SLC 35E2, protein_coding	15,5086	1,150807868	0,70564513	0,337631	3,408475	0,000653	0,027707
ENSG00000111087.9, CAPZA1, protein_coding	61,04183	0,765823342	0,62963262	0,225074	3,40254	0,000668	0,027891
ENSG00000173080.5, RXFP4, protein_coding	51,28045	-0,894713245	-0,70442	0,263435	-3,39633	0,000683	0,028069
ENSG00000230262.6, MIRLET 7DHG, lincRNA	60,85104	0,710721056	0,61045357	0,209482	3,392747	0,000692	0,028069
ENSG00000184620.12, BRX 1, protein_coding	64,8372	0,961874146	0,66596867	0,284793	3,377453	0,000732	0,028761
ENSG00000164754.14, RAD21, protein_coding	108,3293	-0,69603875	-0,6496673	0,207178	-3,35961	0,000781	0,028761
ENSG00000056558.10, T RAF 1, protein_coding	67,86126	1,199633088	0,81780027	0,356719	3,362959	0,000771	0,028761
ENSG00000166105.15, GLBL 3, protein_coding	68,43628	0,770171304	0,65888228	0,229254	3,359468	0,000781	0,028761
ENSG00000187109.13, NAP 1L, protein_coding	27,87156	0,90785584	0,6959513	0,269028	3,374574	0,000739	0,028761
ENSG00000162783.10, IER5, protein_coding	79,92687	0,910651534	0,67956933	0,272717	3,339181	0,00084	0,030152
ENSG00000149476.15, TKFC, protein_coding	70,70571	0,857350007	0,70674951	0,256573	3,341545	0,000833	0,030152
ENSG00000181350.11, LRRC 75A, protein_coding	275,9754	0,792304887	0,61147946	0,240658	3,292249	0,000994	0,034668
ENSG000000247595.4, RP11-504G3.1, protein_coding	56,24375	0,99173488	0,61730646	0,302703	3,276261	0,001052	0,035163
ENSG000000283199.2, ABC 13-47488600E17.1, protein_coding	1073,99	-1,028673055	-0,916823	0,313937	-3,27668	0,00105	0,035163
ENSG00000100979.14, PLTP, protein_coding	19,42708	1,17488095	0,71682881	0,359499	3,275362	0,001055	0,035163
ENSG00000170345.9, FOS, protein_coding	4719704	0,694693934	0,58871417	0,213581	3,252609	0,001144	0,037217
ENSG00000126453.9, BCL2L 12, protein_coding	198,8922	-0,864586991	-0,7984692	0,266403	-3,24541	0,001173	0,037646
ENSG00000120129.5, DUSP 1, protein_coding	44,73206	0,701270051	0,62613747	0,218809	3,204947	0,001351	0,039801
ENSG00000157593.18, SLC 35B2, protein_coding	98,83206	0,872557039	0,63882531	0,271758	3,21079	0,001324	0,039801
ENSG00000245164.6, RP11-622011.2, lincRNA	157,836	0,815913235	0,67078952	0,254248	3,209121	0,001331	0,039801
ENSG00000171223.12, JUNB, protein_coding	54,59044	0,705431217	0,59759273	0,219092	3,219798	0,001283	0,039801
ENSG00000175183.9, CSRP2, protein_coding	34,81189	-0,897009375	-0,6843491	0,281175	-3,19021	0,001422	0,041195
ENSG00000267232.1, CTB-31020.9, lincRNA	18,56216	1,199541382	0,70595056	0,375465	3,194819	0,001399	0,041195
ENSG00000136527.17, T RA2B, protein_coding	20,82036	0,832277632	0,65420841	0,262092	3,175517	0,001496	0,041044
ENSG00000120539.14, MASTL, protein_coding	166,4097	0,846397733	0,68308019	0,266098	3,180769	0,001469	0,041044
ENSG00000074319.12, TSG 101, protein_coding	32,64556	0,871858853	0,66094686	0,274894	3,17621	0,00156	0,041994
ENSG00000203772.7, SPRN, protein_coding	48,31507	-0,690342864	-0,6182646	0,218271	-3,16279	0,001563	0,042057
ENSG00000067082.14, KLF6, protein_coding	51,65126	0,740459175	0,6005021	0,234818	3,153335	0,001614	0,042623
ENSG00000099834.13, CDHR5, protein_coding	19,69995	-0,841289172	-0,716262	0,269653	-3,11989	0,001809	0,045438
ENSG00000103522.15, IL2R, protein_coding	49,239	0,88385105	0,6474824	0,28359	3,11655	0,001829	0,045438
ENSG00000146872.17, TLK2, protein_coding	15,47873	0,98505459	0,70290646	0,320318	3,075235	0,002103	0,049053
ENSG00000167895.14, TMC 8, protein_coding	74,81656	-0,737498217	-0,6717746	0,239226	-3,08285	0,00205	0,049053
ENSG00000142168.14, SOD1, protein_coding	15,36195	0,825718228	0,65651401	0,268761	3,072312	0,002124	0,049053
ENSG00000161981.10, SNRN P25, protein_coding	20,05179	-0,735553427	-0,621398	0,240064	-3,06399	0,002184	0,0491
ENSG00000255302.4, EID1, protein_coding	48,22591	-0,657607124	-0,595301	0,214854	-3,06072	0,002208	0,049841
Diagnosis vs Non-progression							
ENSG00000283199.2, ABC 13-47488600E17.1, protein_coding	1357,476	-1,277594877	-1,1176126	0,309459	-4,12848	3,65E-05	0,030437
ENSG00000158062.20, UBXN 11, protein_coding	365,2557	1,049254268	0,89529413	0,279687	3,751525	0,000176	0,045487
ENSG00000284526.1, RP11-666A8.13, protein_coding	340,5875	1,128409666	0,9245339	0,298199	3,784077	0,000154	0,045487

Table 14. Differentially expressed genes in T-CLL cells. Data analysis was performed as detailed in Materials & Methods.

Gene	Function
UBXN1 CDC14A HOOK2	Actine, microtubule and Rho-GTPase binding proteins
NOA1	Synthesis of nitric oxide
ADAC8 NAPSA FUT8 PRSSI2	Fatty acids and amino acids catabolism
SLC2A3/GLUT3 SLC35A3	Glucose transporters
PTCD1 NSUN4	RNA processing mechanisms
FOSB JUN PRSSI2 FAM46C NAPSA	Immune response and exhaustion
TNS2 FARP2	Adhesion molecules
SPG7 C8orf41 DDX23 ERMPI	Maintenance of OXPHOS
SGPP2 MGAT4B	Synthesis of cellular components
DDX23	RNA processing mechanisms

Table 15. Highlighted dysregulated genes in T-CLL cells at progression. Up-regulated genes (red); down-regulated genes (green).

5.5. PD-1 expression in CD8⁺ T cells is induced by malignant cells via soluble factors including IL-10

In order to gain insight into the functional mechanisms that could trigger the increased exhausted condition observed in CD8⁺ T cells at progression, we co-cultured T cells from patients with CLL (T-CLL) with increasing ratios of either healthy B cells (B-HD) or autologous B-CLL cells at progression and non-progression. We found that PD-1 expression was increased in CD8⁺ T cells in the presence of progressed B-CLL cells at any T to leukemic-cell ratio, while B-HD cells did not induce changes in PD-1 expression (Figure 28A, left). B-CLL cells from non-progressors were also able to induce higher PD-1 levels in autologous CD8⁺ T cells, but only at the highest T to B-cell ratio (Figure 28A, right). This supports that this mechanism is not only dependent on leukemic burden, but intrinsic features of malignant B cells from progressing patients that can contribute to T-cell exhaustion. And by co-culturing T cells from healthy donors (T-HD) with both types of malignant cells we found that progressed B-CLL cells were capable of inducing PD-1 expression even in healthy CD8⁺ T cells whereas non-progressed B-CLL cells were not (Figure 28B). These results indicate that malignant cells at progression are intrinsically more capable of inducing PD-1 expression in both autologous and HD-derived T cells. In addition, CD8⁺ T cells expanded *in vitro* under the influence of leukemic cells showed features of severe exhaustion as denoted by their co-expression of PD-1 and CD244 (Figure 28C). Co-expression of these markers was also induced, but at lower levels, in healthy CD8⁺ T cells co-cultured with leukemic cells at the highest T to B-CLL ratio (Figure 28D), evidencing that T-CLL cells are more predisposed to exhaustion.

Soluble factors play an important role in shaping CLL immune microenvironment (348). To investigate whether the T-cell state induced by CLL cells occurs through a cell-to-cell mediated mechanism or, otherwise, is mediated by soluble factors, T-CLL and B-CLL co-cultures were performed with transwells. We observed that the induction of PD-1 in CD8⁺ T cells was

equivalent when there was no contact between autologous T cells and leukemic cells (**Figure 28E**), suggesting that secretion of soluble factors lead to upregulation of PD-1. CLL cells are known to exhibit features of regulatory B cells, such as IL-10 production (231). Moreover, it has been described that high-expressing-PD-1 tumor infiltrating lymphocytes (TILs) when expanded *in vitro* rapidly re-express high levels of PD-1 after exposure to IL-10 (42). Accordingly, we measured the levels of IL-10 in paired plasma samples from CLL patients and found that plasmatic IL-10 significantly increased at progression while remaining stable over time in non-progressing patients (**Figure 29A**). IL-10 in plasma did not correlate with whole blood count (not shown) and, therefore, higher plasmatic levels at the time of progression are not a consequence of higher tumoral load. To investigate whether malignant cells acquire an increased capacity to produce IL-10 at progression, we assessed the production of IL-10 by CLL cells *in vitro* after microenvironmental stimuli. We detected an increased frequency of IL-10⁺ CLL cells only at progression (**Figure 29B and 29C**), indicating that progressing leukemic cells have indeed increased their immunosuppressive potential. Moreover, the induction of PD-1 expression in CD8⁺ T cells was partially blocked after IL-10 neutralization (**Figure 29D**), supporting the contribution of this cytokine to progression from early stages. IL-10 can also be secreted by other cell types such as MDSCs which can facilitate tumor progression by suppressing T-cell immunity against tumors (349). The analysis of MDSCs by flow cytometry showed an accumulation of these cells over time in CLL patients regardless of their clinical status, although the increment of this population was higher in progressing patients (**Figure 29E**).

These observations indicate that the increased load of leukemic cells at the time of progression is accompanied by an enhanced capacity of IL-10 production in CLL cells. This likely promotes engaging in a positive feed-back system that would increase the CD8⁺ T-cell exhaustion status we have observed at progression.

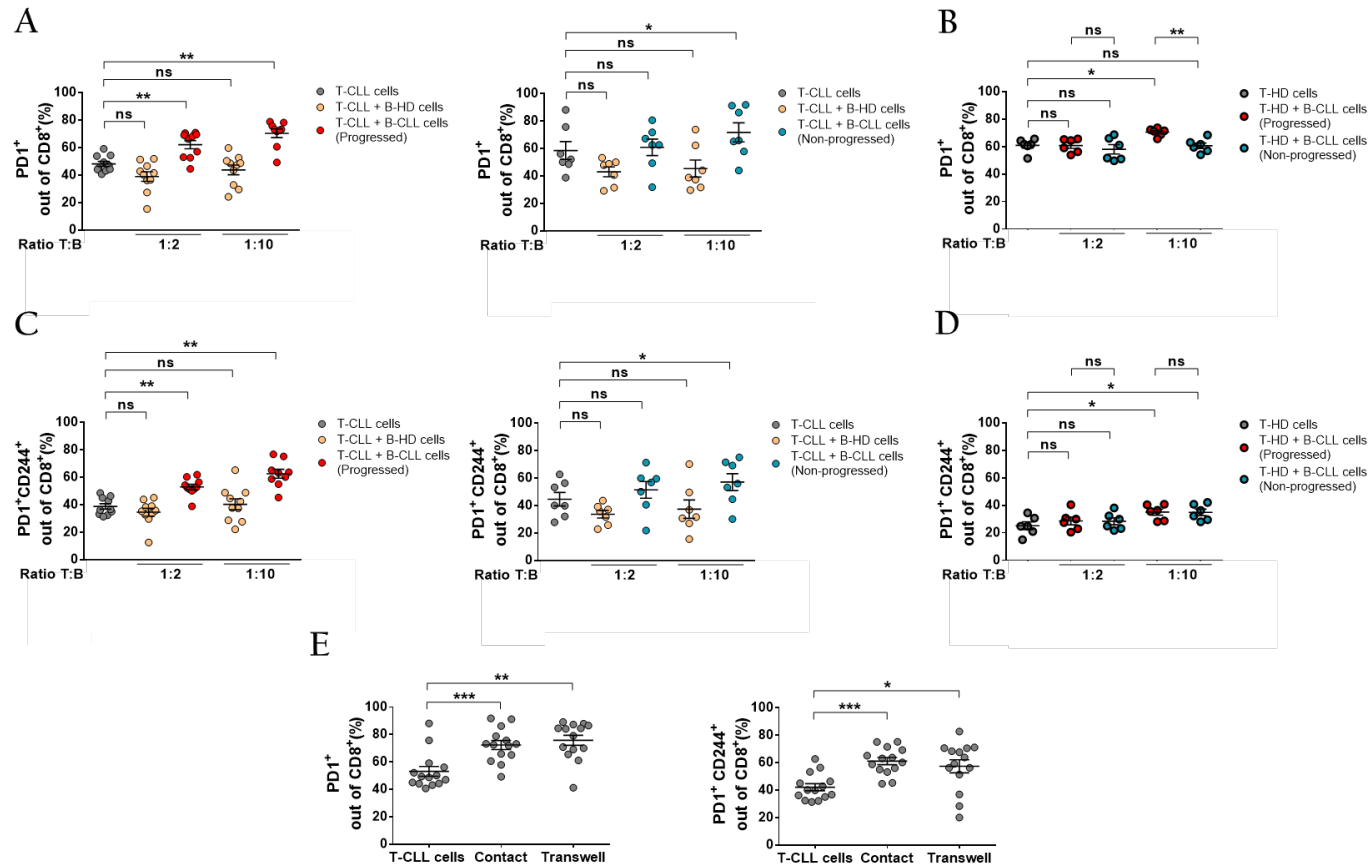


Figure 28. PD1 and CD244 expression in CD8⁺ T cells after co-culture with B-HD cells or B-CLL cells. (A) PD1 expression and (C) co-expression with CD244 in CD8⁺ T cells and from progressing (left, n=10) and non-progressing (right, n=7) CLL patients alone or in presence of B-HD cells or B-CLL cells at the time of progression or non-progression at the indicated T:B ratios. (B) PD1 expression and (D) co-expression with CD244 in CD8⁺ T cells from HD (n=6) alone or in presence of B-CLL cells at progression or non-progression at the indicated T:B ratios. (E) Percentages of PD1⁺CD8⁺ T cells (left) and CD244⁺PD1⁺ out of CD8⁺ T cells (right) from CLL patients in co-cultures performed with transwells at 1:10 T:B ratio (n=14). Co-cultures in (A) (B) and (C) were stimulated with anti-CD3 and anti-CD28 for 7 days. Mean±SEM or paired values; Wilcoxon matched paired test or Mann-Whitney test; *P<0.05; **P<0.01; ***P<0.001.

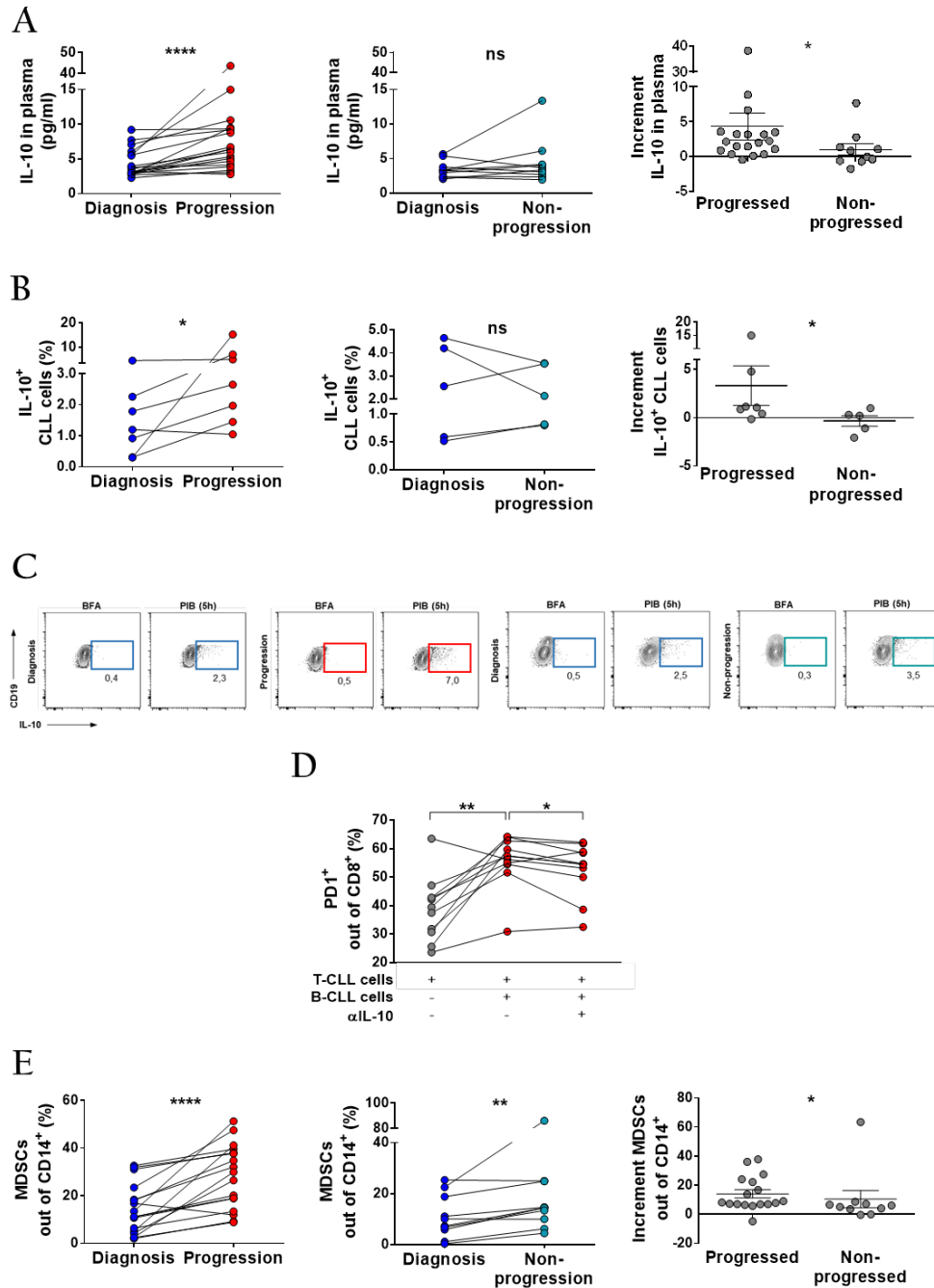


Figure 29. Contribution of soluble factors to progression. (A) Plasmatic IL-10 in progressors (n=19) and non-progressors (n=10) at diagnosis and progression or non-progression; increment between time points comparing progressors (n=19) and non-progressors (n=10). (B) Percentage of IL-10-producing CLL cells in progressors (n=7) and non-progressors (n=5) after the co-culture of paired PBMCs with UE6E7T-2 cells, CD40L and TLR9L for 48h; increment of IL-10-producing CLL cells between time points in progressors (n=7) and non-progressors (n=5). (C) Percentages of PD1⁺CD8⁺ T cells from CLL after co-culture with progressing B-CLL cells at 1:10 T:B ratio and anti-human IL-10 neutralizing antibody for 7 days (n=11). (D) Dot plots of IL-10⁺ B cells gated on CD19⁺CD5⁺ cells after 5 hours of leukocyte stimulation (PIB), or brefeldin A (BFA) as control, from one representative progressed and non-progressed patient. (E) Proportion of MDSCs (CD14⁺HLA-DR^{low/-}) out of CD14⁺ cells in progressing (left, n=17) and non-progressing patients (middle, n=10) at diagnosis and progression or non-progression. Increment of MDSCs between time points comparing progressing and non-progressing patients (right). Mean±SEM or paired values; Wilcoxon matched paired test or Mann-Whitney test; *P<0.05; **P<0.01; ****P<0.0001.

Part II - New therapeutic strategies in PCNSL
and immunomodulatory effects

5.6. DLBCL cell lines have equivalent sensitivity to selinexor regardless of their COO

ABC-DLBCL relies heavily on NF- κ B signaling and shows chronic BCR activation for the survival of malignant cells. ABC and GCB-DLBCL cases display a differential sensitivity to drugs targeting these pathways (350,351). Since increased expression of XPO1 has been related to resistance to chemotherapy and worse prognosis in different neoplasias (352), we studied the potential relationship between expression of XPO1 and sensitivity to selinexor in DLBCL cell lines. Although mRNA expression of XPO1 was significantly higher in ABC-DLBCL cell lines (Figure 30A), we did not find differential *in vitro* sensitivity to selinexor according to the COO (Figure 30B and 30C). We also interrogated the available public data on gene expression of primary DLBCL cases (353) and we did not observe any association between the COO and expression of XPO1 (Figure 30D).

5.7. Selinexor blocks tumor growth and prolongs survival in a orthotopic mouse model of PCNSL

We next assessed the role of XPO1 inhibition in PCNSL using an intracerebral orthotopic xenograft murine model. This model was established by the stereotactic injection of the luciferase-expressing OCI-Ly10 cell line into the cerebral parenchyma of nude athymic mice. We chose this cell line because it derives from a patient diagnosed with ABC-DLBCL and harbors alterations frequently found in PCNSL (354). This includes mutations in *MYD88* (L265P) and *CD79A* (c. 4275_4316del) (355) (further verified in house). Moreover, OCI-Ly10 cells have been used successfully for PCNSL pre-clinical studies using xenograft models in athymic mice (355). Tumor growth was monitored by bioluminescence measurement using IVIS Spectrum.

Eleven days after the injection of cells all animals had developed detectable tumors restricted to the CNS. Then, they were randomly distributed into treatment or vehicle experimental groups (vehicle: n=8, mean radiance= $1.16 \cdot 10^7$ ph/s \pm $0.615 \cdot 10^7$; treatment: n=9, mean radiance= $2.32 \cdot 10^7$ ph/s \pm $1.86 \cdot 10^7$) and dosed with 5 mg/kg of selinexor or vehicle via oral gavage three times a week. Doses were selected based on previous pre-clinical data in mouse models of different neoplasias (356). Bioluminescence was assessed twice a week in order to non-invasively monitor the tumor growth (Figure 30E). We observed a significantly slower increase in the bioluminescence signal in mice treated with selinexor (two-way ANOVA: P=0.0002; Figure 30F). Therefore, the drug was able to slow down the tumor growth. The differences in tumor growth were significant as soon as 12 days after the first dose (or day 23 after injection; mean radiance: vehicle $2.61 \cdot 10^8$ ph/s \pm $8.64 \cdot 10^7$ vs. selinexor $3.73 \cdot 10^7$ ph/s \pm $1.9 \cdot 10^7$; P=0.011) and peaked at day 20 after treatment (or day 31 after injection; mean radiance: vehicle $8.98 \cdot 10^8$ ph/s \pm $3.13 \cdot 10^8$ vs. selinexor $1.19 \cdot 10^8$ ph/s \pm $5.58 \cdot 10^7$; P=0.0037; Figure 30F). Representative cases are depicted in Figure 30H. The blockade of intracerebral lymphoma growth induced by selinexor led to a significant increase in the survival of mice (median survival: vehicle 34 days and selinexor 48 days; P<0.0001; Figure 30G).

Histopathological analysis at the final time-point showed multifocal and infiltrative tumors affecting the cerebral parenchyma and meninges of both hemispheres. Tumor cells were highly proliferative (100% Ki-67⁺) and CD20-positive. They tended to accumulate in the perivascular area resembling the histology of human PCNSLs. Although the injection of cells was performed in the right hemisphere, tumor infiltration was equally observed in both hemispheres. Moreover, we did not observe variations in the intensity of CD20 among mice or within different areas of the same brain. Representative cases are shown in **Figure 30I** and **Figure 3I**.

TIME in B-cell lymphoid malignancies

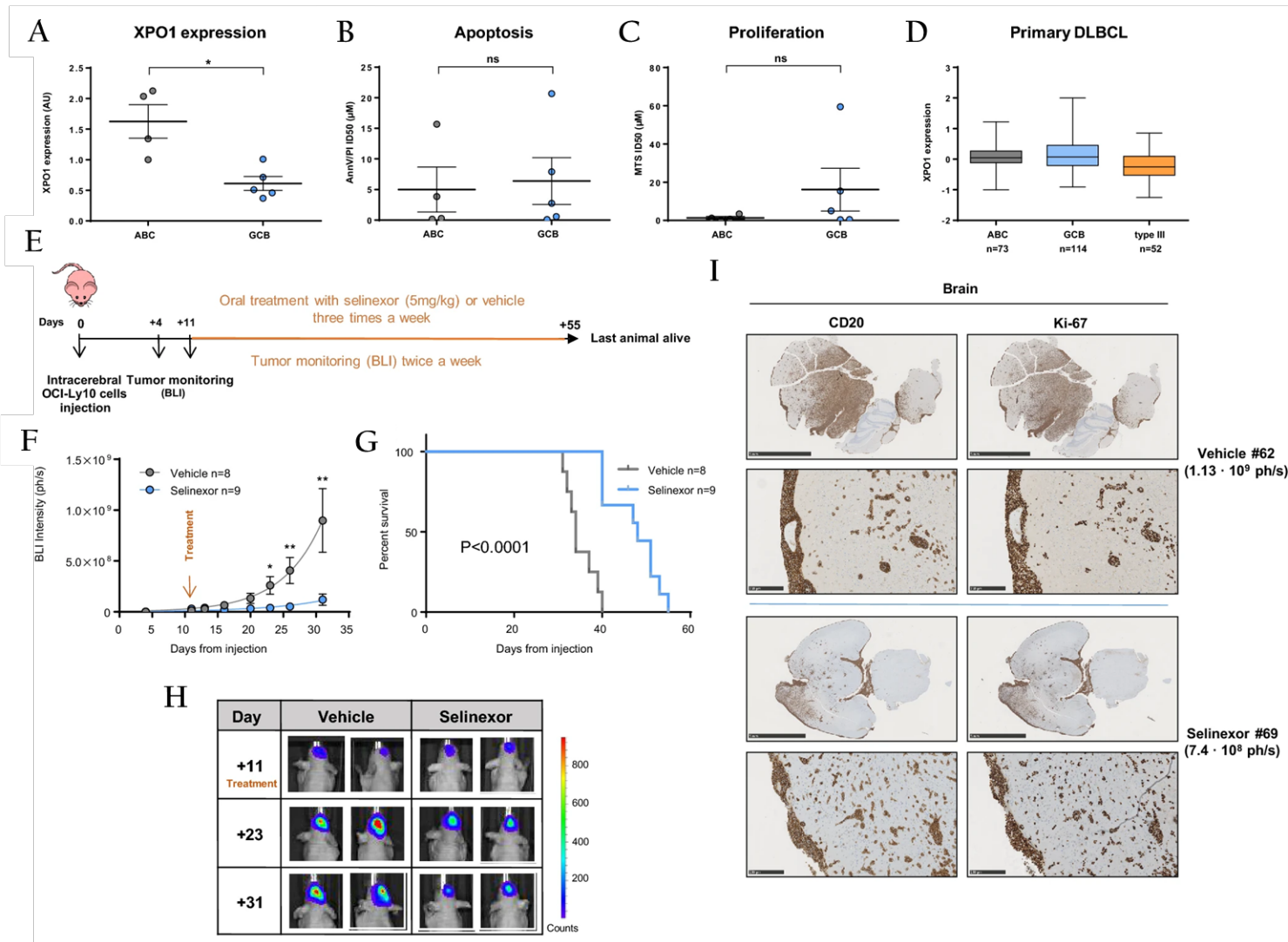


Figure 30. *In vitro* and *in vivo* effects of selinexor in PCNSL models. (A) XPO1 relative expression by qRT-PCR. Cells were treated with increasing doses of selinexor or vehicle (1% DMSO) for 96h. Viability and proliferation was determined by (B) Annexin-V-PI exclusion or (C) MTS method. (D) Relative XPO1 expression in DLBCL patients. (E) Scheme representing mice treatment and monitoring. (F) Tumor size measured by BLI in mice treated with vehicle (n=8) or selinexor (n=9). Data are shown until day 31 (last day when all animals were still alive). Two-way ANOVA analysis (P=0.0002). Asterisks indicate the result of Mann-Whitney test at different time points. *P<0,05; **P<0,01; ***P<0,001. Graphs show mean ± SEM. (G) Survival curves and (H) representative BLI images of tumors. (I) IHC analysis showing the expression of CD20 and Ki-67 in the brain parenchyma and meninges from a representative mouse of each group. Bars represent 5mm in top panels and 250µm in bottom panels.

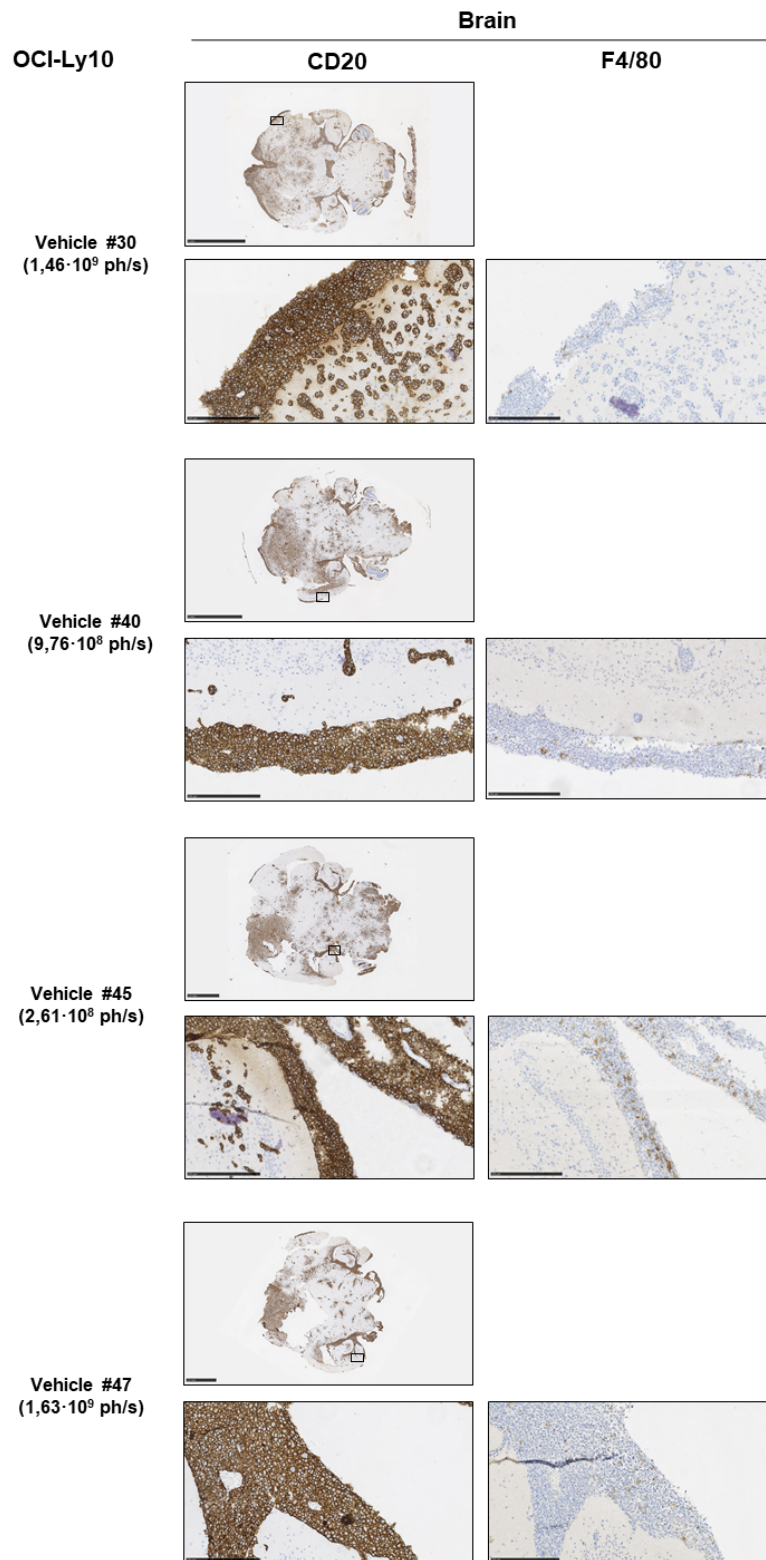


Figure 31. IHC of the brain from representative OCI-Ly10 PCNSL mice. Representative IHC images from brains obtained from 4 nude athymic mice inoculated with OCI-Ly10 cells (24 days after injection). Bars represent 2.5mm in whole brain images and 250 μ m in zoomed in images.

5.8. The combination of selinexor and ibrutinib synergizes *in vitro* in DLBCL cell lines and increases the survival of mice with CNS lymphoma

The high frequency of molecular alterations in components of the BCR pathway can explain the response to BCR inhibitors in PCNSL to some extent. R/R PCNSL patients receiving ibrutinib as monotherapy achieve higher response rates compared to systemic DLBCL patients. Nonetheless, the response is brief (292,293). SINE compounds are able to inhibit the BCR signaling. In primary CLL cells, selinexor inhibits the BCR pathway by downregulating the expression of BTK via enforced I κ B nuclear retention (357) and shows *in vitro* synergism with ibrutinib (358). We also observed reduced BCR signaling in OCI-Ly10 cells after selinexor and ibrutinib treatments (Figure 32A) as well as a reduced BTK expression after 48h of treatment with selinexor (Figure 32B). Accordingly, we hypothesized that combining XPO1 and BTK inhibition in PCNSL could have a synergistic therapeutic effect. To demonstrate this, we first treated a panel of cell lines *in vitro* with increasing doses of both drugs and analyzed apoptosis after 96h. In three out of four ABC-DLBCL cell lines we found a strong synergism between the two compounds (Figure 32C). In addition, the treatment with selinexor sensitized GCB-SUDHL4 cells to ibrutinib as was pointed out by the combination index (CI) values (Figure 32C, right panel).

We next sought to elucidate whether the synergy observed *in vitro* could be translated *in vivo*. For this, we used the mouse model described above. Eleven days after the intracerebral injection of lymphoma cells mice were distributed into the following groups and started therapy: selinexor monotherapy (5 mg/kg twice a week via oral gavage, n=12, mean radiance=3.95 \cdot 10⁶ ph/s), ibrutinib monotherapy (25 mg/kg daily in drinking water, n=9, mean radiance=1.02 \cdot 10⁷ ph/s), combination therapy (n=11, mean radiance =1.02 \cdot 10⁷ ph/s) and vehicle (n =9, mean radiance=3.21 \cdot 10⁶ ph/s). Selinexor dose was adjusted (from three times a week to twice a week) to prevent a potential

toxicity of the drug combination; and ibrutinib dose was chosen based on previous experience in CLL pre-clinical models (**Figure 33A**) (359). It has to be taken into account that ibrutinib is mainly metabolized by cytochrome P450 while selinexor is not. It seems unlikely that their co-administration could result in any effects on the exposure for the other drug (356). Compared to vehicle, all three treatment regimens induced an equivalent significant effect in the tumor growth kinetics in terms of decreased growth rate (**Figure 33B** and **33C**). Interestingly, the combination increased the survival of mice compared to vehicle. Single treatments with ibrutinib or selinexor did not exhibit differences. However, although the median survival of mice treated with the combinations increased up to 55 days the survival curve was not statistically different from mice treated with the individual drugs (median survival: vehicle 35 days vs. selinexor: 40 days, $P=0.001$; vehicle vs. ibrutinib, 43 days, $P=0.0005$; vehicle vs. combination, 55 days, $P=0.0001$; **Figure 33D**).

TIME in B-cell lymphoid malignancies

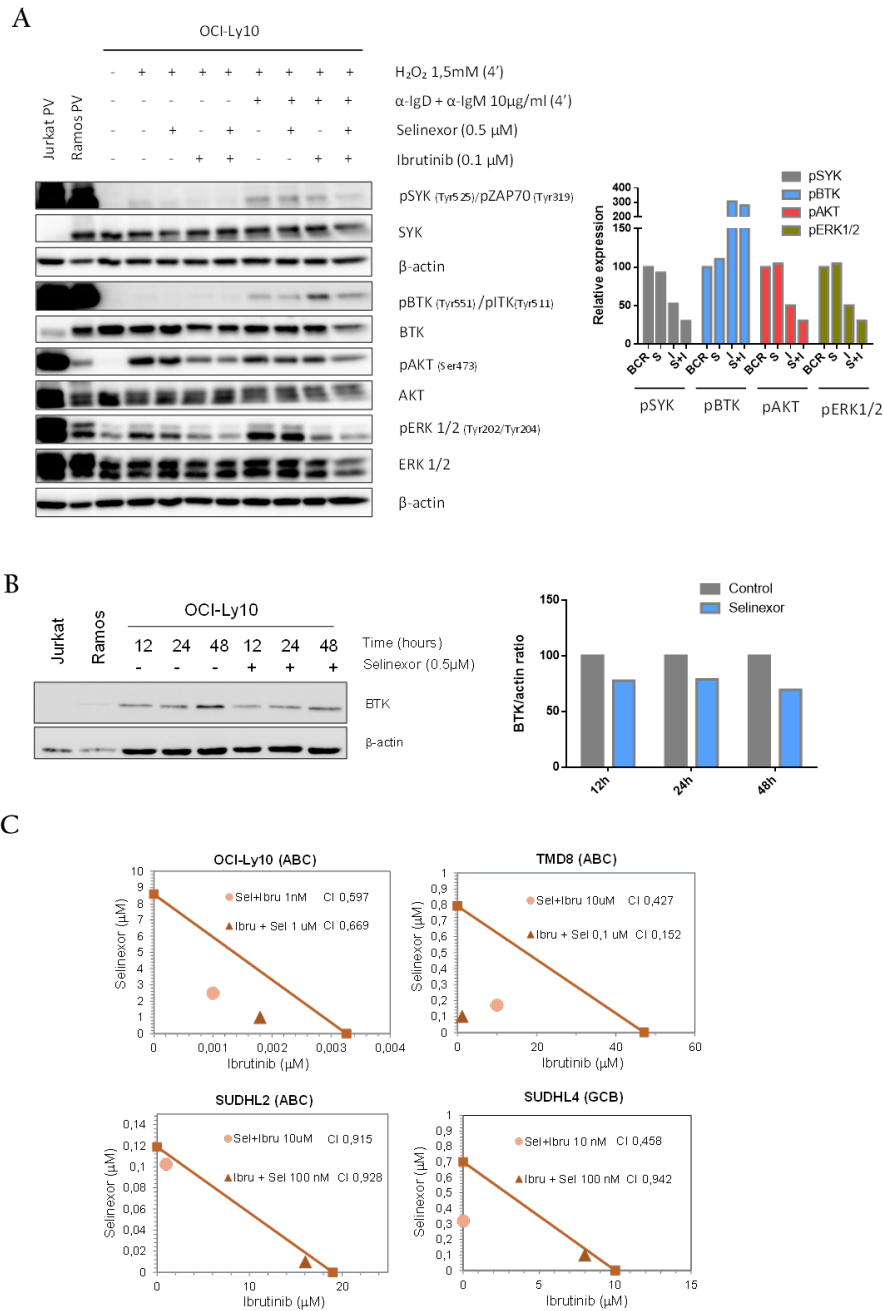


Figure 32. Treatment with selinexor and ibrutinib synergizes in DLBCL cell lines. (A) Phosphorylation of BTK, SYK, AKT and ERK1/2 was analyzed by Western Blot in OCI-Ly10 cells pre-treated with selinexor and/or ibrutinib for 1 hour and stimulated with anti-IgD and anti-IgM for 4 minutes. Quantification of bands is relative to cells stimulated with anti-IgD/IgM using total protein and loading control as calibration. **(B)** Immunoblot showing expression of BTK and β-actin proteins in OCI-Ly10 cells after 12, 24 and 48 hours of treatment with selinexor. Jurkat (T-cell lymphoblastic leukemia) and Ramos (Burkitt's lymphoma) cells were used as negative and positive controls for BTK expression, respectively. **(C)** Isobolograms showing the synergistic effect of combining selinexor and ibrutinib *in vitro*. The X axis shows ID50 of ibrutinib while the Y axis shows ID50 of selinexor as single treatments. ID50 of selinexor or ibrutinib alone (square) or combinations with the sub-ID50 concentration of the other drug (circle and triangle for selinexor and ibrutinib, respectively) are plotted. PV: pervanadate. S: selinexor. I: ibrutinib.

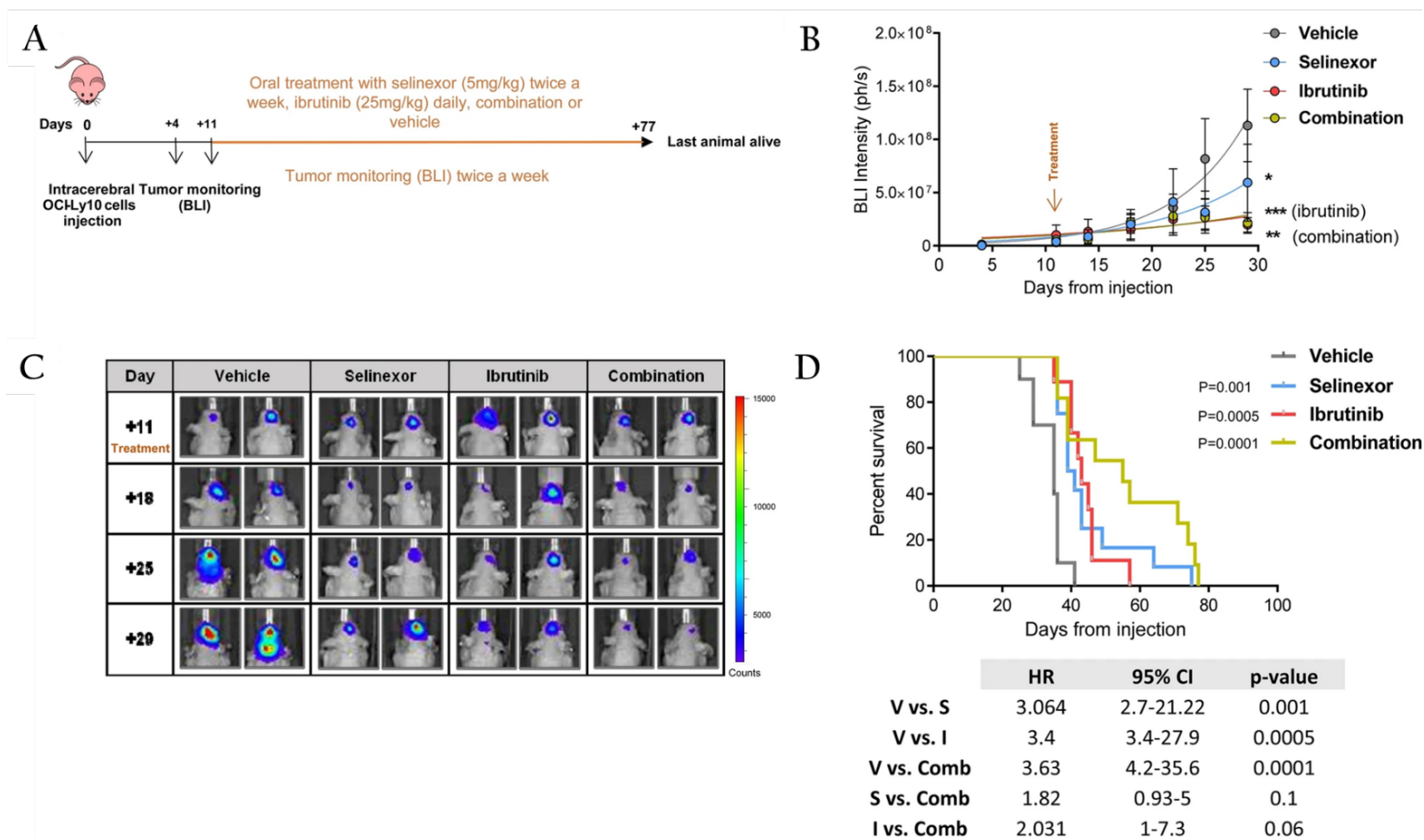


Figure 33. Treatment with selinexor and ibrutinib further increases survival of mice with CNS lymphoma. (A) Scheme representing mice treatment and monitoring. (B) Tumor size as measured by BLI intensity. Data are shown until day 29 (last day when all animals were still alive). * $P < 0.05$; ** $P < 0.01$; *** $P < 0.001$; Mann-Whitney test. Graphs show mean \pm SEM. (C) Representative BLI images in mice from each treatment arm. (D) Survival curves of mice from the four treatment groups. Survival curves were generated using the Kaplan and Meier method, and statistically compared by the log-rank test.

5.9. CNS lymphoma is infiltrated by M2-like macrophages expressing PD-1 and SIRP α

Analysis of the tumor-infiltrating immune microenvironment has shown that tumor cells in PCNSL are mainly accompanied by TAMs and, to a lesser extent, T cells. And this is associated with bad prognosis (298,299,302,360,361). Recently, TAMs in mouse and human colorectal cancer have been described to express the immune checkpoint PD-1 and recover their potential to phagocyte tumor cells after PD-1 blockade (29). To conduct an interactive study of infiltrating innate immune cells and tumor cells, we inoculated OCI-Ly10 cells into the brain parenchyma of nude athymic mice as described above. This model has been used to study the modulation of the innate immune response against PCNSL successfully in previous publications (294,355).

Accordingly, we harvested brains 24 days after the intracerebral injection of OCI-Ly10 cells and further processed the tissue for subsequent IHC and flow cytometry analysis. The histopathological analysis showed that tumors encompassing both cerebral hemispheres were infiltrated by macrophages expressing the surface glycoprotein F4/80, mainly in the meninges but also in the cerebral parenchyma. Notably, F4/80⁺ macrophages were completely absent in areas that were free of tumor cells as well as in healthy brains from control mice (**Figure 34A and Figure 31**). Iba-1 staining further identified microglial cells and TAMs showing an amoeboid morphology when interacting with tumor cells. This might indicate an activation status in macrophages (**Figure 34A**) (362). Macrophages can be polarized towards M1 or M2 phenotypes depending on stimuli from the microenvironment. In the TIME, macrophages generally exhibit a M2-like phenotype but M1 features can also be present in TAMs (22). Hence, we analyzed the proportion of M1 and M2 TAMs and the expression of immune checkpoints in brains from mice with PCNSL using flow cytometry (**Figure 34B**). We found that TAMs were evenly distributed between M1 and M2 phenotypes (**Figure 34C**). Notably, PD-1 expression was mainly found in the pro-tumoral M2 subset (**Figure 34D**). This suggests that a direct interaction between M2 macrophages and PCNSL cells triggers the up-regulation of PD-1. As described in colorectal cancer models (29), the phagocytic ability of PD1-expressing TAMs could also be impaired in

PCNSL. On the other hand, SIRP α in macrophages interacts with CD47 in malignant cells and hampers phagocytosis (33). Here, we observed that SIRP α was also preferentially expressed by M2 TAMs (Figure 34E), and the co-expression of PD-1 and SIRP α was higher in this subset (Figure 34F). These findings point towards an inhibition of the macrophage activity in CNS lymphomas.

In addition, we further analyzed the innate immune composition in an orthotopic xenograft model using PCNSL cells derived from a patient (PDX). The PDX model was developed using NSG mice for the initial expansion of fresh primary malignant cells. Then, $2 \cdot 10^5$ lymphoma cells were inoculated into the brain parenchyma of nude athymic mice (363) and infiltrates of innate immune cells were evaluated at day 18 by IHC and flow cytometry. At that time, brains were already infiltrated by innate immune cells and mice were still alive (median survival of this model: 22 days). We identified TAMs localized only amongst tumor cells as observed in the OCI-Ly10 mouse model (Figure 35A and Figure 36). Moreover, we detected a similar phenotype in TAMs from the PDX model to that found in TAMs from the cell line xenograft model. This consists of similar proportions of M1 and M2 macrophages (Figure 35B) and higher expression of PD-1 and SIRP α in M2 macrophages (Figures 35C-E). However, patient-derived PCNSL cells, unlike OCI-Ly10 cells, did express the SIRP α ligand CD47 (97.61% of CD20 cells \pm 0.62).

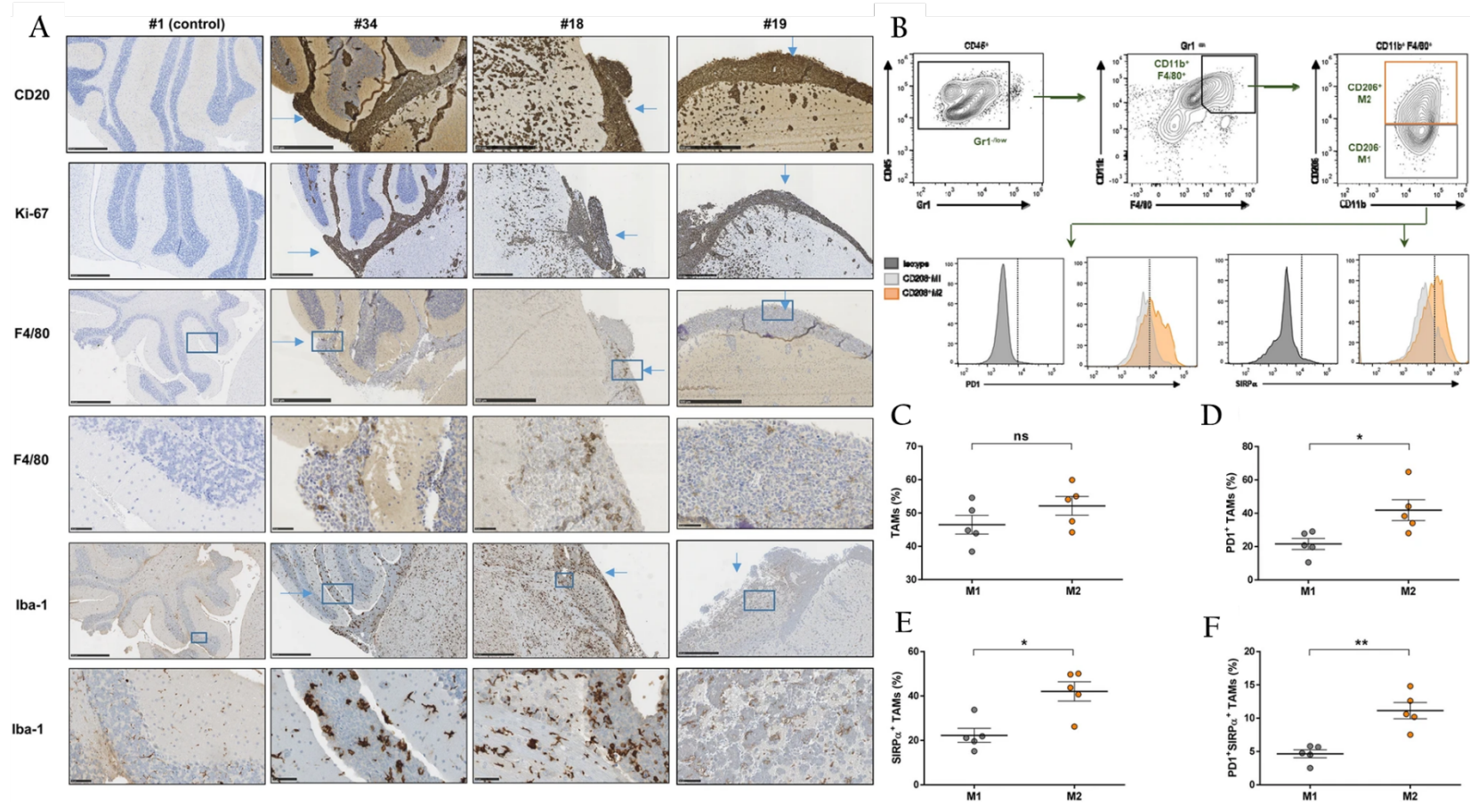


Figure 34. OCI-Ly10 CNS lymphomas are infiltrated by innate immune cells. (A) Representative IHC images from brains obtained from three mice inoculated with OCI-Ly10 cells (24 days after injection). The bar represents 500µm, except for fourth and last rows (50µm). (B) Gating strategy for the analysis of TAMs. (C) Percentage of macrophages (M1/M2) expressing (D) PD-1, (E) SIRPα and (F) co-expressing both. *P<0,05; **P<0,01; Mann-Whitney test. Graphs show mean ± SEM.

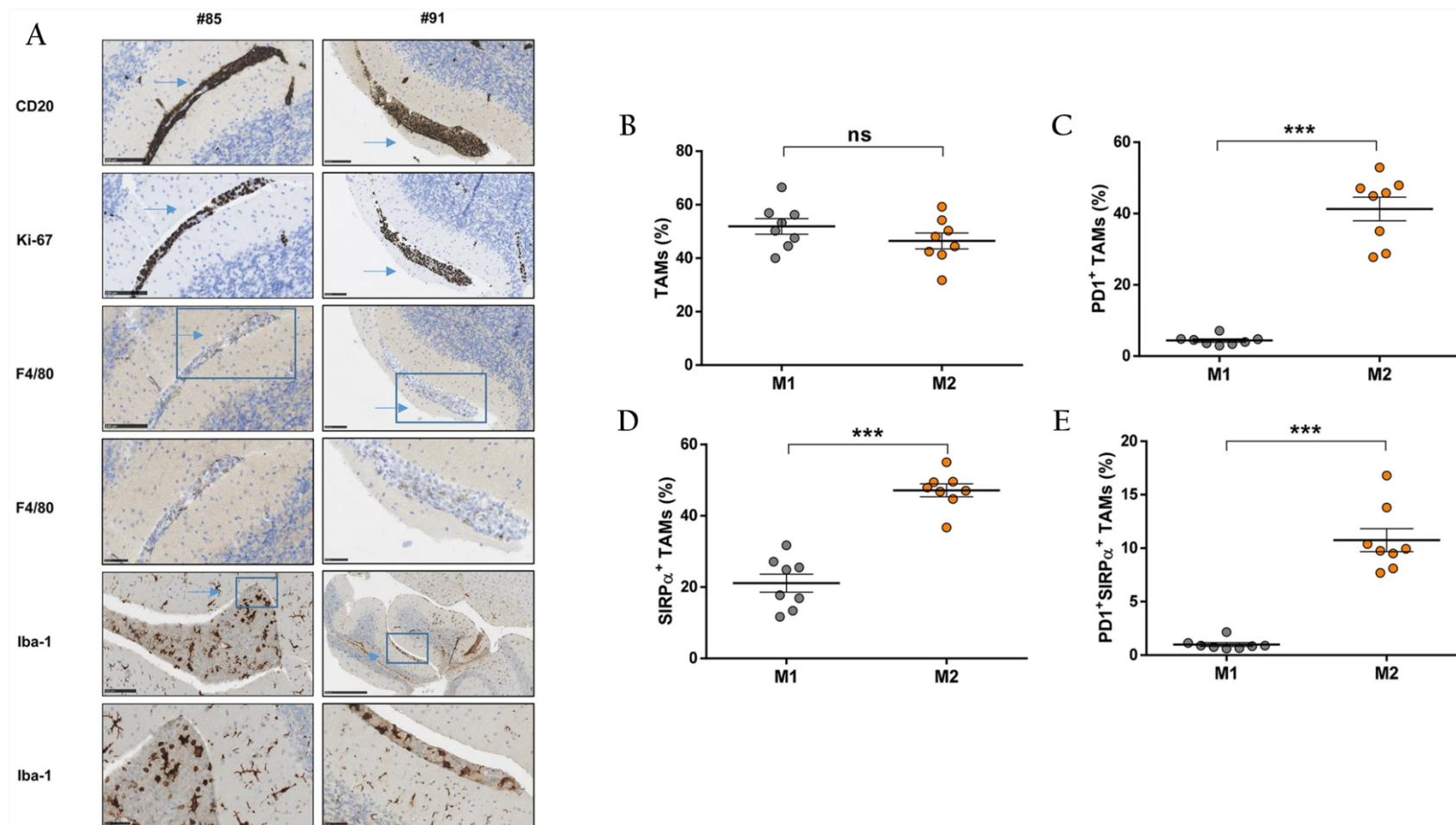


Figure 35. PDX CNS lymphomas are infiltrated by innate immune cells. (A) Representative IHC images from brains obtained from two mice inoculated with patient-derived PCNSL cells (18 days after injection). The bar represents 100 μ m except for the four last rows (50 μ m). (B) Percentage of macrophages (M1/M2) expressing (C) PD-1, (D) SIRP α and (E) co-expressing both. (***) $P < 0.001$; Mann-Whitney test. Graphs show mean \pm SEM).

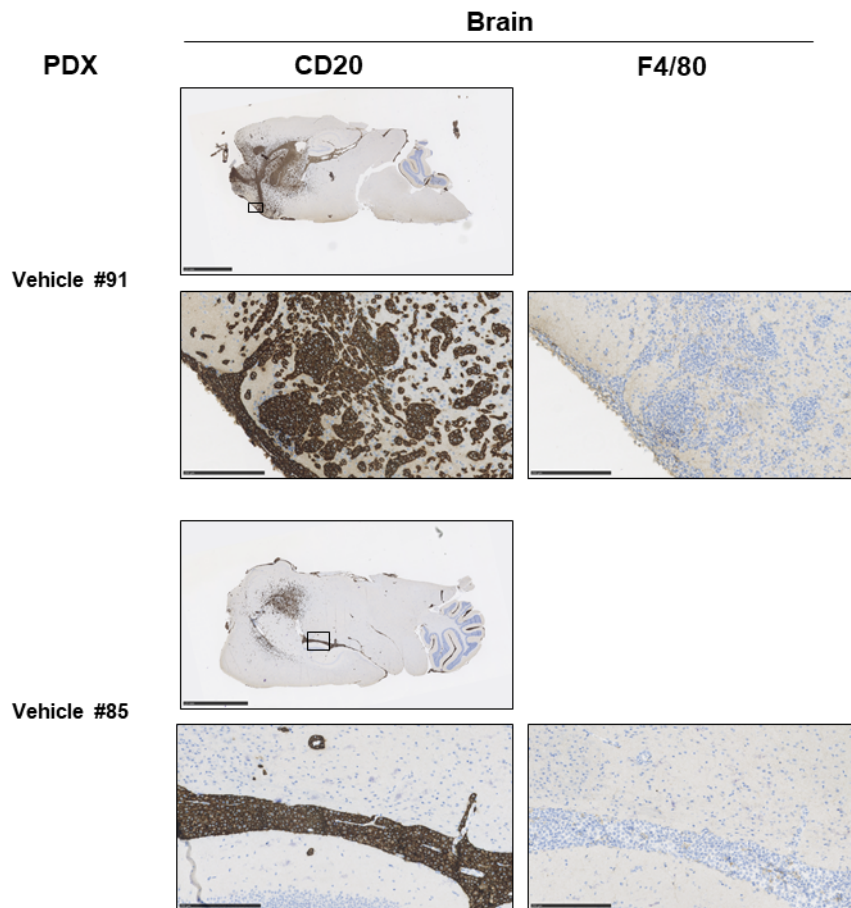


Figure 36. IHC of representative PCNSL PDX tumors. Representative IHC images from brains obtained from 2 nude athymic mice inoculated with patient-derived PCNSL cells (18 days after injection). The bar represents 2.5mm in whole brain images and 250 μ m in zoomed in images.

5.10. Treatment with selinexor and ibrutinib favors TAM polarization toward a pro-inflammatory M1-like phenotype and diminishes PD-1 and SIRP α expression in M2-like TAMs

The BTK protein is crucial for the pro-tumoral function of macrophages in different neoplasias. For instance, its inhibition using ibrutinib modulates TAMs in CLL (364). In addition, other immunomodulatory drugs, such as lenalidomide, not only have a direct anti-tumoral effect but are able to shift macrophage polarization in pre-clinical PCNSL models (294,355). Our study shows that the combination of selinexor and ibrutinib restrains tumor growth and prolongs mice survival. Since both drugs are able to inhibit BTK, we hypothesized that the drugs could also cooperate and modify the innate immune response in PCNSL. To test that, we treated mice bearing OCI-Ly10-CNS lymphomas with selinexor (5 mg/kg twice a week), ibrutinib (25 mg/kg daily) or their combination for two weeks (Figure 37A). Flow cytometry performed at the final time point showed that selinexor monotherapy and its combination with ibrutinib shifted the M1/M2 ratio towards an anti-tumoral M1 phenotype (Figure 37B). Interestingly, while none of the individual treatments induced significant changes in the frequency of M2 macrophages expressing PD-1 and SIRP α , the drug combination significantly reduced the frequency of PD-1-positive, SIRP α -positive and double-positive M2 macrophages (Figure 37C-F). In agreement, CI values indicated that the reduction of the expression of PD-1, SIRP α and their co-expression was synergistic (CI<1). This was accompanied by a decrease in the expression of PD-L1 in malignant cells (Figures 37G and 37H). PD-L1 reduction can be associated with ibrutinib since lower PD-L1 levels were also observed under ibrutinib monotherapy.

In the PDX model the immune analysis was performed after treating mice for 12 days (Figure 38A). Here, single therapies with selinexor and ibrutinib as well as their combination were able

TIME in B-cell lymphoid malignancies

to change the M1/M2 balance towards an inflammatory M1 phenotype (Figure 38B). In addition, mice treated with ibrutinib monotherapy and the combination showed lower frequencies of PD-1-expressing M2 macrophages (Figure 38C). M2 macrophages that expressed SIRP α alone and co-expressed with PD-1 were diminished in all treated mice (Figures 38D and 38E). In this model, neither the percentage of malignant cells nor their PD-L1 expression were affected by the treatments (Figure 38F and 38G). However, CD47 expression in patient-derived PCNSL cells was significantly downregulated in mice treated with the combination (Figure 38H). Accordingly, CI calculations showed that the combination did not improve upon individual treatments for any of the parameters except for the expression of CD47 on malignant cells.

Finally, and in order to identify direct immunomodulatory effects of selinexor and ibrutinib on human macrophages, we treated differentiated-M2 macrophages from HDs *in vitro* with increasing doses of selinexor, ibrutinib or the combination. Derived-M2 macrophages displayed a mean expression of PD-1 of 81.15% \pm 8.8% and a mean expression of SIRP α of 45.53% \pm 9.3%. In agreement with what we observed *in vivo*, these markers were also downregulated *in vitro* by the individual drugs or the combination (Figures 39A-C). However, this did not translate into increased phagocytic activity (Figure 39D). We also analyzed additional characteristic surface markers of M1 and M2 macrophages and the presence of IL-10 in culture supernatants. We found that selinexor induced an increase in the expression of CD86, an M1-like marker associated with activation, while the expression of the M2-like marker CD163 was decreased. Accordingly, this was also observed in human-derived macrophages treated with the combination. In addition, single treatments led to lower levels of PD-L1. Selinexor was also able to reduce the secretion of the anti-inflammatory cytokine IL-10 (Figures 39E-H). This demonstrates that selinexor and ibrutinib are able to modulate M1 and M2 features *in vitro* consistent with a loss of pro-tumoral M2 properties. Nonetheless, the drugs did not induce significant changes in other molecules related to M2 and M1 phenotypes, such as CD206 and HLA-DR (Figures 39I and 39J).

In summary, our findings indicate that the combination of selinexor and ibrutinib is able to block the growth of PCNSL in mice and significantly increase their median survival. It also modulates

in vivo the innate immune microenvironment towards a more anti-tumoral stage. Finally, further studies are needed to demonstrate that a reinvigoration of the anti-tumoral phagocytic function in macrophages after the treatments is responsible for these effects.

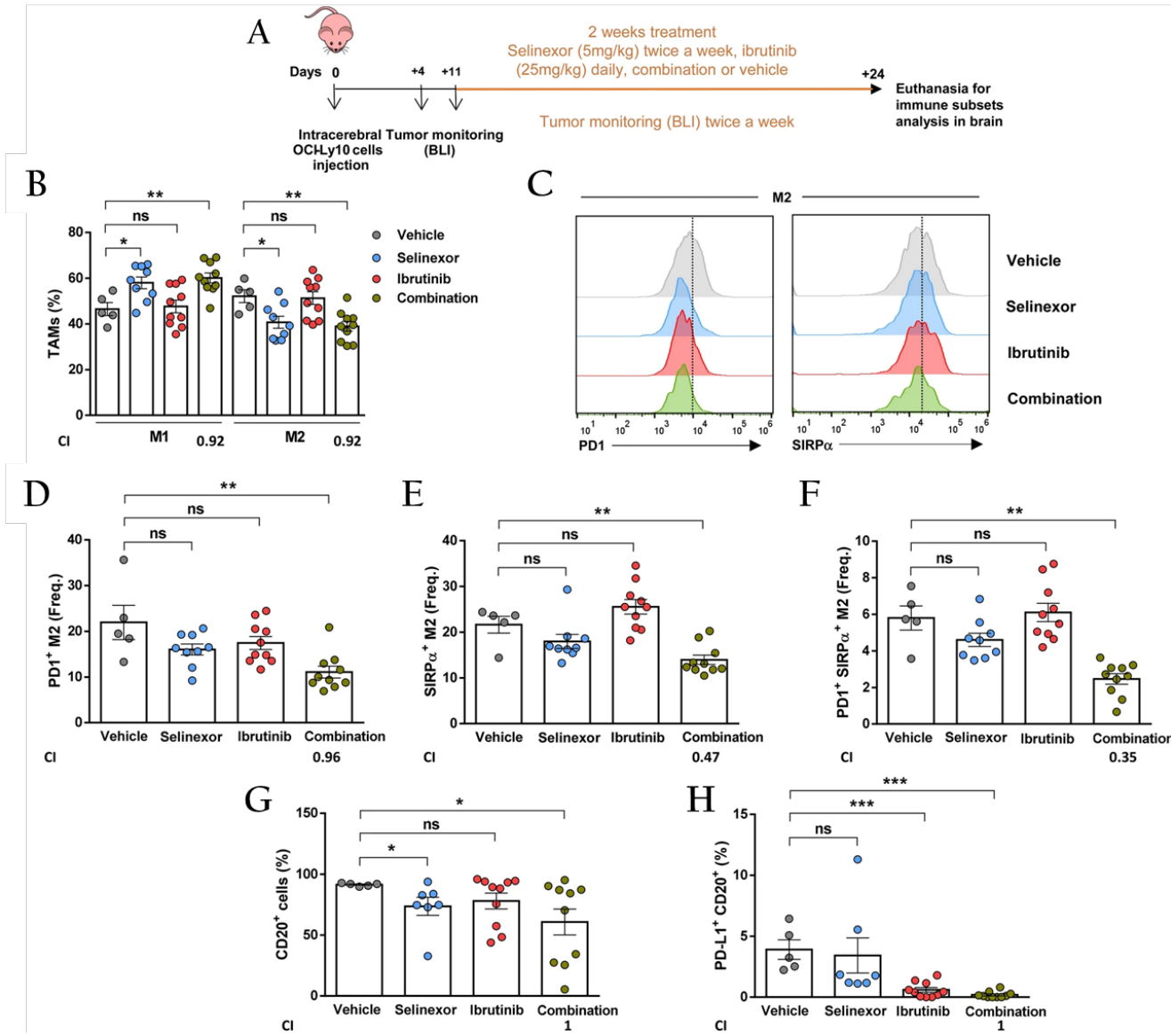


Figure 37. Treatment with selinexor and ibrutinib favors an M1-like response in tumor-associated macrophages from OCI-Ly10-derived CNS lymphomas. (A) Scheme representing mice treatment and monitoring. (B) Percentage of M1 and M2 TAMs by flow cytometry. (C) Histograms of PD-1⁺ M2 and SIRPα⁺ M2 of one representative mouse from each group. Frequency of M2 macrophages that express (D) PD-1, (E) SIRPα or (F) co-express both markers. (G) Percentage of CD20⁺ cells in the brains from mice treated for two weeks. (H) Percentage of CD20⁺ malignant cells expressing PD-L1 in mice from the different treatment groups. *P<0,05; **P<0,01; ***P<0,001; Mann-Whitney test. Graphs show mean ± SEM.

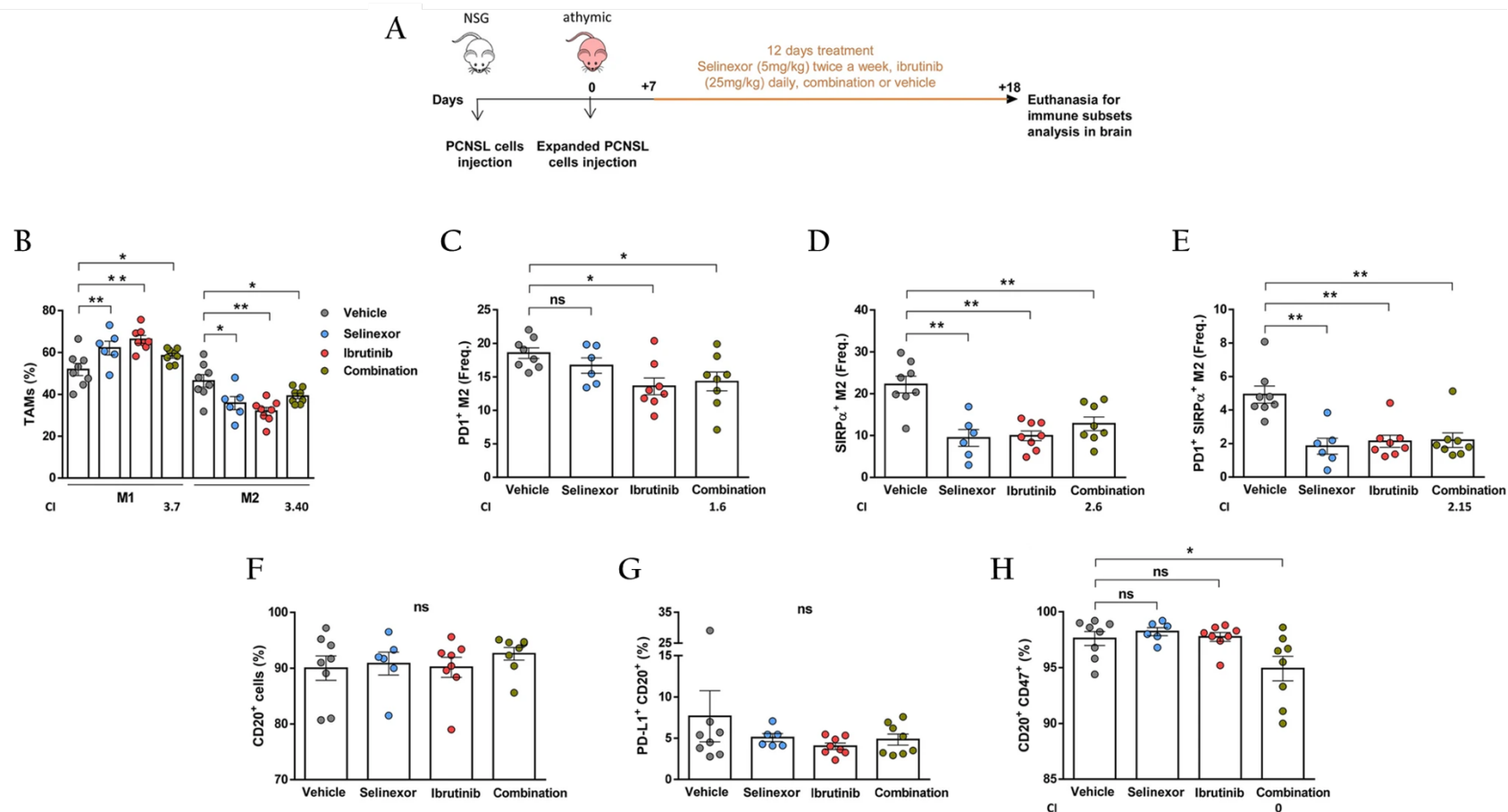


Figure 38. Treatment with selinexor and ibrutinib favors an M1-like response in TAMs in CNS lymphoma PDXs. (A) Scheme representing mice treatment and monitoring. (B) Percentage of M1 and M2 TAMs by flow cytometry. Frequency of M2 macrophages that express (C) PD-1, (D) SIRP α or (E) co-express both markers. (F) Percentage of CD20⁺ cells in the brains from mice. (G) Percentage of malignant cells CD20⁺ expressing PD-L1 in mice from the different treatment groups. Percentage of malignant cells expressing (H) CD47 and (I) co-expressing PD-L1 and CD47. *P<0,05; **P<0,01; ***P<0,001; Mann-Whitney test. Graphs show mean \pm SEM.

TIME in B-cell lymphoid malignancies

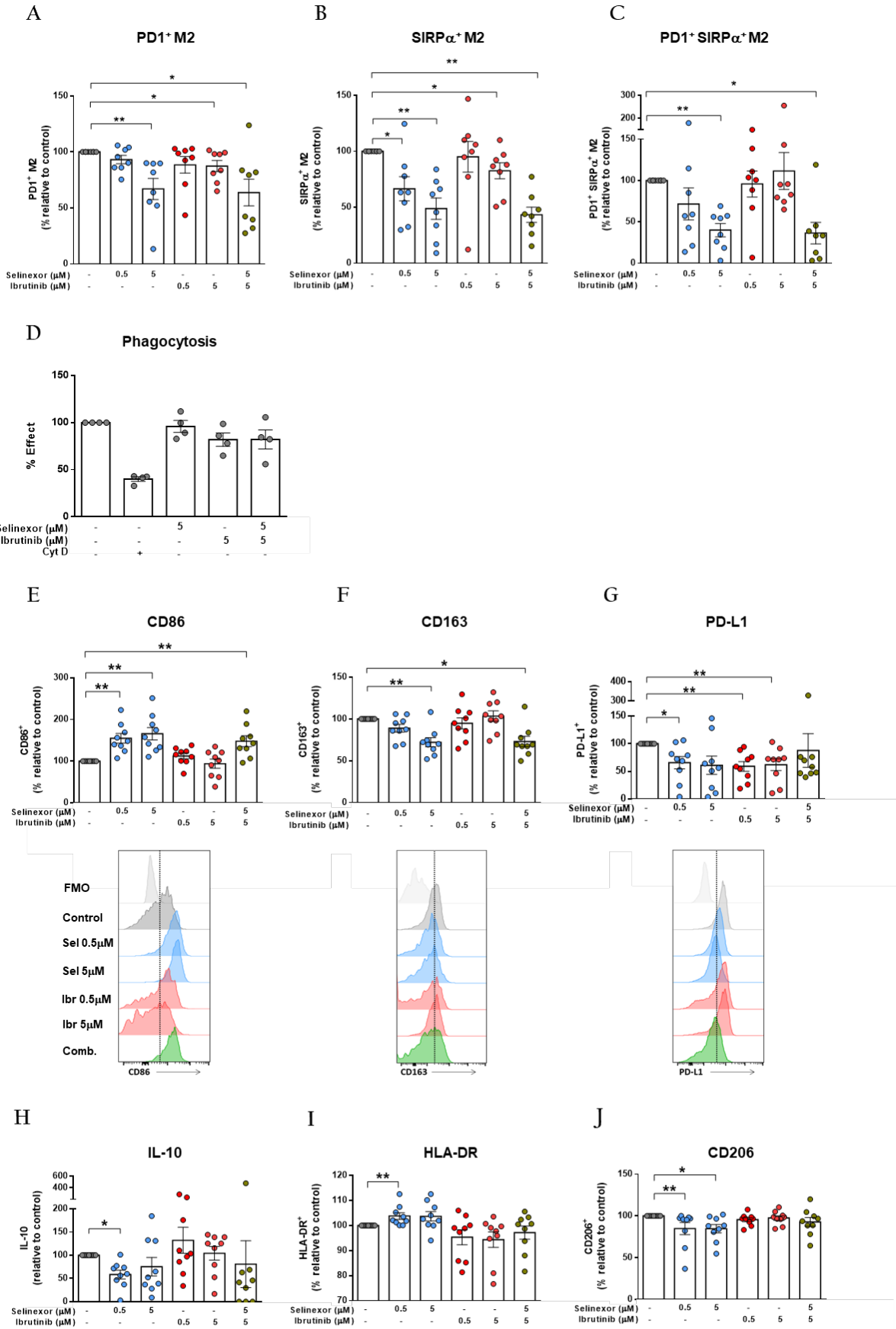


Figure 39 (left). Treatment with selinexor and ibrutinib induces downregulation of PD-1 and SIRP α in human M2 macrophages. Human macrophages differentiated from peripheral blood using M-CSF were pre-incubated with drugs for 30 minutes and then 10ng/ml IL-10 was added for 48h to promote M2 differentiation. After 48 hours the following parameters were analyzed: changes in the expression of PD-1 (A), SIRP α (B) and co-expression of both molecules (C) in human M2 macrophages (CD14⁺CD16⁺CD206⁺) treated with selinexor and/or ibrutinib relative to untreated cells. Changes in phagocytosis (D), CD86 (E), CD163 (F), PD-L1 (G), IL-10 (H), HLA-DR (I) and CD206 (J) in macrophages (CD14⁺CD16⁺) treated with selinexor and/or ibrutinib relative to untreated cells. *P<0.05, **P<0.01, ***P<0.001, Wilcoxon test. Graphs show mean \pm SEM.

6. Discussion



In this doctoral thesis, immune mechanisms that potentially contribute to tumor progression and new therapeutic strategies with immunomodulatory potential focusing on CLL and PCNSL, respectively, have been studied. Results obtained are discussed in this section.

Part I – The genetic and immune landscapes of clinical progression in CLL

The biological processes that lead to clinical progression from early asymptomatic stages in patients diagnosed with CLL are not well understood and, consequently, the pathogenesis behind the natural history of this disease remains unclear. This also limits catching progression in advance or improving the current therapeutic options. Longitudinal studies from diagnosis to clinical progression are essential to elucidate mechanisms of progression. Here, we perform a comprehensive longitudinal analysis of the genetic and immunological processes driving disease progression in CLL. When viewed as a whole our research contributes new insights into CLL progression. The genetic analysis in our series indicates that genetic fluctuations in malignant cells are not always detected during the progression of CLL from early stages, as previously reported by others (131,138,165,168–170,172,173,365). This supports that the immunological changes we describe are of paramount importance in clinical progression. Here, we report an increasingly dysfunctional CD8⁺ T-cell compartment in progressing patients that was not

TIME in B-cell lymphoid malignancies

observed in those patients that remained asymptomatic. We show that soluble factors, such as IL-10 produced by CLL cells, play a role in CD8⁺ T-cell exhaustion and in the progression of the disease. CLL cells exhibit increased capacity to produce IL-10 at progression indicating that malignant cells from progressing patients acquire immune evasion properties along the course of the disease. This promotes engaging in a positive feed-back system that would further increase exhaustion in CD8⁺ T cells and ultimately facilitating the transition from diagnosis to clinical progression. Notably, only one patient (CLL51) (8% of total) clearly showed clonal evolution at progression with increased frequencies in *NFKBIE* and *ATM* genes and gain of del(8p) and del(15p). Deletion of 8p has been previously associated with resistance to ibrutinib while del(15q) includes the driver gene *MGA* (366).

An altered anti-tumor immune response is evidenced in CLL by diverse factors affecting mainly T cells (203,205,219,221,340,341). Recent studies using the TCL1 mouse model indicate that CD8⁺ T cells can delay CLL progression at the same time that the expression of IR progressively increases (243). Accordingly, our longitudinal immune analysis in CLL patients showed that effector memory CD8⁺ subsets expressing PD-1 and CD244 accumulate specifically at clinical progression. In addition, terminally exhausted (T-bet^{dim}/Eomes^{hi}PD-1^{hi}) CD8⁺ T cells accumulated at progression. This denotes an increase in T-cell dysfunction over time. Further studies aimed at the potential recovery of terminally exhausted CD8⁺ T cells are necessary and would help improve anti-tumor T-cell responses. This may be particularly advantageous considering the low functionality of chimeric antigen receptor (CAR) T cells derived from patients in an advanced disease stage (222).

The transcriptome of T cells from progressing and non-progressing patients was also analyzed. Although the low quality of the RNA we obtained hampered this analysis, we were able to identify changes in the transcriptome specifically associated with clinical progression. We found a distinct expression profile in T cells at progression compared to diagnosis and minor differences in T cells from non-progressing patients.

In this study, we also identified that CLL cells *ex vivo* induced the expression of PD-1 in autologous CD8⁺ T cells, indicating that T cells are able to recognize and interact with malignant cells despite their reported failure to mount a functional immune synapse (221). Importantly, we found that PD-1 upregulation depended on soluble factors and provided an association between the enhanced ability of IL-10 production by CLL cells at progression and PD-1 expression in CD8⁺ T cells. However, the neutralization of IL-10 partially blocked the induction of PD-1 in CD8⁺ T cells. Therefore, the role of additional soluble factors in this mechanism needs further investigations.

The accumulation of exhausted CD8⁺ T cells in progressing patients might be a mere consequence of the higher tumoral load characterizing the majority of patients at progression (see Table 17 and Table 18 for clinical data). However, our data highlight a scenario where accumulating malignant cells also acquire higher immunosuppressive properties along the course of the disease, which would promote engaging in a positive feed-back system further increasing CD8⁺ T-cell exhaustion. In this regard, Gonnord *et al.* recently described that CD8⁺ T cells from untreated CLL patients that will need therapy within 6 months after analysis display a unique signature which is not correlated with the time that CD8⁺ T cells have been exposed to CLL cells (218), reinforcing the idea that T-cell exhaustion is not a mere product of increased exposure to malignant cells, either in time or in tumoral load.

Collectively, our findings indicate that at clinical progression CLL cells exhibit limited genetic changes, while CD8⁺ T lymphocytes show increased exhaustion that can be induced by IL-10 secreted by malignant B cells. In contrast, patients without evidence of progression did not experience significant changes over time in their T-cell compartment. Our study could also be of interest to explore the use of early immunotherapeutic interventions to avoid or delay progression or to help improve current therapies in CLL patients.

Part II – New therapeutic strategies in PCNSL and immunomodulatory effects

The blockade of XPO1-mediated nuclear transport using SINEs like selinexor shows anti-neoplastic efficacy against a variety of malignancies (309,311). XPO1 inhibition forces the nuclear localization of tumor suppressors. It also interferes with crucial signaling pathways for the survival of malignant B cells, including the NF- κ B and BCR pathways which are particularly important for the survival of PCNSL cells. The clinical use of selinexor in lymphoma has been studied in a phase I trial in patients diagnosed with R/R NHL and a phase IIb trial in patients with DLBCL (311,313). The latter has led to the FDA approval of selinexor as a therapeutic option in R/R DLBCL patients. Recently, and based on our pre-clinical experience, we have used selinexor in a compassionate way to treat a patient diagnosed with DLBCL who experienced an isolated CNS relapse after several lines of treatment. After one month of treatment, a PR was observed in this patient; and after 5 months, the patient remained asymptomatic and the MRI showed a complete resolution of the brain tumors (314). Furthermore, ibrutinib is able to cross the BBB and has also shown activity against CNS lymphoma cells. Ibrutinib, both as single treatment and combined with chemotherapy, leads to high response rates in PCNSL patients but remissions are short (292,293). Other BTK inhibitors have shown a similar efficacy (367). Here, we study selinexor alone and combined with ibrutinib in pre-clinical models of PCNSL. We report that selinexor blocks tumor growth and prolongs survival in a bioluminescent mouse model of PCNSL and its combination with ibrutinib further increases survival.

The modulation of the immune response against tumors is currently a widespread strategy to treat cancer. In this regard, different approaches are being pursued. Some of them are focused on harnessing the anti-tumoral capacity of T lymphocytes via immune check-point inhibition. The anti-PD-1 antibody nivolumab is an effective treatment for Hodgkin's lymphoma. This is intriguing if we take into account that the expression of PD-1 in T-cells from Hodgkin's lymphoma patients is heterogeneous and tumor cells frequently show PD-L1/2 amplifications as well as a lack of MHC-I expression (368,369). These features might hamper T-cell responses. In

PCNSL, a high percentage of patients are affected by loss of MHC-I and/or PD-L1/2 amplifications suggesting that the evasion of tumor cells from T-cell mediated immune responses is a common mechanism (277). Moreover, cerebral T-cell infiltrates can be observed in patients, even if they are scarce (298,299,360,361). Some immunotherapeutic strategies have shown activity in PCNSL such as anti-CD20 therapies. Recently, nivolumab has shown pre-clinical evidences (370) and also clinical evidences in a small group of four patients (295).

A role for the innate immune system in the development of PCNSL is supported by the expression of PD-1 in TAMs (371). In addition, macrophage-mediated phagocytosis can be inhibited by the MHC-I system in cancer cells (372). Malignant cells that downregulate MHC-I are able to avoid T-cell surveillance, but they are also more exposed to phagocytosis. In this regard, the CR experienced by PCNSL patients treated with nivolumab could be related to a macrophage-mediated anti-tumoral effect after PD-1 blockade rather than an anti-tumoral T-cell effect. This is also supported by the presence of cerebral PD-1-positive M2 macrophages we found in two orthotopic mouse models of PCNSL, including PDXs.

Human malignant cells can be recognized by macrophages from mice as demonstrated in previous studies using PCNSL mouse models (355) and models of colon cancer (29), pancreatic adenocarcinoma (373) and T-cell lymphoma (374). TAMs are related to prognosis of PCNSL patients (302,360) as well as IDO and IL-10, which are mainly produced by macrophages (302,360,375). The expression of PD-1 and SIRP α we found in macrophages responding to and interacting with CNS lymphoma cells *in vivo* suggests that their anti-tumoral effect is partially impaired in this disease. This opens the opportunity to potentially target macrophages using immunotherapies aimed at recovering their anti-tumoral functions. The immunomodulatory drug pomalidomide has already been tested in mouse models of PCNSL in which it has been able to reprogramme M2 macrophages into M1 (355). In the clinical setting, both pomalidomide and lenalidomide are being tested in a phase I trial in patients diagnosed with PCNSL in combination with dexamethasone. Some preliminary therapeutic activity is being observed in this trial (294). Also, lenalidomide in combination with rituximab showed significant clinical activity in R/R

TIME in B-cell lymphoid malignancies

PCNSL patients (375). This indicates that therapies that combine drugs that not only attack the survival of malignant cells but also modulate the immune response are interesting approaches to achieve long-lasting responses. The BTK protein is essential for malignant B-cell survival and the tumor-promoting effects of macrophages (376). Therefore, the combination of selinexor and ibrutinib we test in this study could also be effective in harnessing the innate immune response mediated by TAMs. In this regard, our results show that the combination of selinexor and ibrutinib shifts the innate immune response towards a more inflammatory phenotype. Specifically, the expression of PD-1 and SIRP α in M2 macrophages is downregulated while the proportion of M1 macrophages is increased. In addition, we identify changes in additional M1 and M2-like properties consistent with a loss of pro-tumoral M2 characteristics in macrophages treated *in vitro*. This includes an increase of CD86 expression and a decrease of CD163 expression and IL-10 production. Further analysis of the interactions between malignant cells and immune cells in PCNSL using different *in vivo* models, including syngeneic mice, are needed. This will help confirm the potential clinical value of the combination of selinexor and ibrutinib in patients diagnosed with PCNSL.

7. Conclusions

1. CLL cells show reduced genetic changes at progression indicating that immune variations can facilitate the transition from diagnosis to clinical progression.
2. Progressed CLL patients experience an increase in effector memory and terminally exhausted T-bet^{mid/}Eomes^{hi}PD^{hi} CD8⁺ T cells over time, not observed in non-progressing patients. In addition, T cells at progression acquire a distinct transcriptional profile.
3. Progressed CLL cells are intrinsically more capable of inducing CD8⁺ T-cell exhaustion in both T cells from CLL and healthy T cells by a mechanism dependent on soluble factors including IL-10.
4. Selinexor blocks tumor growth and prolongs survival in a bioluminescent mouse model of PCNSL and its combination with ibrutinib further increases survival.
5. CNS lymphomas from orthotopic xenograft mouse models are infiltrated by pro-tumoral M2 TAMs with an increased expression of PD-1 and SIRP α .
6. Selinexor and ibrutinib exhibit immunomodulatory potential in PCNSL mouse models. Their combination shifts tumor-infiltrating macrophage polarization toward a M1 phenotype and diminishes the expression of PD-1 and SIRP α in M2 macrophages.

8. Prospective research opportunities



Our CLL research demonstrates that clinical progression from its early stages is characterized by a progressive increase in immunosuppressive features, especially in T cells, that may contribute to leukemic cells' evasion from immunosurveillance. Ultimately, this may be one of the main factors that facilitates CLL progression. Based on our data, the next goal is to decipher the immune mechanisms involved in CLL progression and use this information to create better methods for prognostication and treatment selection. In order to achieve this, we are going to study genome-wide expression changes in both CLL and immune cells using RNA-Seq and multiparametric mass cytometry (CyTOF). We also are going to investigate changes in the immune system of mice with the 13q14 deletion according to their CLL development. The deletion of 13q14 is the most common genetic alteration in CLL patients. In animal models it induces the development of CLL with a relatively low incidence which could be related to T-cell immune control. In addition, we will use mice with the 13q14 deletion as a pre-clinical model to test early immunomodulatory therapies that could potentially impede CLL progression. Finally, those altered immune parameters identified in patients and mice will be integrated with other prognostic factors in order to establish an algorithm to predict the time to progression. Ultimately, this project will help better define a patient's prognosis while thoroughly studying the mechanisms of progression in CLL and the potential of early immunomodulating therapies.

The immunomodulatory effect of therapies that blocks the BCR signaling we observed in macrophages as well as the presence of PD-1 in M2 TAMs from CNS lymphomas in mice models have led us to hypothesize that the innate immune system plays a more relevant role than previously believed in the pathogenesis of CNS lymphomas. This is supported by the recent

TIME in B-cell lymphoid malignancies

discovery of PD-1 expression in TAMs from other types of tumors as well as the recovery of their ability to phagocyte tumor cells after a PD-1 blockade. In addition, a high proportion of patients diagnosed with PCNSL show genetic strategies to avoid the recognition of tumor cells by the immune system. This includes PD-L1/PD-L2 amplifications and/or loss of MHC molecules. More than half of patients have amplifications of the ligand of PD-1 in 9p24.1, which increases the negative stimuli in cytotoxic T cells. And 65-79% of patients also lack MHC-I and MHC-II molecules. The loss of MHC-I molecules likely prevents T lymphocytes from recognizing malignant cells and losing MHC-II molecules hampers the ability of malignant cells to present antigens. If all these genetic strategies are circumvented, malignant cells could be less resistant to immune-based therapies. Taking this into account, our next goal is to further evaluate the interactions between immune cells and PCNSL cells. We are going to develop an immunocompetent syngeneic CNS lymphoma model since mouse macrophages are not able to interact with the human MHC-I complex. Therefore, our orthotopic xenograft models would not be appropriate for studying these interactions. This immune analysis we are planning to conduct will unveil the potential role of macrophages in the immune response against CNS lymphoma cells. Importantly, this will also provide pre-clinical evidence for the optimal development of novel immunotherapies targeting myeloid cells in CNS lymphoma patients.

9. Bibliography

1. Zhang Y, Gao S, Xia J, Liu F. Hematopoietic Hierarchy - An Updated Roadmap. *Trends Cell Biol.* 2018;28(12):976–86.
2. Laurenti E, Göttgens B. From haematopoietic stem cells to complex differentiation landscapes. *Nature.* 2018 24;553(7689):418–26.
3. Orkin SH, Zon LI. Hematopoiesis: an evolving paradigm for stem cell biology. *Cell.* 2008 Feb 22;132(4):631–44.
4. Tokoyoda K, Egawa T, Sugiyama T, Choi B-I, Nagasawa T. Cellular niches controlling B lymphocyte behavior within bone marrow during development. *Immunity.* 2004 Jun;20(6):707–18.
5. Herzog S, Reth M, Jumaa H. Regulation of B-cell proliferation and differentiation by pre-B-cell receptor signalling. *Nat Rev Immunol.* 2009 Mar;9(3):195–205.
6. Chaudhuri J, Alt FW. Class-switch recombination: interplay of transcription, DNA deamination and DNA repair. *Nat Rev Immunol.* 2004 Jul;4(7):541–52.
7. Xu Z, Zan H, Pone EJ, Mai T, Casali P. Immunoglobulin class-switch DNA recombination: induction, targeting and beyond. *Nat Rev Immunol.* 2012 Jun 25;12(7):517–31.
8. Melchers F. Checkpoints that control B cell development. *J Clin Invest.* 2015 Jun 1;125(6):2203–10.
9. Basso K, Dalla-Favera R. Germinal centres and B cell lymphomagenesis. *Nat Rev Immunol.* 2015 Mar;15(3):172–84.
10. Roco JA, Mesin L, Binder SC, Neftzger C, Gonzalez-Figueroa P, Canete PF, et al. Class-Switch Recombination Occurs Infrequently in Germinal Centers. *Immunity.* 2019 20;51(2):337–350.e7.
11. Kitano M, Moriyama S, Ando Y, Hikida M, Mori Y, Kurosaki T, et al. Bcl6 Protein Expression Shapes Pre-Germinal Center B Cell Dynamics and Follicular Helper T Cell Heterogeneity. *Immunity.* 2011 Jun;34(6):961–72.
12. Ci W, Polo JM, Cerchiatti L, Shaknovich R, Wang L, Yang SN, et al. The BCL6 transcriptional program features repression of multiple oncogenes in primary B cells and is deregulated in DLBCL. *Blood.* 2009 May 28;113(22):5536–48.
13. Cimmino L, Martins GA, Liao J, Magnusdottir E, Grunig G, Perez RK, et al. Blimp-1 attenuates Th1 differentiation by repression of ifng, tbx21, and bcl6 gene expression. *J Immunol.* 2008 Aug 15;181(4):2338–47.
14. D D-S, Gd V, Cy Y, Rt P, M S, Mc N, et al. The proto-oncogene MYC is required for selection in the germinal center and cyclic reentry [Internet]. *Nature immunology.* 2012 [cited 2020 Sep 10]. Available from: <https://pubmed.ncbi.nlm.nih.gov/23001145/>
15. Cobaleda C, Schebesta A, Delogu A, Busslinger M. Pax5: the guardian of B cell identity and function. *Nature Immunology.* 2007 May;8(5):463–70.
16. Nera K-P, Kohonen P, Narvi E, Peippo A, Mustonen L, Terho P, et al. Loss of Pax5 promotes plasma cell differentiation. *Immunity.* 2006 Mar;24(3):283–93.
17. Küppers R. Mechanisms of B-cell lymphoma pathogenesis. *Nat Rev Cancer.* 2005 Apr;5(4):251–62.

TIME in B-cell lymphoid malignancies

18. Binnewies M, Roberts EW, Kersten K, Chan V, Fearon DF, Merad M, et al. Understanding the tumor immune microenvironment (TIME) for effective therapy. *Nat Med*. 2018;24(5):541–50.
19. McLane LM, Abdel-Hakeem MS, Wherry EJ. CD8 T Cell Exhaustion During Chronic Viral Infection and Cancer. *Annual Review of Immunology*. 2019;37(1):457–95.
20. Vesely MD, Kershaw MH, Schreiber RD, Smyth MJ. Natural innate and adaptive immunity to cancer. *Annu Rev Immunol*. 2011;29:235–71.
21. Yarchoan M, Johnson BA, Lutz ER, Laheru DA, Jaffee EM. Targeting neoantigens to augment antitumour immunity. *Nat Rev Cancer*. 2017;17(4):209–22.
22. Biswas SK, Mantovani A. Macrophage plasticity and interaction with lymphocyte subsets: cancer as a paradigm. *Nature Immunology*. 2010 Oct;11(10):889–96.
23. Mantovani A, Sica A, Sozzani S, Allavena P, Vecchi A, Locati M. The chemokine system in diverse forms of macrophage activation and polarization. *Trends in Immunology*. 2004 Dec 1;25(12):677–86.
24. Raes G, Brys L, Dahal BK, Brandt J, Grooten J, Brombacher F, et al. Macrophage galactose-type C-type lectins as novel markers for alternatively activated macrophages elicited by parasitic infections and allergic airway inflammation. *J Leukoc Biol*. 2005 Mar;77(3):321–7.
25. Recalcati S, Locati M, Marini A, Santambrogio P, Zaninotto F, De Pizzol M, et al. Differential regulation of iron homeostasis during human macrophage polarized activation. *Eur J Immunol*. 2010 Mar;40(3):824–35.
26. Puig-Kröger A, Sierra-Filardi E, Domínguez-Soto A, Samaniego R, Corcuera MT, Gómez-Aguado F, et al. Folate receptor beta is expressed by tumor-associated macrophages and constitutes a marker for M2 anti-inflammatory/regulatory macrophages. *Cancer Res*. 2009 Dec 15;69(24):9395–403.
27. Curiel TJ, Coukos G, Zou L, Alvarez X, Cheng P, Mottram P, et al. Specific recruitment of regulatory T cells in ovarian carcinoma fosters immune privilege and predicts reduced survival. *Nat Med*. 2004 Sep;10(9):942–9.
28. Wong S-C, Puaux A-L, Chittezhath M, Shalova I, Kajiji TS, Wang X, et al. Macrophage polarization to a unique phenotype driven by B cells. *Eur J Immunol*. 2010 Aug;40(8):2296–307.
29. Gordon SR, Maute RL, Dulken BW, Hutter G, George BM, McCracken MN, et al. PD-1 expression by tumor-associated macrophages inhibits phagocytosis and tumor immunity. *Nature*. 2017 May 25;545(7655):495–9.
30. Noy R, Pollard JW. Tumor-associated macrophages: from mechanisms to therapy. *Immunity*. 2014 Jul 17;41(1):49–61.
31. Kren L, Muckova K, Lzicarova E, Sova M, Vybihal V, Svoboda T, et al. Production of immune-modulatory nonclassical molecules HLA-G and HLA-E by tumor infiltrating ameboid microglia/macrophages in glioblastomas: a role in innate immunity? *J Neuroimmunol*. 2010 Mar 30;220(1–2):131–5.

32. Morandi F, Levreri I, Bocca P, Galleni B, Raffaghello L, Ferrone S, et al. Human neuroblastoma cells trigger an immunosuppressive program in monocytes by stimulating soluble HLA-G release. *Cancer Res.* 2007 Jul 1;67(13):6433–41.
33. Jaiswal S, Chao MP, Majeti R, Weissman IL. Macrophages as mediators of tumor immunosurveillance. *Trends Immunol.* 2010 Jun;31(6):212–9.
34. Loke P, Allison JP. PD-L1 and PD-L2 are differentially regulated by Th1 and Th2 cells. *Proc Natl Acad Sci USA.* 2003 Apr 29;100(9):5336–41.
35. Belai EB, de Oliveira CE, Gasparoto TH, Ramos RN, Torres SA, Garlet GP, et al. PD-1 blockage delays murine squamous cell carcinoma development. *Carcinogenesis.* 2014 Feb;35(2):424–31.
36. Ding L, Linsley PS, Huang LY, Germain RN, Shevach EM. IL-10 inhibits macrophage costimulatory activity by selectively inhibiting the up-regulation of B7 expression. *J Immunol.* 1993 Aug 1;151(3):1224–34.
37. Wherry EJ. T cell exhaustion. *Nat Immunol.* 2011 Jun;12(6):492–9.
38. Wherry EJ, Kurachi M. Molecular and cellular insights into T cell exhaustion. *Nat Rev Immunol.* 2015 Aug;15(8):486–99.
39. Schluns KS, Lefrançois L. Cytokine control of memory T-cell development and survival. *Nat Rev Immunol.* 2003 Apr;3(4):269–79.
40. Paley MA, Kroy DC, Odorizzi PM, Johnnidis JB, Dolfi DV, Barnett BE, et al. Progenitor and terminal subsets of CD8⁺ T cells cooperate to contain chronic viral infection. *Science.* 2012 Nov 30;338(6111):1220–5.
41. Blackburn SD, Shin H, Haining WN, Zou T, Workman CJ, Polley A, et al. Coregulation of CD8⁺ T cell exhaustion by multiple inhibitory receptors during chronic viral infection. *Nat Immunol.* 2009 Jan;10(1):29–37.
42. Thommen DS, Koelzer VH, Herzig P, Roller A, Trefny M, Dimeloe S, et al. A transcriptionally and functionally distinct PD-1 + CD8 + T cell pool with predictive potential in non-small-cell lung cancer treated with PD-1 blockade. *Nature Medicine.* 2018 Jul;24(7):994.
43. Yao C, Sun H-W, Lacey NE, Ji Y, Moseman EA, Shih H-Y, et al. Single-cell RNA-seq reveals TOX as a key regulator of CD8⁺ T cell persistence in chronic infection. *Nat Immunol.* 2019;20(7):890–901.
44. Khan O, Giles JR, McDonald S, Manne S, Ngiow SF, Patel KP, et al. TOX transcriptionally and epigenetically programs CD8⁺ T cell exhaustion. *Nature.* 2019;571(7764):211–8.
45. Belkaid Y, Rouse BT. Natural regulatory T cells in infectious disease. *Nat Immunol.* 2005 Apr;6(4):353–60.
46. Gautron A-S, Dominguez-Villar M, de Marcken M, Hafler DA. Enhanced suppressor function of TIM-3⁺ FoxP3⁺ regulatory T cells. *Eur J Immunol.* 2014 Sep;44(9):2703–11.
47. Blackburn SD, Shin H, Freeman GJ, Wherry EJ. Selective expansion of a subset of exhausted CD8 T cells by alphaPD-L1 blockade. *Proc Natl Acad Sci U S A.* 2008 Sep 30;105(39):15016–21.

TIME in B-cell lymphoid malignancies

48. Sade-Feldman M, Yizhak K, Bjorgaard SL, Ray JP, Boer CG de, Jenkins RW, et al. Defining T Cell States Associated with Response to Checkpoint Immunotherapy in Melanoma. *Cell*. 2018 Nov 1;175(4):998-1013.e20.
49. Miller BC, Sen DR, Al Abosy R, Bi K, Virkud YV, LaFleur MW, et al. Subsets of exhausted CD8+ T cells differentially mediate tumor control and respond to checkpoint blockade. *Nat Immunol*. 2019;20(3):326–36.
50. Siddiqui I, Schaeuble K, Chennupati V, Fuertes Marraco SA, Calderon-Copete S, Pais Ferreira D, et al. Intratumoral Tcf1+PD-1+CD8+ T Cells with Stem-like Properties Promote Tumor Control in Response to Vaccination and Checkpoint Blockade Immunotherapy. *Immunity*. 2019 15;50(1):195-211.e10.
51. Swerdlow SH, Campo E, Pileri SA, Harris NL, Stein H, Siebert R, et al. The 2016 revision of the World Health Organization classification of lymphoid neoplasms. *Blood*. 2016 19;127(20):2375–90.
52. Chronic Lymphocytic Leukemia - Cancer Stat Facts [Internet]. SEER. [cited 2019 Dec 5]. Available from: <https://seer.cancer.gov/statfacts/html/clyl.html>
53. Sant M, Allemani C, Tereanu C, De Angelis R, Capocaccia R, Visser O, et al. Incidence of hematologic malignancies in Europe by morphologic subtype: results of the HAEMACARE project. *Blood*. 2010 Nov 11;116(19):3724–34.
54. Rozman C, Montserrat E. Chronic lymphocytic leukemia. *N Engl J Med*. 1995 Oct 19;333(16):1052–7.
55. Bosch F, Dalla-Favera R. Chronic lymphocytic leukaemia: from genetics to treatment. *Nat Rev Clin Oncol*. 2019 Jul 5;
56. Hallek M, Cheson BD, Catovsky D, Caligaris-Cappio F, Dighiero G, Döhner H, et al. iwCLL guidelines for diagnosis, indications for treatment, response assessment, and supportive management of CLL. *Blood*. 2018 Jun 21;131(25):2745–60.
57. Hallek M. Chronic lymphocytic leukemia: 2020 update on diagnosis, risk stratification and treatment. *Am J Hematol*. 2019 Nov;94(11):1266–87.
58. Rawstron AC, Bennett FL, O'Connor SJM, Kwok M, Fenton JAL, Plummer M, et al. Monoclonal B-cell lymphocytosis and chronic lymphocytic leukemia. *N Engl J Med*. 2008 Aug 7;359(6):575–83.
59. Nieto WG, Almeida J, Romero A, Teodosio C, López A, Henriques AF, et al. Increased frequency (12%) of circulating chronic lymphocytic leukemia–like B-cell clones in healthy subjects using a highly sensitive multicolor flow cytometry approach. *Blood*. 2009 Jul 2;114(1):33–7.
60. Strati P, Shanafelt TD. Monoclonal B-cell lymphocytosis and early-stage chronic lymphocytic leukemia: diagnosis, natural history, and risk stratification. *Blood*. 2015 Jul 23;126(4):454–62.
61. Rawstron AC, Kreuzer K-A, Soosapilla A, Spacek M, Stehlikova O, Gambell P, et al. Reproducible diagnosis of chronic lymphocytic leukemia by flow cytometry: An European Research Initiative on CLL (ERIC) & European Society for Clinical Cell Analysis (ESCCA) Harmonisation project. *Cytometry B Clin Cytom*. 2018;94(1):121–8.

62. Moreau EJ, Matutes E, A'Hern RP, Morilla AM, Morilla RM, Owusu-Ankomah KA, et al. Improvement of the chronic lymphocytic leukemia scoring system with the monoclonal antibody SN8 (CD79b). *Am J Clin Pathol*. 1997 Oct;108(4):378–82.
63. Ginaldi L, De Martinis M, Matutes E, Farahat N, Morilla R, Catovsky D. Levels of expression of CD19 and CD20 in chronic B cell leukaemias. *J Clin Pathol*. 1998 May;51(5):364–9.
64. Chiorazzi N, Rai KR, Ferrarini M. Chronic lymphocytic leukemia. *N Engl J Med*. 2005 Feb 24;352(8):804–15.
65. Weide R, Feiten S, Chakupurakal G, Friesenhahn V, Kleboth K, Köppler H, et al. Survival improvement of patients with chronic lymphocytic leukemia (CLL) in routine care 1995–2017. *Leukemia & Lymphoma*. 2020 Feb 23;61(3):557–66.
66. Montserrat E, Sanchez-Bisono J, Viñolas N, Rozman C. Lymphocyte doubling time in chronic lymphocytic leukaemia: analysis of its prognostic significance. *Br J Haematol*. 1986 Mar;62(3):567–75.
67. Hallek M, Wanders L, Ostwald M, Busch R, Senekowitsch R, Stern S, et al. Serum beta(2)-microglobulin and serum thymidine kinase are independent predictors of progression-free survival in chronic lymphocytic leukemia and immunocytoma. *Leuk Lymphoma*. 1996 Aug;22(5–6):439–47.
68. Hallek M, Langenmayer I, Nerl C, Knauf W, Dietzfelbinger H, Adorf D, et al. Elevated serum thymidine kinase levels identify a subgroup at high risk of disease progression in early, nonsmoldering chronic lymphocytic leukemia. *Blood*. 1999 Mar 1;93(5):1732–7.
69. Lee JS, Dixon DO, Kantarjian HM, Keating MJ, Talpaz M. Prognosis of chronic lymphocytic leukemia: a multivariate regression analysis of 325 untreated patients. *Blood*. 1987 Mar;69(3):929–36.
70. Sarfati M, Chevret S, Chastang C, Biron G, Stryckmans P, Delespesse G, et al. Prognostic importance of serum soluble CD23 level in chronic lymphocytic leukemia. *Blood*. 1996 Dec 1;88(11):4259–64.
71. Dürig J, Naschar M, Schmücker U, Renzing-Köhler K, Hölter T, Hüttmann A, et al. CD38 expression is an important prognostic marker in chronic lymphocytic leukaemia. *Leukemia*. 2002 Jan;16(1):30–5.
72. Schroers R, Griesinger F, Trümper L, Haase D, Kulle B, Klein-Hitpass L, et al. Combined analysis of ZAP-70 and CD38 expression as a predictor of disease progression in B-cell chronic lymphocytic leukemia. *Leukemia*. 2005 May;19(5):750–8.
73. Saka B, Aktan M, Sami U, Oner D, Sanem O, Dinçol G. Prognostic importance of soluble CD23 in B-cell chronic lymphocytic leukemia. *Clin Lab Haematol*. 2006 Feb;28(1):30–5.
74. Del Poeta G, Maurillo L, Venditti A, Buccisano F, Epiceno AM, Capelli G, et al. Clinical significance of CD38 expression in chronic lymphocytic leukemia. *Blood*. 2001 Nov 1;98(9):2633–9.
75. Fais F, Ghiotto F, Hashimoto S, Sellars B, Valetto A, Allen SL, et al. Chronic lymphocytic leukemia B cells express restricted sets of mutated and unmutated antigen receptors. *J Clin Invest*. 1998 Oct 15;102(8):1515–25.

TIME in B-cell lymphoid malignancies

76. Damle RN, Wasil T, Fais F, Ghiotto F, Valetto A, Allen SL, et al. Ig V gene mutation status and CD38 expression as novel prognostic indicators in chronic lymphocytic leukemia. *Blood*. 1999 Sep 15;94(6):1840–7.
77. Hamblin TJ, Davis Z, Gardiner A, Oscier DG, Stevenson FK. Unmutated Ig V(H) genes are associated with a more aggressive form of chronic lymphocytic leukemia. *Blood*. 1999 Sep 15;94(6):1848–54.
78. Davis Z, Forconi F, Parker A, Gardiner A, Thomas P, Catovsky D, et al. The outcome of Chronic lymphocytic leukaemia patients with 97% IGHV gene identity to germline is distinct from cases with <97% identity and similar to those with 98% identity. *Br J Haematol*. 2016 Apr;173(1):127–36.
79. Tobin G, Thunberg U, Johnson A, Eriksson I, Söderberg O, Karlsson K, et al. Chronic lymphocytic leukemias utilizing the VH3-21 gene display highly restricted Vλ2-14 gene use and homologous CDR3s: implicating recognition of a common antigen epitope. *Blood*. 2003 Jun 15;101(12):4952–7.
80. Ghiotto F, Fais F, Valetto A, Albesiano E, Hashimoto S, Dono M, et al. Remarkably similar antigen receptors among a subset of patients with chronic lymphocytic leukemia. *J Clin Invest*. 2004 Apr;113(7):1008–16.
81. Messmer BT, Albesiano E, Efremov DG, Ghiotto F, Allen SL, Kolitz J, et al. Multiple Distinct Sets of Stereotyped Antigen Receptors Indicate a Role for Antigen in Promoting Chronic Lymphocytic Leukemia. *J Exp Med*. 2004 Aug 16;200(4):519–25.
82. Tobin G, Thunberg U, Karlsson K, Murray F, Laurell A, Willander K, et al. Subsets with restricted immunoglobulin gene rearrangement features indicate a role for antigen selection in the development of chronic lymphocytic leukemia. *Blood*. 2004 Nov 1;104(9):2879–85.
83. Stamatopoulos K, Belessi C, Moreno C, Boudjograh M, Guida G, Smilevska T, et al. Over 20% of patients with chronic lymphocytic leukemia carry stereotyped receptors: Pathogenetic implications and clinical correlations. *Blood*. 2007 Jan 1;109(1):259–70.
84. Agathangelidis A, Darzentas N, Hadzidimitriou A, Brochet X, Murray F, Yan X-J, et al. Stereotyped B-cell receptors in one-third of chronic lymphocytic leukemia: a molecular classification with implications for targeted therapies. *Blood*. 2012 May 10;119(19):4467–75.
85. Tobin G, Thunberg U, Johnson A, Thörn I, Söderberg O, Hultdin M, et al. Somatically mutated Ig V(H)3-21 genes characterize a new subset of chronic lymphocytic leukemia. *Blood*. 2002 Mar 15;99(6):2262–4.
86. Stamatopoulos K, Agathangelidis A, Rosenquist R, Ghia P. Antigen receptor stereotypy in chronic lymphocytic leukemia. *Leukemia*. 2017 Feb;31(2):282–91.
87. Crespo M, Bosch F, Villamor N, Bellosillo B, Colomer D, Rozman M, et al. ZAP-70 expression as a surrogate for immunoglobulin-variable-region mutations in chronic lymphocytic leukemia. *N Engl J Med*. 2003 May 1;348(18):1764–75.
88. Wiestner A, Rosenwald A, Barry TS, Wright G, Davis RE, Henrickson SE, et al. ZAP-70 expression identifies a chronic lymphocytic leukemia subtype with unmutated immunoglobulin genes, inferior clinical outcome, and distinct gene expression profile. *Blood*. 2003 Jun 15;101(12):4944–51.

89. Campana D, Suzuki T, Todisco E, Kitanaka A. CD38 in hematopoiesis. *Chem Immunol*. 2000;75:169–88.
90. Deaglio S, Capobianco A, Bergui L, Dürig J, Morabito F, Dührsen U, et al. CD38 is a signaling molecule in B-cell chronic lymphocytic leukemia cells. *Blood*. 2003 Sep 15;102(6):2146–55.
91. Hamblin TJ, Orchard JA, Ibbotson RE, Davis Z, Thomas PW, Stevenson FK, et al. CD38 expression and immunoglobulin variable region mutations are independent prognostic variables in chronic lymphocytic leukemia, but CD38 expression may vary during the course of the disease. *Blood*. 2002 Feb 1;99(3):1023–9.
92. Jelinek DF, Tschumper RC, Geyer SM, Bone ND, Dewald GW, Hanson CA, et al. Analysis of clonal B-cell CD38 and immunoglobulin variable region sequence status in relation to clinical outcome for B-chronic lymphocytic leukaemia. *Br J Haematol*. 2001 Dec;115(4):854–61.
93. Shanafelt TD, Geyer SM, Bone ND, Tschumper RC, Witzig TE, Nowakowski GS, et al. CD49d expression is an independent predictor of overall survival in patients with chronic lymphocytic leukaemia: a prognostic parameter with therapeutic potential. *Br J Haematol*. 2008 Mar;140(5):537–46.
94. Rossi D, Zucchetto A, Rossi FM, Capello D, Cerri M, Deambrogi C, et al. CD49d expression is an independent risk factor of progressive disease in early stage chronic lymphocytic leukemia. *Haematologica*. 2008 Oct 1;93(10):1575–9.
95. Gattei V, Bulian P, Del Principe MI, Zucchetto A, Maurillo L, Buccisano F, et al. Relevance of CD49d protein expression as overall survival and progressive disease prognosticator in chronic lymphocytic leukemia. *Blood*. 2008 Jan 15;111(2):865–73.
96. Bulian P, Shanafelt TD, Fegan C, Zucchetto A, Cro L, Nüchel H, et al. CD49d Is the Strongest Flow Cytometry–Based Predictor of Overall Survival in Chronic Lymphocytic Leukemia. *Journal of Clinical Oncology* [Internet]. 2014 Feb 10 [cited 2020 Feb 13]; Available from: <https://ascopubs.org/doi/pdf/10.1200/JCO.2013.50.8515>
97. Döhner H, Stilgenbauer S, Benner A, Leupolt E, Kröber A, Bullinger L, et al. Genomic aberrations and survival in chronic lymphocytic leukemia. *N Engl J Med*. 2000 Dec 28;343(26):1910–6.
98. Australian Pancreatic Cancer Genome Initiative, ICGC Breast Cancer Consortium, ICGC MML-Seq Consortium, ICGC PedBrain, Alexandrov LB, Nik-Zainal S, et al. Signatures of mutational processes in human cancer. *Nature*. 2013 Aug;500(7463):415–21.
99. Caligaris-Cappio F, Gobbi M, Bofill M, Janosy G. Infrequent normal B lymphocytes express features of B-chronic lymphocytic leukemia. *J Exp Med*. 1982 Feb 1;155(2):623–8.
100. Caligaris-Cappio F. B-chronic lymphocytic leukemia: a malignancy of anti-self B cells. *Blood*. 1996 Apr 1;87(7):2615–20.
101. Fischer M, Klein U, Küppers R. Molecular single-cell analysis reveals that CD5-positive peripheral blood B cells in healthy humans are characterized by rearranged V κ genes lacking somatic mutation. *J Clin Invest*. 1997 Oct 1;100(7):1667–76.
102. Bhat NM, Kantor AB, Bieber MM, Stall AM, Herzenberg LA, Teng NN. The ontogeny and functional characteristics of human B-1 (CD5+ B) cells. *Int Immunol*. 1992 Feb;4(2):243–52.

TIME in B-cell lymphoid malignancies

103. Casali P, Notkins AL. Probing the human B-cell repertoire with EBV: polyreactive antibodies and CD5⁺ B lymphocytes. *Annu Rev Immunol.* 1989;7:513–35.
104. Mantovani L, Wilder RL, Casali P. Human rheumatoid B-1a (CD5⁺ B) cells make somatically hypermutated high affinity IgM rheumatoid factors. *J Immunol.* 1993 Jul 1;151(1):473–88.
105. Kasaian MT, Casali P. B-1 cellular origin and VH segment structure of IgG, IgA, and IgM anti-DNA autoantibodies in patients with systemic lupus erythematosus. *Ann N Y Acad Sci.* 1995 Sep 29;764:410–23.
106. Küppers R, Klein U, Hansmann ML, Rajewsky K. Cellular origin of human B-cell lymphomas. *N Engl J Med.* 1999 Nov 11;341(20):1520–9.
107. Klein U, Tu Y, Stolovitzky GA, Mattioli M, Cattoretti G, Husson H, et al. Gene expression profiling of B cell chronic lymphocytic leukemia reveals a homogeneous phenotype related to memory B cells. *J Exp Med.* 2001 Dec 3;194(11):1625–38.
108. Rosenwald A, Alizadeh AA, Widhopf G, Simon R, Davis RE, Yu X, et al. Relation of gene expression phenotype to immunoglobulin mutation genotype in B cell chronic lymphocytic leukemia. *J Exp Med.* 2001 Dec 3;194(11):1639–47.
109. Ha YJ, Mun Y-C, Seong C-M, Lee JR. Characterization of phenotypically distinct B-cell subsets and receptor-stimulated mitogen-activated protein kinase activation in human cord blood B cells. *Journal of Leukocyte Biology.* 2008;84(6):1557–64.
110. Sims GP, Ettinger R, Shirota Y, Yarboro CH, Illei GG, Lipsky PE. Identification and characterization of circulating human transitional B cells. *Blood.* 2005 Jun 1;105(11):4390–8.
111. Seifert M, Sellmann L, Bloehdorn J, Wein F, Stilgenbauer S, Dürig J, et al. Cellular origin and pathophysiology of chronic lymphocytic leukemia. *J Exp Med.* 2012 Nov 19;209(12):2183–98.
112. Kikushige Y, Ishikawa F, Miyamoto T, Shima T, Urata S, Yoshimoto G, et al. Self-renewing hematopoietic stem cell is the primary target in pathogenesis of human chronic lymphocytic leukemia. *Cancer Cell.* 2011 Aug 16;20(2):246–59.
113. Marsilio S, Khiabani H, Fabbri G, Vergani S, Scuoppo C, Montserrat E, et al. Somatic CLL mutations occur at multiple distinct hematopoietic maturation stages: documentation and cautionary note regarding cell fraction purity. *Leukemia.* 2018 Apr;32(4):1040–3.
114. Barrio S, Shanafelt TD, Ojha J, Chaffee KG, Secreto C, Kortüm KM, et al. Genomic Characterization of High-Count MBL Cases Indicates that Early Detection of Driver Mutations and Subclonal Expansion are Predictors of Adverse Clinical Outcome. *Leukemia.* 2017 Jan;31(1):170–6.
115. Rossi D, Gaidano G. Richter syndrome: pathogenesis and management. *Seminars in Oncology.* 2016 Apr 1;43(2):311–9.
116. Fabbri G, Khiabani H, Holmes AB, Wang J, Messina M, Mullighan CG, et al. Genetic lesions associated with chronic lymphocytic leukemia transformation to Richter syndrome. *J Exp Med.* 2013 Oct 21;210(11):2273–88.

117. Chigrinova E, Rinaldi A, Kwee I, Rossi D, Rancoita PMV, Strefford JC, et al. Two main genetic pathways lead to the transformation of chronic lymphocytic leukemia to Richter syndrome. *Blood*. 2013 Oct 10;122(15):2673–82.
118. Grever MR, Lucas DM, Dewald GW, Neuberg DS, Reed JC, Kitada S, et al. Comprehensive assessment of genetic and molecular features predicting outcome in patients with chronic lymphocytic leukemia: results from the US Intergroup Phase III Trial E2997. *J Clin Oncol*. 2007 Mar 1;25(7):799–804.
119. Marasca R, Maffei R, Martinelli S, Fiorcari S, Bulgarelli J, Debbia G, et al. Clinical heterogeneity of de novo 11q deletion chronic lymphocytic leukaemia: prognostic relevance of extent of 11q deleted nuclei inside leukemic clone. *Hematol Oncol*. 2013 Jun;31(2):88–95.
120. Tam CS, Shanafelt TD, Wierda WG, Abruzzo LV, Van Dyke DL, O'Brien S, et al. De novo deletion 17p13.1 chronic lymphocytic leukemia shows significant clinical heterogeneity: the M. D. Anderson and Mayo Clinic experience. *Blood*. 2009 Jul 30;114(5):957–64.
121. Oscier DG, Gardiner AC, Mould SJ, Glide S, Davis ZA, Ibbotson RE, et al. Multivariate analysis of prognostic factors in CLL: clinical stage, IGVH gene mutational status, and loss or mutation of the p53 gene are independent prognostic factors. *Blood*. 2002 Aug 15;100(4):1177–84.
122. Strati P, Abruzzo LV, Wierda WG, O'Brien S, Ferrajoli A, Keating MJ. Second cancers and Richter transformation are the leading causes of death in patients with trisomy 12 chronic lymphocytic leukemia. *Clin Lymphoma Myeloma Leuk*. 2015 Jul;15(7):420–7.
123. Rossi D, Cerri M, Capello D, Deambrogi C, Rossi FM, Zucchetto A, et al. Biological and clinical risk factors of chronic lymphocytic leukaemia transformation to Richter syndrome. *Br J Haematol*. 2008 Jun;142(2):202–15.
124. Thompson PA, Tam CS, O'Brien SM, Wierda WG, Stingo F, Plunkett W, et al. Fludarabine, cyclophosphamide, and rituximab treatment achieves long-term disease-free survival in IGHV-mutated chronic lymphocytic leukemia. *Blood*. 2016 Jan 21;127(3):303–9.
125. Herling CD, Klaumünzer M, Rocha CK, Altmüller J, Thiele H, Bahlo J, et al. Complex karyotypes and KRAS and POT1 mutations impact outcome in CLL after chlorambucil-based chemotherapy or chemoimmunotherapy. *Blood*. 2016 21;128(3):395–404.
126. Baliakas P, Jeromin S, Iskas M, Puiggros A, Plevova K, Nguyen-Khac F, et al. Cytogenetic complexity in chronic lymphocytic leukemia: definitions, associations, and clinical impact. *Blood*. 2019 14;133(11):1205–16.
127. Leeksma AC, Baliakas P, Moysiadis T, Puiggros A, Plevova K, Kevie-Kersemaekers A-M van der, et al. Genomic arrays identify high-risk chronic lymphocytic leukemia with genomic complexity: a multi-center study. *Haematologica* [Internet]. 2020 Jan 23 [cited 2020 Jun 23]; Available from: <http://www.haematologica.org/content/early/2020/01/21/haematol.2019.239947>
128. Landau DA, Tausch E, Taylor-Weiner AN, Stewart C, Reiter JG, Bahlo J, et al. Mutations driving CLL and their evolution in progression and relapse. *Nature*. 2015 Oct;526(7574):525–30.

TIME in B-cell lymphoid malignancies

129. Wang L, Lawrence MS, Wan Y, Stojanov P, Sougnez C, Stevenson K, et al. SF3B1 and other novel cancer genes in chronic lymphocytic leukemia. *N Engl J Med*. 2011 Dec 29;365(26):2497–506.
130. Quesada V, Conde L, Villamor N, Ordóñez GR, Jares P, Bassaganyas L, et al. Exome sequencing identifies recurrent mutations of the splicing factor SF3B1 gene in chronic lymphocytic leukemia. *Nat Genet*. 2011 Dec 11;44(1):47–52.
131. Landau DA, Carter SL, Stojanov P, McKenna A, Stevenson K, Lawrence MS, et al. Evolution and impact of subclonal mutations in chronic lymphocytic leukemia. *Cell*. 2013 Feb 14;152(4):714–26.
132. Puente XS, Pinyol M, Quesada V, Conde L, Ordonez GR, Villamor N, et al. Whole-genome sequencing identifies recurrent mutations in chronic lymphocytic leukaemia. *Nature*. 2011 Jun 5;475(7354):101–5.
133. O'Neil J, Grim J, Strack P, Rao S, Tibbitts D, Winter C, et al. FBW7 mutations in leukemic cells mediate NOTCH pathway activation and resistance to γ -secretase inhibitors. *J Exp Med*. 2007 Aug 6;204(8):1813–24.
134. Jeromin S, Weissmann S, Haferlach C, Dicker F, Bayer K, Grossmann V, et al. SF3B1 mutations correlated to cytogenetics and mutations in NOTCH1, FBXW7, MYD88, XPO1 and TP53 in 1160 untreated CLL patients. *Leukemia*. 2014 Jan;28(1):108–17.
135. Ramsay AJ, Quesada V, Foronda M, Conde L, Martínez-Trillos A, Villamor N, et al. POT1 mutations cause telomere dysfunction in chronic lymphocytic leukemia. *Nat Genet*. 2013 May;45(5):526–30.
136. Ljungström V, Cortese D, Young E, Pandzic T, Mansouri L, Plevova K, et al. Whole-exome sequencing in relapsing chronic lymphocytic leukemia: clinical impact of recurrent RPS15 mutations. *Blood*. 2016 Feb 25;127(8):1007–16.
137. Baliakas P, Hadzidimitriou A, Sutton L-A, Rossi D, Minga E, Villamor N, et al. Recurrent mutations refine prognosis in chronic lymphocytic leukemia. *Leukemia*. 2015 Feb;29(2):329–36.
138. Nadeu F, Delgado J, Royo C, Baumann T, Stankovic T, Pinyol M, et al. Clinical impact of clonal and subclonal TP53, SF3B1, BIRC3, NOTCH1, and ATM mutations in chronic lymphocytic leukemia. *Blood*. 2016 Apr 28;127(17):2122–30.
139. Rossi D, Rasi S, Fabbri G, Spina V, Fangazio M, Forconi F, et al. Mutations of NOTCH1 are an independent predictor of survival in chronic lymphocytic leukemia. *Blood*. 2012 Jan 12;119(2):521–9.
140. Guruharsha KG, Kankel MW, Artavanis-Tsakonas S. The Notch signalling system: recent insights into the complexity of a conserved pathway. *Nat Rev Genet*. 2012 Sep;13(9):654–66.
141. Zenz T, Eichhorst B, Busch R, Denzel T, Häbe S, Winkler D, et al. TP53 mutation and survival in chronic lymphocytic leukemia. *J Clin Oncol*. 2010 Oct 10;28(29):4473–9.
142. Zenz T, Kröber A, Scherer K, Häbe S, Bühler A, Benner A, et al. Monoallelic TP53 inactivation is associated with poor prognosis in chronic lymphocytic leukemia: results from a detailed genetic characterization with long-term follow-up. *Blood*. 2008 Oct 15;112(8):3322–9.

143. Stilgenbauer S, Schnaiter A, Paschka P, Zenz T, Rossi M, Döhner K, et al. Gene mutations and treatment outcome in chronic lymphocytic leukemia: results from the CLL8 trial. *Blood*. 2014 May 22;123(21):3247–54.
144. Gonzalez D, Martinez P, Wade R, Hockley S, Oscier D, Matutes E, et al. Mutational status of the TP53 gene as a predictor of response and survival in patients with chronic lymphocytic leukemia: results from the LRF CLL4 trial. *J Clin Oncol*. 2011 Jun 1;29(16):2223–9.
145. Rossi D, Cerri M, Deambrogi C, Sozzi E, Cresta S, Rasi S, et al. The prognostic value of TP53 mutations in chronic lymphocytic leukemia is independent of Del17p13: implications for overall survival and chemorefractoriness. *Clin Cancer Res*. 2009 Feb 1;15(3):995–1004.
146. Levine AJ, Momand J, Finlay CA. The p53 tumour suppressor gene. *Nature*. 1991 Jun;351(6326):453–6.
147. Rossi D, Rasi S, Spina V, Brusca A, Monti S, Ciardullo C, et al. Integrated mutational and cytogenetic analysis identifies new prognostic subgroups in chronic lymphocytic leukemia. *Blood*. 2013 Feb 21;121(8):1403–12.
148. Rossi D, Spina V, Deambrogi C, Rasi S, Laurenti L, Stamatopoulos K, et al. The genetics of Richter syndrome reveals disease heterogeneity and predicts survival after transformation. *Blood*. 2011 Mar 24;117(12):3391–401.
149. Knight S, Yau C, Clifford R, Timbs AT, Sadighi Akha E, Dréau HM, et al. Quantification of subclonal distributions of recurrent genomic aberrations in paired pre-treatment and relapse samples from patients with B-cell chronic lymphocytic leukemia. *Leukemia*. 2012 Jul;26(7):1564–75.
150. Amin NA, Seymour E, Saiya-Cork K, Parkin B, Shedden K, Malek SN. A Quantitative Analysis of Subclonal and Clonal Gene Mutations before and after Therapy in Chronic Lymphocytic Leukemia. *Clin Cancer Res*. 2016 Sep 1;22(17):4525–35.
151. Guarini A, Marinelli M, Tavolaro S, Bellacchio E, Magliozzi M, Chiaretti S, et al. ATM gene alterations in chronic lymphocytic leukemia patients induce a distinct gene expression profile and predict disease progression. *Haematologica*. 2012 Jan;97(1):47–55.
152. Austen B, Powell JE, Alvi A, Edwards I, Hooper L, Starczynski J, et al. Mutations in the ATM gene lead to impaired overall and treatment-free survival that is independent of IGVH mutation status in patients with B-CLL. *Blood*. 2005 Nov 1;106(9):3175–82.
153. Austen B, Skowronska A, Baker C, Powell JE, Gardiner A, Oscier D, et al. Mutation status of the residual ATM allele is an important determinant of the cellular response to chemotherapy and survival in patients with chronic lymphocytic leukemia containing an 11q deletion. *J Clin Oncol*. 2007 Dec 1;25(34):5448–57.
154. Skowronska A, Parker A, Ahmed G, Oldreive C, Davis Z, Richards S, et al. Biallelic ATM inactivation significantly reduces survival in patients treated on the United Kingdom Leukemia Research Fund Chronic Lymphocytic Leukemia 4 trial. *J Clin Oncol*. 2012 Dec 20;30(36):4524–32.
155. Agathangelidis A, Ljungström V, Scarfò L, Fazi C, Gounari M, Pandzic T, et al. Highly similar genomic landscapes in monoclonal B-cell lymphocytosis and ultra-stable chronic lymphocytic leukemia with low frequency of driver mutations. *Haematologica*. 2018 May 1;103(5):865–73.

156. Ojha J, Secreto C, Rabe K, Ayres-Silva J, Tschumper R, Dyke DV, et al. Monoclonal B-cell lymphocytosis is characterized by mutations in CLL putative driver genes and clonal heterogeneity many years before disease progression. *Leukemia*. 2014 Dec;28(12):2395–8.
157. Rossi D, Fangazio M, Rasi S, Vaisitti T, Monti S, Cresta S, et al. Disruption of BIRC3 associates with fludarabine chemorefractoriness in TP53 wild-type chronic lymphocytic leukemia. *Blood*. 2012 Mar 22;119(12):2854–62.
158. Zarnegar BJ, Wang Y, Mahoney DJ, Dempsey PW, Cheung HH, He J, et al. Activation of noncanonical NF- κ B requires coordinated assembly of a regulatory complex of the adaptors cIAP1, cIAP2, TRAF2, TRAF3 and the kinase NIK. *Nat Immunol*. 2008 Dec;9(12):1371–8.
159. Rossi D, Brusca A, Spina V, Rasi S, Khiabani H, Messina M, et al. Mutations of the SF3B1 splicing factor in chronic lymphocytic leukemia: association with progression and fludarabine-refractoriness. *Blood*. 2011 Dec 22;118(26):6904–8.
160. Wang L, Lawrence MS, Wan Y, Stojanov P, Sougnez C, Stevenson K, et al. SF3B1 and other novel cancer genes in chronic lymphocytic leukemia. *N Engl J Med*. 2011 Dec 29;365(26):2497–506.
161. Wang L, Brooks AN, Fan J, Wan Y, Gambe R, Li S, et al. Transcriptomic Characterization of SF3B1 Mutation Reveals Its Pleiotropic Effects in Chronic Lymphocytic Leukemia. *Cancer Cell*. 2016 Nov 14;30(5):750–63.
162. Martínez-Trillos A, Pinyol M, Navarro A, Aymerich M, Jares P, Juan M, et al. Mutations in TLR/MYD88 pathway identify a subset of young chronic lymphocytic leukemia patients with favorable outcome. *Blood*. 2014 Jun 12;123(24):3790–6.
163. Puente XS, Beà S, Valdés-Mas R, Villamor N, Gutiérrez-Abril J, Martín-Subero JI, et al. Non-coding recurrent mutations in chronic lymphocytic leukaemia. *Nature*. 2015 Oct;526(7574):519–24.
164. Oscier D, Fitchett M, Herbert T, Lambert R. Karyotypic evolution in B-cell chronic lymphocytic leukaemia. *Genes Chromosomes Cancer*. 1991 Jan;3(1):16–20.
165. Stilgenbauer S, Sander S, Bullinger L, Benner A, Leupolt E, Winkler D, et al. Clonal evolution in chronic lymphocytic leukemia: acquisition of high-risk genomic aberrations associated with unmutated VH, resistance to therapy, and short survival. *Haematologica*. 2007 Sep;92(9):1242–5.
166. Fernandez V, Jares P, Salaverria I, Gine E, Bea S, Aymerich M, et al. Gene expression profile and genomic changes in disease progression of early-stage chronic lymphocytic leukemia. *Haematologica*. 2008 Jan;93(1):132–6.
167. Shanafelt TD, Witzig TE, Fink SR, Jenkins RB, Paternoster SF, Smoley SA, et al. Prospective evaluation of clonal evolution during long-term follow-up of patients with untreated early-stage chronic lymphocytic leukemia. *J Clin Oncol*. 2006 Oct 1;24(28):4634–41.
168. Gunnarsson R, Mansouri L, Isaksson A, Goransson H, Cahill N, Jansson M, et al. Array-based genomic screening at diagnosis and during follow-up in chronic lymphocytic leukemia. *Haematologica*. 2011 Aug;96(8):1161–9.

169. Smith EN, Ghia EM, DeBoever CM, Rassenti LZ, Jepsen K, Yoon K-A, et al. Genetic and epigenetic profiling of CLL disease progression reveals limited somatic evolution and suggests a relationship to memory-cell development. *Blood Cancer J*. 2015 Apr;5(4):e303.
170. Rose-Zerilli MJ, Gibson J, Wang J, Tapper W, Davis Z, Parker H, et al. Longitudinal copy number, whole exome and targeted deep sequencing of “good risk” IGHV-mutated CLL patients with progressive disease. *Leukemia*. 2016;30(6):1301–10.
171. Nadeu F, Clot G, Delgado J, Martín-García D, Baumann T, Salaverria I, et al. Clinical impact of the subclonal architecture and mutational complexity in chronic lymphocytic leukemia. *Leukemia*. 2018;32(3):645–53.
172. Hernández-Sánchez M, Kotaskova J, Rodríguez AE, Radova L, Tamborero D, Abáigar M, et al. CLL cells cumulate genetic aberrations prior to the first therapy even in outwardly inactive disease phase. *Leukemia*. 2018 Sep 12;
173. Ramassone A, D’Argenio A, Veronese A, Basti A, Soliman SHA, Volinia S, et al. Genetic dynamics in untreated CLL patients with either stable or progressive disease: a longitudinal study. *J Hematol Oncol*. 2019 Nov 19;12(1):114.
174. Oakes CC, Claus R, Gu L, Assenov Y, Hüllein J, Zucknick M, et al. Evolution of DNA methylation is linked to genetic aberrations in chronic lymphocytic leukemia. *Cancer Discov*. 2014 Mar;4(3):348–61.
175. Rossi D, Spina V, Gaidano G. Biology and treatment of Richter syndrome. *Blood*. 2018 Jun 21;131(25):2761–72.
176. Villamor N, Conde L, Martínez-Trillos A, Cazorla M, Navarro A, Beà S, et al. NOTCH1 mutations identify a genetic subgroup of chronic lymphocytic leukemia patients with high risk of transformation and poor outcome. *Leukemia*. 2013 Apr;27(5):1100–6.
177. Rossi D, Rasi S, Spina V, Fangazio M, Monti S, Greco M, et al. Different impact of NOTCH1 and SF3B1 mutations on the risk of chronic lymphocytic leukemia transformation to Richter syndrome. *British Journal of Haematology*. 2012;158(3):426–9.
178. Pasqualucci L, Dalla-Favera R. The Genetic Landscape of Diffuse Large B Cell Lymphoma. *Seminars in hematology*. 2015 Apr;52(2):67.
179. Beà S, López-Guillermo A, Ribas M, Puig X, Pinyol M, Carrió A, et al. Genetic imbalances in progressed B-cell chronic lymphocytic leukemia and transformed large-cell lymphoma (Richter’s syndrome). *Am J Pathol*. 2002 Sep;161(3):957–68.
180. Timár B, Fülöp Z, Csernus B, Angster C, Bognár A, Szepesi A, et al. Relationship between the mutational status of VH genes and pathogenesis of diffuse large B-cell lymphoma in Richter’s syndrome. *Leukemia*. 2004 Feb;18(2):326–30.
181. Jones J, Mato A, Coutre S, Byrd JC, Furman RR, Hillmen P, et al. Evaluation of 230 patients with relapsed/refractory deletion 17p chronic lymphocytic leukaemia treated with ibrutinib from 3 clinical trials. *British Journal of Haematology*. 2018;182(4):504–12.
182. Rossi D, Khiabanian H, Spina V, Ciardullo C, Brusca A, Famà R, et al. Clinical impact of small TP53 mutated subclones in chronic lymphocytic leukemia. *Blood*. 2014 Apr 3;123(14):2139–47.

183. Fischer K, Bahlo J, Fink AM, Goede V, Herling CD, Cramer P, et al. Long-term remissions after FCR chemoimmunotherapy in previously untreated patients with CLL: updated results of the CLL8 trial. *Blood*. 2016 Jan 14;127(2):208–15.
184. Hallek M, Fischer K, Fingerle-Rowson G, Fink AM, Busch R, Mayer J, et al. Addition of rituximab to fludarabine and cyclophosphamide in patients with chronic lymphocytic leukaemia: a randomised, open-label, phase 3 trial. *The Lancet*. 2010 Oct 2;376(9747):1164–74.
185. Goede V, Fischer K, Busch R, Engelke A, Eichhorst B, Wendtner CM, et al. Obinutuzumab plus Chlorambucil in Patients with CLL and Coexisting Conditions. *New England Journal of Medicine*. 2014 Mar 20;370(12):1101–10.
186. Woyach JA, Ruppert AS, Heerema NA, Zhao W, Booth AM, Ding W, et al. Ibrutinib Regimens versus Chemoimmunotherapy in Older Patients with Untreated CLL. *New England Journal of Medicine*. 2018 Dec 27;379(26):2517–28.
187. Moreno C, Greil R, Demirkan F, Tedeschi A, Anz B, Larratt L, et al. Ibrutinib plus obinutuzumab versus chlorambucil plus obinutuzumab in first-line treatment of chronic lymphocytic leukaemia (iLLUMINATE): a multicentre, randomised, open-label, phase 3 trial. *The Lancet Oncology*. 2019 Jan 1;20(1):43–56.
188. Shanafelt TD, Wang V, Kay NE, Hanson CA, O'Brien SM, Barrientos JC, et al. A Randomized Phase III Study of Ibrutinib (PCI-32765)-Based Therapy Vs. Standard Fludarabine, Cyclophosphamide, and Rituximab (FCR) Chemoimmunotherapy in Untreated Younger Patients with Chronic Lymphocytic Leukemia (CLL): A Trial of the ECOG-ACRIN Cancer Research Group (E1912). *Blood*. 2018 Nov 29;132(Supplement 1):LBA-4-LBA-4.
189. O'Brien S, Furman RR, Coutre S, Flinn IW, Burger JA, Blum K, et al. Single-agent ibrutinib in treatment-naïve and relapsed/refractory chronic lymphocytic leukemia: a 5-year experience. *Blood*. 2018 26;131(17):1910–9.
190. Seymour JF, Kipps TJ, Eichhorst B, Hillmen P, D'Rozario J, Assouline S, et al. Venetoclax–Rituximab in Relapsed or Refractory Chronic Lymphocytic Leukemia. *New England Journal of Medicine*. 2018 Mar 22;378(12):1107–20.
191. Furman RR, Sharman JP, Coutre SE, Cheson BD, Pagel JM, Hillmen P, et al. Idelalisib and Rituximab in Relapsed Chronic Lymphocytic Leukemia. *New England Journal of Medicine*. 2014 Mar 13;370(11):997–1007.
192. Weerdt I de, Koopmans SM, Kater AP, Gelder M van. Incidence and management of toxicity associated with ibrutinib and idelalisib: a practical approach. *Haematologica* [Internet]. 2017 Aug 3 [cited 2020 Jun 24]; Available from: <http://www.haematologica.org/content/early/2017/07/31/haematol.2017.164103>
193. Jones JA, Mato AR, Wierda WG, Davids MS, Choi M, Cheson BD, et al. Venetoclax for chronic lymphocytic leukaemia progressing after ibrutinib: an interim analysis of a multicentre, open-label, phase 2 trial. *Lancet Oncol*. 2018;19(1):65–75.
194. Purroy N, Abrisqueta P, Carabia J, Carpio C, Palacio C, Bosch F, et al. Co-culture of primary CLL cells with bone marrow mesenchymal cells, CD40 ligand and CpG ODN promotes proliferation of chemoresistant CLL cells phenotypically comparable to those proliferating in vivo. *Oncotarget*. 2015 Apr 10;6(10):7632–43.

195. Burger JA, Ghia P, Rosenwald A, Caligaris-Cappio F. The microenvironment in mature B-cell malignancies: a target for new treatment strategies. *Blood*. 2009 Oct 15;114(16):3367–75.
196. Marquez M-E, Hernández-Uzcátegui O, Cornejo A, Vargas P, Costa OD. Bone marrow stromal mesenchymal cells induce down regulation of CD20 expression on B-CLL: implications for rituximab resistance in CLL. *British Journal of Haematology*. 2015;169(2):211–8.
197. Jitschin R, Braun M, Qorraj M, Saul D, Le Blanc K, Zenz T, et al. Stromal cell-mediated glycolytic switch in CLL cells involves Notch-c-Myc signaling. *Blood*. 2015 May 28;125(22):3432–6.
198. Ten Hacken E, Burger JA. Microenvironment interactions and B-cell receptor signaling in Chronic Lymphocytic Leukemia: Implications for disease pathogenesis and treatment. *Biochim Biophys Acta*. 2016 Mar;1863(3):401–13.
199. Cols M, Barra CM, He B, Puga I, Xu W, Chiu A, et al. Stromal endothelial cells establish a bidirectional crosstalk with chronic lymphocytic leukemia cells through the TNF-related factors BAFF, APRIL, and CD40L. *J Immunol*. 2012 Jun 15;188(12):6071–83.
200. Maffei R, Fiorcari S, Bulgarelli J, Martinelli S, Castelli I, Deaglio S, et al. Physical contact with endothelial cells through $\beta 1$ - and $\beta 2$ - integrins rescues chronic lymphocytic leukemia from spontaneous and drug-induced apoptosis and induces a peculiar gene expression profile on leukemic cells. *Haematologica* [Internet]. 2011 Dec 29 [cited 2020 Aug 21]; Available from: <http://www.haematologica.org/content/early/2011/12/16/haematol.2011.054924>
201. Elston L, Fegan C, Hills R, Hashimdeen SS, Walsby E, Henley P, et al. Increased frequency of CD4+ PD-1+ HLA-DR+ T cells is associated with disease progression in CLL. *Br J Haematol*. 2020 Mar;188(6):872–80.
202. Catakovic K, Gassner FJ, Ratswohl C, Zaborsky N, Rebhandl S, Schubert M, et al. TIGIT expressing CD4+T cells represent a tumor-supportive T cell subset in chronic lymphocytic leukemia. *Oncoimmunology*. 2017;7(1):e1371399.
203. Riches JC, Davies JK, McClanahan F, Fatah R, Iqbal S, Agrawal S, et al. T cells from CLL patients exhibit features of T-cell exhaustion but retain capacity for cytokine production. *Blood*. 2013 Feb 28;121(9):1612–21.
204. Liu Z, Fan H, Jiang S. CD4(+) T-cell subsets in transplantation. *Immunological reviews*. 2013;
205. Palma M, Gentilcore G, Heimersson K, Mozaffari F, Näsman-Glaser B, Young E, et al. T cells in chronic lymphocytic leukemia display dysregulated expression of immune checkpoints and activation markers. *Haematologica*. 2017;102(3):562–72.
206. Bürgler S, Gimeno A, Parente-Ribes A, Wang D, Os A, Devereux S, et al. Chronic lymphocytic leukemia cells express CD38 in response to Th1 cell-derived IFN- γ by a Tbet-dependent mechanism. *J Immunol*. 2015 Jan 15;194(2):827–35.
207. Görgün G, Holderried TAW, Zahrieh D, Neuberg D, Gribben JG. Chronic lymphocytic leukemia cells induce changes in gene expression of CD4 and CD8 T cells. *J Clin Invest*. 2005 Jul 1;115(7):1797–805.

TIME in B-cell lymphoid malignancies

208. Rossmann ED, Lewin N, Jeddi-Tehrani M, Osterborg A, Mellstedt H. Intracellular T cell cytokines in patients with B cell chronic lymphocytic leukaemia (B-CLL). *Eur J Haematol*. 2002 May;68(5):299–306.
209. Buggins AGS, Patten PEM, Richards J, Thomas NSB, Mufti GJ, Devereux S. Tumor-derived IL-6 may contribute to the immunological defect in CLL. *Leukemia*. 2008 May;22(5):1084–7.
210. Roessner PM, Hanna BS, Öztürk S, Schulz R, Cid LL, Yazdanparast H, et al. TBET-expressing Th1 CD4+ T cells accumulate in chronic lymphocytic leukaemia without affecting disease progression in E μ -TCL1 mice. *British Journal of Haematology*. 2020;189(1):133–45.
211. Jain P, Javdan M, Feger FK, Chiu PY, Sison C, Damle RN, et al. Th17 and non-Th17 interleukin-17-expressing cells in chronic lymphocytic leukemia: delineation, distribution, and clinical relevance. *Haematologica*. 2012 Apr;97(4):599–607.
212. Ahearne MJ, Willimott S, Piñon L, Kennedy DB, Miall F, Dyer MJS, et al. Enhancement of CD154/IL4 proliferation by the T follicular helper (Tfh) cytokine, IL21 and increased numbers of circulating cells resembling Tfh cells in chronic lymphocytic leukaemia. *British Journal of Haematology*. 2013;162(3):360–70.
213. Beyer M, Kochanek M, Darabi K, Popov A, Jensen M, Endl E, et al. Reduced frequencies and suppressive function of CD4+CD25hi regulatory T cells in patients with chronic lymphocytic leukemia after therapy with fludarabine. *Blood*. 2005 Sep 15;106(6):2018–25.
214. Lad DP, Varma S, Varma N, Sachdeva MUS, Bose P, Malhotra P. Regulatory T-cells in B-cell chronic lymphocytic leukemia: their role in disease progression and autoimmune cytopenias. *Leuk Lymphoma*. 2013 May;54(5):1012–9.
215. D’Arena G, Simeon V, D’Auria F, Statuto T, Sanzo PD, Martino LD, et al. Regulatory T-cells in chronic lymphocytic leukemia: actor or innocent bystander? *Am J Blood Res*. 2013 Jan 17;3(1):52–7.
216. Sallusto F, Geginat J, Lanzavecchia A. Central memory and effector memory T cell subsets: function, generation, and maintenance. *Annu Rev Immunol*. 2004;22:745–63.
217. Nunes C, Wong R, Mason M, Fegan C, Man S, Pepper C. Expansion of a CD8(+)/PD-1(+) replicative senescence phenotype in early stage CLL patients is associated with inverted CD4:CD8 ratios and disease progression. *Clin Cancer Res*. 2012 Feb 1;18(3):678–87.
218. Gonnord P, Costa M, Abreu A, Peres M, Ysebaert L, Gadat S, et al. Multiparametric analysis of CD8+ T cell compartment phenotype in chronic lymphocytic leukemia reveals a signature associated with progression toward therapy. *Oncoimmunology* [Internet]. 2019 Feb 7 [cited 2020 Jan 23];8(4). Available from: <https://www.ncbi.nlm.nih.gov/pmc/articles/PMC6422371/>
219. Ramsay AG, Clear AJ, Fatah R, Gribben JG. Multiple inhibitory ligands induce impaired T-cell immunologic synapse function in chronic lymphocytic leukemia that can be blocked with lenalidomide: establishing a reversible immune evasion mechanism in human cancer. *Blood*. 2012 Aug 16;120(7):1412–21.
220. van Bruggen JAC, Martens AWJ, Fraietta JA, Hofland T, Tonino SH, Eldering E, et al. Chronic lymphocytic leukemia cells impair mitochondrial fitness in CD8+ T cells and impede CAR T-cell efficacy. *Blood*. 2019 04;134(1):44–58.

221. Ramsay AG, Johnson AJ, Lee AM, Gorgün G, Le Dieu R, Blum W, et al. Chronic lymphocytic leukemia T cells show impaired immunological synapse formation that can be reversed with an immunomodulating drug. *J Clin Invest*. 2008 Jul;118(7):2427–37.
222. Porter DL, Hwang W-T, Frey NV, Lacey SF, Shaw PA, Loren AWW, et al. Chimeric antigen receptor T cells persist and induce sustained remissions in relapsed refractory chronic lymphocytic leukemia. *Sci Transl Med*. 2015 Sep 2;7(303):303ra139.
223. Maffei R, Bulgarelli J, Fiorcari S, Bertonecchi L, Martinelli S, Guarnotta C, et al. The monocytic population in chronic lymphocytic leukemia shows altered composition and deregulation of genes involved in phagocytosis and inflammation. *Haematologica*. 2013 Jul;98(7):1115–23.
224. Schulz A, Toedt G, Zenz T, Stilgenbauer S, Lichter P, Seiffert M. Inflammatory cytokines and signaling pathways are associated with survival of primary chronic lymphocytic leukemia cells in vitro: a dominant role of CCL2. *Haematologica*. 2011 Mar 1;96(3):408–16.
225. Jitschin R, Braun M, Buttner M, Dettmer-Wilde K, Bricks J, Berger J, et al. CLL-cells induce IDOhi CD14+HLA-DRlo myeloid-derived suppressor cells that inhibit T-cell responses and promote TRegs. *Blood*. 2014 Jul 31;124(5):750–60.
226. LIU J, ZHOU Y, HUANG Q, QIU L. CD14+HLA-DRlow/- expression: A novel prognostic factor in chronic lymphocytic leukemia. *Oncol Lett*. 2015 Mar;9(3):1167–72.
227. Huergo-Zapico L, Acebes-Huerta A, Gonzalez-Rodriguez AP, Contesti J, Gonzalez-García E, Payer AR, et al. Expansion of NK Cells and Reduction of NKG2D Expression in Chronic Lymphocytic Leukemia. Correlation with Progressive Disease. *PLOS ONE*. 2014 Oct 6;9(10):e108326.
228. Palmer S, Hanson CA, Zent CS, Porrata LF, LaPlant B, Geyer SM, et al. Prognostic importance of T and NK-cells in a consecutive series of newly diagnosed patients with chronic lymphocytic leukaemia. *British Journal of Haematology*. 2008;141(5):607–14.
229. Wild J, Schmiedel BJ, Maurer A, Raab S, Prokop L, Stevanović S, et al. Neutralization of (NK-cell-derived) B-cell activating factor by Belimumab restores sensitivity of chronic lymphoid leukemia cells to direct and Rituximab-induced NK lysis. *Leukemia*. 2015 Aug;29(8):1676–83.
230. Heinig K, Gätjen M, Grau M, Stache V, Anagnostopoulos I, Gerlach K, et al. Access to Follicular Dendritic Cells Is a Pivotal Step in Murine Chronic Lymphocytic Leukemia B-cell Activation and Proliferation. *Cancer Discov*. 2014 Dec 1;4(12):1448–65.
231. DiLillo DJ, Weinberg JB, Yoshizaki A, Horikawa M, Bryant JM, Iwata Y, et al. Chronic lymphocytic leukemia and regulatory B cells share IL-10 competence and immunosuppressive function. *Leukemia*. 2013 Jan;27(1):170–82.
232. Ringelstein-Harlev S, Avivi I, Fanadka M, Horowitz NA, Katz T. Chronic lymphocytic leukemia cells acquire regulatory B-cell properties in response to TLR9 and CD40 activation. *Cancer Immunol Immunother*. 2018 May;67(5):739–48.
233. Mockridge CI, Potter KN, Wheatley I, Neville LA, Packham G, Stevenson FK. Reversible anergy of sIgM-mediated signaling in the two subsets of CLL defined by VH-gene mutational status. *Blood*. 2007 May 15;109(10):4424–31.

TIME in B-cell lymphoid malignancies

234. Dühren-von Minden M, Übelhart R, Schneider D, Wossning T, Bach MP, Buchner M, et al. Chronic lymphocytic leukaemia is driven by antigen-independent cell-autonomous signalling. *Nature*. 2012 Sep 13;489(7415):309–12.
235. Burger JA. Treatment of Chronic Lymphocytic Leukemia. *N Engl J Med*. 2020 30;383(5):460–73.
236. Woyach JA, Ruppert AS, Guinn D, Lehman A, Blachly JS, Lozanski A, et al. BTKC481S-Mediated Resistance to Ibrutinib in Chronic Lymphocytic Leukemia. *J Clin Oncol*. 2017 May 1;35(13):1437–43.
237. Woyach J, Huang Y, Rogers K, Bhat SA, Grever MR, Lozanski A, et al. Resistance to Acalabrutinib in CLL Is Mediated Primarily By BTK Mutations. *Blood*. 2019 Nov 13;134(Supplement_1):504–504.
238. Pascutti MF, Jak M, Tromp JM, Derks IAM, Remmerswaal EBM, Thijssen R, et al. IL-21 and CD40L signals from autologous T cells can induce antigen-independent proliferation of CLL cells. *Blood*. 2013 Oct 24;122(17):3010–9.
239. Bhattacharya N, Reichenzeller M, Caudron-Herger M, Haebe S, Brady N, Diener S, et al. Loss of cooperativity of secreted CD40L and increased dose-response to IL4 on CLL cell viability correlates with enhanced activation of NF- κ B and STAT6. *Int J Cancer*. 2015 Jan 1;136(1):65–73.
240. Buschle M, Campana D, Carding SR, Richard C, Hoffbrand AV, Brenner MK. Interferon gamma inhibits apoptotic cell death in B cell chronic lymphocytic leukemia. *J Exp Med*. 1993 Jan 1;177(1):213–8.
241. Gauthier M, Durrieu F, Martin E, Peres M, Vergez F, Filleron T, et al. Prognostic role of CD4 T-cell depletion after frontline fludarabine, cyclophosphamide and rituximab in chronic lymphocytic leukaemia. *BMC Cancer*. 2019 Aug 14;19(1):809.
242. Kocher T, Asslaber D, Zaborsky N, Flenady S, Denk U, Reinthaler P, et al. CD4+ T cells, but not non-classical monocytes, are dispensable for the development of chronic lymphocytic leukemia in the TCL1-tg murine model. *Leukemia*. 2016 Jun;30(6):1409–13.
243. Hanna BS, Roessner PM, Yazdanparast H, Colomer D, Campo E, Kugler S, et al. Control of chronic lymphocytic leukemia development by clonally-expanded CD8+ T-cells that undergo functional exhaustion in secondary lymphoid tissues. *Leukemia*. 2018 Sep 28;
244. Vardi A, Vlachonikola E, Karypidou M, Stalika E, Bikos V, Gemenetzi K, et al. Restrictions in the T-cell repertoire of chronic lymphocytic leukemia: high-throughput immunoprofiling supports selection by shared antigenic elements. *Leukemia*. 2017;31(7):1555–61.
245. Lewinsky H, Barak AF, Huber V, Kramer MP, Radomir L, Sever L, et al. CD84 regulates PD-1/PD-L1 expression and function in chronic lymphocytic leukemia. *J Clin Invest*. 2018 Dec 3;128(12):5465–78.
246. Dong S, Harrington BK, Hu EY, Greene JT, Lehman AM, Tran M, et al. PI3K p110 δ inactivation antagonizes chronic lymphocytic leukemia and reverses T cell immune suppression. *J Clin Invest*. 2019 Jan 2;129(1):122–36.
247. Villano JL, Koshy M, Shaikh H, Dolecek TA, McCarthy BJ. Age, gender, and racial differences in incidence and survival in primary CNS lymphoma. *Br J Cancer*. 2011 Oct 25;105(9):1414–8.

248. O'Neill BP, Decker PA, Tieu C, Cerhan JR. The changing incidence of primary central nervous system lymphoma is driven primarily by the changing incidence in young and middle-aged men and differs from time trends in systemic diffuse large B-cell non-Hodgkin's lymphoma. *Am J Hematol*. 2013 Dec;88(12):997–1000.
249. Cai Q, Fang Y, Young KH. Primary Central Nervous System Lymphoma: Molecular Pathogenesis and Advances in Treatment. *Transl Oncol*. 2019 Jan 4;12(3):523–38.
250. Grommes C, DeAngelis LM. Primary CNS Lymphoma. *J Clin Oncol*. 2017 Jul 20;35(21):2410–8.
251. Schlegel U, Schmidt-Wolf IG, Deckert M. Primary CNS lymphoma: clinical presentation, pathological classification, molecular pathogenesis and treatment. *J Neurol Sci*. 2000 Dec 1;181(1–2):1–12.
252. Hill QA, Owen RG. CNS prophylaxis in lymphoma: who to target and what therapy to use. *Blood Rev*. 2006 Nov;20(6):319–32.
253. Abrey LE, Batchelor TT, Ferreri AJM, Gospodarowicz M, Pulczynski EJ, Zucca E, et al. Report of an international workshop to standardize baseline evaluation and response criteria for primary CNS lymphoma. *J Clin Oncol*. 2005 Aug 1;23(22):5034–43.
254. Hegde U, Filie A, Little RF, Janik JE, Grant N, Steinberg SM, et al. High incidence of occult leptomeningeal disease detected by flow cytometry in newly diagnosed aggressive B-cell lymphomas at risk for central nervous system involvement: the role of flow cytometry versus cytology. *Blood*. 2005 Jan 15;105(2):496–502.
255. Bobillo S, Crespo M, Escudero L, Mayor R, Raheja P, Carpio C, et al. Cell free circulating tumor DNA in cerebrospinal fluid detects and monitors central nervous system involvement of B-cell lymphomas. *Haematologica*. 2020 Feb 20;
256. Ferreri AJM, Blay J-Y, Reni M, Pasini F, Spina M, Ambrosetti A, et al. Prognostic scoring system for primary CNS lymphomas: the International Extranodal Lymphoma Study Group experience. *J Clin Oncol*. 2003 Jan 15;21(2):266–72.
257. Abrey LE, Ben-Porat L, Panageas KS, Yahalom J, Berkey B, Curran W, et al. Primary central nervous system lymphoma: the Memorial Sloan-Kettering Cancer Center prognostic model. *J Clin Oncol*. 2006 Dec 20;24(36):5711–5.
258. Sasayama T, Nakamizo S, Nishihara M, Kawamura A, Tanaka H, Mizukawa K, et al. Cerebrospinal fluid interleukin-10 is a potentially useful biomarker in immunocompetent primary central nervous system lymphoma (PCNSL). *Neuro Oncol*. 2012 Mar;14(3):368–80.
259. Rubenstein JL, Wong VS, Kadoch C, Gao H-X, Barajas R, Chen L, et al. CXCL13 plus interleukin 10 is highly specific for the diagnosis of CNS lymphoma. *Blood*. 2013 Jun 6;121(23):4740–8.
260. Camilleri-Broët S, Martin A, Moreau A, Angonin R, Hénin D, Gontier MF, et al. Primary central nervous system lymphomas in 72 immunocompetent patients: pathologic findings and clinical correlations. Groupe Ouest Est d'étude des Leucémies et Autres Maladies du Sang (GOELAMS). *Am J Clin Pathol*. 1998 Nov;110(5):607–12.
261. Montesinos-Rongen M, Brunn A, Bentink S, Basso K, Lim WK, Klapper W, et al. Gene expression profiling suggests primary central nervous system lymphomas to be derived from a late germinal center B cell. *Leukemia*. 2008 Feb;22(2):400–5.

TIME in B-cell lymphoid malignancies

262. Levy O, DeAngelis LM, Filippa DA, Panageas KS, Abrey LE. Bcl-6 predicts improved prognosis in primary central nervous system lymphoma. *Cancer*. 2008;112(1):151–6.
263. Braaten KM, Betensky RA, de Leval L, Okada Y, Hochberg FH, Louis DN, et al. BCL-6 expression predicts improved survival in patients with primary central nervous system lymphoma. *Clin Cancer Res*. 2003 Mar;9(3):1063–9.
264. Kreher S, Jöhrens K, Strehlow F, Martus P, Borowiec K, Radke J, et al. Prognostic impact of B-cell lymphoma 6 in primary CNS lymphoma. *Neuro-oncology*. 2015 Jul;17(7):1016–21.
265. Montesinos-Rongen M, Van Roost D, Schaller C, Wiestler OD, Deckert M. Primary diffuse large B-cell lymphomas of the central nervous system are targeted by aberrant somatic hypermutation. *Blood*. 2004 Mar 1;103(5):1869–75.
266. Montesinos-Rongen M, Schmitz R, Courts C, Stenzel W, Bechtel D, Niedobitek G, et al. Absence of Immunoglobulin Class Switch in Primary Lymphomas of the Central Nervous System. *The American Journal of Pathology*. 2005 Jun 1;166(6):1773–9.
267. Deckert M, Montesinos-Rongen M, Brunn A, Siebert R. Systems biology of primary CNS lymphoma: from genetic aberrations to modeling in mice. *Acta Neuropathol*. 2014 Feb;127(2):175–88.
268. Montesinos-Rongen M, Zühlke-Jenisch R, Gesk S, Martín-Subero JI, Schaller C, Van Roost D, et al. Interphase cytogenetic analysis of lymphoma-associated chromosomal breakpoints in primary diffuse large B-cell lymphomas of the central nervous system. *J Neuropathol Exp Neurol*. 2002 Oct;61(10):926–33.
269. Pasqualucci L, Neumeister P, Goossens T, Nanjangud G, Chaganti RS, Küppers R, et al. Hypermutation of multiple proto-oncogenes in B-cell diffuse large-cell lymphomas. *Nature*. 2001 Jul 19;412(6844):341–6.
270. Cady FM, O'Neill BP, Law ME, Decker PA, Kurtz DM, Giannini C, et al. Del(6)(q22) and BCL6 rearrangements in primary CNS lymphoma are indicators of an aggressive clinical course. *J Clin Oncol*. 2008 Oct 10;26(29):4814–9.
271. Montesinos-Rongen M, Siebert R, Deckert M. Primary lymphoma of the central nervous system: just DLBCL or not? *Blood*. 2009 Jan 1;113(1):7–10.
272. Courts C, Montesinos-Rongen M, Brunn A, Bug S, Siemer D, Hans V, et al. Recurrent inactivation of the PRDM1 gene in primary central nervous system lymphoma. *J Neuropathol Exp Neurol*. 2008 Jul;67(7):720–7.
273. Schwindt H, Vater I, Kreuz M, Montesinos-Rongen M, Brunn A, Richter J, et al. Chromosomal imbalances and partial uniparental disomies in primary central nervous system lymphoma. *Leukemia*. 2009 Oct;23(10):1875–84.
274. Montesinos-Rongen M, Schäfer E, Siebert R, Deckert M. Genes regulating the B cell receptor pathway are recurrently mutated in primary central nervous system lymphoma. *Acta Neuropathol*. 2012 Dec;124(6):905–6.
275. Montesinos-Rongen M, Godlewska E, Brunn A, Wiestler OD, Siebert R, Deckert M. Activating L265P mutations of the MYD88 gene are common in primary central nervous system lymphoma. *Acta Neuropathol*. 2011 Dec 1;122(6):791–2.

276. Gonzalez-Aguilar A, Idbah A, Boisselier B, Habbita N, Rossetto M, Laurence A, et al. Recurrent Mutations of MYD88 and TBL1XR1 in Primary Central Nervous System Lymphomas. *Clin Cancer Res*. 2012 Oct 1;18(19):5203–11.
277. Chapuy B, Roemer MGM, Stewart C, Tan Y, Abo RP, Zhang L, et al. Targetable genetic features of primary testicular and primary central nervous system lymphomas. *Blood*. 2016 Feb 18;127(7):869–81.
278. Chen BJ, Chapuy B, Ouyang J, Sun HH, Roemer MGM, Xu ML, et al. PD-L1 expression is characteristic of a subset of aggressive B-cell lymphomas and virus-associated malignancies. *Clin Cancer Res*. 2013 Jul 1;19(13):3462–73.
279. Charette M de, Houot R. Hide or defend, the two strategies of lymphoma immune evasion: potential implications for immunotherapy. 1. 2018 Aug 1;103(8):1256–68.
280. Booman M, Douwes J, Glas AM, Riemersma SA, Jordanova ES, Kok K, et al. Mechanisms and Effects of Loss of Human Leukocyte Antigen Class II Expression in Immune-Privileged Site-Associated B-Cell Lymphoma. *Clin Cancer Res*. 2006 May 1;12(9):2698–705.
281. Braggio E, McPhail ER, Macon W, Lopes MB, Schiff D, Law M, et al. Primary Central Nervous System Lymphomas: A Validation Study of Array-Based Comparative Genomic Hybridization in Formalin-Fixed Paraffin-Embedded Tumor Specimens. *Clin Cancer Res*. 2011 Jul 1;17(13):4245–53.
282. Morris PG, Correa DD, Yahalom J, Raizer JJ, Schiff D, Grant B, et al. Rituximab, methotrexate, procarbazine, and vincristine followed by consolidation reduced-dose whole-brain radiotherapy and cytarabine in newly diagnosed primary CNS lymphoma: final results and long-term outcome. *J Clin Oncol*. 2013 Nov 1;31(31):3971–9.
283. Ferreri AJM, Cwynarski K, Pulczynski E, Ponzoni M, Deckert M, Politi LS, et al. Chemoimmunotherapy with methotrexate, cytarabine, thiotepa, and rituximab (MATRix regimen) in patients with primary CNS lymphoma: results of the first randomisation of the International Extranodal Lymphoma Study Group-32 (IELSG32) phase 2 trial. *Lancet Haematol*. 2016 May;3(5):e217-227.
284. Nelson DF, Martz KL, Bonner H, Nelson JS, Newall J, Kerman HD, et al. Non-Hodgkin's lymphoma of the brain: can high dose, large volume radiation therapy improve survival? Report on a prospective trial by the Radiation Therapy Oncology Group (RTOG): RTOG 8315. *Int J Radiat Oncol Biol Phys*. 1992;23(1):9–17.
285. Correa DD, Shi W, Abrey LE, Deangelis LM, Omuro AM, Deutsch MB, et al. Cognitive functions in primary CNS lymphoma after single or combined modality regimens. *Neuro-oncology*. 2012 Jan;14(1):101–8.
286. Soussain C, Hoang-Xuan K, Taillandier L, Fourme E, Choquet S, Witz F, et al. Intensive chemotherapy followed by hematopoietic stem-cell rescue for refractory and recurrent primary CNS and intraocular lymphoma: Société Française de Greffe de Moëlle Osseuse-Thérapie Cellulaire. *J Clin Oncol*. 2008 May 20;26(15):2512–8.
287. Omuro A, Chinot O, Taillandier L, Ghesquieres H, Soussain C, Delwail V, et al. Methotrexate and temozolomide versus methotrexate, procarbazine, vincristine, and cytarabine for primary CNS lymphoma in an elderly population: an intergroup ANOCEF-GOELAMS randomised phase 2 trial. *Lancet Haematol*. 2015 Jun;2(6):e251-259.

TIME in B-cell lymphoid malignancies

288. Jahnke K, Thiel E, Martus P, Herrlinger U, Weller M, Fischer L, et al. Relapse of primary central nervous system lymphoma: clinical features, outcome and prognostic factors. *J Neurooncol.* 2006 Nov;80(2):159–65.
289. Reni M, Ferreri AJM, Villa E. Second-line treatment for primary central nervous system lymphoma. *Br J Cancer.* 1999 Feb;79(3–4):530–4.
290. Pentsova E, Deangelis LM, Omuro A. Methotrexate re-challenge for recurrent primary central nervous system lymphoma. *J Neurooncol.* 2014 Mar;117(1):161–5.
291. Plotkin SR, Betensky RA, Hochberg FH, Grossman SA, Lesser GJ, Nabors LB, et al. Treatment of Relapsed Central Nervous System Lymphoma with High-Dose Methotrexate. *Clin Cancer Res.* 2004 Sep 1;10(17):5643–6.
292. Grommes C, Pastore A, Palaskas N, Tang SS, Campos C, Scharz D, et al. Ibrutinib Unmasks Critical Role of Bruton Tyrosine Kinase in Primary CNS Lymphoma. *Cancer Discov.* 2017;7(9):1018–29.
293. Lionakis MS, Dunleavy K, Roschewski M, Widemann BC, Butman JA, Schmitz R, et al. Inhibition of B Cell Receptor Signaling by Ibrutinib in Primary CNS Lymphoma. *Cancer Cell.* 2017 12;31(6):833–843.e5.
294. Tun HW, Johnston PB, DeAngelis LM, Atherton PJ, Pederson LD, Koenig PA, et al. Phase 1 study of pomalidomide and dexamethasone for relapsed/refractory primary CNS or vitreoretinal lymphoma. *Blood.* 2018 22;132(21):2240–8.
295. Nayak L, Iwamoto FM, LaCasce A, Mukundan S, Roemer MGM, Chapuy B, et al. PD-1 blockade with nivolumab in relapsed/refractory primary central nervous system and testicular lymphoma. *Blood.* 2017 08;129(23):3071–3.
296. Arvanitis CD, Ferraro GB, Jain RK. The blood-brain barrier and blood-tumour barrier in brain tumours and metastases. *Nat Rev Cancer.* 2020;20(1):26–41.
297. Marcelis L, Antoranz A, Delsupehe A-M, Biesemans P, Ferreira JF, Debackere K, et al. In-depth characterization of the tumor microenvironment in central nervous system lymphoma reveals implications for immune-checkpoint therapy. *Cancer Immunol Immunother.* 2020 Sep;69(9):1751–66.
298. Venetz D, Ponzoni M, Schiraldi M, Ferreri AJM, Bertoni F, Doglioni C, et al. Perivascular expression of CXCL9 and CXCL12 in primary central nervous system lymphoma: T-cell infiltration and positioning of malignant B cells. *Int J Cancer.* 2010 Nov 15;127(10):2300–12.
299. Chang C, Lin C-H, Cheng A-L, Medeiros LJ, Chang K-C. Primary central nervous system diffuse large B-cell lymphoma has poorer immune cell infiltration and prognosis than its peripheral counterpart. *Histopathology.* 2015 Nov;67(5):625–35.
300. Rimsza LM, Roberts RA, Miller TP, Unger JM, LeBlanc M, Brazier RM, et al. Loss of MHC class II gene and protein expression in diffuse large B-cell lymphoma is related to decreased tumor immunosurveillance and poor patient survival regardless of other prognostic factors: a follow-up study from the Leukemia and Lymphoma Molecular Profiling Project. *Blood.* 2004 Jun 1;103(11):4251–8.
301. Riemersma SA, Oudejans JJ, Vonk MJ, Dreef EJ, Prins FA, Jansen PM, et al. High numbers of tumour-infiltrating activated cytotoxic T lymphocytes, and frequent loss of HLA class

- I and II expression, are features of aggressive B cell lymphomas of the brain and testis. *J Pathol.* 2005 Jul;206(3):328–36.
302. Sasayama T, Tanaka K, Mizowaki T, Nagashima H, Nakamizo S, Tanaka H, et al. Tumor-Associated Macrophages Associate with Cerebrospinal Fluid Interleukin-10 and Survival in Primary Central Nervous System Lymphoma (PCNSL). *Brain Pathology.* 2016;26(4):479–87.
 303. Berghoff AS, Ricken G, Widhalm G, Rajky O, Hainfellner JA, Birner P, et al. PD1 (CD279) and PD-L1 (CD274, B7H1) expression in primary central nervous system lymphomas (PCNSL). *Clin Neuropathol.* 2014 Feb;33(1):42–9.
 304. Ou A, Sumrall A, Phuphanich S, Spetzler D, Gatalica Z, Xiu J, et al. Primary CNS lymphoma commonly expresses immune response biomarkers. *Neuro Oncol Adv* [Internet]. 2020 Jan 1 [cited 2020 Sep 1];2(1). Available from: <https://academic.oup.com/nea/article/2/1/vdaa018/5740887>
 305. Miyasato Y, Takashima Y, Takeya H, Yano H, Hayano A, Nakagawa T, et al. The expression of PD-1 ligands and IDO1 by macrophage/microglia in primary central nervous system lymphoma. *J Clin Exp Hematop.* 2018;58(2):95–101.
 306. Cho I, Lee H, Yoon SE, Ryu KJ, Ko YH, Kim WS, et al. Serum levels of soluble programmed death-ligand 1 (sPD-L1) in patients with primary central nervous system diffuse large B-cell lymphoma. *BMC Cancer* [Internet]. 2020 Feb 13 [cited 2020 Sep 2];20. Available from: <https://www.ncbi.nlm.nih.gov/pmc/articles/PMC7020571/>
 307. Rubenstein JL. Biology of CNS lymphoma and the potential of novel agents. *Hematology Am Soc Hematol Educ Program.* 2017 Dec 8;2017(1):556–64.
 308. Korfel A, Schlegel U, Herrlinger U, Dreyling M, Schmidt C, von Baumgarten L, et al. Phase II Trial of Temsirolimus for Relapsed/Refractory Primary CNS Lymphoma. *J Clin Oncol.* 2016 20;34(15):1757–63.
 309. Das A, Wei G, Parikh K, Liu D. Selective inhibitors of nuclear export (SINE) in hematological malignancies. *Exp Hematol Oncol.* 2015;4:7.
 310. Nachmias B, Schimmer AD. Targeting nuclear import and export in hematological malignancies. *Leukemia.* 2020 Jul 5;1–12.
 311. Kuruvilla J, Savona M, Baz R, Mau-Sorensen PM, Gabrail N, Garzon R, et al. Selective inhibition of nuclear export with selinexor in patients with non-Hodgkin lymphoma. *Blood.* 2017 15;129(24):3175–83.
 312. Chari A, Vogl DT, Gavriatopoulou M, Nooka AK, Yee AJ, Huff CA, et al. Oral Selinexor-Dexamethasone for Triple-Class Refractory Multiple Myeloma. *N Engl J Med.* 2019 22;381(8):727–38.
 313. Kalakonda N, Maerevoet M, Cavallo F, Follows G, Goy A, Vermaat JSP, et al. Selinexor in patients with relapsed or refractory diffuse large B-cell lymphoma (SADAL): a single-arm, multinational, multicentre, open-label, phase 2 trial. *The Lancet Haematology.* 2020 Jul 1;7(7):e511–22.
 314. Bobillo S, Abrisqueta P, Carpio C, Raheja P, Castellví J, Crespo M, et al. Promising activity of selinexor in the treatment of a patient with refractory diffuse large B-cell lymphoma and central nervous system involvement. *Haematologica.* 2018 Feb;103(2):e92–3.

TIME in B-cell lymphoid malignancies

315. Cabanillas R, Diñeiro M, Cifuentes GA, Castillo D, Pruneda PC, Álvarez R, et al. Comprehensive genomic diagnosis of non-syndromic and syndromic hereditary hearing loss in Spanish patients. *BMC Med Genomics*. 2018 Jul 9;11(1):58.
316. Bolger AM, Lohse M, Usadel B. Trimmomatic: a flexible trimmer for Illumina sequence data. *Bioinformatics*. 2014 Aug 1;30(15):2114–20.
317. Li H, Durbin R. Fast and accurate long-read alignment with Burrows-Wheeler transform. *Bioinformatics*. 2010 Mar 1;26(5):589–95.
318. Li H, Handsaker B, Wysoker A, Fennell T, Ruan J, Homer N, et al. The Sequence Alignment/Map format and SAMtools. *Bioinformatics*. 2009 Aug 15;25(16):2078–9.
319. Tarasov A, Vilella AJ, Cuppen E, Nijman IJ, Prins P. Sambamba: fast processing of NGS alignment formats. *Bioinformatics*. 2015 Jun 15;31(12):2032–4.
320. Puente XS, Pinyol M, Quesada V, Conde L, Ordóñez GR, Villamor N, et al. Whole-genome sequencing identifies recurrent mutations in chronic lymphocytic leukaemia. *Nature*. 2011 Jun 5;475(7354):101–5.
321. Kumar P, Henikoff S, Ng PC. Predicting the effects of coding non-synonymous variants on protein function using the SIFT algorithm. *Nat Protoc*. 2009;4(7):1073–81.
322. Choi Y, Sims GE, Murphy S, Miller JR, Chan AP. Predicting the functional effect of amino acid substitutions and indels. *PLoS ONE*. 2012;7(10):e46688.
323. Reva B, Antipin Y, Sander C. Predicting the functional impact of protein mutations: application to cancer genomics. *Nucleic Acids Res*. 2011 Sep 1;39(17):e118.
324. Schwarz JM, Cooper DN, Schuelke M, Seelow D. MutationTaster2: mutation prediction for the deep-sequencing age. *Nat Methods*. 2014 Apr;11(4):361–2.
325. Chun S, Fay JC. Identification of deleterious mutations within three human genomes. *Genome Res*. 2009 Sep;19(9):1553–61.
326. Dong C, Wei P, Jian X, Gibbs R, Boerwinkle E, Wang K, et al. Comparison and integration of deleteriousness prediction methods for nonsynonymous SNVs in whole exome sequencing studies. *Hum Mol Genet*. 2015 Apr 15;24(8):2125–37.
327. Shihab HA, Gough J, Mort M, Cooper DN, Day INM, Gaunt TR. Ranking non-synonymous single nucleotide polymorphisms based on disease concepts. *Hum Genomics*. 2014 Jun 30;8:11.
328. Sundaram L, Gao H, Padigepati SR, McRae JF, Li Y, Kosmicki JA, et al. Predicting the clinical impact of human mutation with deep neural networks. *Nat Genet*. 2018;50(8):1161–70.
329. Raimondi D, Tanyalcin I, Ferte J, Gazzo A, Orlando G, Lenaerts T, et al. DEOGEN2: prediction and interactive visualization of single amino acid variant deleteriousness in human proteins. *Nucleic Acids Res*. 2017 03;45(W1):W201–6.
330. Davydov EV, Goode DL, Sirota M, Cooper GM, Sidow A, Batzoglou S. Identifying a high fraction of the human genome to be under selective constraint using GERP++. *PLoS Comput Biol*. 2010 Dec 2;6(12):e1001025.

331. Valdés-Mas R, Bea S, Puente DA, López-Otín C, Puente XS. Estimation of copy number alterations from exome sequencing data. *PLoS ONE*. 2012;7(12):e51422.
332. Shinde J, Bayard Q, Imbeaud S, Hirsch TZ, Liu F, Renault V, et al. Palimpsest: an R package for studying mutational and structural variant signatures along clonal evolution in cancer. *Bioinformatics*. 2018 01;34(19):3380–1.
333. Dobin A, Davis CA, Schlesinger F, Drenkow J, Zaleski C, Jha S, et al. STAR: ultrafast universal RNA-seq aligner. *Bioinformatics*. 2013 Jan;29(1):15–21.
334. Li B, Dewey CN. RSEM: accurate transcript quantification from RNA-Seq data with or without a reference genome. *BMC Bioinformatics*. 2011 Aug 4;12(1):323.
335. Love MI, Huber W, Anders S. Moderated estimation of fold change and dispersion for RNA-seq data with DESeq2. *Genome Biol*. 2014;15(12):550.
336. Pösel C, Möller K, Boltze J, Wagner D-C, Weise G. Isolation and Flow Cytometric Analysis of Immune Cells from the Ischemic Mouse Brain. *J Vis Exp*. 2016 Feb 12;(108):53658.
337. Tallarida RJ. An overview of drug combination analysis with isobolograms. *J Pharmacol Exp Ther*. 2006 Oct;319(1):1–7.
338. Chou T-C. Drug combination studies and their synergy quantification using the Chou-Talalay method. *Cancer Res*. 2010 Jan 15;70(2):440–6.
339. Gonzalez-Perez A, Perez-Llamas C, Deu-Pons J, Tamborero D, Schroeder MP, Jene-Sanz A, et al. IntOGen-mutations identifies cancer drivers across tumor types. *Nature Methods*. 2013 Nov;10(11):1081–2.
340. Mackus WJM, Frakking FNJ, Grummels A, Gamadia LE, De Bree GJ, Hamann D, et al. Expansion of CMV-specific CD8+CD45RA+CD27- T cells in B-cell chronic lymphocytic leukemia. *Blood*. 2003 Aug 1;102(3):1057–63.
341. Brusa D, Serra S, Coscia M, Rossi D, D’Arena G, Laurenti L, et al. The PD-1/PD-L1 axis contributes to T-cell dysfunction in chronic lymphocytic leukemia. *Haematologica*. 2013 Jun;98(6):953–63.
342. Gros A, Robbins PF, Yao X, Li YF, Turcotte S, Tran E, et al. PD-1 identifies the patient-specific CD8(+) tumor-reactive repertoire infiltrating human tumors. *J Clin Invest*. 2014 May;124(5):2246–59.
343. Ahmadzadeh M, Johnson LA, Heemskerk B, Wunderlich JR, Dudley ME, White DE, et al. Tumor antigen-specific CD8 T cells infiltrating the tumor express high levels of PD-1 and are functionally impaired. *Blood*. 2009 Aug 20;114(8):1537–44.
344. Thommen DS, Schumacher TN. T Cell Dysfunction in Cancer. *Cancer Cell*. 2018 09;33(4):547–62.
345. Best JA, Blair DA, Knell J, Yang E, Mayya V, Doedens A, et al. Transcriptional insights into the CD8(+) T cell response to infection and memory T cell formation. *Nat Immunol*. 2013 Apr;14(4):404–12.
346. Schoggins JW, Wilson SJ, Panis M, Murphy MY, Jones CT, Bieniasz P, et al. A diverse range of gene products are effectors of the type I interferon antiviral response. *Nature*. 2011 Apr 28;472(7344):481–5.

TIME in B-cell lymphoid malignancies

347. Schietinger A, Philip M, Krisnawan VE, Chiu EY, Delrow JJ, Basom RS, et al. Tumor-Specific T Cell Dysfunction Is a Dynamic Antigen-Driven Differentiation Program Initiated Early during Tumorigenesis. *Immunity*. 2016 16;45(2):389–401.
348. Burger JA, Quiroga MP, Hartmann E, Bürkle A, Wierda WG, Keating MJ, et al. High-level expression of the T-cell chemokines CCL3 and CCL4 by chronic lymphocytic leukemia B cells in nurselike cell cocultures and after BCR stimulation. *Blood*. 2009 Mar 26;113(13):3050–8.
349. Azzaoui I, Uhel F, Rossille D, Pangault C, Dulong J, Priol JL, et al. T-cell defect in diffuse large B-cell lymphomas involves expansion of myeloid-derived suppressor cells. *Blood*. 2016 Aug 25;128(8):1081–92.
350. Yang Y, Shaffer AL, Emre NCT, Ceribelli M, Zhang M, Wright G, et al. Exploiting synthetic lethality for the therapy of ABC diffuse large B cell lymphoma. *Cancer Cell*. 2012 Jun 12;21(6):723–37.
351. Wilson WH, Gerecitano JF, Goy A, de Vos S, Kenkre VP, Barr PM, et al. The Bruton's Tyrosine Kinase (BTK) Inhibitor, Ibrutinib (PCI-32765), Has Preferential Activity in the ABC Subtype of Relapsed/Refractory De Novo Diffuse Large B-Cell Lymphoma (DLBCL): Interim Results of a Multicenter, Open-Label, Phase 2 Study. *Blood*. 2012 Nov 16;120(21):686–686.
352. Turner JG, Dawson J, Sullivan DM. Nuclear export of proteins and drug resistance in cancer. *Biochem Pharmacol*. 2012 Apr 15;83(8):1021–32.
353. Rosenwald A, Wright G, Chan WC, Connors JM, Campo E, Fisher RI, et al. The use of molecular profiling to predict survival after chemotherapy for diffuse large-B-cell lymphoma. *N Engl J Med*. 2002 Jun 20;346(25):1937–47.
354. Nakamura T, Tateishi K, Niwa T, Matsushita Y, Tamura K, Kinoshita M, et al. Recurrent mutations of CD79B and MYD88 are the hallmark of primary central nervous system lymphomas. *Neuropathol Appl Neurobiol*. 2016 Apr;42(3):279–90.
355. Li Z, Qiu Y, Personett D, Huang P, Edenfield B, Katz J, et al. Pomalidomide Shows Significant Therapeutic Activity against CNS Lymphoma with a Major Impact on the Tumor Microenvironment in Murine Models. *PLOS ONE*. 2013 Aug 5;8(8):e71754.
356. Abdul Razak AR, Mau-Soerensen M, Gabrail NY, Gerecitano JF, Shields AF, Unger TJ, et al. First-in-Class, First-in-Human Phase I Study of Selinexor, a Selective Inhibitor of Nuclear Export, in Patients With Advanced Solid Tumors. *J Clin Oncol*. 2016;34(34):4142–50.
357. Zhong Y, El-Gamal D, Dubovsky JA, Beckwith KA, Harrington BK, Williams KE, et al. Selinexor suppresses Downstream Effectors of B-cell activation, proliferation and migration in chronic lymphocytic leukemia cells. *Leukemia*. 2014 May;28(5):1158–63.
358. Hing ZA, Mantel R, Beckwith KA, Guinn D, Williams E, Smith LL, et al. Selinexor is effective in acquired resistance to ibrutinib and synergizes with ibrutinib in chronic lymphocytic leukemia. *Blood*. 2015 May 14;125(20):3128–32.
359. Ponader S, Chen S-S, Buggy JJ, Balakrishnan K, Gandhi V, Wierda WG, et al. The Bruton tyrosine kinase inhibitor PCI-32765 thwarts chronic lymphocytic leukemia cell survival and tissue homing in vitro and in vivo. *Blood*. 2012 Feb 2;119(5):1182–9.

360. Nam SJ, Kim S, Kwon D, Kim H, Kim S, Lee E, et al. Prognostic implications of tumor-infiltrating macrophages, M2 macrophages, regulatory T-cells, and indoleamine 2,3-dioxygenase-positive cells in primary diffuse large B-cell lymphoma of the central nervous system. *Oncoimmunology*. 2018;7(7):e1442164.
361. He M, Zuo C, Wang J, Liu J, Jiao B, Zheng J, et al. Prognostic significance of the aggregative perivascular growth pattern of tumor cells in primary central nervous system diffuse large B-cell lymphoma. *Neuro Oncol*. 2013 Jun;15(6):727–34.
362. Colonna M, Butovsky O. Microglia Function in the Central Nervous System During Health and Neurodegeneration. *Annu Rev Immunol*. 2017 26;35:441–68.
363. Pouzoulet F, Alentorn A, Royer-Perron L, Assayag F, Mokhtari K, Labiod D, et al. Primary CNS lymphoma patient-derived orthotopic xenograft model capture the biological and molecular characteristics of the disease. *Blood Cells Mol Dis*. 2019;75:1–10.
364. Niemann CU, Herman SEM, Maric I, Gomez-Rodriguez J, Biancotto A, Chang BY, et al. Disruption of in vivo Chronic Lymphocytic Leukemia Tumor-Microenvironment Interactions by Ibrutinib--Findings from an Investigator-Initiated Phase II Study. *Clin Cancer Res*. 2016 Apr 1;22(7):1572–82.
365. Leeksma AC, Taylor J, Wu B, Gardner JR, He J, Nahas M, et al. Clonal diversity predicts adverse outcome in chronic lymphocytic leukemia. *Leukemia*. 2019 Feb;33(2):390.
366. Burger JA, Landau DA, Taylor-Weiner A, Bozic I, Zhang H, Sarosiek K, et al. Clonal evolution in patients with chronic lymphocytic leukaemia developing resistance to BTK inhibition. *Nat Commun*. 2016 20;7:11589.
367. Munakata W, Ando K, Hatake K, Fukuhara N, Kinoshita T, Fukuhara S, et al. Phase I study of tirabrutinib (ONO-4059/GS-4059) in patients with relapsed or refractory B-cell malignancies in Japan. *Cancer Sci*. 2019 May;110(5):1686–94.
368. Ansell SM, Lesokhin AM, Borrello I, Halwani A, Scott EC, Gutierrez M, et al. PD-1 blockade with nivolumab in relapsed or refractory Hodgkin's lymphoma. *N Engl J Med*. 2015 Jan 22;372(4):311–9.
369. Reichel J, Chadburn A, Rubinstein PG, Giulino-Roth L, Tam W, Liu Y, et al. Flow sorting and exome sequencing reveal the oncogenome of primary Hodgkin and Reed-Sternberg cells. *Blood*. 2015 Feb 12;125(7):1061–72.
370. Qiu Y, Li Z, Pouzoulet F, Vishnu P, Copland JA, Knutson KL, et al. Immune checkpoint inhibition by anti-PDCD1 (anti-PD1) monoclonal antibody has significant therapeutic activity against central nervous system lymphoma in an immunocompetent preclinical model. *Br J Haematol*. 2018;183(4):674–8.
371. Gordon SR, Maute RL, Dulken BW, Hutter G, George BM, McCracken MN, et al. PD-1 expression by tumour-associated macrophages inhibits phagocytosis and tumour immunity. *Nature*. 2017 25;545(7655):495–9.
372. Barkal AA, Weiskopf K, Kao KS, Gordon SR, Rosental B, Yiu YY, et al. Engagement of MHC class I by the inhibitory receptor LILRB1 suppresses macrophages and is a target of cancer immunotherapy. *Nat Immunol*. 2018 Jan;19(1):76–84.
373. Massó-Vallés D, Jauset T, Serrano E, Sodir NM, Pedersen K, Affara NI, et al. Ibrutinib exerts potent antifibrotic and antitumor activities in mouse models of pancreatic adenocarcinoma. *Cancer Res*. 2015 Apr 15;75(8):1675–81.

TIME in B-cell lymphoid malignancies

374. Horwitz SM, Koch R, Porcu P, Oki Y, Moskowitz A, Perez M, et al. Activity of the PI3K- δ,γ inhibitor duvelisib in a phase I trial and preclinical models of T-cell lymphoma. *Blood*. 2018 22;131(8):888–98.
375. Rubenstein JL, Geng H, Fraser EJ, Formaker P, Chen L, Sharma J, et al. Phase I investigation of lenalidomide/rituximab plus outcomes of lenalidomide maintenance in relapsed CNS lymphoma. *Blood Adv*. 2018 10;2(13):1595–607.
376. Nguyen P-H, Fedorchenko O, Rosen N, Koch M, Barthel R, Winarski T, et al. LYN Kinase in the Tumor Microenvironment Is Essential for the Progression of Chronic Lymphocytic Leukemia. *Cancer Cell*. 2016 10;30(4):610–22.

10. Annexes


10.1. Scientific articles and communications

Jiménez I, Carabia J, Bobillo S, Palacio C, Abrisqueta P, Pagès C, et al. Repolarization of tumor infiltrating macrophages and increased survival in mouse primary CNS lymphomas after XPO1 and BTK inhibition. *J Neurooncol.* 2020 Jul 20.

Jiménez I, Bobillo S, Abrisqueta P, Tazón B, Palacio C, Nieto JC, et al. Clinical Progression of Chronic Lymphocytic Leukemia (CLL) Is Characterized By a Progressive Increase of the Exhausted T-Cell Phenotype and Immunosuppression Induced By Leukemic Cells. *Blood.* 2017 Dec 7;130(Supplement 1):1713–1713.



Repolarization of tumor infiltrating macrophages and increased survival in mouse primary CNS lymphomas after XPO1 and BTK inhibition

Isabel Jiménez^{1,2} · Júlia Carabia^{1,2} · Sabela Bobillo^{2,3} · Carles Palacio^{2,3} · Pau Abrisqueta^{2,3} · Carlota Pagès^{1,2} · Juan C. Nieto^{1,2} · Josep Castellví⁴ · Francisco Martínez-Ricarte⁵ · Lourdes Escoda⁶ · Cristóbal Perla⁷ · Dennis H. Céspedes Torrez⁷ · Joan Boix^{1,2} · Noelia Purroy^{1,2,10} · Lluís Puigdefàbregas^{1,2} · Joan Seoane^{2,8,9} · Francesc Bosch^{2,3} · Marta Crespo^{1,2} 

Received: 20 March 2020 / Accepted: 2 July 2020
© The Author(s) 2020

Abstract

Background Patients diagnosed with primary central nervous system lymphoma (PCNSL) often face dismal outcomes due to the limited availability of therapeutic options. PCNSL cells frequently have deregulated B-cell receptor (BCR) signaling, but clinical responses to its inhibition using ibrutinib have been brief. In this regard, blocking nuclear export by using selinexor, which covalently binds to XPO1, can also inhibit BCR signaling. Selinexor crosses the blood–brain barrier and was recently shown to have clinical activity in a patient with refractory diffuse large B-cell lymphoma in the CNS. We studied selinexor alone or in combination with ibrutinib in pre-clinical mouse models of PCNSL.

Methods Orthotopic xenograft models were established by injecting lymphoma cells into the brain parenchyma of athymic mice. Tumor growth was monitored by bioluminescence. Malignant cells and macrophages were studied by immunohistochemistry and flow cytometry.

Results Selinexor blocked tumor growth and prolonged survival in a bioluminescent mouse model, while its combination with ibrutinib further increased survival. CNS lymphoma in mice was infiltrated by tumor-promoting M2-like macrophages expressing PD-1 and SIRP α . Interestingly, treatment with selinexor and ibrutinib favored an anti-tumoral immune response by shifting polarization toward inflammatory M1-like and diminishing PD-1 and SIRP α expression in the remaining tumor-promoting M2-like macrophages.

Conclusions These data highlight the pathogenic role of the innate immune microenvironment in PCNSL and provide pre-clinical evidence for the development of selinexor and ibrutinib as a new promising therapeutic option with cytotoxic and immunomodulatory potential.

Keywords PCNSL · XPO1 · BTK · Innate immune system

Abbreviations

PCNSL Primary central nervous system lymphoma
BCR B-cell receptor

NHL	Non-Hodgkin lymphoma
ABC-DLBCL	Activated B-cell diffuse large B-cell lymphoma
GCB-DLBCL	Germinal center B-cell diffuse large B-cell lymphoma
SINE	Selective inhibitor of nuclear export
BBB	Blood–brain barrier
BLI	Bioluminescence imaging
PDX	Patient derived xenograft
NSG	NOD-SCID- γ : non-obese diabetic- severe combined immune deficiency- interleukin 2 receptor gamma chain
IHC	Immunohistochemistry
SEM	Standard error of the mean

Isabel Jiménez, Júlia Carabia and Francesc Bosch, Marta Crespo have contributed equally to this work

Electronic supplementary material The online version of this article (<https://doi.org/10.1007/s11060-020-03580-y>) contains supplementary material, which is available to authorized users.

✉ Marta Crespo
macrespo@vhio.net

Extended author information available on the last page of the article

COO	Cell of origin
CLL	Chronic lymphocytic leukemia
TAM	Tumor-associated macrophages
M-CSF	Macrophage colony-stimulating factor
IDO	Indoleamine 2, 3 dioxygenase
MRI	Magnetic resonance imaging
CI	Combination index

Background

Primary central nervous system lymphoma (PCNSL) is a rare and aggressive non-Hodgkin lymphoma (NHL) localized to the CNS in the absence of systemic involvement that represents around 4% of all brain tumors and 4 to 6% of all extranodal lymphomas [1]. Approximately 95% of PCNSL are classified as activated B-cell diffuse large B-cell lymphoma (ABC-DLBCL) based on histopathology, gene expression and mutational landscape [2]. Current treatment options for PCNSL include high doses of chemotherapy able to cross the blood–brain barrier (BBB) combined with anti-CD20 monoclonal antibodies and the addition of whole brain radiation in some settings; also, autologous stem cell transplantation is considered for young patients. Patients diagnosed with PCNSL respond poorly to the available treatments and often face dismal outcomes, especially in the relapsed setting, with an estimated overall survival of 30% at 5 years [3]. This notion of the poor prognosis of PCNSL can be explained by particular biological characteristics of the tumor. First, PCNSL are characterized by a high frequency of concomitant MYD88 and CD79B mutations [4] along with lesions related to B-cell development and function (e.g. BLIMP1), and the NF- κ B pathway (e.g. CARD11 or TBL1XR1). The involvement of the BCR signaling in PCNSL has prompted the use of the BTK inhibitor ibrutinib, that, although it can cross the BBB [5], achieves wide but short duration responses [6–8]. In addition, PCNSL develop in a special microenvironment of unique immune surveillance, which could contribute to an inefficient response of the immune system against lymphoma cells. In this regard, the few reports examining the tumor-infiltrating immune microenvironment show that it is mainly composed by macrophages and by T-cells to a lesser extent [9–13]. Also, an intriguing high proportion of PCNSL have genetic lesions that potentially avoid being recognized by T-cells, namely HLA losses and PD-L1/2 amplifications found in up to 80% of patients [14]. Finally, the poor prognosis can also be explained by the diminished capacity of some drugs to cross the BBB. Selinexor (KPT-330), a BBB permeable small molecule [15], is a Selective Inhibitor of Nuclear Export (SINE) compound that binds to the cargo binding pocket of XPO1 (exportin-1/CRM1) and inhibits its activity. This results in the nuclear accumulation of tumor

suppressor proteins and cell cycle regulators together with the activation of tumor suppressor proteins, which translates in cell cycle arrest and specific anti-cancer activity across a wide range of hematological and solid malignancies [16]. In July 2019, selinexor was approved by the FDA to treat patients with multiple myeloma while in May 2020 it was approved for systemic relapsed/refractory DLBCL after positive results in a phase IIb trial [17]. Also, the ability of selinexor to inhibit both the BCR and the NF- κ B signaling pathways makes this drug interesting for studies in NHL [16, 18]. Recently, in a clinical case study, selinexor was reported to inhibit refractory DLBCL with CNS involvement [19]. In order to provide a pre-clinical rationale for the design of new therapeutic strategies for patients diagnosed with PCNSL, herein we evaluate the role of XPO1 and BTK inhibition in intracerebral xenograft murine models, focusing on malignant cells and the innate immune microenvironment.

Materials and methods

In vivo modeling of PCNSL

All animal experiments were approved by the local Ethical Committee for the Use of Experimental Animals. Detailed methods including treatment schedules can be found in *Supplementary information*. Briefly, brains of eight-week-old athymic female mice were injected with OCI-Ly10 cells stably transfected with luciferase, as previously reported [20]. Tumor growth was monitored by bioluminescence imaging (BLI) using IVIS® Spectrum system and Living Image software (PerkinElmer).

Patient derived xenograft (PDX) model was established by intracerebral injection of human lymphoma cells isolated from a brain biopsy in eight-week-old NOD-SCID- γ (NSG) female mice. Next, expanded CD19⁺ tumor cells were inoculated into the brain parenchyma of eight-week-old athymic female mice as specified above. Human tumor sample was obtained from a patient diagnosed with PCNSL at Hospital Universitari Joan XIII, Tarragona (Spain) after approval from the local Clinical Research Ethics Committee according to the principles of the Declaration of Helsinki and obtaining written informed consent from the patient.

Flow cytometry and immunohistochemistry (IHC) analysis

Mice brains were collected in cold RPMI-1640 medium immediately after euthanasia and the two hemispheres were separated with a razor blade. One hemisphere was used for IHC and the other one was processed for flow cytometry. Detailed methods can be found in *Supplementary information*.

Statistical analysis

Results are expressed as the mean \pm standard error of the mean (SEM) of at least four independent experiments or subjects. The statistically significant differences between groups were analyzed using the Mann–Whitney test or one or two-way ANOVA, and $P < 0.05$ was considered significant. Detailed methods can be found in *Supplementary information*.

Results

DLBCL cell lines have equivalent sensitivity to selinexor regardless of their cell of origin (COO)

ABC-DLBCL relies heavily on NF- κ B signaling and shows chronic BCR activation that is needed for survival, which translates into differential sensitivity to drugs targeting these pathways between ABC and GCB DLBCL cases [21, 22]. Since increased expression of XPO1 has been related to resistance to chemotherapy and worse prognosis in different neoplasias [23], we studied the potential relationship between expression of XPO1 and sensitivity to selinexor in DLBCL cell lines. Although mRNA expression of XPO1 was significantly higher in ABC-DLBCL cell lines (Fig. 1a), we did not find differential in vitro sensitivity to selinexor according to COO (Fig. 1b, c). Finally, we interrogated the publicly available data on gene expression of primary DLBCL cases [24] and we did not observe any association between the COO and the expression of XPO1 (Fig. 1d).

Selinexor blocks tumor growth and prolongs survival in a bioluminescent orthotopic mouse model of PCNSL.

We next assessed the role of XPO1 inhibition in PCNSL using an intracerebral orthotopic xenograft murine model established by stereotactic injection of the luciferase-expressing OCI-Ly10 cell line into the cerebral parenchyma of nude athymic mice. OCI-Ly10 cell line was selected because it is derived from a patient diagnosed with ABC-DLBCL and its genetic profile includes mutations in *MYD88* (L265P) and *CD79A* (c. 4275_4316del) genes [20] (further verified in house), frequent in PCNSL [4]. Additionally, OCI-Ly10 cells have successfully been used before in a PCNSL xenograft model in athymic mice for pre-clinical studies [20]. Tumoral growth was monitored using IVIS-Spectrum bioluminescence measurement. Eleven days after the injection of cells, all animals had developed detectable tumors restricted to the CNS and were randomly distributed into treatment or vehicle experimental groups (vehicle: $n = 8$, mean radiance = $1.16 \cdot 10^7$ ph/s \pm $0.615 \cdot 10^7$; treatment: $n = 9$,

mean radiance = $2.32 \cdot 10^7$ ph/s \pm $1.86 \cdot 10^7$). Mice were dosed with 5 mg/kg of selinexor or vehicle via oral gavage three times a week and subsequently, in order to non-invasively monitor the tumor growth, bioluminescence was assessed twice a week (Fig. 1e). Dose was selected based on previous pre-clinical data in mouse models of different neoplasias [25]. Treated mice showed a significantly slower increase in bioluminescence signal along time (two-way ANOVA: $p = 0.0002$; Fig. 1f) indicating that the treatment with selinexor was able to notably slow down tumor growth. Specific time-point analysis showed that differences were significant as soon as 12 days after start of treatment (day 23 after injection: vehicle mean radiance $2.61 \cdot 10^8$ ph/s \pm $8.64 \cdot 10^7$ vs. $3.73 \cdot 10^7$ ph/s \pm $1.9 \cdot 10^7$ in selinexor; $p = 0.011$) while differences peaked at day 20 after treatment (day 31 after injection: $8.98 \cdot 10^8$ ph/s \pm $3.13 \cdot 10^8$ in vehicle vs. $1.19 \cdot 10^8$ ph/s \pm $5.58 \cdot 10^7$ in selinexor group; $p = 0.0037$; Fig. 1f, representative cases can be seen in Fig. 1h). The blockage of intracerebral lymphoma growth induced by selinexor translated into a significantly increased survival, with a median survival of 48 days in the treatment group compared to 34 days in the vehicle group ($p < 0.0001$; Fig. 1g). At final point, histopathological analysis showed multifocal and infiltrative tumors affecting cerebral parenchyma and meninges of both cerebral hemispheres. Cells were highly proliferative (Ki-67 100%), CD20-positive and were often found in the perivascular space resembling human PCNSL histology. Remarkably, infiltration was observed in both hemispheres, showing no preference for the right hemisphere, where the original inoculation of malignant cells was performed. Also, we did not observe variations in CD20 intensity among mice or within different areas of the same brain (representative cases shown at Fig. 1i and Supplemental Figure S1).

The combination of selinexor and ibrutinib synergizes in vitro in DLBCL cell lines and increases survival of mice with CNS lymphoma

The high frequency of molecular alterations in components of the BCR pathway can in part explain the response to BCR inhibitors in PCNSL. In this regard, ibrutinib in monotherapy in patients diagnosed with relapsed or refractory PCNSL achieves higher response rates compared to systemic DLBCL, however, the duration of the response is brief [5–7]. Alongside this, SINE compounds have also been shown to inhibit BCR signaling by downregulating the protein expression of BTK via enforced I κ B nuclear retention in primary cells from patients with chronic lymphocytic leukemia (CLL) [16]. Moreover, the combination of selinexor and ibrutinib has shown in vitro synergism in CLL cells [18]. Accordingly, we observed reduced BCR signaling after treatment of OCI-Ly10 cells with selinexor and ibrutinib (Supplementary Figure S2A), as well as reduced BTK

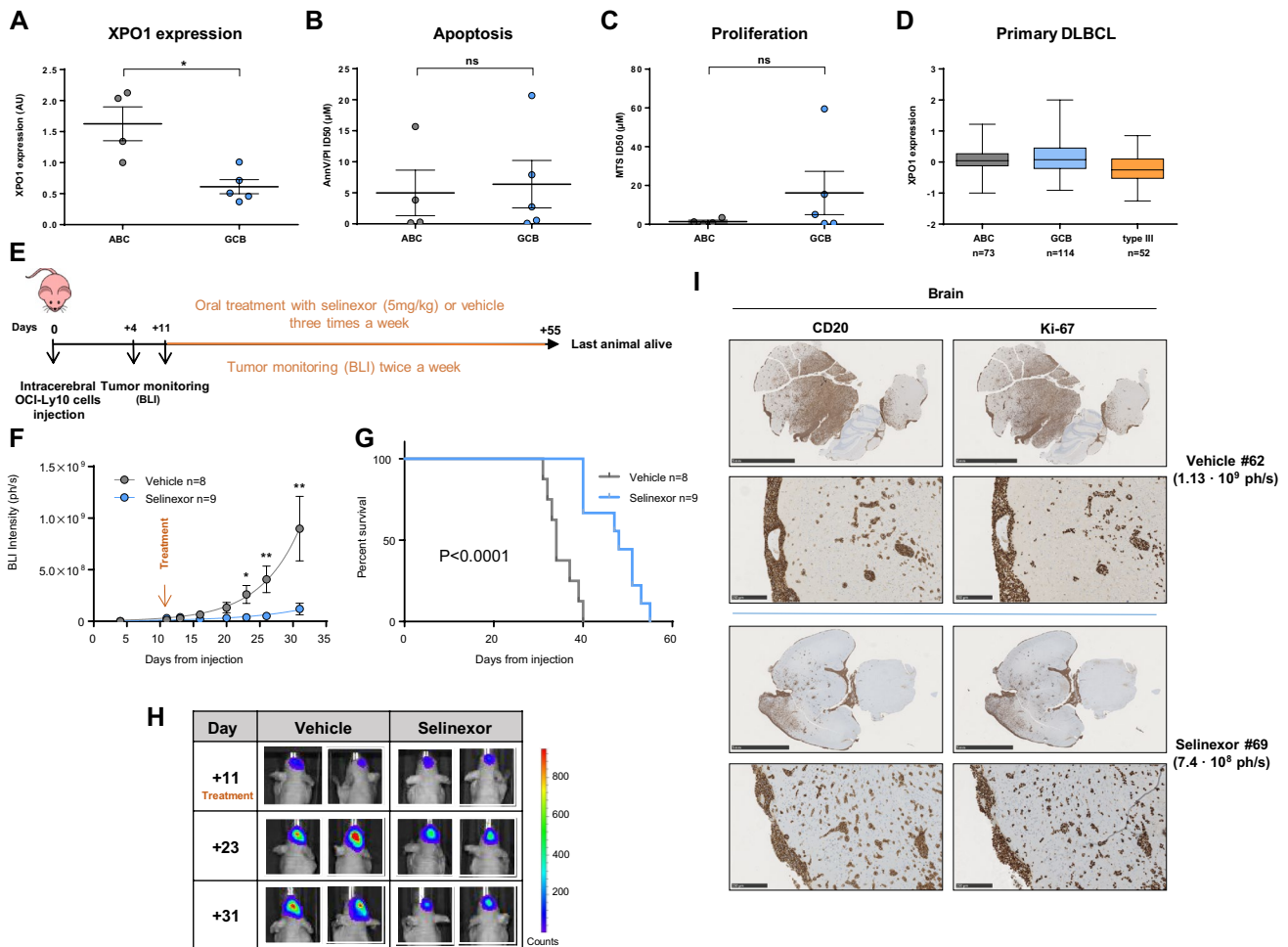


Fig. 1 In vitro and in vivo effects of selinexor in PCNSL models. **a** XPO1 relative expression by QRT-PCR. Cells were treated with increasing doses of selinexor or vehicle (1% DMSO) for 96 h and viability and proliferation was determined by Annexin-V-PI exclusion (**b**) or MTS method (**c**). **d** Relative XPO1 expression in DLBCL patients, using public data from ref [24]. **e** Scheme representing mice treatment and monitoring. **f** Tumor size as measured by BLI in mice treated with vehicle ($n=8$) or selinexor ($n=9$). Data is shown until day 31, last day when all animals were still alive. Two-way ANOVA analysis ($P=0.0002$). Asterisks indicate the result of Mann–Whitney

test at different time points. ($*P<0.05$, $**P<0.01$, $***P<0.001$. Graphs show mean \pm SEM) (**g**) Survival curves and (**h**) representative BLI images of the CNS tumors. **i** IHC analysis showing expression of CD20 and Ki-67 in representative mice brain parenchyma and meninges. The bars represent 5 mm in top panels and 250 μ m in bottom panels. ID50: inhibitory dose 50. ABC: activated-B cell. GCB: germinal center B-cell. BLI: bioluminescence imaging. Ph/s: photons per second. ($*P<0.05$, $**P<0.01$, Mann–Whitney test. Graphs show mean \pm SEM)

expression after 48 h of treatment with selinexor (Supplementary Figure S2B). Against this background, we hypothesized that combining XPO1 and BTK inhibition in PCNSL would have a synergistic therapeutic effect in our models. Firstly we treated a panel of cell lines in vitro with increasing doses of both drugs and analyzed apoptosis after 96 h. In three out of four ABC-DLBCL cell lines we observed a strong synergism between the two compounds (Supplementary Figure S2C); remarkably, treatment with selinexor sensitized GCB-SUDHL4 cells to ibrutinib, as shown by the combination index values indicating strong synergism

between the two drugs (CI) (Supplementary Figure S2C, right panel).

We next sought to elucidate whether the synergy observed in vitro could be translated in vivo. Importantly, while ibrutinib is mainly metabolized by cytochrome P450, the metabolism of selinexor is independent of it, therefore it is unlikely that their co-administration could result in any effects on the exposure for the other drug [25, 26]. By using the same animal model described above, mice were distributed into the following four groups and started therapy 11 days after intracerebral injection of lymphoma cells:

selinexor monotherapy (5 mg/kg twice a week via oral gavage, $n=12$, mean radiance = $3.95 \cdot 10^6$ ph/s), ibrutinib monotherapy (25 mg/kg daily in drinking water, $n=9$, mean radiance = $1.02 \cdot 10^7$ ph/s), combination therapy ($n=11$, mean radiance = $1.02 \cdot 10^7$ ph/s) and vehicle ($n=9$, mean radiance = $3.21 \cdot 10^6$ ph/s). Selinexor dose was adjusted (from three times a week to twice a week) in order to prevent potential toxicity of the drug combination, while ibrutinib dose was based on previous experience in CLL preclinical models [27] (Fig. 2a). Compared to vehicle, all three treatment regimens induced an equivalent significant effect in tumor growth kinetics in terms of decreased growth rate (Fig. 2b and c). Interestingly, the combination increased the survival of mice compared to vehicle, whereas there was no significant difference between ibrutinib and selinexor alone. Although the median survival increased up to 55 days, the survival curve of the mice treated with the combination was not statistically different from the ones from mice treated with the individual treatments (median survival of mice treated with vehicle: 35 days vs. survival for mice treated with selinexor: 40 days, $p=0.001$; vehicle vs. ibrutinib, 43 days, $p=0.0005$; vehicle vs. combination, 55 days, $p=0.0001$; Fig. 2d).

CNS lymphoma is infiltrated by tumor-promoting M2-like macrophages expressing PD-1 and SIRPα

Analysis of the tumor-infiltrating immune microenvironment has shown that tumoral cells in PCNSL are accompanied by tumor-associated macrophages (TAMs) and T-cells to less extent, which is related to bad prognosis. [9–13] Remarkably, TAMs in mouse and human colorectal cancer have been recently described to express the immune checkpoint PD-1 and to recover their potential to phagocyte tumoral cells when PD-1 is blocked [28]. To conduct an interactive study of the infiltrating innate immune cells and PCNSL, we inoculated OCI-Ly10 cells into the brain parenchyma of nude athymic mice, an experimental *in vivo* model that has been previously successfully used to study the modulation of the innate immune response against PCNSL [20, 29]. Brains were harvested after 24 days of cell injection and further processed for subsequent analysis. Histopathological analysis showed that tumors encompassing both cerebral hemispheres were infiltrated by macrophages expressing the surface glycoprotein F4/80, mainly in the meninges but also in the cerebral parenchyma; notably, F4/80-positive macrophages

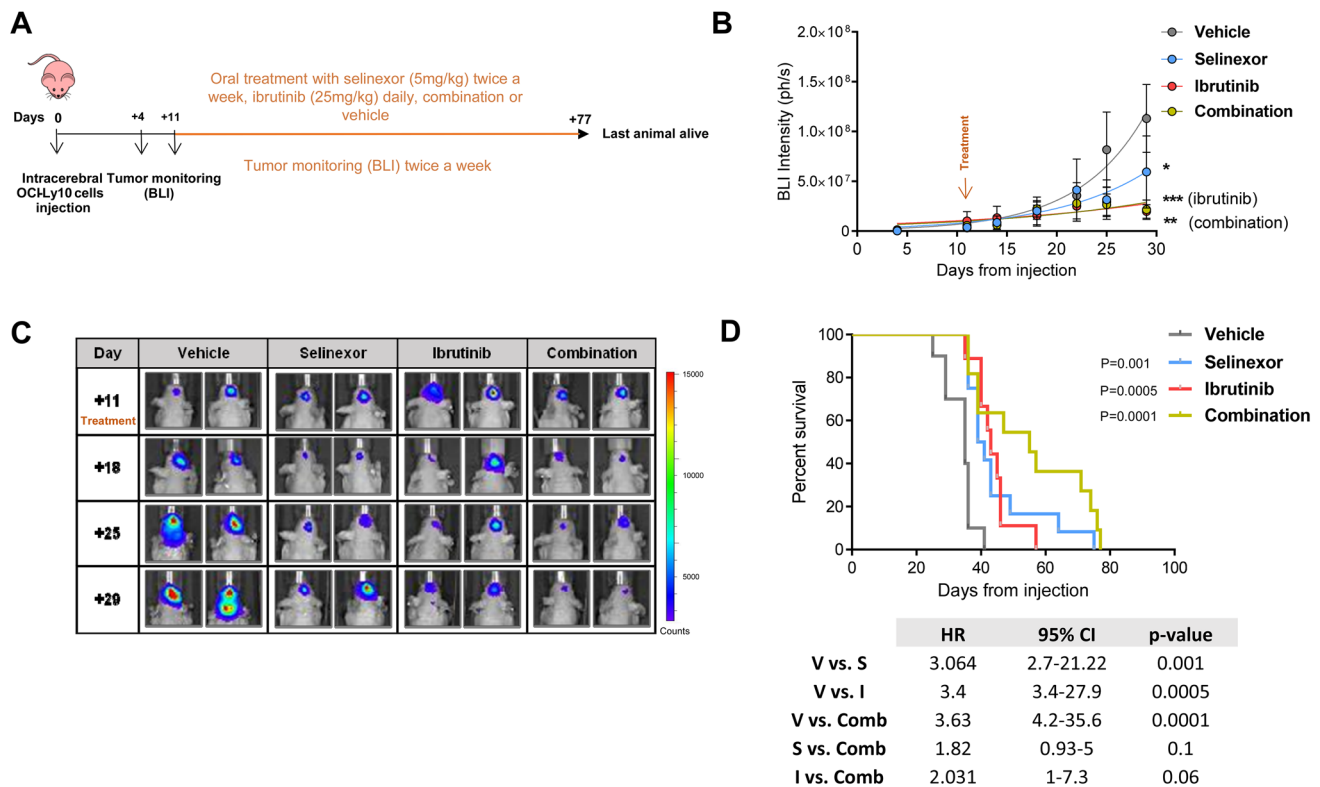


Fig. 2 Treatment with selinexor and ibrutinib further increases survival of mice with CNS lymphoma. **a** Scheme representing mice treatment and monitoring. **b** Tumor size as measured by BLI intensity. Data is shown until day 29, last day when all animals were still alive. (* $P < 0.05$, ** $P < 0.01$, *** $P < 0.001$, Mann–Whitney test.

Graphs show mean \pm SEM). **c** Representative BLI images in mice from every treatment arm. **d** Survival curves of mice in the four treatment groups. Survival curves were generated using the Kaplan and Meier method, and statistically compared by the log-rank test. *HR* hazard ratio, *CI* confidence interval, *BLI* bioluminescence imaging

were completely absent in the areas of the brain that were not invaded by tumoral cells (Figs. 3a and Supplemental figure S1) as well as in healthy brains from control mice (Fig. 3a). Iba-1 staining further identified microglial cells and TAMs, which showed an amoeboid morphology when interacting with tumoral cells, consistent with an active state (Fig. 3a) [30]. TAMs can be polarized towards a pro-inflammatory (M1) or a tumor-promoting (M2) state, depending on microenvironment and external stimuli [31]. By flow cytometry, we analyzed the proportion of M1 and M2 TAMs and their expression of immune checkpoints in brains from mice with PCNSL. First, we observed that TAMs were evenly distributed between M1 and M2 (Fig. 3c). Of note, TAMs expressed PD-1, mainly the tumor promoting M2 subset (Fig. 3d). This suggests that the direct interaction of M2 macrophages with the tumor triggers the upregulation of PD-1 and thus impairs their phagocytic capacity, as has been recently discovered in an analogous role to tumor-infiltrating T-cells using both immunocompetent syngeneic and athymic xenograft mouse models [28]. SIRP α is a well described regulatory checkpoint on macrophages, its interaction with CD47 on malignant cells hampering the phagocytosis by macrophages [32]. Herein we observed that SIRP α was also preferentially expressed by M2 TAMs (Fig. 3e) and that

the co-expression of PD-1 and SIRP α was also higher in the M2 subset (Fig. 3f), pointing out towards a severe inhibition of macrophage activity in CNSL.

The response of the innate immune system to PCNSL cells derived from a patient was further analyzed. For that, we developed an orthotopic PDX model using NSG mice to initially expand the freshly obtained primary malignant cells, as previously described by Rubenstein et al. and following the detailed protocol described in Supplementary methods [33] Next, we inoculated $2 \cdot 10^5$ lymphoma cells into the brain parenchyma of nude athymic mice [34]. Since the median survival of this mouse model was 22 days, infiltration by immune cells was analyzed after 18 days of tumor injection allowing infiltration by innate immune cells. In this model, TAMs were also found only amongst tumoral cells (Figs. 4a and Supplemental Figure S3) as assessed by IHC. TAMs from the PDX model displayed an immunophenotypic profile resembling the one found in TAMs from the cell line xenograft model. Along this line, a similar proportion of M1 and M2 (Fig. 4b) and a more frequent expression of PD-1 and SIRP α in M2 tumor-promoting macrophages was observed (Fig. 4c, d, e). In contrast to the OCI-Ly10 model, patient-derived PCNSL cells did express the SIRP α ligand CD47 (97.61% of CD20 cells \pm 0.62).

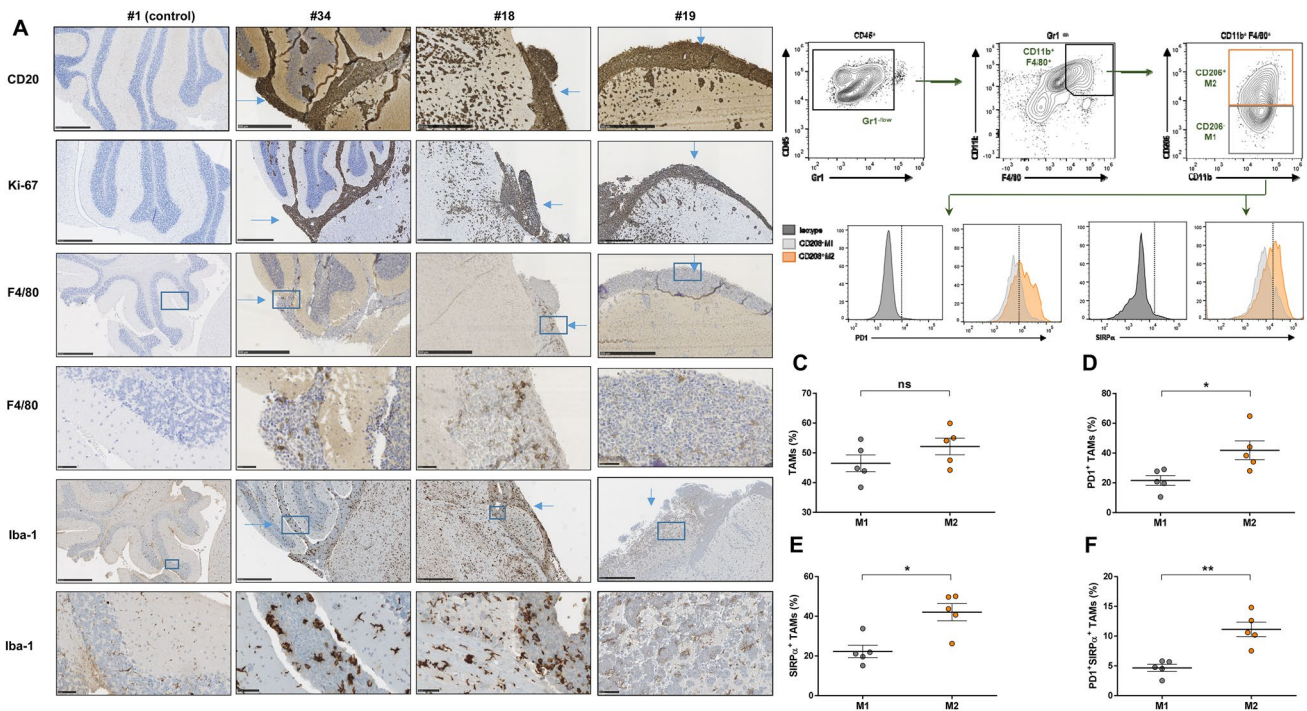


Fig. 3 OCI-Ly10 CNS lymphomas are infiltrated by innate immune cells. **a** Representative IHC images from brains obtained from three mice inoculated with OCI-Ly10 cells (24 days after injection). The bar represents 500 μ m, except for fourth and last rows (50 μ m). **b** Gat-

ing strategy for the analysis of TAMs. Percentage of macrophages (M1/M2) (c) expressing PD-1 (d), SIRP α (e) and co-expressing both (f)

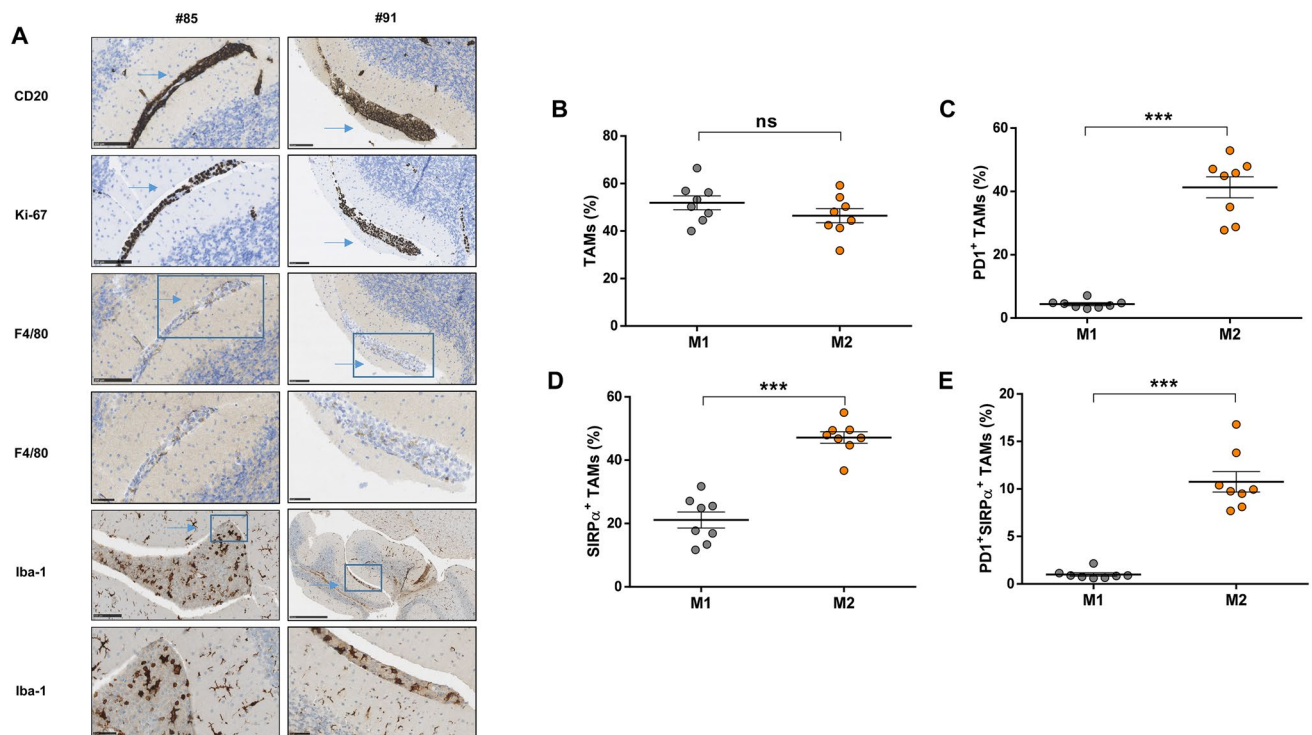


Fig. 4 PDX CNS lymphomas are infiltrated by innate immune cells. **a** Representative IHC images from brains obtained from two mice inoculated with patient-derived PCNSL cells (18 days after injection). The bar represents 100 μm except for the four last rows (50 μm). Per-

centage of macrophages (M1/M2) (**b**) expressing PD-1 (**c**), SIRP α (**d**) and co-expressing both (**e**). (* $P < 0.05$, ** $P < 0.01$, *** $P < 0.001$, Mann–Whitney test. Graphs show mean \pm SEM)

Treatment with selinexor and ibrutinib favors TAM polarization toward pro-inflammatory M1-like and diminishes PD-1 and SIRP α expression in M2-like TAMs

BTK protein has been shown to be crucial for tumor-promoting function of macrophages in different neoplasias, especially in CLL, where modulation of TAMs has been shown to be also a relevant mode of action of ibrutinib [35, 36]. Therefore, after showing that the combination of selinexor and ibrutinib restrains tumor growth and prolongs mice survival, and since both drugs are able to inhibit BTK, we hypothesized that these drugs could also cooperate to modify the innate immune response in PCNSL. In this regard, pre-clinical PCNSL models have previously demonstrated how immunomodulating drugs are able to shift macrophages polarization as well as have direct antitumoral effect. [20, 29] To test that, we treated mice bearing OCI-Ly10-CNS lymphomas with selinexor 5 mg/kg twice a week, ibrutinib 25 mg/kg daily or the combination of the two drugs for two weeks by oral gavage (Fig. 5a). We observed that selinexor and the combination shifted the M1/M2 ratio towards predominance of anti-tumoral M1 (Fig. 5b). Interestingly, while none of the individual treatments induced significant changes in the frequency of PD-1 or SIRP α -positive M2

macrophages, the drug combination significantly reduced the frequency of PD-1-positive, SIRP α -positive (Fig. 5c, d, e) and double-positive M2 macrophages (Fig. 5f). In agreement the (CI) that the reduction of the expression of PD-1, SIRP α and their co-expression was synergistic (CI < 1). This was accompanied by a reduction in PD-L1-expressing malignant cells (Fig. 5g, h) that was attributable to ibrutinib action since it was also observed under ibrutinib monotherapy.

In the PDX model, the study of immunomodulation was performed 18 days after cell injection preceded by 12 days of oral gavage treatment as described earlier (Fig. 6a). Both treatments alone or in combination were able to change the M1/M2 balance towards a more anti-tumoral or inflammatory response (Fig. 6b). Moreover, treatment with ibrutinib only or with the drug combination was able to diminish the frequency of PD-1-positive M2 macrophages (Fig. 6c). The frequency of SIRP α -positive M2 macrophages was also diminished by both individual treatments, as well as the double positive M2 cells (Fig. 6d and e). In this mouse model we did not observe any effect in the expression of PD-L1 by the malignant cells, while the percentage of malignant cells was also not affected by the short term treatment (Fig. 6f and g). Expression of CD47 by patient-derived PCNSL cells was significantly down-regulated after treatment with the combination (Fig. 6h).

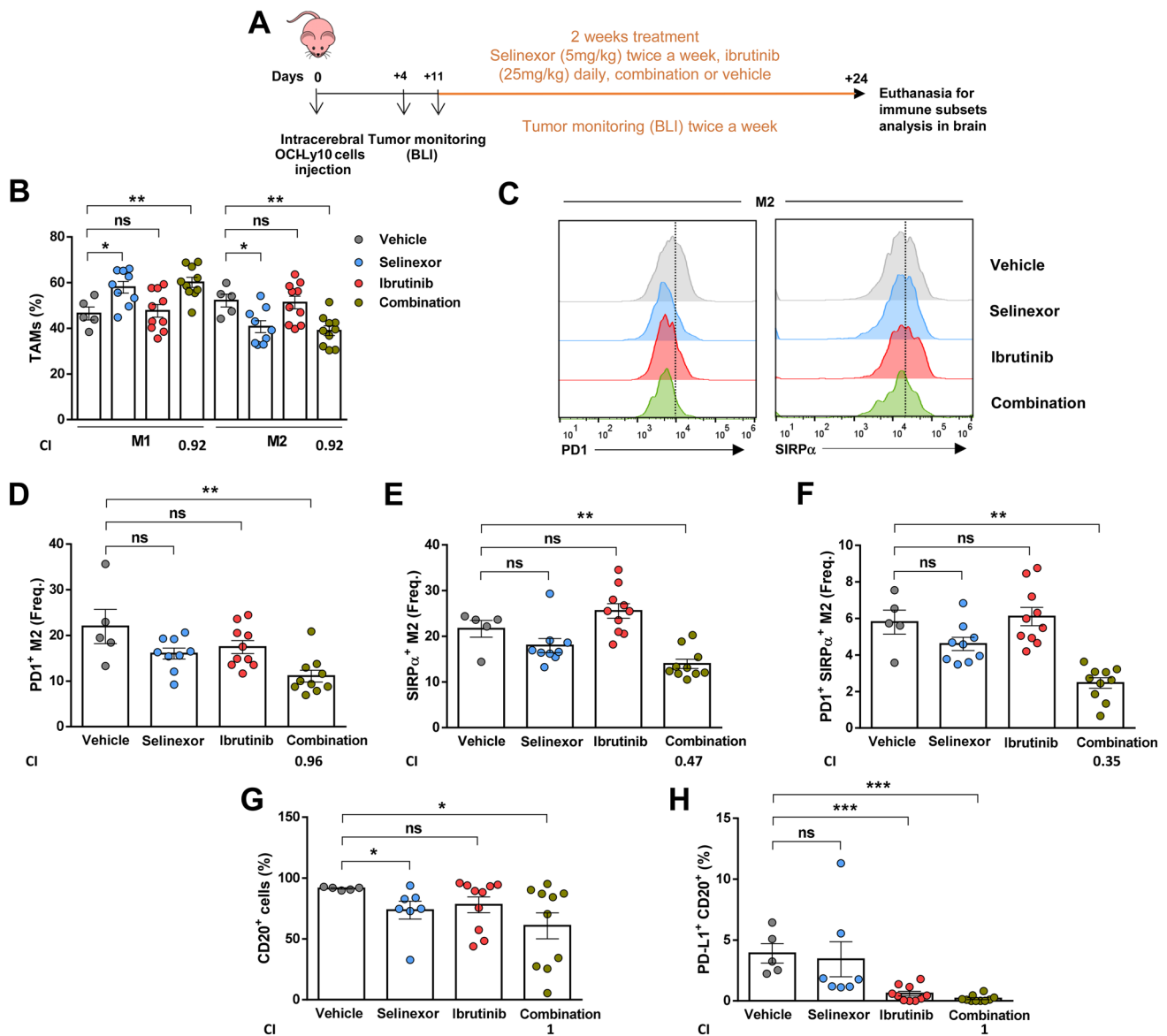


Fig. 5 Treatment with selinexor and ibrutinib favors M1-like response in tumor-associated macrophages in OCI-Ly10-derived CNS lymphomas. **a** Scheme representing mice treatment and monitoring. **b** Percentage of M1 and M2 TAMs by flow cytometry. **c** Histograms of PD1⁺ M2 and SIRP α ⁺ M2 of one representative mouse from each group. Frequency of M2 macrophages that express PD-1 (**d**), SIRP α

(**e**) or co-express both markers (**f**). **g** Percentage of CD20⁺ cells in the brains from mice treated for two weeks. **h** Percentage of CD20⁺ malignant cells expressing PD-L1 in the different treatment groups. (* $P < 0.05$, ** $P < 0.01$, *** $P < 0.001$, Mann-Whitney test. Graphs show mean \pm SEM). *CI* combination index, *BLI* bioluminescence imaging

Accordingly, CI calculations show that the combination did not improve upon individual treatments for any of the parameters except for the expression of CD47 on malignant cells. In order to identify direct immunomodulatory effects of selinexor and ibrutinib on human macrophages, we treated peripheral blood-derived macrophages in vitro with increasing doses of selinexor, ibrutinib or the combination for 30 min before inducing differentiation to M2 using macrophage colony-stimulating factor (M-CSF) and IL-10 (see *Supplementary information* for detailed

methods). M2 macrophages derived from 8 healthy donors had a mean expression of PD-1 of 81.15% \pm 8.8 and mean expression of SIRP α of 45.53% \pm 9.3. Firstly, we made sure that the drugs did not affect survival of macrophages at the concentrations used (data not shown). Next, in agreement with what we observed in vivo, we observed downregulation of the expression of both PD-1 and SIRP α caused by individual drugs or the combination. (Supplementary Figures S4A, S4B and S4C). However,

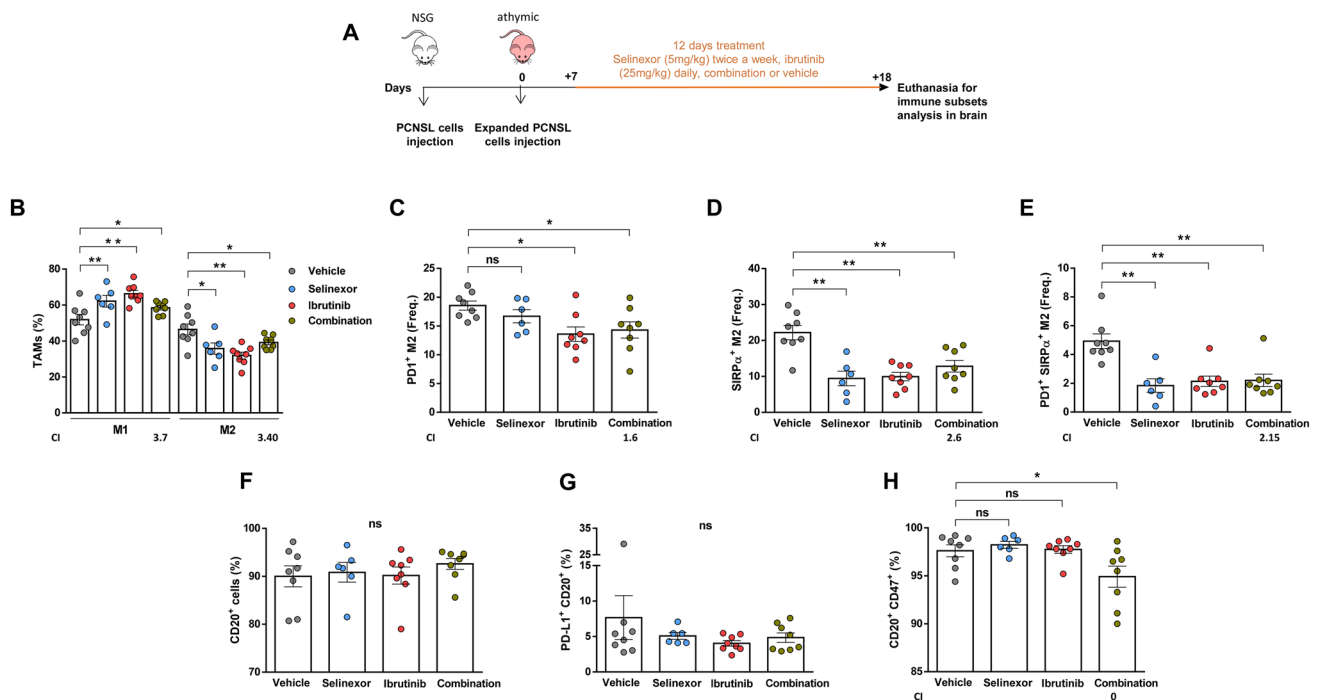


Fig. 6 Treatment with selinexor and ibrutinib favors M1-like response in tumor-associated macrophages in CNS lymphoma PDXs. **a** Scheme representing mice treatment and monitoring. **b** Percentage of M1 and M2 TAMs by flow cytometry. Frequency of M2 macrophages that express PD-1 (**c**), SIRP α (**d**) or co-express both markers (**e**). **f** Percentage of CD20⁺ cells in the brains from mice. **g**

Percentage of malignant cells CD20⁺ expressing PD-L1 in the different treatment groups. Percentage of malignant cells expressing CD47 (**h**) and co-expressing PD-L1 and CD47 (**i**). (* $P < 0.05$, ** $P < 0.01$, *** $P < 0.001$, Mann-Whitney test. Graphs show mean \pm SEM). *CI* combination index

this did not translate into increased phagocytic activity (Supplementary Figure S4D).

Also, using the same experimental setting we analyzed the effect of selinexor, ibrutinib or the combination in interfering with M2 polarization by analyzing additional M1 and M2-like markers and IL-10 production. We found an increase in the expression of the activation and M1-like marker CD86 and a decrease in the M2-like marker CD163 as well as lower levels of PD-L1 and the anti-inflammatory cytokine IL-10 after treatment with selinexor and ibrutinib (Supplementary Figures S4E-H). However, we did not see any significant effect in the expression of CD206 or HLA-DR (Supplementary Figures S4I-J). In vitro modulation of additional surface markers and cytokines is consistent with the loss of pro-tumoral M2 properties after treatment with selinexor and ibrutinib.

Altogether these results indicate that the combination of selinexor and ibrutinib is able to block tumoral growth, to significantly increase the median survival of mice with PCNSL and to modulate the innate immune microenvironment towards a more anti-tumoral stage, likely reinvigorating the anti-tumoral phagocytic function of the tumor infiltrating macrophage population in vivo.

Discussion

Blockage of XPO1-mediated nuclear transport using SINEs like selinexor has been shown to be an effective anti-neoplastic approach in a variety of malignancies. [17, 37, 38] XPO1 inhibition forces nuclear localization of tumor suppressors and also interferes with additional signaling pathways, including NF- κ B and BCR, which are crucial for survival of malignant B cells in general and for PCNSL cells in particular. The clinical use of selinexor in lymphoma has been studied in a phase I trial studying patients diagnosed with relapsed/refractory NHL and a phase IIb study in patients with DLBCL [17], which has led to a recent approval by the FDA in such an adverse setting. Additionally, based on our pre-clinical experience, we recently used selinexor in a compassionate way for a patient diagnosed with DLBCL who developed an isolated CNS relapse after several lines of treatment. After a month of treatment a partial response was already observed while after 5 months of selinexor the patient remained asymptomatic and the MRI (magnetic resonance imaging) showed a complete resolution of the brain tumors [19]. Ibrutinib

is also able to cross the BBB and is active against CNS lymphoma cells. In this setting, ibrutinib has been assayed alone [6, 7] or in combination with chemotherapy [5], showing high response rates but relatively short remissions, while other BTK inhibitors have showed similar efficacy [39]. Based on all these data, herein we proposed to combine selinexor with ibrutinib in models of PCNSL.

Exploitation of the immune response to a neoplastic process is currently a widespread strategy to treat cancer. To achieve this, different approaches are being pursued, specially focused on harnessing the anti-tumoral capacity of T lymphocytes via checkpoint inhibition [40]. Intriguingly, evading a T-cell mediated immune response seems to be a common feature of PCNSL since a high percentage of cases are affected by both MHC-I loss and/or PD-L1/2 amplification [14], and the infiltration by T lymphocytes is scarce while present [9–12]. However, some immunotherapies have already shown to be effective in PCNSL, such as anti-CD20 and, more recently, anti-PD-1 therapy, with both preclinical [41] and clinical evidences, although with only information for four patients, where responses lasted a median of 15 months [42]. In agreement, anti-PD-1 is highly effective in Hodgkin's lymphoma [43] even though the expression of PD-1 on T-cells is heterogeneous and PD-L1/2 amplification and lack of MHC-I expression on tumoral cells are common, characteristics that should hamper a T-cell mediated response [44]. In this regard, a role for the innate immune system in the development of PCNSL is further supported by recent discovery of PD-1 expression in TAMs [28] and the fact that these immune cells have also been found to be suppressed by the MHC-I system in cancer cells, rendering malignant cells that downregulate MHC-I to avoid T cell surveillance exposed to macrophage phagocytosis [45]. Therefore, paralleling the few PCNSL patients treated with anti-PD-1 achieving a complete response, this effect may be related to a macrophage-mediated anti-tumoral effect after PD-1 pharmacological blockage. Supporting that, herein we describe the presence of brain PD-1-positive M2 macrophages in two orthotopic mouse models of PCNSL, including PDXs. The recognition of human malignant cells by mice macrophages has been previously demonstrated in mice models of PCNSL [20, 46] and other tumoral models such as colon cancer [28], pancreatic adenocarcinoma [47] and T-cell lymphoma [48]. TAMs in CNLS have been found to be supportive of the tumoral growth and related to prognosis of patients [9, 13]. Also, indoleamine 2,3 dioxygenase (IDO) and IL-10, which may be markers of macrophage infiltration, are related to prognosis or response to immunomodulatory therapy [9, 13, 49]. The observed expression of PD-1 and SIRP α by innate immune cells responding to and interacting with CNS lymphoma cells in vivo indicates that their anti-tumoral effect is partially impaired but also opens the opportunity to potentially target these cells by

immunotherapies that aim at potentiating the autologous anti-tumoral immune response. In this regard, it has been previously shown how immunomodulation by pomalidome in mouse models of PCNSL results in reprogramming of M2 macrophages into M1 [20]. In the clinical setting, both pomalidomide and lenalidomide are showing preliminary therapeutic activity in a phase I study in patients diagnosed with PCNSL (combined with dexamethasone) [29]. Also, lenalidomide in combination with rituximab showed significant clinical activity in relapsed/refractory PCNSL patients [49, 50]. Combination therapies that not only directly attack the survival of malignant cells but also alter the immune function are therefore an interesting approach when aiming at achieving long lasting responses. In this regard, inhibiting BTK can have this double effect in B-cell malignancies, since BTK protein is not only involved in malignant B-cell survival but is also required for the tumor-promoting effect of macrophages [35, 36]. Taking this into account, we hypothesized that combining ibrutinib with selinexor would also be effective in harnessing the innate immune response mediated by TAMs in PCNSL. In fact, selinexor and ibrutinib combination treatment was able to not only increase mouse survival but to shift the innate immune response towards a more inflammatory phenotype, specifically defined by downregulation of PD-1 and SIRP α in M2 macrophages and increased proportion of M1 macrophages as well as modulation of additional M1 and M2-like properties consistent with loss of pro-tumoral M2 characteristics. Confirmation of these results and additional studies in the interaction of malignant cells and the immune system in PCNSL using different in vivo models, including syngeneic mice, is needed to further confirm the potential clinical value of the combination of selinexor and ibrutinib in patients diagnosed with PCNSL.

Conclusions

Our results show that selinexor blocks tumor growth and prolongs survival in a bioluminescent mouse model, while its combination with ibrutinib further increases survival. Alongside this, treatment with this combination not only had a direct cytotoxic effect in malignant cells but also favored an anti-tumoral innate immune response by shifting polarization of tumor-infiltrating macrophages toward inflammatory M1 and diminishing PD-1 and SIRP α expression in the remaining tumor-promoting M2 macrophages, highlighting the pathogenic role of the innate immune microenvironment in PCNSL. Herein we provide pre-clinical evidence for the development of selinexor and ibrutinib as a new therapeutic option with cytotoxic and immunomodulatory potential for patients diagnosed with PCNSL, aiming at a durable

response to improve the fatal prognosis of patients diagnosed with this disease.

Acknowledgements Authors want to thank Dr. Francesc Graus and Josep González from IDIBAPS, University of Barcelona, Spain and Dr. Andreu Gabarrós, from IDIBELL, University of Barcelona, Spain, for their commitment and support in this project. Authors thank the Cellex Foundation for providing research facilities and equipment.

Author contributions Designed research and supervised the work: MC and FB. Performed experiments: IJ, JC, SB, C.Pagès. JCN, JB, NP, LP. Analyzed and interpreted data: MC, FB, JS, IJ, JC. Contributed primary samples and analysis: SB, PA, JC, LE, CP, DHC, FM-R. Wrote the manuscript: IJ, JC, MC, FB. Revised the manuscript: all authors.

Funding This work was supported by research funding from the Instituto de Salud Carlos III, Fondo de Investigaciones Sanitarias (PI17/00950, M.C., PI17/00943, F.B, PI18/01392, P.A., PI16/01278, J.S) cofinanced by the European Regional Development Fund (ERDF); Fundación Asociación Española Contra el Cáncer (M.C. and P.A.) and Gilead Fellowships (GLD16/00144, GLD18/00047, F.B). M.C. holds a contract from Ministerio de Ciencia, Innovación y Universidades (RYC-2012-12018). S.B. is the recipient of a postdoctoral fellowship from Fundación Alfonso Martin Escudero.

Data availability The datasets used and/or analyzed and materials from the current study are available from the corresponding author on reasonable request.

Compliance with ethical standards

Conflicts of interest M. C. has received research funding from Karyopharm, Pharmacyclics, Roche, Arqule and AstraZeneca. F.B. has received research funding and honoraria from Roche, Celgene, Takeda, AstraZeneca, Novartis, Abbie and Janssen. J.S. is a co-founder of Mosaic Biomedicals and Northern Biologics. J.S. received grant/research support from Mosaic Biomedicals, Northern Biologics and Roche/Glycart. PA has received honorarium for advisory and speaker faculty from Janssen, Roche, Celgene, and Abbvie. All remaining authors have declared no conflicts of interest.

Ethics approval and consent to participate All animal experiments were approved by the local Ethical Committee for the Use of Experimental Animals. The use of primary cells from patients was approved by the local Clinical Research Ethics Committee according to the principles of the Declaration of Helsinki and after obtaining written informed consent from the patient.

Informed consent Not applicable.

Open Access This article is licensed under a Creative Commons Attribution 4.0 International License, which permits use, sharing, adaptation, distribution and reproduction in any medium or format, as long as you give appropriate credit to the original author(s) and the source, provide a link to the Creative Commons licence, and indicate if changes were made. The images or other third party material in this article are included in the article's Creative Commons licence, unless indicated otherwise in a credit line to the material. If material is not included in the article's Creative Commons licence and your intended use is not permitted by statutory regulation or exceeds the permitted use, you will need to obtain permission directly from the copyright holder. To view a copy of this licence, visit <http://creativecommons.org/licenses/by/4.0/>.


References

1. Maher EA, Fine HA (1999) Primary CNS lymphoma. *Semin Oncol* 26(3):346–356
2. Camilleri-Broët S, Crinière E, Broët P et al (2006) A uniform activated B-cell-like immunophenotype might explain the poor prognosis of primary central nervous system lymphomas: analysis of 83 cases. *Blood* 107(1):190–196
3. Kerbauy MN, Moraes FY, Lok BH et al (2017) Challenges and opportunities in primary CNS lymphoma: a systematic review. *Radiother Oncol J Eur Soc Ther Radiol Oncol* 122(3):352–361
4. Nakamura T, Tateishi K, Niwa T et al (2016) Recurrent mutations of CD79B and MYD88 are the hallmark of primary central nervous system lymphomas. *Neuropathol Appl Neurobiol* 42(3):279–290
5. Lionakis MS, Dunleavy K, Roschewski M et al (2017) Inhibition of B cell receptor signaling by ibrutinib in primary CNS lymphoma. *Cancer Cell* 31(6):833–843.e5
6. Grommes C, Pastore A, Palaskas N et al (2017) Ibrutinib unmasks critical role of bruton tyrosine kinase in primary CNS lymphoma. *Cancer Discov* 7(9):1018–1029
7. Soussain C, Choquet S, Blonski M et al (1990) Ibrutinib monotherapy for relapse or refractory primary CNS lymphoma and primary vitreoretinal lymphoma: final analysis of the phase II “proof-of-concept” iLOC study by the Lymphoma study association (LYSA) and the French oculo-cerebral lymphoma (LOC) network. *Eur J Cancer Oxf Engl* 2019(117):121–130
8. Grommes C, Tang SS, Wolfe J et al (2019) Phase 1b trial of an ibrutinib-based combination therapy in recurrent/refractory CNS lymphoma. *Blood* 133(5):436–445
9. Nam SJ, Kim S, Kwon D et al (2018) Prognostic implications of tumor-infiltrating macrophages, M2 macrophages, regulatory T-cells, and indoleamine 2,3-dioxygenase-positive cells in primary diffuse large B-cell lymphoma of the central nervous system. *Oncoimmunology* 7(7):e1442164
10. He M, Zuo C, Wang J et al (2013) Prognostic significance of the aggregative perivascular growth pattern of tumor cells in primary central nervous system diffuse large B-cell lymphoma. *Neuro-Oncol* 15(6):727–734
11. Chang C, Lin C-H, Cheng A-L, Medeiros LJ, Chang K-C (2015) Primary central nervous system diffuse large B-cell lymphoma has poorer immune cell infiltration and prognosis than its peripheral counterpart. *Histopathology* 67(5):625–635
12. Venetz D, Ponzoni M, Schiraldi M et al (2010) Perivascular expression of CXCL9 and CXCL12 in primary central nervous system lymphoma: T-cell infiltration and positioning of malignant B cells. *Int J Cancer* 127(10):2300–2312
13. Sasayama T, Tanaka K, Mizowaki T et al (2016) Tumor-associated macrophages associate with cerebrospinal fluid interleukin-10 and survival in primary central nervous system lymphoma (PCNSL). *Brain Pathol Zurich Switz* 26(4):479–487
14. Chapuy B, Roemer MGM, Stewart C et al (2016) Targetable genetic features of primary testicular and primary central nervous system lymphomas. *Blood* 127(7):869–881
15. Etchin J, Berezovskaya A, Conway AS et al (2017) KPT-8602, a second-generation inhibitor of XPO1-mediated nuclear export, is well tolerated and highly active against AML blasts and leukemia-initiating cells. *Leukemia* 31(1):143–150
16. Zhong Y, El-Gamal D, Dubovsky JA et al (2014) Selinexor suppresses downstream effectors of B-cell activation, proliferation and migration in chronic lymphocytic leukemia cells. *Leukemia* 28(5):1158–1163
17. Kuruvilla J, Savona M, Baz R et al (2017) Selective inhibition of nuclear export with selinexor in patients with non-Hodgkin lymphoma. *Blood* 129(24):3175–3183

18. Hing ZA, Mantel R, Beckwith KA et al (2015) Selinexor is effective in acquired resistance to ibrutinib and synergizes with ibrutinib in chronic lymphocytic leukemia. *Blood* 125(20):3128–3132
19. Bobillo S, Abrisqueta P, Carpio C, et al. 2017. Promising activity of selinexor in the treatment of a patient with refractory diffuse large B-cell lymphoma and central nervous system involvement. *Haematologica*.
20. Li Z, Qiu Y, Personett D et al (2013) Pomalidomide shows significant therapeutic activity against CNS lymphoma with a major impact on the tumor microenvironment in murine models. *PLoS ONE* 8(8):e71754
21. Yang Y, Shaffer AL 3rd, Emre NCT et al (2012) Exploiting synthetic lethality for the therapy of ABC diffuse large B cell lymphoma. *Cancer Cell* 21(6):723–737
22. Wilson WH, Gerecitano JF, Goy A et al (2012) The Bruton's Tyrosine Kinase (BTK) Inhibitor, Ibrutinib (PCI-32765), has preferential activity in the ABC subtype of relapsed/refractory de novo diffuse large B-Cell lymphoma (DLBCL): interim results of a multicenter, open-label, phase 2 study. *ASH Annu Meet Abstr* 120(21):686
23. Turner JG, Dawson J, Sullivan DM (2012) Nuclear export of proteins and drug resistance in cancer. *Biochem Pharmacol* 83(8):1021–1032
24. Rosenwald A, Wright G, Chan WC et al (2002) The use of molecular profiling to predict survival after chemotherapy for diffuse large-B-cell lymphoma. *N Engl J Med* 346(25):1937–1947
25. Abdul Razak AR, Mau-Soerensen M, Gabrail NY et al (2016) First-in-class, first-in-human phase I study of selinexor, a selective inhibitor of nuclear export, in patients with advanced solid tumors. *J Clin Oncol Off J Am Soc Clin Oncol* 34(34):4142–4150
26. de Vries R, Smit JW, Hellemans P et al (2016) Stable isotope-labelled intravenous microdose for absolute bioavailability and effect of grapefruit juice on ibrutinib in healthy adults. *Br J Clin Pharmacol* 81(2):235–245
27. Ponader S, Chen S-S, Buggy JJ et al (2012) The Bruton tyrosine kinase inhibitor PCI-32765 thwarts chronic lymphocytic leukemia cell survival and tissue homing in vitro and in vivo. *Blood* 119(5):1182–1189
28. Gordon SR, Maute RL, Dulken BW et al (2017) PD-1 expression by tumour-associated macrophages inhibits phagocytosis and tumour immunity. *Nature* 545(7655):495–499
29. Tun HW, Johnston PB, DeAngelis LM et al (2018) Phase 1 study of pomalidomide and dexamethasone for relapsed/refractory primary CNS or vitreoretinal lymphoma. *Blood* 132(21):2240–2248
30. Colonna M, Butovsky O (2017) Microglia function in the central nervous system during health and neurodegeneration. *Annu Rev Immunol* 35:441–468
31. Sica A, Schioppa T, Mantovani A, Allavena P. (2006). Tumour-associated macrophages are a distinct M2 polarised population promoting tumour progression: potential targets of anti-cancer therapy. *Eur J Cancer Oxf Engl*, 1990, 42(6): 717–727
32. Matlung HL, Szilagy K, Barclay NA, van den Berg TK (2017) The CD47-SIRP α signaling axis as an innate immune checkpoint in cancer. *Immunol Rev* 276(1):145–164
33. Rubenstein JL, Wong VS, Kadoch C et al (2013) CXCL13 plus interleukin 10 is highly specific for the diagnosis of CNS lymphoma. *Blood* 121(23):4740–4748
34. Pouzoulet F, Alentorn A, Royer-Perron L et al (2019) Primary CNS lymphoma patient-derived orthotopic xenograft model capture the biological and molecular characteristics of the disease. *Blood Cells Mol Dis* 75:1–10
35. Nguyen P-H, Fedorchenko O, Rosen N et al (2016) LYN kinase in the tumor microenvironment is essential for the progression of chronic lymphocytic leukemia. *Cancer Cell* 30(4):610–622
36. Ping L, Ding N, Shi Y et al (2017) The Bruton's tyrosine kinase inhibitor ibrutinib exerts immunomodulatory effects through regulation of tumor-infiltrating macrophages. *Oncotarget* 8(24):39218–39229
37. Das A, Wei G, Parikh K, Liu D (2015) Selective inhibitors of nuclear export (SINE) in hematological malignancies. *Exp Hematol Oncol* 4:7
38. Gravina GL, Mancini A, Colapietro A et al (2017) Pharmacological treatment with inhibitors of nuclear export enhances the anti-tumor activity of docetaxel in human prostate cancer. *Oncotarget* 8(67):111225–111245
39. Nagane M, Narita Y, Mishima K, et al. (2019). Phase 1/2 study of tirabrutinib (ONO/GS-4059), a Next-Generation Bruton's Tyrosine Kinase (BTK) inhibitor, monotherapy in patients with relapsed/refractory primary central nervous system Lymphoma (PCNSL). *Blood*, 134(Supplement_1): 1586–1586.
40. Robert C, Ribas A, Wolchok JD et al (2014) Anti-programmed-death-receptor-1 treatment with pembrolizumab in ipilimumab-refractory advanced melanoma: a randomised dose-comparison cohort of a phase 1 trial. *Lancet Lond Engl* 384(9948):1109–1117
41. Qiu Y, Li Z, Pouzoulet F et al (2018) Immune checkpoint inhibition by anti-PDCD1 (anti-PD1) monoclonal antibody has significant therapeutic activity against central nervous system lymphoma in an immunocompetent preclinical model. *Br J Haematol* 183(4):674–678
42. Nayak L, Iwamoto FM, LaCasce A, et al. 2017. PD-1 blockade with nivolumab in relapsed/refractory primary central nervous system and testicular lymphoma. *Blood*.
43. Ansell SM, Lesokhin AM, Borrello I et al (2015) PD-1 blockade with nivolumab in relapsed or refractory Hodgkin's lymphoma. *N Engl J Med* 372(4):311–319
44. Reichel J, Chadburn A, Rubinstein PG et al (2015) Flow sorting and exome sequencing reveal the oncogenome of primary Hodgkin and reed-sternberg cells. *Blood* 125(7):1061–1072
45. Barkal AA, Weiskopf K, Kao KS et al (2018) Engagement of MHC class I by the inhibitory receptor LILRB1 suppresses macrophages and is a target of cancer immunotherapy. *Nat Immunol* 19(1):76–84
46. Yushi Q, Li Z, Von Roemeling CA et al (2016) Osteopontin is a multi-faceted pro-tumorigenic driver for central nervous system lymphoma. *Oncotarget* 7(22):32156–32171
47. Massó-Vallés D, Jauset T, Serrano E et al (2015) Ibrutinib exerts potent antifibrotic and antitumor activities in mouse models of pancreatic adenocarcinoma. *Cancer Res* 75(8):1675–1681
48. Horwitz SM, Koch R, Porcu P et al (2018) Activity of the PI3K- δ , γ inhibitor duvelisib in a phase 1 trial and preclinical models of T-cell lymphoma. *Blood* 131(8):888–898
49. Rubenstein JL, Geng H, Fraser EJ et al (2018) Phase 1 investigation of lenalidomide/rituximab plus outcomes of lenalidomide maintenance in relapsed CNS lymphoma. *Blood Adv* 2(13):1595–1607
50. Ghesquieres H, Chevrier M, Laadhari M et al (2019) Lenalidomide in combination with intravenous rituximab (REVRI) in relapsed/refractory primary CNS lymphoma or primary intraocular lymphoma: a multicenter prospective “proof of concept” phase II study of the French Oculo-Cerebral lymphoma (LOC) Network and the Lymphoma Study Association (LYSA)†. *Ann Oncol Off J Eur Soc Med Oncol* 30(4):621–628

Publisher's Note Springer Nature remains neutral with regard to jurisdictional claims in published maps and institutional affiliations.

Affiliations

Isabel Jiménez^{1,2} · Júlia Carabia^{1,2} · Sabela Bobillo^{2,3} · Carles Palacio^{2,3} · Pau Abrisqueta^{2,3} · Carlota Pagès^{1,2} · Juan C. Nieto^{1,2} · Josep Castellví⁴ · Francisco Martínez-Ricarte⁵ · Lourdes Escoda⁶ · Cristóbal Perla⁷ · Dennis H. Céspedes Torrez⁷ · Joan Boix^{1,2} · Noelia Purroy^{1,2,10} · Lluís Puigdefàbregas^{1,2} · Joan Seoane^{2,8,9} · Francesc Bosch^{2,3} · Marta Crespo^{1,2} 

¹ Experimental Hematology, Vall d'Hebron Institute of Oncology (VHIO), Vall d'Hebron Barcelona Hospital Campus, C/Natzaret, 115-117, Barcelona 08035, Spain

² Department of Medicine, Universitat Autònoma de Barcelona, Bellaterra 08193, Spain

³ Department of Hematology, Experimental Hematology, Vall d'Hebron Hospital Universitari, Vall d'Hebron Institute of Oncology (VHIO), Vall d'Hebron Barcelona Hospital Campus, Passeig Vall d'Hebron 119-129, Barcelona 08035, Spain

⁴ Department of Pathology, Vall d'Hebron Hospital Universitari, Vall d'Hebron Barcelona Hospital Campus, Passeig Vall d'Hebron 119-129, Barcelona 08035, Spain

⁵ Department of Neurosurgery, Vall d'Hebron Hospital Universitari, Vall d'Hebron Barcelona Hospital Campus, Passeig Vall d'Hebron 119-129, Barcelona 08035, Spain

⁶ Department of Hematology, Hospital Universitari Joan XXIII, Tarragona, Spain

⁷ Department of Neurosurgery, Hospital Universitari Joan XXIII, Tarragona, Spain

⁸ Translational Research Program, Vall d'Hebron Institute of Oncology (VHIO), Vall d'Hebron Barcelona Hospital Campus, C/Natzaret, 115-117, 08035 Barcelona, Spain

⁹ Institució Catalana de Recerca I Estudis Avançats (ICREA), CIBERONC, Barcelona, Spain

¹⁰ Department of Medical Oncology, Dana-Farber Cancer Institute, Boston, Massachusetts and Broad Institute of MIT and Harvard, Cambridge, MA, UK

Clinical Progression of Chronic Lymphocytic Leukemia (CLL) Is Characterized By a Progressive Increase of the Exhausted T-Cell Phenotype and Immunosuppression Induced By Leukemic Cells

Isabel Jiménez, MSc, Sabela Bobillo, MD, Pau Abrisqueta, MD PhD, Bárbara Tazón, PhD, Carles Palacio, MD, Juan C Nieto, PhD, Júlia Carabía, MSc, María José Terol, MD PhD, Jose García-Marco, MD PhD, Joan Boix, BSc, Magdalena Munuera, BSc, Lluís Puigdefàbregas, Elisa Roldán, Marta Crespo, PhD, Francesc Bosch



Blood (2017) 130 (Supplement 1): 1713.

https://doi.org/10.1182/blood.V130.Suppl_1.1713.1713

Split-Screen Share Tools

Abstract

The mechanisms leading to clinical progression of CLL from early asymptomatic stages are not fully elucidated, being the acquisition of molecular alterations an infrequent phenomenon. Abrogation of autologous immune response against neoplastic processes is a key feature defining cancer. In CLL, malignant cells are able to evade immune anti-tumoral responses through inhibitory ligand signaling and defective immune synapse with T cells, which in turn exhibit an impaired proliferation and cytotoxic activity as well as high expression of exhaustion markers. In addition, other immunosuppressive features, such as production of IL-10 by CLL cells, are observed in these patients. Against this background, we hypothesize that evasion from immune surveillance is a mechanism of clinical progression from early stages in CLL that potentially opens a new field of therapeutic opportunities.

To study changes in the immune system related to clinical progression, we performed flow cytometry analysis in paired samples from 19 patients with CLL at diagnosis and progression (median time to progression: 2.2 years), and in paired samples from 5 CLL patients without clinical progression (median follow-up: 2.7 years) as controls. At progression, we observed a significant increase in the absolute numbers of the CD45RA⁺CCR7⁻ effector memory (EM) subset in both CD4⁺ and CD8⁺ T cells; CD4⁺ and CD8⁺ EM also had increased expression of PD1 at progression. Of note, there was no increase in PD1 in patients that did not progress; pointing out that PD1 plays a relevant role in CLL progression (Figure 1). Moreover, the inhibitory receptors CD244 and CD160 were significantly increased in CD8⁺ T cells and the co-expression of these receptors was also significantly higher in CD8⁺ cells at the time of progression. Differential expression of the transcription factors T-bet and Eomes defines the progenitor (T-bet^{hi}PD1^{int}) and the terminal (Eomes^{hi}PD1^{hi}) exhausted CD8⁺ T-cell subsets. In CLL, the Eomes^{hi}PD1^{hi} CD8⁺ terminal subpopulation was significantly increased at progression, whereas the T-bet^{hi}PD1^{int} CD8⁺ progenitor subset was stable, indicating the predominance of a more severe exhausted subset. In addition, myeloid-derived suppressor cells (MDSCs) were significantly increased and NK cells were decreased at late stages, while in contrast regulatory T cells remained unchanged. To further evaluate the increase of immunosuppression during progression, we studied IL-10 production in paired CLL samples. After 48 hours of microenvironmental stimuli, expression of IL-10 by CLL cells was significantly higher in samples obtained at the time of progression. In agreement with this, IL-10 plasma levels were higher at progression (n=9 pairs). This enhancement of regulatory B cell properties in CLL cells may also contribute to the increase of exhausted T-cell phenotype observed at clinical progression. To study the influence of B-CLL cells in T cells, we modeled progression *in vitro* by co-culturing T cells from CLL patients with increasing ratios of autologous CLL cells during 7 days. Under this setting, CLL cells induced a higher expression of PD1 (Figure 2) and CD244 in CD8⁺ T cells compared to healthy B cells, this increase being dependent on the T:B ratio. To evaluate the contribution of IL-10 to the induction of T-cell exhaustion *in vitro* we are currently blocking its production from CLL cells and these results will be ready at the time of the meeting. Finally, to rule out the putative contribution of genetic clonal evolution on CLL progression, we analyzed by deep sequencing (median deepness of 16000X) mutations in 8 driver genes (MYD88, NOTCH1, SF3B1, BIRC3, TP53, XPO1, ATM and POT1) and the size of the subclones affected at diagnosis and progression. Out of the 17 cases analyzed, we found driver mutations at diagnosis in 10 patients, from which only one showed clonal evolution at progression (increased allele frequency in SF3B1 and ATM mutations).

Taking these results together, we conclude that clinical progression of CLL is potentially driven by an increasingly severe exhausted T-cell phenotype and by an enhancement in immunosuppressive features such as accumulation of MDSCs and elevated IL-10, pointing towards an impaired anti-neoplastic autologous immune response as a main mechanism of clinical progression. These results support the design of new immunotherapeutic strategies for patients in early stages that are likely to progress.

